Heidelberg University

Institute for Theoretical Physics

Phenomenology of Extra Abelian Gauge Symmetries

Dissertation

by

Patrick Foldenauer

Dissertation

submitted to the

Combined Faculties for the Natural Sciences and for Mathematics
of the Ruperto-Carola University of Heidelberg, Germany

for the degree of

Doctor of Natural Sciences

Put forward by

Patrick Foldenauer

born in Kirchheim unter Teck, Germany

Oral examination: July 3, 2019

Phenomenology of Extra Abelian Gauge Symmetries

Referees: Prof. Dr. Jörg Jäckel
Jun.-Prof. Dr. Susanne Westhoff

Zusammenfassung

Auf der Suche nach neuer Physik bieten Theorien mit zusätzlichen $U(1)$ Eichsymmetrien ein simples, aber facettenreiches theoretisches Modell um Defizite des Standard Modells zu verringern. Um die physikalische Vorhersagekraft solcher Modelle systematisch zu untersuchen, betrachten wir drei verschiedene phänomenologische Aspekte von zusätzlichen $U(1)$ Eichsymmetrien.
Zuerst identifizieren wir unter Berücksichtigung von flavorverletzenden neutralen Strömen, welche durch ein effektives schweres Z'-Boson induziert werden, die jeweils stärksten Einschränkungen für alle möglichen Kombinationen von quark- und leptonflavorverletzenden Kopplungen. In Bereichen des Parameterraums, in denen es keine starke Einschränkung durch Mesonmischung gibt, können Resonanzsuchen am LHC die stärkste Einschränkung liefern. Solche Szenarien können die Anomalien, welche in $(g-2)_\mu$ und Tau-Zerfällen gemessen wurden, erklären.
Anschließend betrachten wir den Fall, dass das „Hidden Photon“ das Eichboson der anomaliefreien Gruppen $U(1)_{B-L}$, $U(1)_{L_\mu - L_e}$, $U(1)_{L_e - L_\tau}$ oder $U(1)_{L_\mu - L_\tau}$ ist. Unter Berücksichtigung von schleifeninduziertem kinetischem Mischen führen wir eine umfassende Analyse aller Einschränkungen auf „Hidden Photons“ in diesen Modellen durch. Während diese Modelle allgemein stark durch Neutrinoexperimente eingeschränkt sind, kann die $(g-2)_\mu$ Anomalie in einem $U(1)_{L_\mu - L_\tau}$ Modell erklärt werden.
Zuletzt finden wir, dass durch Erweiterung des zuvor betrachteten $U(1)_{L_\mu - L_\tau}$ Modells um ein vektorartiges Fermion χ die $(g-2)_\mu$ Anomalie und die heutige Dichte der Dunklen Materie gleichzeitig erklärt werden können.

Abstract

In the search for new physics, models of extra $U(1)$ symmetries provide a simple but versatile theoretical framework to attenuate shortcomings of the Standard Model (SM). In an effort to systematically survey the physical prospects of such theories, we study three different phenomenological aspects of extra $U(1)$ symmetries.
First, studying Flavor-Changing Neutral Currents (FCNC) mediated by an effective heavy Z' boson, we identify the most stringent constraints for all possible combinations of lepton and quark flavor violating couplings. In regions of parameter space where severe bounds from meson mixing are avoided, LHC resonance searches can provide the leading constraint. Such scenarios are able to explain the observed $(g-2)_\mu$ and tau decay anomalies.
Second, we consider the possibility that the hidden photon is the gauge boson of the anomaly-free groups $U(1)_{B-L}$, $U(1)_{L_\mu - L_e}$, $U(1)_{L_e - L_\tau}$ or $U(1)_{L_\mu - L_\tau}$. Taking into account loop-induced kinetic mixing, we perform a comprehensive analysis of all hidden photon constraints in these scenarios. While generically stringent bounds arise due to neutrino couplings, for $U(1)_{L_\mu - L_\tau}$ an explanation of the $(g-2)_\mu$ anomaly is possible.
Finally, extending the previously considered $U(1)_{L_\mu - L_\tau}$ model by a vector-like fermion χ, we find that the $(g-2)_\mu$ anomaly and the dark matter relic abundance can be simultaneously explained.

Contents

Preface

The research presented in this thesis was conducted at the Institute for Theoretical Physics at Heidelberg University in the years 2016 to 2019. Chapter 3 is based on research in collaboration with J. Jaeckel (Heidelberg U.) that was previously published in the article

[1] P. Foldenauer and J. Jaeckel,
Purely flavor-changing Z' bosons and where they might hide,
JHEP **05** (2017) 010, [1612.07789].

Chapter 4 is based on research in collaboration with M. Bauer (Durham U., IPPP) and J. Jaeckel (Heidelberg U.) that was published in

[2] M. Bauer, P. Foldenauer and J. Jaeckel,
Hunting All the Hidden Photons,
JHEP **07** (2018) 094, [1803.05466].

Finally, the contents presented in Chapter 5 are based on the article

[3] P. Foldenauer,
Light dark matter in a gauged $U(1)_{L_\mu - L_\tau}$ model,
Phys. Rev. **D99** (2019) 035007, [1808.03647].

Furthermore, the author contributed to the "Fourth workshop of the LHC LLP Community" and is endorser of the resulting white paper

[4] J. Alimena *et al.*,
Searching for long-lived particles beyond the Standard Model at the Large Hadron Collider,
1903.04497.

Finally, the author is involved in ongoing research, which has not been published at the time of writing this thesis.

Chapter 1

Introduction

The tantalizing precision with which modern particle physics describes nature at the smallest experimentally accessible scales is rooted in the successful unification of two of the most fundamental concepts of modern physics – quantum mechanics and special relativity – within the framework of quantum field theory (QFT) [1–5]. Only the formulation of the Standard Model (SM) of particle physics [6–8] as a local QFT subject to an $SU(3) \times SU(2) \times U(1)$ symmetry group has permitted particle physics to embark on an era of precision tests. In this context, one of the most celebrated predictions of the SM is that of the electron magnetic moment with an accuracy of better than 10^{-12} [9, 10]. The discovery of the Higgs boson in 2012 at the LHC [11, 12] marked the ultimate triumph of the SM, when finally its last elusive piece had been found. With all its postulated particles discovered and its huge precision in predicting observables, the SM today is established as a very successful theory of particle physics. However, in spite of its tremendous success, the SM suffers from a number of fundamental shortcomings, which might motivate us to go beyond the SM in our theoretical efforts.

To begin with, all the success of the SM in making high precision predictions is conditional on the precise knowledge of its 19 free input parameters [13]. Considering the SM to be a purely descriptive model, it might appear appealing to view the SM input parameters as *a priori* arbitrary and to determine them experimentally. However, from a theoretical point of view this is deeply unsatisfactory and indeed there is reason to believe that the exact values of the SM parameters are not pure coincidence. For example, consider an alternative incarnation of the SM with the same field content, but with the values of the u- and d-quark Yukawa couplings (i.e. the quark masses) interchanged. Suddenly, the proton would be heavier than the neutron. This would have drastic consequences for our universe as the hydrogen atom would become unstable. Its nucleus (i.e. the proton) would decay into a neutron, a positron and an electron-neutrino. The released positron would annihilate with the electron into pairs of characteristic 511 keV photons and the universe would be mainly filled with stable thermal neutrons [14]. Considerations of the like show us that the existence of the universe as we know it critically depends on the exact values of the SM parameters. This might be reason to believe that a deeper mechanism beyond the SM exists which sets those values.

Moreover, within the SM the three fundamental interactions of elementary particles – the strong, the weak and the hypercharge interaction – are described in terms of quantum

field theories. At energies accessible with modern particle accelerators, it is sufficient to take into account only these three interactions to get an accurate description of the physics. However, at energies exceeding the Planck mass $m_{Pl} = \sqrt{\hbar c/G}$, or equivalently at distances smaller than the Planck length $\ell_{Pl} = \sqrt{\hbar G/c^3}$, we expect gravitational effects to become as important as quantum effects [15,16]. In this sense, the Planck scale gives the quantum limit of general relativity [17] and conventionally it is assumed that a theory of quantum gravity should resolve this by setting all the fundamental interactions (including gravity) on equal footing. However, the SM is not concerned with gravity at all and it is therefore not expected to give an accurate description of particle physics at or beyond the Planck scale.

This fact tells us that indeed the SM cannot be a complete theory of particle physics up to arbitrarily high scales in the ultraviolet (UV). Instead, it must rather be a low-energy effective theory that is valid up to some scale $\Lambda < m_{Pl}$ [18]. However, considering the SM to be valid up to scales substantially higher than the electroweak scale is problematic from the point of view of an effective field theory (EFT). As in an EFT all operators $\mathcal{O}^d$ of dimension d should have their dimensionality set by the cutoff scale Λ [19], their coefficients should be $c\,\Lambda^{4-d}$ with a parameter $c \approx 1$. For the $d = 2$ Higgs mass operator, this would mean that

$$\mathcal{L}_{d=2} = c\,\Lambda^2 |H|^2 \,. \tag{1.1}$$

From the measurement of the physical Higgs mass M_h we know, however, that $M_h \sim v$ is of the order of the electroweak vacuum expectation value (VEV) v. In contrast to what we just said, this would require $c = v^2/\Lambda^2 \ll 1$ to be unnaturally small [20]. This apparent fine-tuning problem is often referred to as the Electroweak Hierarchy Problem.

The aforementioned theoretical issues can be considered purely aesthetic if the SM itself is regarded as a mere low-energy effective theory. In this case it should at the least accurately describe particle physics at comparatively small energies, as accessible in laboratory experiments or in processes governing the universe today. Contrary to these considerations, the SM cannot give a complete description of particle physics at low energies as soon as we are also concerned with astrophysics and cosmology.

If we consider the total energy budget of the universe today, we find that only $\sim 5\%$ of the energy density consists of baryonic matter [21], which can be described by SM physics. The fact that there is at all a net relic baryon abundance is attributed to baryogenesis, a mechanism that under very general assumptions requires violation of baryon number B, C- and CP-violation, as well as out-of-equilibrium interactions [22]. However, the SM can most probably not be the (only) source of baryogenesis [23]. For example, in order for electroweak baryogenesis to work, a strong first order phase transition is required [24, 25]. This is not the situation that we have in the SM and hence sphaleron processes could attenuate any created baryon asymmetry. Second, the SM is believed not provide enough CP-violation [26–29] to have generated the observed asymmetry.

Another $\sim 27\%$ of the energy density of the universe consists of non-baryonic matter referred to as Dark Matter (DM). The remaining $\sim 68\%$ are due to a substance with negative pressure called Dark Energy (DE), which in the common Standard Model of Cosmology is just given by a cosmological constant Λ. Neither DM nor DE are described by SM physics. Hence, (at least) $\sim 95\%$ of the total energy budget of the universe is

unaccounted for by the SM, making the need for physics Beyond the Standard Model (BSM) all the more pressing.

Apart from the theoretical issues of the SM that could potentially be addressed with new physics, there are a number of observational hints of where such new physics might be hiding.

- One observation exhibiting a feature that can potentially be attributed to new physics is the measured cosmic ray positron spectrum. The positron fraction observed first with PAMELA [30,31] and later with Fermi-LAT [32] and AMS-02 [33,34] shows a rise at energies between 10 to 100 GeV. While there is some general debate whether this excess can be explained from astrophysical sources or secondary particle production during cosmic ray propagation [35, 36], it has also immediately been interpreted as potentially coming from a possible DM remnant [37–41].

- A number of analyses of gamma ray data of the galactic centre taken with Fermi-LAT [42] revealed an excess peak at energies of around 1 to 5 GeV, which has commonly been interpreted as coming from the annihilation of DM [43–50]. That being said, in recent years an alternative explanation of the excess has ben attributed to gamma-ray pulsars [51, 52].

- The data taken with the full 2.46 t×yr exposure of the DAMA/NaI and DAMA/LIBRA experiments show evidence for an annual modulation signal consistent with the DM hypothesis at 12.9 σ C.L. [53, 54]. The findings of the DAMA experiments are subject to an ongoing controversial debate. While attempts to attribute the observed signal to a potential background process [55–60] have been futile, the DAMA signal as being due to DM has been firmly ruled out by a number of complementary experiments [61–71]. Independent measurements with very similar detector designs might help in the future to resolve this tension [72].

- LHCb has performed a number of measurements to test lepton flavor universality. Most prominently, the individual measurements of the B meson decay ratios

$$R_K = \frac{\mathrm{Br}(B^+ \to K^+ \mu^+\mu^-)}{\mathrm{Br}(B^+ \to K^+ e^+e^-)}\,, \qquad R_{K^*} = \frac{\mathrm{Br}(B^0 \to K^{*0} \mu^+\mu^-)}{\mathrm{Br}(B^0 \to K^{*0} e^+e^-)}\,, \tag{1.2}$$

  are compatible with their SM prediction at the $\sim 2\,\sigma$ level [73, 74]. However, the combination of these measurements is very sensitive to new physics contributions [75,76] and indeed displays a deviation from the SM expectation of $\sim 4-5\sigma$ [77–83]. Similarly, experimental determinations of the individual ratios

$$R_D = \frac{\mathrm{Br}(\bar{B} \to D\,\tau^-\bar{\nu}_\tau)}{\mathrm{Br}(\bar{B} \to D\,\ell^-\bar{\nu}_\tau)}\,, \qquad R_{D^*} = \frac{\mathrm{Br}(\bar{B} \to D^*\,\tau^-\bar{\nu}_\tau)}{\mathrm{Br}(\bar{B} \to D^*\,\ell^-\bar{\nu}_\tau)}\,, \tag{1.3}$$

  with $\ell = e, \mu$, are compatible with the SM at the $\sim 2\,\sigma$ level [84–87]. The combined analysis of R_D and R_{D^*} on the other hand is in tension with the SM prediction at the $\sim 4\,\sigma$ level [88–90].

- Finally, one of the most longstanding tensions between experiment and theory is certainly the excess in the observed muon anomalous magnetic moment $a_\mu = (g-2)_\mu/2$. The value of a_μ, experimentally determined at the BNL E821 experiment [91–93], deviates from the SM prediction by about $\sim 3\,\sigma$ [94, 95]. The successor experiment E989 at Fermilab, which already started taking data, is aiming at a factor-of-20 improvement in the muon statistics, thereby reaching a fourfold improvement in the uncertainty [96,97]. If the excess in a_μ is due to new physics and the central value does not change, this will push the significance above $5\,\sigma$, thereby making it a discovery of new physics.

Together with the previously discussed theoretical shortcomings that the SM is suffering from, this list of observational hints provides ample motivation to consider new physics. Ultimately, a UV-complete "theory of everything" should address and resolve all of the aforementioned issues in a comprehensive and unified framework. One possible example of such theories might be string theory, as e.g. argued for in [98]. However, the complexity of string theory makes it very hard to make clear experimentally testable predictions.

Rather than trying to construct such a "theory of everything", in this thesis we follow a more humble bottom-up approach to address new physics. In this approach, we will ask ourselves in Chapter 2 how to incorporate new physics effects addressing (part of) the issues discussed here into the SM. Therefore, we will start out in Section 2.1 to investigate strategies to extend the SM in a consistent way. This will bring us to the concept of portal interactions of new physics with the SM. As we will see in Section 2.2, renormalizability and gauge invariance allow for three different portal interactions – the Higgs, neutrino and vector portal. Of these three portals, the vector portal motivates the presence of a new fundamental abelian gauge interaction. This will serve us as a motivation to study general models of extra $U(1)$ symmetries in Section 2.3 as one representative class of theories that incorporate new physics into the SM in a consistent way. As a possible example of such an extension, we study in Chapter 3 the phenomenology of an effective $U(1)$ model with an associated Z' boson that exposes exclusively flavor-violating couplings to the SM. We will see that such models are subject to severe constraints from flavor observables. Nevertheless, they provide for a possible simultaneous explanation of the $(g-2)_\mu$ excess and a small tension in the tau decay ratio to muons and electrons. Starting out from a secluded $U(1)_X$ hidden photon model, we discuss the phenomenological consequences on the hidden gauge bosons of the four anomaly-free groups $U(1)_{L_\mu - L_e}$, $U(1)_{L_e - L_\tau}$, $U(1)_{L_\mu - L_\tau}$ and $U(1)_{B-L}$ in Chapter 4. Apart from the vector portal interaction, the associated bosons of these groups also take part in gauge interactions with SM particles. We will see that this makes them subject to stringent bounds from neutrino experiments. Furthermore, we will see that while an explanation of $(g-2)_\mu$ is still possible in the case of $U(1)_{L_\mu - L_\tau}$, part of the relevant parameter space can be excluded from novel white dwarf cooling constraints. In Chapter 5, we will extend the phenomenologically interesting $U(1)_{L_\mu - L_\tau}$ model by a vector-like fermion χ. The results of our analysis of such a model show that χ is a viable DM candidate, which enables a simultaneous explanation of the DM relic abundance $\Omega_{\rm DM}$ and the $(g-2)_\mu$ excess. Finally, we summarize our results and draw some concluions in Chapter 6.

Chapter 2

Fundamentals of extra abelian gauge symmetries

In this chapter, we want to motivate and review models of extra $U(1)$ gauge symmetries as candidate theories of new physics. Driven by the question of how we can consistently incorporate new physics effects into the SM, our discussion in Section 2.1 will bring us to the special role that dimension-four operators play in the construction of quantum field theoretic models of new physics. As the three gauge invariant dimension-four operators, we will review the Higgs, neutrino and vector portal in Section 2.2. Intriguingly, the vector portal coupling of the associated boson of a new $U(1)$ gauge group to the SM hypercharge boson naturally combines the principles of renormalizability and symmetry. The postulation of a new abelian gauge symmetry is a unique feature of the vector portal and serves us as a motivation to study general $U(1)$ extensions of the SM in Section 2.3. In this discussion, we will go beyond the case of pure portal interactions with the SM and allow for gauge couplings of the new bosons to SM fields. This general discussion will set the stage for our phenomenological studies of various aspects of extra $U(1)$ gauge symmetries in Chapters 3 to 5.

2.1 New Physics from the bottom up

The tremendous success of the SM is in its essence built upon the concept of symmetry. The idea that nature can be described by a renormalizable quantum field theory which is invariant under local symmetry transformations is at the heart of the SM. We can now ask ourselves if we can consistently incorporate new physics into the SM without giving up on these successful concepts.

When constructing models for new physics, we might ask for some guiding principles. In an attempt to formulate a quantum field theory for new physics, we will hence follow the very successful approach of canonical quantization in quantum mechanics [99]. In canonical quantization we obtain the quantized theory from its classical analogue by promoting the field variables $\varphi(x)$ (and their conjugate momenta) to operators and imposing commutation relations on them. All the dynamics of the system is then encoded in the Lagrangian $\mathcal{L}$. The fundamental building blocks of a quantum field theory containing a

quantum field φ are the n-point correlation functions [100]

$$\langle 0|T\,\varphi(x_1)\,\varphi(x_2)\ldots|0\rangle = \frac{1}{i}\frac{\delta}{\delta J(x_1)}\,\frac{1}{i}\frac{\delta}{\delta J(x_2)}\cdots \int \mathcal{D}\varphi\; e^{i\int \mathrm{d}^4x(\mathcal{L}[\varphi]+J\varphi)}\Bigg|_{J=0}. \tag{2.1}$$

Thus, the quantity determining the behavior of the quantum theory is the action governed by the Lagrangian,

$$S = \int \mathrm{d}^4x\; \mathcal{L}[\varphi]\,. \tag{2.2}$$

If we want to construct a theory for BSM physics, we will be concerned with the question of how to consistently modify this quantity in order to incorporate new physics effects. In the action appears the Lagrangian density $\mathcal{L}$ consisting of a sum of local operators $\mathcal{O}$ times couplings g. In order to gain a better understanding of which kind of operators $\mathcal{O}$ we may add to the Lagrangian of the SM, it is insightful to perform some dimensional analysis.

As we work in units where $\hbar = c = 1$, we can relate length L and time T to units of inverse mass M^{-1} via $T = c^{-1}L$ and $L = \hbar c^{-1}M^{-1}$. Effectively, we can therefore assign units of mass to some power to every quantity Q. Henceforth, we will denote this **mass dimension** by $[Q]$. As the action S appears in the exponential in Eq. (2.1), it must be dimensionless $[S] = 0$. From the four-dimensional space-time integral appearing in Eq. (2.2) it follows immediately that the Lagrangian has mass dimension $[\mathcal{L}] = 4$. So for every term in the Lagrangian it must hold that

$$[\mathcal{L}] = 4 = [g] + [\mathcal{O}]. \tag{2.3}$$

This means that we can only add terms to the Lagrangian which have an overall mass dimension of four. Indeed, it turns out that operators of mass dimension $[\mathcal{O}] \leq 4$ are special for a number of reasons.

2.1.1 Operators of dimension four and less

In a generic Lagrangian QFT, UV divergencies might appear when we want to calculate correlation functions or scattering amplitudes, respectively. However, if we want the theory to be predictive we might want to find a way to regulate the divergencies such that the expressions for physical quantities stay finite. If it is possible to absorb the appearing divergencies into coefficients of terms in the Lagrangian or to cancel them by adding a finite number of counterterms, we call the theory **renormalizable**.

In order to understand under which conditions a theory is renormalizable we will follow the reasoning of Weinberg [101][1] and classify the divergent behavior of a generic theory. In general, the theory will contain various different types of interactions labeled i, which are characterized by the number n_{if} of fields of type f and the number d_i of derivatives acting on them. For any connected one-particle irreducible (1PI) Feynman diagram with I_f internal and E_f external lines of type f and N_i vertices of type i we can calculate its **superficial degree of divergence** D. Roughly speaking, D is the power of internal momenta in the numerator minus the power of internal momenta in the denominator of the

[1] For variations in the treatment of this analysis we refer the reader to [100, 102, 103].

amplitude corresponding to the 1PI Feynman diagram. In the ultraviolet where all internal momenta go to infinity with a common factor $\kappa \to \infty$ the amplitude will asymptotically behave as

$$\int^{\infty} \kappa^{D-1} \mathrm{d}\kappa \,. \tag{2.4}$$

In other words, for $D > 0$ the diagram will diverge with the power of D, for $D = 0$ it will diverge logarithmically and for $D < 0$ it will converge in the UV.

In order to calculate D, we first note that the propagator of field f has an asymptotic momentum behavior of

$$\Delta_f(k) \propto k^{-2+2s_f} \,, \tag{2.5}$$

with $s_f = 0$ for scalars, $s_f = 1/2$ for Dirac fermions and $s_f = 1$ for massive vector particles[2]. Taken together, all the propagators in the diagram will add a total power of momenta to the amplitude equal to

$$\sum_f 2\, I_f (s_f - 1) \,. \tag{2.6}$$

The derivatives in the interaction of type i will yield at each vertex an additional power d_i of momenta totaling to

$$\sum_i N_i d_i \,. \tag{2.7}$$

Finally, we have to integrate over the internal momenta. *A priori* each internal line I_f will contribute one such four-momentum integration. However, the delta functions accompanying each vertex will linearly relate the internal momenta with each other. Taking further into account that one delta function enforces total momentum conservation, the full momentum integration will contribute another power of momenta of

$$4 \left[\sum_f I_f - \left(\sum_i N_i - 1 \right) \right] \,. \tag{2.8}$$

We can now determine D by simply adding up all these contributions. However, we can make some further simplifications to bring D into a more insightful form. Therefore, we remember that each vertex of type i has n_{if} lines of field type f attached to it. So in total there will be $\sum_i N_i\, n_{if}$ lines of field type f ending in all the vertices of the diagram. Taking into account that the full diagram has E_f external and I_f internal lines of field type f and each internal line I_f will end at two different vertices implies the topological identities

$$E_f + 2I_f = \sum_i N_i\, n_{if} \,. \tag{2.9}$$

Eliminating I_f by use of these identities leaves us with the following expression

$$D = 4 - \sum_f E_f (s_f + 1) - \sum_i N_i\, \Delta_i \,, \tag{2.10}$$

[2]For example, in the case of a massless photon cancellations in the propagator lead to $s_f = 0$. as pointed out in [101], due to gauge invariance such cancellations even occur for massive vector fields if they are coupled to a conserved current, leading also to $s_f = 0$. Otherwise, we might think of s_f as the spin of the particle.

where we have identified the canonical mass dimension of the coupling associated with the interaction of type i,

$$\Delta_i \equiv 4 - d_i - \sum_f n_{if}(s_f + 1)\,. \tag{2.11}$$

From Eq. (2.10) it follows immediately that interactions with $\Delta_i < 0$ cannot be renormalizable. This becomes immediately clear as for any given number of external lines $\sum_f E_f$ the degree of divergence grows as we add more and more of the corresponding vertices. Eventually, this will always render D positive and consequently deteriorate the divergent behavior of the amplitude with increasing number of vertices. Interactions with $\Delta_i < 0$ are therefore called perturbatively **non-renormalizable**. Interactions with $\Delta_i = 0$ are perturbatively **renormalizable** as the divergencies can be absorbed by a finite number of counterterms and the asymptotic divergent behavior of the amplitude does not change if more vertices are added. Finally, interactions with $\Delta_i > 0$ are called perturbatively **super-renormalizable** as the divergent behavior of the amplitude even improves with more and more vertices added (D eventually becomes negative and the amplitude converges).

As mentioned before we can regard the SM as an effective field theory (EFT) at low energies, in this case the electroweak scale v. In this spirit, we can try to incorporate new physics effects originating from a UV-complete theory into such a low-energy EFT. Formally, we can write down the EFT Lagrangian as an infinite sum over operators $\mathcal{O}_i$ of mass dimension $[\mathcal{O}_i] = \delta_i$ times couplings g_i with $[g_i] = \Delta_i$,

$$\mathcal{L}_{\text{EFT}} = \sum_i g_i\, \mathcal{O}_i = \sum_i \frac{c_i}{\Lambda^{\delta_i - 4}}\, \mathcal{O}_i\,. \tag{2.12}$$

For the second equality, we have introduced the dimensionless coupling coefficient $c_i = \Lambda^{\delta_i - 4} g_i$, where the cutoff Λ of the EFT is around the typical energy scale $M \gg v$ of the full UV-complete theory (and hence $c_i = \mathcal{O}(1)$). If we want to consider a process at an energy E we can dimensionally estimate the magnitude of the ith term in the action [19] to be

$$\int \mathrm{d}^4x\; g_i\, \mathcal{O}_i \sim c_i \left(\frac{E}{\Lambda}\right)^{\delta_i - 4}\,. \tag{2.13}$$

This allows us to classify operators as **relevant**, **marginal** or **irrelevant** depending on whether their energy scaling lets the corresponding amplitude grow, invariant or decrease when going to small energies [104,105]. Together with our renormalizability considerations from before we can group interactions $g_i\,\mathcal{O}_i$ into three classes as summarized in Table 2.1. Hence, we find that relevant and marginal operators of EFTs, i.e. operators with $\delta_i \leq 4$, are exactly those that have potentially large effects at low energies where we can make experiments to test the theory. If we are thus interested in the phenomenology of a potential UV completion of the SM, we should make sure that we include all operators of $\delta_i \leq 4$ in our low energy theory when calculating observables.

On the other hand, we have seen from dimensional analysis that for non-renormalizable interactions the coupling has mass dimension $[g_i] = \Delta_i < 0$. As these interactions are a residual low-energy effect of the full UV-complete theory, it is reasonable to assume that the coupling g_i is suppressed with the mass scale of the full theory,

$$g_i \sim M^{\Delta_i}\,. \tag{2.14}$$

δ_i	Δ_i	behavior for $E \to 0$		
< 4	> 0	growing	relevant	super-renormalizable
$= 4$	$= 0$	constant	marginal	renormalizable
> 4	< 0	falling	irrelevant	non-renormalizable

Table 2.1: Classification of operators according to their low-energy behavior.

From our simple order of magnitude estimate Eq. (2.13) we can conclude that at low energies $E \ll M$ the effect of non-renormalizable interactions stemming from the UV theory will be suppressed by a factor $(E/M)^{-\Delta_i}$ and can thus safely be neglected at leading order.

2.2 Portals to pew physics

In the discussion of the previous section, we have seen that if we want to consistently include new physics into our theory we should first and foremost be concerned with operators of dimension $\delta_i \leq 4$. These are exactly the operators that will be renormalizable and therefore do not introduce uncontrollable divergencies into the theory. Furthermore, we expect these operators to have large effects at low energies and therefore to be most relevant for experimental searches for new physics. From an EFT perspective, they are the first operators to appear at low energies as they are unsuppressed by the scale M of the full UV theory.

This leads us to the important concept of **portal interactions** or **portals**. The idea of portals is to systematically incorporate new physics into the SM via operators $\mathcal{O}_i$ with $\delta_i \leq 4$ by coupling combinations of SM fields which are singlets under the SM gauge group to some new hidden sector (HS) fields. The general strategy to construct such portals can be summed up as follows:

- Replace (combinations of) SM fields that are total singlets under the SM gauge group by HS fields.
- Replace dimensionfull SM couplings (i.e. $[g] > 0$) by HS fields.

In the following, we want to give a short overview over the three different SM portals to new physics and analyze them in some detail.

2.2.1 Higgs portal

The SM Lagrangian features only strictly renormalizable terms (i.e. operators with $\delta_i = 4$) with the exception of one super-renormalizable term with a positive-mass dimension coupling, the Higgs mass term (with $\delta_i = 2$)

$$\mathcal{L} = -\mu^2 H^\dagger H \,. \tag{2.15}$$

Indeed, the scalar, dimension-two combination $H^\dagger H$ is a total singlet under the SM gauge group G_{SM}. This offers the possibility to couple it to a HS singlet scalar in a

(super-)renormalizable operator [106]. The simplest choice for such a new HS field is a real scalar S [107, 108], which transforms as a total singlet under all symmetries of the theory. This allows both for a direct trilinear and quartic coupling to the SM Higgs boson of the type

$$\mathcal{L} = -(\omega\, S - \lambda_{HS}\, S^2) H^\dagger H\,. \tag{2.16}$$

In this minimal choice of an extra real, total-singlet scalar, the most general potential for H and S [109, 110] is then given by

$$V_0(H,S) = -\mu^2\, H^\dagger H + \lambda (H^\dagger H)^2 - \mu_S^2 S^2 - \alpha S^3 + \lambda_S S^4 - \omega\, S H^\dagger H + \lambda_{HS}\, S^2 H^\dagger H\,, \tag{2.17}$$

where the parameters μ, μ_S, α and ω have positive mass dimension.

In many realizations of the Higgs portal, the new scalar field S plays the role of a Higgs field and induces spontaneous breaking of a new extra dark symmetry G_d [111]. In this case, however, the scalar S cannot transform as a singlet under the dark symmetry G_d, but must rather transform under some non-trivial representation. In this case, we can still construct a Higgs portal interaction of $\delta_i = 4$ by replacing $S^2 \to S^\dagger S$ in Eq. (2.16). Similarly, such scalar portals are often studied in the context of dark matter extensions (see e.g. [112–114]). In this case the new scalar S plays the role of the DM candidate. It must therefore be protected from decays in order to be stable at cosmological scales. This requires S to be (at least) odd under an extra $\mathbb{Z}_2$ symmetry. Imposing such a symmetry removes all terms with odd powers of S in the potential,

$$V_0(H,S) = -\mu^2\, H^\dagger H + \lambda (H^\dagger H)^2 - \mu_S^2 S^\dagger S + \lambda_S (S^\dagger S)^2 + \lambda_{HS}\, S^\dagger S H^\dagger H\,. \tag{2.18}$$

If the scalar S acquires a vacuum expectation value $\langle S \rangle = w$ this will lead to an off-diagonal mass matrix for the two scalars h and s after symmetry breaking

$$\mathcal{M}^2 = \begin{pmatrix} 2\lambda v^2 & \lambda_{HS}\, vw \\ \lambda_{HS}\, vw & 2\lambda_S w^2 \end{pmatrix}\,. \tag{2.19}$$

This mass matrix can be diagonalized by a simple orthogonal rotation $O^T \mathcal{M}^2 O$ about an angle θ that is defined by

$$\tan\theta = \frac{\lambda_{HS}\, vw}{\lambda_S w^2 - \lambda v^2}\,. \tag{2.20}$$

However, this has interesting phenomenological consequences as it mixes h and s in the mass eigenstates

$$\begin{pmatrix} H_1 \\ H_2 \end{pmatrix} = \begin{pmatrix} \cos\theta\, h - \sin\theta\, s \\ \cos\theta\, s + \sin\theta\, h \end{pmatrix}\,. \tag{2.21}$$

This mixing will modify the couplings of the SM-like Higgs. Hence Higgs coupling measurements can be used to constrain such a scenario [115, 116].

In principle, there are two different cases. If the new scalar, typically identified with H_2, is heavier than the SM-like scalar H_1 it can be searched for e.g. in WW, ZZ or dihiggs final states [117–119]. The second heavier Higgs H_2 can actually help to stabilize the Higgs potential, if it is sufficiently heavy [120, 121]. In general, the portal coupling can be constrained by demanding that $\lambda_{HS} > 0$ up to the Planck scale M_{Pl}. In case that the

new scalar H_2 is lighter than H_1, it is typically subject to strong constraints from direct searches [122].

While the Higgs portal provides in general for a very rich phenomenology we will refrain from a detailed discussion here and refer the reader to Refs. [123, 124] for recent reviews.

2.2.2 Neutrino portal

In the SM, the Higgs mechanism is responsible for giving all the fermions and gauge bosons their masses. After Electroweak Symmetry Breaking (EWSB) the Higgs acquires a VEV,

$$H = \frac{1}{\sqrt{2}} \begin{pmatrix} 0 \\ v + h \end{pmatrix} , \tag{2.22}$$

generating a mass term for the fermions from the Yukawa terms. For example, in the quarks sector the corresponding Yukawa terms are given by

$$\mathcal{L}_{\text{YukQ}} = -Y^D_{\alpha\beta}\ \bar{Q}_\alpha H\, d_{R\beta} - Y^U_{\alpha\beta}\ \bar{Q}_\alpha \tilde{H}\, u_{R\beta} + h.c.\,, \tag{2.23}$$

where Y^D and Y^U are the down- and up-type Yukawa matrices and $\tilde{H} = i\tau_2 H^*$. As in the SM there are no right-handed neutrinos, the equivalent of the up-type Yukawa coupling is absent in the lepton sector. Hence, neutrinos are exactly massless within the SM.

However, it is worthwhile noticing that the spin-1/2 operator $\bar{L}\tilde{H}$, which would be required for the neutrino Yukawa coupling term, transforms as a total singlet under the SM gauge group G_{SM}. Hence, from this operator we can build another portal interaction of $\delta_i = 4$ by coupling it to $\mathcal{N}$ gauge-singlet fermions N_I ($I = 1, \ldots, \mathcal{N}$) [125]. Due to their singlet nature these fermions do not take part in any of the SM model interactions, which is why they are often called **sterile neutrinos** in contrast to their active SM counterparts. In so-called **neutrino portal** interactions, these new right-handed sterile neutrinos are coupled to the SM left-handed neutrinos

$$\mathcal{L}_{\text{Neutrino portal}} = -Y^\nu_{\alpha I}\ \bar{L}_\alpha \tilde{H}\, N_I + h.c.\,, \tag{2.24}$$

where Y^ν is in general a complex $3 \times \mathcal{N}$ Yukawa coupling matrix. For $\mathcal{N} = 3$ each left-handed SM neutrino obtains its right-handed partner and the SM three-family structure is fully recovered. In the broken phase, the neutrino portal Eq. (2.24) generates a Dirac mass term with $m_D = Y^\nu v$ for the neutrinos. From cosmological observations we know, however, that the sum of the masses of the active neutrinos has to be quite small $\sum_\nu m_\nu < 0.12$ eV [21]. If these small mass are to be generated from a pure Dirac mass term, this usually requires quite a substantial amount of fine-tuning of the neutrino Yukawa coupling and therefore seems to be rather unnatural[3].

This is where sterile neutrinos come into play to offer a compelling explanation for the smallness of the active neutrino masses. As the new fermions N_I are singlets under the full SM group, gauge invariance allows for a Majorana mass term of the form

$$\mathcal{L}_{\text{Majorana}} = -\frac{1}{2}\bar{N}^C \mathcal{M}_M N + h.c.\,, \tag{2.25}$$

[3]However, some mechanisms have been proposed that could explain such small Dirac masses for neutrinos in extradimensional theories [126–128] or in models of composite neutrinos [129] without fine-tuning of the Yukawa couplings or the introduction of a new fundamental heavy scale.

where the matrix $\mathcal{M}_M$ is *a priori* unconstrained. We can write the full neutrino mass term in the following way

$$\mathcal{L}_{\text{mass}} = -\frac{1}{2}(\bar{\nu}, \bar{N}^C) \begin{pmatrix} 0 & m_D \\ m_D^T & \mathcal{M}_M \end{pmatrix} \begin{pmatrix} \nu^C \\ N \end{pmatrix} + h.c.\,. \tag{2.26}$$

If the Majorana mass term is large, in particular if all the eigenvalues of $\mathcal{M}_M$ are much larger than the elements of m_D, the mass matrix of Eq. (2.26) can be brought into block-diagonal form by a unitary transformation [130]. In this case, the upper 3×3 block is approximately given by

$$m_\nu \simeq -m_D^T \, \mathcal{M}_M^{-1} \, m_D \,, \tag{2.27}$$

and the corresponding mass eigenstates are mostly active neutrino-like. This means that the masses of the active neutrinos are proportional to m_D, but suppressed by the small factor $m_D^T \, \mathcal{M}_M^{-1}$ and are therefore naturally small. In other words, the heavy Majorana masses of the sterile neutrinos give rise to the small masses of the active neutrinos, which is why it is called the **(type-I) seesaw mechanism** [131–138]. In this scenario, the mass matrix of the lower $\mathcal{N} \times \mathcal{N}$ block corresponds approximately to the heavy Majorana mass matrix $m_{\text{heavy}} \simeq \mathcal{M}_M$ and the corresponding mass eigenstates are mostly sterile neutrino-like. These heavy neutrinos consequently can be integrated out at low scales and play no role for the phenomenology of the light neutrinos.

In their simplest incarnation, the gauge-singlet sterile neutrinos N_I with their Majorana mass term do not carry lepton number. As they do not take part in any gauge interaction they couple to the SM only very weakly such that they can be out of equilibrium early in the universe. Furthermore, as their Yukawa interactions in principle allow for large CP-violating phases, sterile neutrinos are ideal candidates to help with the generation of the baryon asymmetry of the universe via leptogenesis [139]. In the early universe the out-of-equilibirum sterile neutrinos can generate a net lepton number which is then transported to the baryon sector via electroweak sphalerons at high temperatures $T > T_{EW}$ (see e.g. [140–142] for some reviews).

Another phenomenologically interesting aspect of sterile neutrinos is their capacity to play the role of DM. The fact that sterile neutrinos are neutral, massive and have very weak interactions makes them a natural candidate for DM [143]. Contrary to many other proposed DM candidates, sterile neutrinos are not stable due to their mixing with the light SM neutrinos. However, as this mixing is typically very small they can still have lifetimes significantly larger than the lifetime of the universe. Moreover, sterile neutrinos are typically not produced from thermal freeze-out, but rather from electroweak processes via the mixing with the active neutrinos. For a recent review on sterile neutrino dark matter we refer the reader to [144].

In general, the neutrino portal and sterile neutrinos have a very rich and interesting phenomenology of which we can only give a very limited and imbalanced selection. As sterile neutrinos are not the focus of this thesis, instead we want to refer to one of the many good review papers (see e.g. [145]) as a starting point for further detailed study of the topic.

2.2.3 Vector portal

A fundamental concept that has lead to the construction of the SM is gauge invariance. In any gauge theory, we demand that all terms in the action are invariant under gauge transformations. So for a pure free Yang-Mills theory we demand that under a gauge transformation

$$A_\mu \to \Omega(x) A_\mu \Omega^{-1}(x) + i\Omega(x)\partial_\mu \Omega^{-1}(x)\,, \tag{2.28}$$

of the gauge potential A_μ the Yang-Mills action

$$S_{\mathrm{YM}} = -\frac{1}{4}\int \mathrm{d}^4x \ \mathrm{tr}\, F_{\mu\nu}F^{\mu\nu}\,, \tag{2.29}$$

stays invariant. One can verify by a staight-forward calculation that under the gauge transformation Eq. (2.28) the field strength tensor transforms as

$$F_{\mu\nu} \to \Omega(x) F_{\mu\nu} \Omega^{-1}(x)\,. \tag{2.30}$$

Hence, by construction of the kinetic term Eq. (2.29) via the trace, the Yang-Mills action stays invariant under a general gauge transformation. Remarkably, for abelian gauge symmetries with the transformations $\Omega(x) = e^{i\omega(x)}$, the field strength tensor $F_{\mu\nu}$ is a gauge invariant quantity by itself. Noting further that the field strength has mass dimension $\delta = 2$ we can construct the renormalizable, gauge-invariant **vector portal** interaction of $\delta = 4$ by coupling the field strength tensors of two different abelian symmetries to each other

$$\mathcal{L}_{\text{Vector portal}} = -\frac{\epsilon}{2} F_{\mu\nu}F'^{\mu\nu}\,. \tag{2.31}$$

This type of mixed kinetic term of two abelian gauge bosons is often referred to as **kinetic mixing**. It was first considered in the context of quantum electrodynamics (QED) by Okun [146] and Holdom [147]. In the case of the Higgs and neutrino portals, we could just postulate some new particles *ad hoc*. For the vector portal to work, however, we have to introduce a new $U(1)$ gauge group in order not to spoil renormalizability and gauge invariance of the term in Eq. (2.31). Effectively, this is equivalent to introducing a new fundamental interaction.

The fact that the vector portal should be accompanied by a new fundamental gauge interaction sets this case apart from the Higgs and neutrino portal. In the minimal realization of such a model, any possible new fields ψ carrying charge under the new symmetry are completely secluded from the SM sector, i.e. ψ are SM singlets. In such secluded $U(1)_X$ models, the only interaction of the fields ψ with the SM occurs via the kinetic mixing portal term in Eq. (2.31). This has important phenomenological consequences (for reviews discussing the minimal $U(1)_X$ case see e.g. [148, 149]).

While all portal interactions are interesting by themselves, we will use the fact that the vector portal is accompanied by a new fundamental gauge interaction as a motivation to study the addition of a new $U(1)$ symmetry in more detail. In this context, we will go beyond the concept of a purely secluded $U(1)_X$ and also consider the case where (part of) the SM fields are charged under the new symmetry.

2.3 The Physics of extra abelian symmetries

The possibility of having an extra $U(1)$ factor in the SM has been considered by theorists for a long time [150]. Apart from the interesting phenomenology that it implies, the presence of such extra $U(1)$ groups can be theoretically very well motivated from grand unification or string theories. In this section, we want to study the general physical implications of adding a second $U(1)_X$ to the SM group $G_{\rm SM}$. Having no specific setup in mind, we can start from writing down the most general renormalizable Lagrangian invariant under $G_{\rm SM} \times U(1)_X$,

$$\mathcal{L} = \mathcal{L}_{\rm SM} - \frac{1}{4}\hat{X}_{\mu\nu}\hat{X}^{\mu\nu} - \frac{\epsilon_Y}{2}\hat{B}_{\mu\nu}\hat{X}^{\mu\nu} - \frac{M_X^2}{2}\hat{X}_\mu\hat{X}^\mu - g_x\, j_\mu^x \hat{X}^\mu\,, \tag{2.32}$$

where $\mathcal{L}_{\rm SM}$ denotes the usual SM Lagrangian and $\hat{B}^{\mu\nu}$ and $\hat{X}^{\mu\nu}$ denote the field strength tensors of the hypercharge $U(1)_Y$ and the new $U(1)_X$ symmetry in the gauge basis, respectively. We will see in Section 2.3.2 that the mass term in Eq. (2.32), contrary to intuition, can be made gauge invariant, if it comes from a Stückelberg mechanism. If the extra $U(1)_X$ is Higgsed, the mass term will of course originate from spontaneous symmetry breaking and therefore cannot be gauge invariant anymore[4]. The new gauge field $\hat{X}_\mu$ couples to fields ψ that are charged under $U(1)_X$ via the conserved gauge current

$$j_\mu^x = \sum_\psi \bar{\psi}\,\gamma_\mu\,(Q_L^\psi P_L + Q_R^\psi P_R)\,\psi\,, \tag{2.33}$$

where Q_L^ψ and Q_R^ψ are the charges of the left- and right-handed components of the Dirac field ψ. In a secluded $U(1)_X$ model, only (heavy) hidden sector fields may carry charge under the new symmetry, while all SM fields remain uncharged. In this thesis, however, we will also explicitly consider scenarios where the fields ψ can be SM fields. As we will see, this leads to a very different phenomenology than in the $U(1)_X$ case.

If the mass of the new gauge boson is due to a Stückelberg mechanism, the Lagrangian in Eq. (2.32) alone fully defines the theory of the extra $U(1)_X$ symmetry. In order to gain some physical intuition, we will have a closer look at individual terms and discuss their physical implications in the following.

2.3.1 Origin of kinetic mixing

As we have seen, the vector portal interaction Eq. (2.31) is a fully renormalizable and gauge-invariant operator. Hence, the kinetic mixing parameter ϵ_Y can be viewed as a free parameter of the theory. However, if we view the extra $U(1)_X$ symmetry to be a low-energy remnant of a UV-complete theory that is broken at some high scale $\Lambda \gg v$, we will typically expect to have some additional heavy fields ψ with masses of the order of the breaking scale Λ in the spectrum. In particular, if the new abelian group originates from the breaking of a grand unified theory (GUT), $G_{\rm GUT} \to G_{\rm SM} \times U(1)_X$, the heavy fields ψ are usually charged under both $U(1)_X$ and the SM $U(1)_Y$. These heavy fermions induce

[4] If the new symmetry breaking scalar is also charged under the SM, it can generate an effective mass mixing term $\delta M\, X^\mu B_\mu$ [151, 152]. However, in this work we will not entertain such a possibility and therefore assume $\delta M = 0$ throughout this thesis.

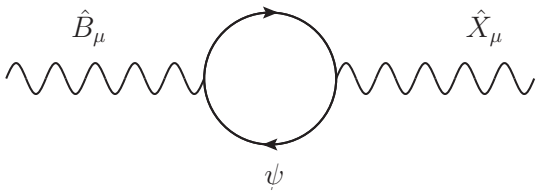

Figure 2.1: Prototypical diagram leading to loop-induced kinetic mixing between the hypercharge gauge boson $\hat{B}_\mu$ and the $U(1)_X$ gauge boson $\hat{X}_\mu$ from a fermion ψ running in the loop.

kinetic mixing between the hypercharge boson $\hat{B}_\mu$ and the new boson $\hat{X}_\mu$ from loop-effects as shown in Fig. 2.1. The resulting loop-induced effective kinetic mixing $\epsilon_Y(q^2)$ depends on the momentum transfer q^2 and is given by

$$\epsilon_Y(q^2) = \frac{g_1\, g_x}{4\pi^2} \int_0^1 dx\; x(1-x)\; \log\left[\prod_{\psi_L,\psi_R}\left(\frac{m_\psi^2 - x(1-x)\,q^2}{\mu^2}\right)^{N_\psi^c Y_\psi Q_\psi}\right], \tag{2.34}$$

where g_1 denotes the $U(1)_Y$ hypercharge coupling constant and m_ψ, N_ψ^c, Y_ψ and Q_ψ are the mass, color factor, hypercharge and $U(1)_X$ charge of the fermion ψ[5]. The renormalization scale $\mu \lesssim \Lambda$ is the scale at which the loop integral is regularized and below which the induced kinetic mixing term is valid from an EFT perspective.

Parametrically, we can estimate the order of magnitude of the induced kinetic mixing in the infrared, i.e. for $q^2 \ll \mu^2$, to

$$\epsilon_Y(q^2) \approx \underbrace{\frac{g_1\, g_x}{4\pi^2}}_{10^{-3}\ldots 10^{-5}} \sum_\psi Y_\psi Q_\psi \underbrace{\log\left(\frac{m_\psi^2}{\mu^2}\right)}_{1\ldots 10} \sim 10^{-2}\ldots 10^{-5}\,, \tag{2.35}$$

where we have assumed that the masses of the extra fermions ψ lie around or above the high scale $m_\psi \gtrsim \Lambda$ and that the new $U(1)_X$ symmetry is weakly coupled $g_x \lesssim \mathcal{O}(10^{-1})$.

These considerations naturally motivate the range of small values $10^{-5} \lesssim \epsilon_Y \lesssim 10^{-2}$ for the kinetic mixing. However, for example in "LARGE" volume compactifications of string theory [153] very small gauge couplings g_x can arise for extra hidden gauge groups $U(1)_X$. In this context, one can also naturally obtain kinetic mixings significantly below the loop suggested value of $\epsilon_Y \sim 10^{-3}$ [154].

2.3.2 Gauge boson mass

The gauge boson $\hat{X}_\mu$ associated with the new $U(1)_X$ can in principle remain massless if the symmetry is unbroken. This possibility has been studied in the context of DM, where

[5]Note that the product in Eq. (2.34) runs over left- and right-handed components of ψ, individually. As hypercharge is chiral (and, depending on the charge assignments, $U(1)_X$ might be as well) left- and right-handed fields contribute differently.

the associated boson mediates interactions between dark sector particles [155]. The kinetic mixing interaction will typically lead to effective milli-charges of the DM particles [156].

In general, the new boson $\hat{X}_\mu$ can acquire mass either by breaking of the $U(1)_X$ symmetry or from a bare or Stückelberg mass term. In this section, we want to study these two different mass generation mechanisms.

Stückelberg mechanism

In his seminal 1938 papers [157, 158], Stückelberg developed a method to write down a gauge-invariant mass term for a vector field $\hat{X}_\mu$. Starting from the Lagrangian of a free massive vector field

$$\mathcal{L} = -\frac{1}{4}\hat{X}_{\mu\nu}\hat{X}^{\mu\nu} - \frac{1}{2}M_X^2\hat{X}_\mu\hat{X}^\mu\,, \tag{2.36}$$

we can split off the longitudinal degree of freedom into a pseudo-scalar field $\hat{\sigma}$ via $\hat{X}_\mu \to \hat{X}_\mu + \frac{1}{M_X}\,\partial_\mu\hat{\sigma}$. Under this decomposition the vector field Lagrangian reads

$$\mathcal{L} = -\frac{1}{4}\hat{X}_{\mu\nu}\hat{X}^{\mu\nu} - \frac{1}{2}M_X^2\left(\hat{X}_\mu + \frac{1}{M_X}\,\partial_\mu\hat{\sigma}\right)\left(\hat{X}^\mu + \frac{1}{M_X}\,\partial^\mu\hat{\sigma}\right)\,. \tag{2.37}$$

This Lagrangian can now be made gauge-invariant by imposing under a general gauge transformation that the two fields transform as

$$\delta\hat{X}_\mu = \partial_\mu\lambda(x)\,, \qquad \delta\hat{\sigma} = -M_X\lambda(x)\,. \tag{2.38}$$

It is worth noting that for $\lambda(x) = \lambda$, the pseudo-scalar is subject to an additional Peccei-Quinn shift-symmetry. Therefore, $\hat{\sigma}$ is sometimes also called an axion.

If one fixes the gauge by adding the term

$$\mathcal{L}_{\text{gf}} = -\frac{1}{2\xi}(\partial_\mu\hat{X}^\mu + \xi M_X\hat{\sigma})^2\,, \tag{2.39}$$

the cross terms of $\hat{X}_\mu$ and $\hat{\sigma}$ are eliminated and the two fields are fully decoupled [159]. The full Lagrangian can then be written as

$$\mathcal{L} = -\frac{1}{4}\hat{X}_{\mu\nu}\hat{X}^{\mu\nu} - \frac{1}{2}M_X^2\hat{X}_\mu\hat{X}^\mu - \frac{1}{2\xi}\,(\partial_\mu\hat{X}^\mu)^2 - \frac{1}{2}\,\partial_\mu\hat{\sigma}\partial^\mu\hat{\sigma} - \xi\frac{M_X^2}{2}\,\hat{\sigma}^2\,. \tag{2.40}$$

In this form, the Lagrangian is not only gauge-invariant under the transformations of Eq. (2.38). Under addition of the appropriate ghost terms, the Stückelberg Lagrangian is also guaranteed to be renormalizable and unitary [160]. This situation is indeed unique for abelian gauge symmetries. There have been many attempts to generalize the Stückelberg mechanism to non-abelian gauge theories, however, the trick of decoupling the longitudinal mode of the vector field violates unitarity [161].

In the case of an extension of the SM, however, the Stückelberg mechanism is a minimal way to give the new boson mass without the need of a Higgs field and an explicit symmetry breaking [162]. As the Stückelberg mass is not induced by the VEV of a symmetry breaking scalar, it is *a priori* a free parameter of the theory and is not subject to strong constraints from the scalar sector.

Higgs mechanism

In the SM, the electroweak bosons $W^{\pm}$ and Z receive their mass from a Higgs mechanism via spontaneous symmetry breaking (SSB) of the electroweak symmetry $SU(2)_L \times U(1)_Y \to U(1)_{\text{QED}}$. Once the Higgs acquires a VEV in the symmetry breaking phase, the weak bosons develop a mass term from their coupling to the Higgs through the kinetic term. On the other hand, as the SM Higgs is a color singlet, $SU(3)_C$ is not broken by the Higgs VEV and the gluons stay exactly massless.

In the same spirit, if there is a new scalar field ϕ charged under the new $U(1)_X$ symmetry, the associated boson $\hat{X}_\mu$ can acquire mass via a Higgs mechanism. In order for the scalar to acquire a VEV it needs a potential that allows for symmetry breaking. The minimal choice is a complex scalar ϕ with a SM-like potential [163]

$$V(\phi) = -\mu'^2|\phi|^2 + \lambda'|\phi|^4 \,. \tag{2.41}$$

The symmetry breaking proceeds analogously to the SM such that the new scalar ϕ will acquire a VEV $f = \sqrt{\mu'^2/\lambda}$. The new physical Higgs mode h' will generate fluctuations of the scalar field around this vacuum. Thus, we can consider fluctuations around the vacuum by rewriting the complex scalar in unitary gauge as $\phi = (f + h')/\sqrt{2}$. The kinetic term in this expansion reads

$$\mathcal{L}_{\phi,\text{kin}} = (D_\mu \phi)^* D^\mu \phi \supset \frac{g_x^2 f^2}{2} \hat{X}_\mu \hat{X}^\mu \,. \tag{2.42}$$

As expected, the Higgs mechanism generates a mass $M_X = g_x f$ for the $U(1)_X$ gauge boson that is proportional to the VEV of ϕ. Furthermore, SSB will generate a number of interactions for the physical Higgs. In unitary gauge these read

$$\mathcal{L}_{\text{int}} = \frac{M_X^2}{f} h' \hat{X}_\mu \hat{X}^\mu + \frac{M_X^2}{f^2} h'^2 \hat{X}_\mu \hat{X}^\mu - \frac{m_{h'}^2}{2f} h'^3 - \frac{m_{h'}^2}{8f^2} h'^4 \,. \tag{2.43}$$

In general, these interactions of h' will open additional possibilities for testing such a model. Depending on the relative size of the coupling constant g_x to the quartic coupling λ, the Higgs h' can be lighter or heavier than the gauge boson $\hat{X}_\mu$. In particular in the case that $m_{h'} \geq 2\, M_X$ decays of the Higgs into two vector bosons would become possible and might lead to observable consequences at collider experiments. On the other hand, if $m_{h'} < M_X$ the Higgs could become (very) long-lived as it would have to decay via two off-shell $\hat{X}$ bosons [164]. In addition, there might be a portal coupling of h' to the SM Higgs H as discussed in Section 2.2.1, which could lead to a much richer phenomenology. Finally, the symmetry breaking scalar receives an effective fractional electric charge also referred to as minicharge, which can lead to severe constraints in particular for very light bosons ($M_X \lesssim$ MeV) [165].

2.3.3 Diagonalization of neutral boson mass matrix

When we were writing down the full Lagrangian for a kinetically mixed $U(1)_X$ in Eq. (2.32) due to the presence of the kinetic mixing portal the kinetic terms of the $U(1)$ bosons were

not canonically normalized. If we want to calculate amplitudes for scattering processes involving the boson fields in this basis, this will make the calculations very tedious. Starting from the Lagrangian,

$$\mathcal{L} = -\frac{1}{4}\hat{B}_{\mu\nu}\hat{B}^{\mu\nu} - \frac{\epsilon_Y}{2}\hat{B}_{\mu\nu}\hat{X}^{\mu\nu} - \frac{1}{4}\hat{X}_{\mu\nu}\hat{X}^{\mu\nu} - g_1\, j_\mu^Y \hat{B}^\mu - g_x\, j_\mu^x \hat{X}^\mu + \frac{1}{2}M_X^2 \hat{X}_\mu \hat{X}^\mu\,, \quad (2.44)$$

we can go to a basis where all kinetic terms have the proper canonical normalization. We can do this by performing a linear field redefinition of the $U(1)$ gauge fields. This field redefinition can be expressed as a $GL(3,\mathbb{R})$ transformation $G(\epsilon_Y)$ on the space of the three electroweak gauge bosons

$$\begin{pmatrix} \hat{B}_\mu \\ \hat{W}_\mu^3 \\ \hat{X}_\mu \end{pmatrix} = G(\epsilon_Y) \begin{pmatrix} B_\mu \\ W_\mu^3 \\ X_\mu \end{pmatrix}\,, \quad (2.45)$$

in which W_μ^3 denotes the third $SU(2)_L$ gauge boson, and one choice for the transformation is given by

$$G(\epsilon_Y) = \begin{pmatrix} 1 & 0 & -\dfrac{\epsilon_Y}{\sqrt{1-\epsilon_Y^2}} \\ 0 & 1 & 0 \\ 0 & 0 & \dfrac{1}{\sqrt{1-\epsilon_Y^2}} \end{pmatrix}\,. \quad (2.46)$$

By virtue of this redefinition of the gauge fields the kinetic terms are now diagonal and canonically normalized. However, this comes at the cost that the canonically normalized field X_μ picks up a coupling to the hypercharge current j_μ^Y. Furthermore, the X_μ boson will now mix into the B_μ mass terms. This leads to an off-diagonal mass for the three neutral electroweak gauge bosons B_μ, W_μ^3, and X_μ. As we have argued in Section 2.3.1, we expect the kinetic mixing parameter to be rather small $\epsilon_Y \ll 1$. In the limit of small ϵ_Y, the mass matrix then reads

$$\mathcal{M}^2 = \frac{v^2}{4}\begin{pmatrix} g_1^2 & -g_1\, g_2 & -g_1^2\epsilon_Y \\ -g_1\, g_2 & g_2^2 & g_1\, g_2\, \epsilon_Y \\ -g_1^2\epsilon_Y & g_1\, g_2\epsilon_Y & \dfrac{4M_X^2}{v^2}(1+\epsilon_Y^2) + g_1^2\epsilon_Y^2 \end{pmatrix} + \mathcal{O}(\epsilon_Y^3), \quad (2.47)$$

where g_2 and g_1 denote the $SU(2)_L$ and $U(1)_Y$ gauge couplings, respectively. This mass matrix can be diagonalized through a combination of two block-diagonal rotations with the weak mixing angle θ_w and an additional angle ξ. Performing these transformations, we change to the mass eigenstates (A_μ, Z_μ, Z'_μ) of the three neutral electroweak bosons with diagonal mass matrix $R_1(\xi)R_2(\theta_w)\mathcal{M}^2\, R_2(\theta_w)^T R_1(\xi)^T = \mathrm{diag}\,(M_A^2, M_Z^2, M_{Z'}^2)$, with the rotation matrices

$$R_1(\xi)R_2(\theta_w) = \begin{pmatrix} 1 & 0 & 0 \\ 0 & \cos\xi & \sin\xi \\ 0 & -\sin\xi & \cos\xi \end{pmatrix}\begin{pmatrix} \cos\theta_w & \sin\theta_w & 0 \\ -\sin\theta_w & \cos\theta_w & 0 \\ 0 & 0 & 1 \end{pmatrix}\,. \quad (2.48)$$

Analogously to the SM, the Weinberg angle in this case is defined by the relation

$$\tan\theta_w = \frac{g_1}{g_2}\,. \tag{2.49}$$

In the second rotation, only the lower right 2×2 block of the mass matrix is non-diagonal and has to be transformed. If we define the coupling

$$g_Z = \frac{g_1}{\sin\theta_w} = \frac{g_2}{\cos\theta_w} = \sqrt{g_1^2+g_2^2}\,, \tag{2.50}$$

the remaining non-diagonal block gets diagonalized for

$$\tan 2\xi = \frac{2\,\sin\theta_w\epsilon_Y}{1-\sin\theta_w^2\epsilon_Y^2 - \frac{4M_X^2}{g_Z^2v^2}(1+\epsilon_Y^2)}\,. \tag{2.51}$$

After the full diagonalization procedure we find the mass eigenvalues in terms of the rotation angles θ_w and ξ as

$$M_A^2 = 0\,, \qquad M_{Z/Z'}^2 = \frac{g_Z^2v^2}{4}\left[1-\frac{\sin\theta_w\epsilon_Y}{\tan 2\xi}\left(1\pm\sqrt{1+\tan^2(2\xi)}\right)\right]\,. \tag{2.52}$$

The photon stays exactly massless as it corresponds to the gauge boson of the unbroken $U(1)_{\rm QED}$. In the SM, the mass of the Z is given by $M_Z^{\rm SM} = g_Z\,v/2$. From Eq. (2.52) we see that this relation gets corrected by the second term in the square brackets. However, we demand that the mass of the physical Z stays compatible with its experimentally determined value from e.g. LEP measurements [166]. This leads in general to quite strong constraints on $Z-Z'$ mixing [167, 168].

2.3.4 Origin of flavor-changing neutral currents

In our discussion of the gauge current Eq. (2.33), we have not specified the structure of the fermion charges. In particular, if (some of) the SM quarks and leptons are charged under the new $U(1)_X$ symmetry, their charges can *a priori* differ across generations. Consider for example a family of n same-type fermions ψ_i charged under $U(1)_X$. In the gauge basis, they will contribute to the gauge current as

$$j_\mu^x \supset \sum_i \bar\psi_{iL}\,\gamma_\mu\,Q^\psi_{i,L}\,\psi_{iL} + \bar\psi_{iR}\,\gamma_\mu\,Q^\psi_{i,R}\,\psi_{iR}\,, \tag{2.53}$$

where $Q^\psi_{i,L}$ and $Q^\psi_{i,R}$ are the elements of the diagonal charge matrices in flavor space. The gauge eigenstates are linked to their corresponding mass eigenstates via unitary transformations,

$$f_{\alpha L} = V^\psi_{L,\alpha i}\;\psi_{iL}\,, \qquad f_{\alpha R} = V^\psi_{R,\alpha i}\;\psi_{iR}\,. \tag{2.54}$$

The gauge current Eq. (2.53) translated into the mass basis via these transformations reads

$$j_\mu^x \supset \sum_{\alpha,\beta} \bar f_{\alpha L}\,\gamma_\mu\,Q^f_{\alpha\beta,L}\,f_{\beta L} + \bar f_{\alpha R}\,\gamma_\mu\,Q^f_{\alpha\beta,R}\,f_{\beta R}\,, \tag{2.55}$$

where

$$Q_L^f = V_L^\psi \, Q_L^\psi \, V_L^{\psi\dagger} \,, \qquad Q_R^f = V_R^\psi \, Q_R^\psi \, V_R^{\psi\dagger} \,. \tag{2.56}$$

If the charge matrices Q^ψ in the gauge basis are not proportional to the unit matrix, the charge matrices of the mass eigenstates Eq. (2.56) will not be diagonal, i.e. $Q^f_{\alpha\beta} \neq 0$ for $\alpha \neq \beta$.

For a model in which SM quarks and/or leptons are charged under $U(1)_X$ with flavor non-universal charges this will introduce flavor-changing neutral currents (FCNCs) amongst the corresponding mass eigenstates. In this case, the CKM and PMNS mixing matrices are given by

$$V^{\text{CKM}} = V_L^u V_L^{d\dagger} \,, \qquad V^{\text{PMNS}} = V_L^\nu V_L^{e\dagger} \,. \tag{2.57}$$

These two matrices determine the mixing of quarks and leptons in weak charge currents (CC) and are experimentally accessible (cf. e.g. [13, 169] for recent reviews). The unitary transformation matrices V_L^f and V_R^f, however, do not feature in any observables and are therefore not measurable. In turn, this means that even if we have knowledge of the (flavor non-universal) quark and lepton charges under $U(1)_X$, the model additionally needs to predict the transformation matrices V_L^f and V_R^f in order to determine the flavor off-diagonal charge matrices Q_L^f and Q_R^f for the mass eigenstates.

2.4 Summary

Let us briefly summarize what we have achieved in this chapter. We started out from the general question of how we can construct models of new physics by consistently extending the SM in a bottom-up approach. Relying on the principles of renormalizability and gauge invariance, we saw that operators of mass dimension $\delta_i \leq 4$ play a special role in constructing consistent theories of new physics. After identifying the three portal interactions (Higgs, neutrino and vector portal) which are strictly of mass dimension four, we used the fact that the vector portal motivates the presence of a new abelian gauge symmetry to study general models of extra $U(1)$ symmetries. In our discussion of such models we have been agnostic about the origin of such a new symmetry and hence have not specified the interactions of the associated gauge boson or the mechanism by which it acquires mass. In particular, we have also allowed for SM fields to be charged under the new symmetry.

In order to develop a global picture of the implications of an extra $U(1)$ symmetry, we want to consider different realizations of such $U(1)$ models and focus on different phenomenological aspects in the following chapters. First, we will consider the impact of flavor-changing couplings of an effective heavy $U(1)$ gauge boson in Chapter 3. In Chapter 4, we will investigate the possibility that instead of introducing a new symmetry *ad hoc* one of the four anomaly-free symmetries of the SM, $U(1)_{L_\mu - L_e}$, $U(1)_{L_e - L_\tau}$, $U(1)_{L_\mu - L_\tau}$ or $U(1)_{B-L}$, is gauged. Finally, we will study the DM properties of $U(1)$ symmetries in Chapter 5 for the example of a vector-like fermion χ charged under a gauged $U(1)_{L_\mu - L_\tau}$ symmetry.

Chapter 3

Flavor violation in a phenomenological Z' model

The contents of this chapter and the related Appendix A correspond to work done in collaboration with J. Jaeckel (Heidelberg U.) and are published as Ref. [170]. In this work, we reinterpreted ATLAS limits on a sequential standard model Z' from a resonance search in flavor-violating dilepton final states. The author was responsible for the numerical implementation of the Monte Carlo simulations required for the reinterpretation. In particular, the credit for the derivation of the muon decay limits is entirely entitled to J. Jaeckel. Nearly all the results in this chapter, including the plots and tables as well as a significant part of the text, are identical to those in the publication.

3.1 Introduction

A large class of BSM theories contains extended gauge sectors leading to the presence of extra gauge bosons. The fact that these bosons have so far escaped detection requires them to be either very weakly coupled to the SM, heavy, or both. If these bosons are massive, the extended gauge group has to be broken at some scale Λ. Typically, the breaking of these extended gauge sectors leads to the presence of extra $U(1)$ symmetries in the low-energy theory. Depending on the representations under which the fermions transform under the full gauge group, the remnant extra $U(1)$ symmetry can have flavor-specific interactions.

Scenarios with extended gauge sectors have traditionally been studied in the context of gauge coupling unification in GUTs. The motivations that lead to the development of the original $SU(5)$ GUT[1] [172] – the minimal simple group that can contain the full SM group – were the inability of the SM to unify the three fundamental interactions, the presence of the hand-crafted three generations of fermions and the large set of free parameters of the SM. The failure of the minimal $SU(5)$ GUT to predict the correct proton lifetime τ_p and Weinberg angle θ_W [173] lead to an increased interest in supersymmetric GUTs. In this

[1]Note that historically the first grand unified theory was the $SU(4)_C \times SU(2)_L \times SU(2)_R$ Pati-Salam model [171] in which all left-handed fermion fields are unified in one $(\mathbf{4}, \mathbf{2}, \mathbf{1})$ representation and all right-handed ones in a $(\overline{\mathbf{4}}, \mathbf{1}, \mathbf{2})$, respectively. However, as the group is not simple it does not lead to gauge coupling unification.

context, especially GUTs with an effective E_6 gauge group rejoiced from a strong interest after it had been shown that heterotic supersymmetric string theory with an $E_8 \times E_8$ gauge group is anomaly-free [174]. The reason for this interest was the fact that E_8 can be broken to an effective E_6 by compactification of the additional 6 dimensions. The effective E_6 gauge group can account for chiral fermions and can be further broken down in the cascade [175]

$$E_6 \quad \to \quad SO(10) \times U(1)_\psi \quad \to \quad (SU(5) \times U(1)_\chi) \times U(1)_\psi \,, \tag{3.1}$$

where the rank-four $SU(5)$ factor contains the SM gauge group. Thus, one obtains two additional effective $U(1)$ gauge factors from the breaking of E_6. However, in many models it is assumed that only one of the corresponding gauge bosons Z' is relevant at low energy scales [176–179].

Alternatively, an additional $U(1)$ symmetry could be the remnant of a solution to the still unsolved question of the origin of the flavor structure of the SM. Indeed, one of the earliest approaches towards an explanation of Yukawa coupling patterns and the family structure of the SM fermions was the introduction of so-called horizontal or gauged flavor symmetries [180–185]. For example, the different copies of up- and down-type quarks, charged leptons and neutrinos can transform in a multiplet representation under a new horizontal $SU(2)$ symmetry group. Such a gauged flavor group could be broken down to a $U(1)$ subgroup. Under appropriate charge assignments, the $U(1)$ could function as the flavor group itself. The breaking of such symmetries generally leads to the emergence of new massive gauge bosons mediating FCNCs. In such scenarios, care has to be taken in that the magnitude of such an effect does not violate experimental constraints [186]. Nevertheless, gauged flavor models have been enjoying a renewed popularity [187, 188]. Especially, the case of a new $U(1)$ gauge symmetry has been extensively studied in the past (see Refs. [189, 190] for reviews). The charge assignment of the fermions determines the coupling structure of the associated massive Z'. As analyzed in Section 2.3.4, family non-universal $U(1)$ charges can induce FCNCs due to the rotation to the mass basis of the fermions. In the literature, such flavor-violating interactions have been partially investigated, for example, in the context of the flavor anomalies $R_{D^{(\star)}}$ and $R_{K^{(\star)}}$ [191,192]. In this chapter, however, we want to study such flavor-violating Z' couplings to quarks and leptons in a systematic way. In this case severe constraints arise from precision tests of FCNCs, in particular on mesons. Yet we will see that there are still interesting areas of parameter space that can be probed with direct production at the LHC and "non-flavored" measurements such as $(g-2)$.

In this study we rely on the purely phenomenological approach of extending the SM by a neutral massive Z' boson, which is possibly the remnant of a broken gauge symmetry, with the simplest possibility being an $U(1)$ group[2]. Not specifying any underlying gauge structure, we consider models with exclusively flavor-changing couplings, one in the quark and one in the lepton sector. This is parametrized by the effective Lagrangian

$$\mathcal{L}_{Z'} = \bar{q}\,\gamma^\mu \left[g^L_{qq'}\,P_L + g^R_{qq'}\,P_R\right] q'\,Z'_\mu + \bar{\ell}\,\gamma^\mu \left[g^L_{\ell\ell'}\,P_L + g^R_{\ell\ell'}\,P_R\right] \ell'\,Z'_\mu + h.c.\,, \tag{3.2}$$

[2]In the following we do not take care of anomalies. For our simple phenomenological considerations we implicitly assume that anomalies will be canceled in an underlying complete model.

with $q \neq q'$ and $\ell \neq \ell'$. Here, $g^L_{qq'}, g^R_{qq'}, g^L_{\ell\ell'}$ and $g^R_{\ell\ell'}$ are the effective left- and right-handed flavor-changing couplings in the quark and in the lepton sector. Purely flavor-changing interactions provide a simple but interesting test case. On the one hand, they provide a maximally flavor-changing effect. On the other hand, they are often more difficult to detect. For example, if the quark part of the interaction involves a b- and an s-quark, production at proton colliders like the LHC requires reliance on the sea-quarks in the protons which are less abundant[3]. Similarly, at LEP simple s-channel production of Z' bosons via the lepton couplings is not possible as the initial state is not flavored.

The aim of this study is to identify powerful probes of the interplay of such prototypic purely flavor-violating interactions in both the quark and the lepton sector. This will be done in a comprehensive way by studying the constraining power of different flavored and non-flavored observables on all combinations of quark and lepton flavor transitions. In this analysis, a special emphasis will be put on the complementarity of LHC resonance searches in flavor-violating dilepton final states compared to classical probes of flavor-violation like semi-hadronic meson decays and meson oscillations.

The remainder of this chapter is organized as follows: In Section 3.2 we will give a detailed account of the LHC resonance searches as probes for flavor-violation. In Section 3.3, we will discuss a large set of observables constraining these types of flavor-violating interactions in the quark and/or lepton sector. In Section 3.4, we will present the results of our analysis and discuss our findings. Finally, we will draw some conclusions in Section 3.5.

3.2 Flavor violation complementarity at the LHC

When studying flavor-violation, the typical standard probes to take into account are flavor and electroweak precision experiments (see Section 3.3). One main goal of this study is to explore the complementarity of these standard tests with LHC resonance searches in flavored neutral dilepton channels in the context of a flavor-changing Z' boson.

In a previous study [193], Davidson et al. have investigated flavor violation at multipurpose detectors at the LHC in an EFT approach in four-quark contact interactions, which are the low-energy residue from new physics at a high scale $\Lambda \gg M_W$. For this purpose the coefficients of an almost complete basis of four-quark contact interaction operators have been constrained by LHC dijet searches. The basis under study also contained quark flavor-violating operators, which are of the type

$$\mathcal{O}^{XY}_{minj} = (\bar{q}_m \, \gamma^\mu \, P_X \, q_i)(\bar{q}_n \, \gamma_\mu \, P_Y \, q_j) \,, \tag{3.3}$$

where $X, Y \in \{L, R\}$ and m, i, n, j denote flavor indices.

The models considered in this chapter, however, are concerned with combined lepton and quark flavor violation. While the effective operators of Eq. (3.3) will also be generated by these models, additional contact interaction of quarks and leptons of the type

$$\mathcal{O}^{XY}_{ijkl} = (\bar{q}_i \, \gamma^\mu \, P_X \, q_j)(\bar{\ell}_k \gamma_\mu \, P_Y \, \ell_l) \,, \tag{3.4}$$

[3]This is also the reason why we do not consider interactions involving t-quarks. The corresponding limits are much weaker.

will arise. In our phenomenological model, such operators are generated from a Z'-exchange $\bar{q}_i q_j \to Z' \to \bar{\ell}_k \ell_l$. In the following, we hence want to reinterpret an existing ATLAS analysis of heavy neutral resonances decaying to $e\mu$, $e\tau$ or $\mu\tau$ [194] in the light of our flavor-violating Z' model.

3.2.1 Reinterpretation of ATLAS dilepton resonance search

As in our phenomenological model we have knowledge of the underlying Lagrangian Eq. (3.2), we can directly work in this model basis and do not have to consider contact interactions for the LHC processes. In order to constrain the relevant couplings $g_{qq'}$ and $g_{\ell\ell'}$, we first need an expression for the corresponding cross section within our model. Introducing the non-chiral reduced coupling

$$\bar{g} = \sqrt{\frac{g_L^2 + g_R^2}{2}}\,, \tag{3.5}$$

we can derive an approximate expression for the scaling of the tree-level cross section of the process $qq' \to Z' \to \ell\ell'$ as

$$\sigma(s) \approx \frac{1}{3}\,\frac{s}{M_{Z'}^4}\,\frac{\bar{g}_{qq'}^2\,\bar{g}_{\ell\ell'}^2}{3\,\bar{g}_{qq'}^2 + \bar{g}_{\ell\ell'}^2}\,. \tag{3.6}$$

This expression accurately estimates the tree-level cross section at the parton level. Unfortunately, the parton-level cross section is not directly accessible at the LHC. Apart from higher order corrections, we have to take into account parton distribution functions (PDFs) and hadronization, as the LHC is a hadron collider. Moreover, the observable cross section will also be affected by a number of detector effects like finite resolution, mistags, acceptance, etc..

Our approach to incorporate all these effects is quite straight forward. For a given combination $\{qq', \ell\ell'\}$ of flavor-violating interactions we determine the total cross section σ_{MC} for the process $pp \to Z' \to \ell\ell'$ from Monte Carlo simulations. By virtue of the approximate cross section scaling Eq. (3.6) we can turn the corresponding ATLAS limit on the cross section σ_{lim} into a limit on the couplings. Taking the ratio $\sigma_{\text{MC}}/\sigma_{\text{lim}}$ allows us to derive an approximate limit on the off-diagonal quark coupling $\bar{g}_{qq'}$ as a function of the lepton coupling $\bar{g}_{\ell\ell'}$ according to[4]

$$|\bar{g}_{qq'}| \leq \left[\frac{\sigma_{\text{MC}}}{\sigma_{\text{lim}}}\,\frac{3+r^2}{r^2\,\bar{g}_{qq',\text{MC}}^2} - \frac{3}{\bar{g}_{\ell\ell'}^2}\right]^{-\frac{1}{2}}\,, \tag{3.8}$$

[4]Note that Eq. (3.8) has a pole for

$$\bar{g}_{\ell\ell'}^2 = \frac{\sigma_{\text{lim}}}{\sigma_{\text{MC}}}\,\frac{3\,r^2\,\bar{g}_{qq',\text{MC}}^2}{3+r^2}\,. \tag{3.7}$$

This simply indicates that for values of $\bar{g}_{\ell\ell'}$ close to this pole the lepton coupling is so weak that even for a very large value of the quark coupling $\bar{g}_{qq'}$ the signal cannot be distinguished from background, i.e. the process is unobservable at the LHC.

where $\bar{g}_{qq',\mathrm{MC}}$ and $\bar{g}_{\ell\ell',\mathrm{MC}}$ denote the values of the reduced couplings we used in our simulation and their ratio is defined as

$$r = \frac{\bar{g}_{\ell\ell',\mathrm{MC}}}{\bar{g}_{qq',\mathrm{MC}}} \,. \tag{3.9}$$

In defining the ratios of left- to right-handed couplings

$$\rho_q \equiv \frac{g^L_{qq'}}{g^R_{qq'}} \,, \qquad\qquad \rho_\ell \equiv \frac{g^L_{\ell\ell'}}{g^R_{\ell\ell'}} \,, \tag{3.10}$$

we always can express the derived bounds as limits in terms of the right-handed coupling g^R and the corresponding ratio ρ to the left-handed coupling. We want to point out, however, that in our analysis we always assumed exclusively right-handed lepton couplings and indicated effects from left-handed couplings by dotted lines in the exclusion plots in Figs. 3.14 to 3.16.

With these definitions the limit on the quark couplings from Eq. (3.8) as a function of the reduced lepton coupling $\bar{g}_{\ell\ell'}$ reads

$$g^R_{qq'}(M_{Z'}, \rho_q, \bar{g}_{\ell\ell'}) \lesssim \sqrt{\frac{2}{1+\rho_q^2}} \times \left[\frac{\sigma_{\mathrm{MC}}(M_{Z'})}{\sigma_{\mathrm{lim}}(M_{Z'})} \, \frac{3+r^2}{r^2\,\bar{g}^2} - \frac{3}{\bar{g}^2_{\ell\ell'}} \right]^{-\frac{1}{2}} \,. \tag{3.11}$$

Let us now describe the three-step process by which we have estimated the cross section σ_{MC}, necessary for the limit determination from Eq. (3.8).

- Having implemented our model in `Feynrules` [195] we can calculate the tree-level leading order (LO) cross section σ_{LO} for $pp \to Z' \to \ell\ell'$ with `MadGraph5 v2.3.3` [196]. This way we incorporate PDF effects into our estimate.

- Next, we take into account next-to-next-to leading order (NNLO) effects by determining a mass-dependent K-factor. For this purpose, we make use of the NNLO cross sections, which have been provided for a Z' of the Sequential Standard Model (SSM) in the auxiliary material of the ATLAS study [194]. By calculating the LO cross section for the SSM Z' with `Pythia v8.215` [197], we can determine the values of the K-factor from the ratio to the ATLAS NNLO results

  $$K(M_{Z'}) = \frac{\sigma_{\mathrm{NNLO}}(M_{Z'})}{\sigma_{\mathrm{LO}}(M_{Z'})} \,. \tag{3.12}$$

  For completeness, the correspondingly determined values that we used for our analysis are summarized in Appendix A.2 in Table A.1.

- Finally, we need to determine an effective mass-dependent acceptance times efficiency $A \times \epsilon$. We estimate $A \times \epsilon$ from the ratio of the number of events that survived the detector plus analysis cuts in the ATALS study to the expected total number of events at NNLO

  $$[A \times \epsilon](M_{Z'}) = \frac{N_{\mathrm{survive}}(M_{Z'})}{N_{\mathrm{NNLO}}(M_{Z'})} \,. \tag{3.13}$$

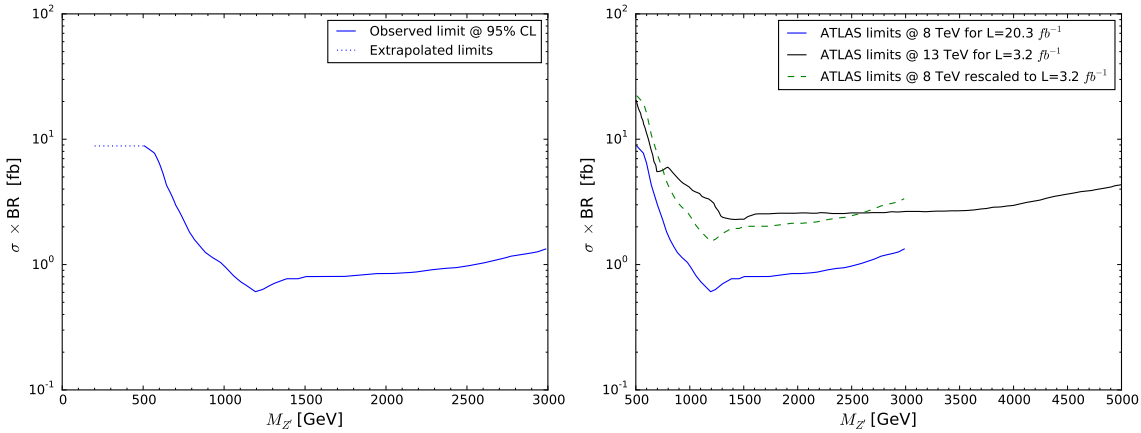

Figure 3.1: (Left) Observed exclusion limits on the branching fraction times cross section in the $e\mu$ channel [194]. The limits have been extrapolated down to masses of 200 GeV by applying a constant continuation. (Right) The blue curve shows the exclusion limits on the branching fraction times cross section at $\sqrt{s} = 8$ TeV given in Ref. [194]. The black curve shows the limit of Ref. [199] derived at $\sqrt{s} = 13$ TeV with 3.2 fb^{-1} of data. The green curve depicts the 8 TeV limit rescaled to the 13 TeV luminosity. The order of magnitude agreement between this curve and the 13 TeV limit in this region indicate that our luminosity rescaling is sensible. Figure taken from [170].

> The number of events at NNLO $N_{\mathrm{NNLO}} = \sigma_{\mathrm{NNLO}} \times \int \mathrm{d}t\, \mathscr{L}$ is simply obtained from multiplying the cross section by the integrated luminosity. The numerical values of the determined acceptance times efficiency we used in our analysis can be found in Appendix A.2 in Table A.2.

In summary, the total observable cross section at the LHC for the process $pp \to Z' \to \ell\ell'$ can be estimated by

$$\sigma_{\mathrm{MC}} = \sigma_{\mathrm{LO}} \times K \times [A \times \epsilon]\,. \tag{3.14}$$

In this work, we have derived these limits from the ATLAS resonance search in flavor-violating dilepton final states for Z' masses in the range of 200 GeV to 3 TeV and for flavor-violating coupling combinations $qq' \in \{sd, bs, bd, cu\}$ and $\ell\ell' \in \{e\mu, e\tau, \mu\tau\}$. In Section 3.4 an example exclusion plot for each flavor combination is given for a benchmark scenario of a Z' boson with $M_{Z'} = 1$ TeV. The entire set of exclusion plots for all coupling combinations and Z' masses produced in this work can be found at the URL in [198].

In deriving these limits, we have performed an optimistic extrapolation of the ATLAS limits for Z' bosons masses below 500 GeV. As shown in the left panel of Fig. 3.1, we assume a constant continuation of the ATLAS limits down to masses of $M_{Z'} = 200$ GeV. This appears to be justified as the resonance search under consideration was designed for heavy mediators [194]. The main reason why the Z' limits are usually not derived for masses below ~ 500 GeV are the huge SM backgrounds (cf. invariant mass distributions in [194, 200, 201]). However, it might be hoped that a dedicated analysis in the low-mass region could yield better limits than the extrapolation of Fig. 3.1.

Furthermore, in our analysis we have projected the limits deduced at $\sqrt{s} = 8$ TeV and 20.3 fb^{-1} of data to a Run 2 scenario (LHC Run II) of $\sqrt{s} = 13$ TeV and 100 fb^{-1} and a high luminosity scenario (HL-LHC) of $\sqrt{s} = 13$ TeV and 3000 fb^{-1}. Therefore, we have rescaled the exclusion limits on the cross section by the respective luminosities

$$\sigma_{\text{lim}}^{(13)} = \sqrt{\frac{\int \mathrm{d}t\ \mathscr{L}_8}{\int \mathrm{d}t\ \mathscr{L}_{13}}}\ \sigma_{\text{lim}}^{(8)}\,, \tag{3.15}$$

assuming that the scaling of the limits is only due to statistics. As a cross-check for this prescription to work, we have compared luminosity-rescaled limits from the ATLAS 8 TeV analysis to first limits obtained by ATLAS[5] at $\sqrt{s} = 13$ TeV with 3.2 fb^{-1} of data in the $e\mu$-channel [199]. As shown in the right panel of Fig. 3.1, this method seems to give sufficiently accurate results for the purpose of a rough projection.

In Section 3.4, we show the limits derived from reinterpreting the ATLAS analysis [194] as just described as red areas in the exclusion plots in Figs. 3.14 to 3.16. The projections to the LHC Run II scenario are illustrated by the red dash-dotted lines and the projections to the HL-LHC scenario by the red dotted lines.

3.3 Constraints

The central goal of this chapter is to identify sensitive probes for all possible combinations of simultaneous quark and lepton flavor violation. In this context, we want to asses in particular the sensitivity of resonance searches with multipurpose experiments at the LHC compared to more traditional probes of flavor violation. Therefore, we want to give a detailed account in the following section of the large set of flavored and non-flavored observables that constrain our model Eq. (3.2). We will first discuss pure quark-sector constraints from meson mixing before considering mixed quark- and lepton-sector constraints from meson decays into charged leptons and neutrinos. Finally, we will analyze pure lepton-sector constraints coming from lepton decays, muonium oscillations, LEP searches and anomalous magnetic moment measurements.

3.3.1 Meson mixing

One of the strongest probes for flavor violation in the quark sector is provided by meson mixing, where a meson $\mathcal{M}$ oscillates into its conjugate state $\overline{\mathcal{M}}$. The meson oscillation processes require FCNCs. These processes are strongly suppressed within the SM as they are only mediated via electroweak loop-processes and the corresponding matrix elements are very small. This makes meson mixing very sensitive to new physics featuring quark flavor-changing couplings. In the model under consideration in this chapter meson mixing arises at tree level via Z' exchange from the diagrams shown in Fig. 3.2.

[5]Notice that after the original publication of the results presented in this chapter, both ATLAS [200] and CMS [201] have performed dedicated resonance searches in all three lepton flavor violating final states $e\mu$, $e\tau$ and $\mu\tau$ at $\sqrt{s} = 13$ TeV.

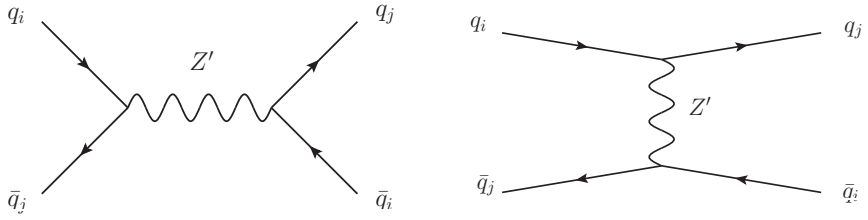

Figure 3.2: Tree-level meson mixing via Z'.

An appropriate observable to test flavor violation is the mass splitting $\Delta M_{\mathcal{M}}$ of the conjugate meson states. As $\Delta M_{\mathcal{M}}$ is given by the real part of the transition matrix element M_{12} of the meson oscillation process,

$$\Delta M_{\mathcal{M}} = 2\,\mathrm{Re}(M_{12}) \propto g_{qq'}^2\,, \tag{3.16}$$

it is directly proportional to the square of the flavor-violating coupling $g_{qq'}$ and hence very sensitive to Z'-induced flavor violation.

Meson mixing is a low-energy effect, which makes it suitable for investigation in an EFT framework. In this spirit we follow Ref. [202] and investigate the Z' effects on meson mixing in an EFT approach, where we integrate out the Z' at the high scale $\mu_{\text{in}} \sim M_{Z'}$. The resulting four-quark operators describing the low-energy phenomenology of the Z'-induced FCNCs are given by [202, 203][6]

$$\mathcal{O}_1^{\text{VLL}} = (\bar{q}\,\gamma^\mu P_L\,q')(\bar{q}\,\gamma^\mu P_L\,q')\,, \tag{3.17}$$
$$\mathcal{O}_1^{\text{VRR}} = (\bar{q}\,\gamma^\mu P_R\,q')(\bar{q}\,\gamma^\mu P_R\,q')\,, \tag{3.18}$$
$$\mathcal{O}_1^{\text{LR}} = (\bar{q}\,\gamma^\mu P_L\,q')(\bar{q}'\,\gamma^\mu P_R\,q')\,, \tag{3.19}$$
$$\mathcal{O}_2^{\text{LR}} = (\bar{q}\,P_L\,q')(\bar{q}'\,P_R\,q')\,. \tag{3.20}$$

After matching the operators of Eqs. (3.17) to (3.20) to the full theory we find the corresponding Wilson coefficients at the high scale μ_{in}. With the off-diagonal transition matrix element given in an effective Hamiltonian framework by $M_{12}^* = \langle\overline{\mathcal{M}}|\mathcal{H}_{\text{eff}}^{\Delta S=2}|\mathcal{M}\rangle$, we find for the mass splitting [202][7]

$$\Delta M_{\mathcal{M}}^{\text{NP}} = \frac{M_{\mathcal{M}}\,f_{\mathcal{M}}^2}{3}\,\frac{\left(g_{qq'}^R\right)^2}{M_{Z'}^2}\left[R_1^{\text{VLL}}(\mu)\,P_1^{\text{VLL}}\,(1+\rho_q^2) + \left(R_1^{\text{LR}}(\mu)\,P_1^{\text{LR}} + R_2^{\text{LR}}(\mu)\,P_2^{\text{LR}}\right)\,\rho_q\right], \tag{3.21}$$

where the P_i denote the hadronic matrix elements corresponding to the operators $\mathcal{O}_i$. We calculate the hadronic matrix elements for K, B_d and B_s mesons mainly from the relations given in Refs. [202, 203] and the lattice bag parameters from quenched QCD calculations given in [204, 205]. For D mesons we rely on the relations given in Ref. [206]. The $R_i(\mu)$

[6] It should be noted that the operator $\mathcal{O}_2^{\text{LR}}$ is generated only through operator mixing due to QCD-loop effects in the renormalization group evolution of the operators from the high to the low scale.

[7] We use $P_1^{\text{VLL}} = P_1^{\text{VRR}}$ to simplify the expression.

are the renormalization group evolution coefficients encoding the running of the operators $\mathcal{O}_i$ due to NLO QCD effects. They are normalized such that $R_i(\mu_{\text{in}}) = 1$ at the scale μ_{in} where the Z' is integrated out. The coefficients are given by [202]

$$R_1^{\text{VLL}}(\mu) = R_1^{\text{VRR}}(\mu) = 1 + \frac{\alpha_s}{4\pi}\left(\frac{11}{3} - 2\,\log\frac{M_{Z'}^2}{\mu^2}\right), \tag{3.22}$$

$$R_1^{\text{LR}}(\mu) = 1 - \frac{\alpha_s}{4\pi}\left(\frac{1}{6} + \log\frac{M_{Z'}^2}{\mu^2}\right), \tag{3.23}$$

$$R_2^{\text{LR}}(\mu) = \quad -\frac{\alpha_s}{4\pi}\left(1 + 6\,\log\frac{M_{Z'}^2}{\mu^2}\right). \tag{3.24}$$

Finally, we can use Eq. (3.21) to constrain the coupling $g^R_{qq'}$ by knowledge of the observed meson mass splitting $\Delta M_{\mathcal{M}}$. We can derive a stringent limit from constraining the Z' contribution to the mass splitting to be smaller than the maximally allowed deviation between the measured value and the SM prediction,

$$\Delta M_{\mathcal{M}}^{\text{NP}} < \Delta M_{\mathcal{M}}^{\text{obs}} - \Delta M_{\mathcal{M}}^{\text{SM}}\,. \tag{3.25}$$

In our analysis, we use the measured values of the meson mass splittings provided by the UTfit collaboration [207] to set our limit.

Cancellation

The strategy discussed in the last section to constrain the flavor-violating quark-sector couplings $g^R_{qq'}$ will in general lead to stringent bounds on the Z' parameter space However, there is an important subtlety to these considerations that alters the picture just enough to serve as motivation for a search of Z' induced FCNCs with multipurpose experiments at the LHC. The term in brackets in Eq. (3.21) is a quadratic form in the parameter ρ_q. Thus, if the discriminant

$$\Delta = \left(R_1^{\text{LR}}(\mu)\,P_1^{\text{LR}} + R_2^{\text{LR}}(\mu)\,P_2^{\text{LR}}\right)^2 - 4\;R_1^{\text{VLL}}(\mu)\,P_1^{\text{VLL}}\left(R_1^{\text{LR}}(\mu)\,P_1^{\text{LR}} + R_2^{\text{LR}}(\mu)\,P_2^{\text{LR}}\right), \tag{3.26}$$

is greater than zero, the quadratic form has two solutions ρ_0 for which the mass splitting due to Z' exchange vanishes exactly. In turn, this means that for a ratio ρ_0 of left- to right-handed couplings, the meson mass splitting is not sensitive to the flavor-violating couplings at all. In this work, we will always only consider the solution that has mostly right-handed couplings as an example. The second solution is simply given by $1/\rho_0$ and has essentially the same behavior.

In this chapter, we are interested in comparing flavor bounds on the Z' couplings to the collider bounds from the dilepton ATLAS search. Therefore, we define an upper and lower tolerance $\Delta\rho_-$ and $\Delta\rho_+$, such that the mixing limit on the coupling $g^{\text{lim}}_{qq'}$ in the interval $[\rho_0 - \Delta\rho_-,\ \rho_0 + \Delta\rho_+]$ enveloping the cancellation point ρ_0 is less stringent than a reference value g^*, i.e.

$$\forall\ \rho_q \in I_0 := [\rho_0 - \Delta\rho_-,\ \rho_0 + \Delta\rho_+]:\ g^{\text{lim}}_{qq'}(\rho_q) \geq g^*\,. \tag{3.27}$$

With this definition we can find an interval I_0 enveloping the cancellation solution ρ_0, where the limit due to meson mixing is subdominant compared to the strongest bound $g^* = \min(g^{\text{col}}_{qq'})$ we can set from the ATLAS search across the entire Z' mass range.

So far, our treatment of the cancellation in meson mixing has been restricted to tree-level effects only. However, we have to ensure that these effects persist at higher orders. Therefore, we have to investigate the impact of one-loop corrections on the cancellation solution ρ_0 and the associated tolerance interval I_0. We leave the discussion of higher-order corrections for Appendix A.1 and only briefly comment on our results. We find that the cancellation solution ρ_0 and the interval I_0 both receive an overall shift $\delta\rho$ at the one-loop level. However, this shift is negligible in the sense that $\delta\rho < \rho_0$ in the region of parameter space that is probed by the ATLAS analysis. Hence, higher-order effects do not destroy the leading-order cancellation effect and in the tolerance intervals I_0 the limit from meson mixing is subdominant.

In our analysis of the constraints on flavor-violation for the different Z' coupling combinations, we will make use of the previous discussion and always focus on the region of parameter space where cancellation in the Z' contribution to meson mixing occurs. Hence, all the exclusion plots we show in Figs. 3.14 to 3.16 in Section 3.4.1 show the limits for the ratio ρ_0 of left- to right-handed quark couplings, where limits from meson mixing exactly vanish.

3.3.2 Meson decays

Another process in the meson sector that directly constrains our model is rare neutral meson decay $\mathcal{M}^0 \to \ell^+\ell'^-$, where $\mathcal{M}^0$ can be the K, D, B_d or B_s meson. As these decays involve two flavor-changing vertices they are highly suppressed in the SM, whereas they are generated at tree level in our Z' model. As these decays are low-energy processes, it is once more convenient to perform the analysis in an EFT framework. In analogy to our treatment of meson mixing in the last section, from the Lagrangian in Eq. (3.2) we can immediately construct the relevant four-fermion operators [208]

$$\mathcal{O}_1 = (\bar{\ell}\,\gamma_\mu\, P_L\, \ell')(\bar{q}\,\gamma^\mu\, P_L\, q')\,, \qquad \mathcal{O}_6 = \mathcal{O}_1(L \leftrightarrow R)\,, \tag{3.28}$$

$$\mathcal{O}_2 = (\bar{\ell}\,\gamma_\mu\, P_R\, \ell')(\bar{q}\,\gamma^\mu\, P_L\, q')\,, \qquad \mathcal{O}_7 = \mathcal{O}_2(L \leftrightarrow R)\,, \tag{3.29}$$

with corresponding Wilson coefficients

$$C_1 = \frac{g^L_{\ell\ell'}\, g^L_{qq'}}{M^2_{Z'}}\,, \qquad C_2 = \frac{g^R_{\ell\ell'}\, g^L_{qq'}}{M^2_{Z'}}\,, \qquad C_6 = \frac{g^R_{\ell\ell'}\, g^R_{qq'}}{M^2_{Z'}}\,, \qquad C_7 = \frac{g^L_{\ell\ell'}\, g^R_{qq'}}{M^2_{Z'}}\,. \tag{3.30}$$

With knowledge of the relevant operators and their associated Wilson coefficients we can calculate the branching ratio $\text{BR}(\mathcal{M}^0 \to \ell^+\ell'^-)$ for the different mesons [208, 209]

$$\text{BR}(\mathcal{M}^0 \to \ell^+\ell'^-) = \frac{f^2_{\mathcal{M}^0}\; M_{\mathcal{M}^0}\; m^2_\ell}{32\,\pi\,\Gamma_{\mathcal{M}^0}\, M^4_{Z'}} \left(1 - \frac{m^2_\ell}{M^2_{\mathcal{M}^0}}\right)^2 (g^L_{\ell\ell'} - g^R_{\ell\ell'})^2 \left(g^L_{qq'} - g^R_{qq'}\right)^2\,, \tag{3.31}$$

where $f_{\mathcal{M}^0}, M_{\mathcal{M}^0}$ and $\Gamma_{\mathcal{M}^0}$ are the decay constant, the mass and the total width of the decaying meson. Furthermore, we assume that ℓ is the heavier of the two leptons and

neglect the mass of the lighter one. Of course, these decays are only possible if the mass of the meson is bigger than the combined mass of the two final-state leptons. Based on Eq. (3.31) we can derive a limit on the Z' coupling given by

$$|g^R_{qq'}| \leq \left[\frac{32\,\pi\ \mathrm{BR}(\mathcal{M}^0 \to \ell^+\ell'^-)\,\Gamma_{\mathcal{M}^0}\,M^4_{Z'}}{M_{\mathcal{M}^0}\,f^2_{\mathcal{M}^0}\,m^2_\ell\left(1-\frac{m^2_\ell}{M^2_{\mathcal{M}^0}}\right)^2}\right]^{\frac{1}{2}} \frac{1}{g^R_{\ell\ell'}\ |1-\rho_\ell|\ |1-\rho_q|}\,, \tag{3.32}$$

where we have made use of the relations in Eq. (3.10).

In the exclusion plots in Figs. 3.14 to 3.16, the corresponding meson decay limits are depicted by the green areas. The constraining power of the meson decay limits is due to the fact that the matrix element is proportional to the product of quark- and lepton-sector couplings $g_{qq'}\,g_{\ell\ell'}$. Therefore, meson decays can probe regions in parameter space where one of the two coupling is very small while the other one is big, a region hard to probe with ATLAS. However, the ATLAS limits are generally more stringent in the region of parameter space where both couplings become small but comparable in size. With Run II or HL-LHC data, improvements of the meson decay limits can mainly be expect in that region of parameter space.

3.3.3 Neutrino limits

It seems reasonable that an extension of the SM should preserve the $SU(2)_L$ gauge symmetry at high energies. In turn, this means for our effective model that the Z' gauge boson should couple to the quark and lepton doublets Q_L and L_L, if left-handed couplings are present. In this scenario, the Z' couples to the neutrinos ν_i and ν_j with equal strength $g^L_{\ell_i\ell_j}$ as to the left-handed charged leptons ℓ_i and ℓ_j. The coupling to neutrinos opens up a new class of constraints to such a model. Especially, meson decays featuring neutrino final states like $\mathcal{M}_1^{0,\pm} \to \mathcal{M}_2^{0,\pm}\,\bar\nu\,\nu$ can be a sensitive probe for the presence of left-handed lepton flavor-violating Z' couplings.

In this section, we will investigate the impact of such decays of the different neutral mesons on our model. In particular, we consider decays of kaons and B-mesons. The corresponding measurements in the D-meson sector are not (very) restricting and hence are not discussed.

Kaons

In the case of non-zero Z'-couplings to the first two generations of quarks, we can constrain the left-handed lepton couplings from the kaon decay $K^+ \to \pi^+\nu\bar\nu$. In order to extract a constraint on $g^L_{\ell_i\ell_j}$, we will calculate the branching ratio $\mathrm{BR}(K^+ \to \pi^+\nu\bar\nu)$ in the following. For a detailed derivation of this branching ratio we refer the reader to [210].

Within the SM the leading-order contributions to this decay are due to electroweak loop-processes shown in the upper panels of Fig. 3.3. Being at the one-loop level, we expect the SM contribution to these decays to be rather small. In the flavor-violating Z' model such a decay can already arise at tree level as shown in the lower panel of Fig. 3.3. Hence, the Z'-mediated process can potentially give a sizable contribution to the branching fraction of this decay. In order to quantify the magnitude of the Z' contribution, we will

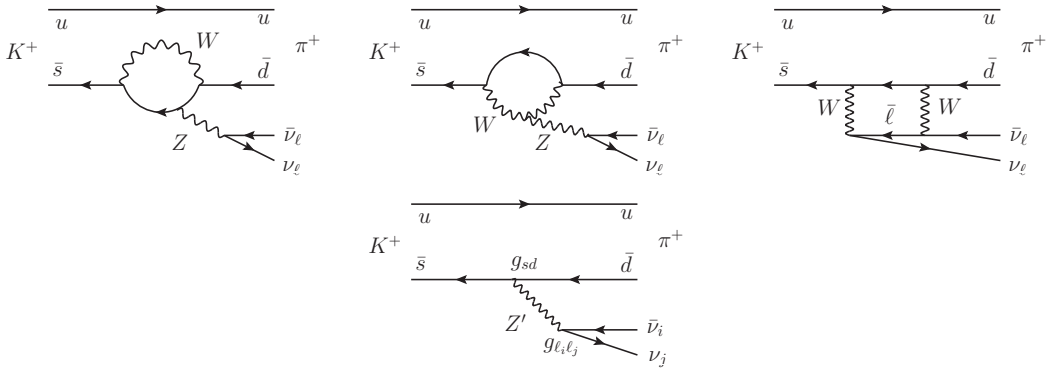

Figure 3.3: (Upper panels) Leading order SM contributions to the decay $K^+ \to \pi^+ \nu\bar{\nu}$. (Lower panel) Leading order Z' contribution to the decay $K^+ \to \pi^+ \nu\bar{\nu}$.

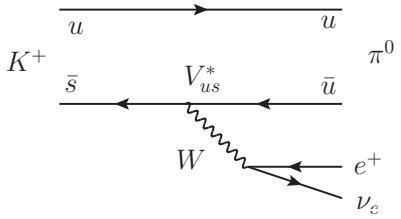

Figure 3.4: Decay $K^+ \to \pi^0\, e^+\, \nu_e$ in the SM.

again calculate the corresponding amplitudes in an EFT approach. Adopting the notation of Ref. [210], where $(\bar{s}d)_{V\pm A} \equiv \bar{s}\gamma_\mu(1 \pm \gamma_5)d$, the relevant operators for this process in the low-energy theory read

$$\mathcal{O}^L_{K^0} = (\bar{s}d)_{V-A}\ (\bar{\nu}_i\nu_j)_{V-A}\,, \qquad \mathcal{O}^R_{K^0} = (\bar{s}d)_{V+A}\ (\bar{\nu}_i\nu_j)_{V-A}\,, \tag{3.33}$$

with their corresponding matched Wilson coefficients

$$C^L_{K^0} = \frac{g^L_{sd}\, g^L_{\ell_i\ell_j}}{4\, M^2_{Z'}}\,, \qquad C^R_{K^0} = \frac{g^R_{sd}\, g^L_{\ell_i\ell_j}}{4\, M^2_{Z'}}\,. \tag{3.34}$$

If we want to calculate the relevant matrix element for this process, we require knowledge of the corresponding hadronic matrix element $\langle\pi^+|(\bar{s}d)|K^+\rangle$. By use of isospin symmetry [210], we are able to extract the hadronic matrix element for $(\bar{s}d)_{V-A}$ from the decay $K^+ \to \pi^0\, e^+\, \nu_e$ shown in Fig. 3.4,

$$\langle\pi^+|(\bar{s}d)_{V-A}|K^+\rangle = \sqrt{2}\,\langle\pi^0|(\bar{s}u)_{V\pm A}|K^+\rangle\,. \tag{3.35}$$

Additionally we take the hadronic matrix elements of the left- and right-handed currents to be equal [211]. As the kaon decay is governed entirely by QCD, it should be independent of the underlying chirality structure. The corresponding effective operator relevant for the process in Fig. 3.4 reads

$$\mathcal{O}^L_{K^+} = (\bar{s}u)_{V-A}\,(\bar{\nu}_e e)_{V-A}\,, \tag{3.36}$$

and the associated Wilson coefficient is given by

$$C^L_{K^+} = \frac{G_F}{\sqrt{2}} V^*_{us}\,, \tag{3.37}$$

where we have denoted the us-element of the CKM matrix by V_{us}. If we now further assume the positron in the process of Fig. 3.4 to be massless, we can assume equality of the leptonic matrix elements $\langle \bar{\nu}_e e^+ | (\bar{\nu}_e e^+)_{V-A} | 0 \rangle = \langle \bar{\nu}_i \nu_j | (\bar{\nu}_i \nu_j)_{V-A} | 0 \rangle$. With these simplifications, we can finally write the fraction of the branching ratios of the two processes as

$$\frac{\mathrm{BR}(K^+ \to \pi^+ \nu\bar{\nu})}{\mathrm{BR}(K^+ \to \pi^0 e^+ \bar{\nu})} = \left(\frac{\sqrt{2}\, g^L_{\ell_i \ell_j}}{4\, G_F\, M^2_{Z'}} \right)^2 \frac{\left| g^L_{sd} \langle \pi^+ | (\bar{s}d)_{V-A} | K^+ \rangle + g^R_{sd} \langle \pi^+ | (\bar{s}d)_{V+A} | K^+ \rangle \right|^2}{|V^*_{us}|^2 \; |\langle \pi^0 | (\bar{s}u)_{V-A} | K^+ \rangle|^2} \tag{3.38}$$

$$= \frac{g^{L\,2}_{\ell_i \ell_j}\; g^{R\,2}_{sd}\; |1 + \rho_q|^2}{4\, |V^*_{us}|^2\, G^2_F\, M^4_{Z'}}\,, \tag{3.39}$$

where in the second line we have assumed isospin symmetry (cf. Eq. (3.35)). To turn this into a limit on g^R_{sd} we only consider the part of the branching fraction not explained by the SM

$$\mathrm{BR}(K^+ \to \pi^+ \nu\bar{\nu})^{\mathrm{NP}} = \mathrm{BR}(K^+ \to \pi^+ \nu\bar{\nu})^{\mathrm{exp}} - \mathrm{BR}(K^+ \to \pi^+ \nu\bar{\nu})^{\mathrm{SM}}\,, \tag{3.40}$$

where we used for our analysis

$$\mathrm{BR}(K^+ \to \pi^+ \nu\bar{\nu})^{\mathrm{exp}} = (1.73^{+1.15}_{-1.05}) \times 10^{-10}\,, \qquad \text{(cf. Ref. [212])}\,, \tag{3.41}$$

$$\mathrm{BR}(K^+ \to \pi^+ \nu\bar{\nu})^{\mathrm{SM}} = (9.1 \pm 0.7) \times 10^{-11}\,, \qquad \text{(cf. Ref. [213])}\,. \tag{3.42}$$

Finally, we obtain the constraint on the sd flavor-changing Z' coupling to be given by

$$|g^R_{sd}| \leq \frac{2\, |V_{us}|\, G_F\, M^2_{Z'}}{|g^L_{\ell_i \ell_j}|\, |1 + \rho_q|} \left[\frac{\mathrm{BR}(K^+ \to \pi^+ \nu\bar{\nu})^{\mathrm{NP}}}{\mathrm{BR}(K^+ \to \pi^0 e^+ \bar{\nu})} \right]^{\frac{1}{2}}\,. \tag{3.43}$$

The resulting limits on the Z' couplings are depicted by the black dotted lines in the lower left panels in Figs. 3.14 to 3.16 in Section 3.4.1. The neutrino limits in the kaon sector are quite strong and as the limits from decays into charged leptons discussed in the previous section constrain the product $g_{qq'} g_{\ell\ell'}$. Especially in the $e\tau$ and $\mu\tau$ sector, the neutrino limits from kaon decay exclude all regions of parameter space that can be hoped to be tested with multipurpose experiments at the LHC. However, as mentioned in the beginning of this section, the neutrino limits are only valid if we take the lepton couplings to be left-handed and can be fully circumvented by only considering right-handed lepton couplings.

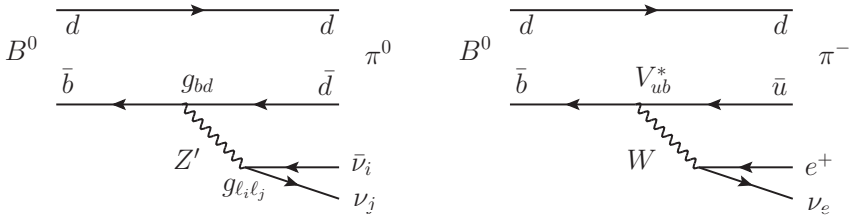

Figure 3.5: (Left) Decay $B^0 \to \pi^0\,\bar{\nu}_i\,\nu_j$ mediated by the Z' boson. (Right) SM decay $B^0 \to \pi^-\,e^+\,\nu_e$ mediated by the W boson.

B mesons

Our strategy to derive a limit on g_{bd} from $b \to d\nu\bar{\nu}$ transitions in B-meson decays is exactly the same as for kaons in the previous section. However, in this case the process that is induced through non-zero g_{bd} and $g_{\ell_i\ell_j}$ couplings is $B^0 \to \pi^0\,\bar{\nu}_i\,\nu_j$. This is shown in the left panel of Fig. 3.5. As in the case for the kaons we will extract the hadronic matrix element from the related decay $B^0 \to \pi^-\,e^+\,\nu_e$ (shown in the right panel of Fig. 3.5) via isospin symmetry. A limit on the coupling g_{bd} can be derived from the fraction of the branching ratios of the two B^0 decays. With the PDG values [214] for the respective branching ratios

$$\mathrm{BR}(B^0 \to \pi^0\,\bar{\nu}\,\nu)^{\mathrm{lim}} < 6.9 \times 10^{-5}\,, \tag{3.44}$$

$$\mathrm{BR}(B^0 \to \pi^-\,e^+\,\nu_e) = (1.45 \pm 0.05) \times 10^{-4}\,, \tag{3.45}$$

we can then set a limit in analogy to Eq. (3.43)[8]

$$|g_{bd}^R| \leq \frac{4\,|V_{ub}|\,G_F\,M_{Z'}^2}{|g_{\ell_i\ell_j}^L|\,|1+\rho_q|}\left[\frac{\mathrm{BR}(B^0 \to \pi^0\,\bar{\nu}\,\nu)^{\mathrm{lim}}}{\mathrm{BR}(B^0 \to \pi^-\,e^+\,\nu_e)}\right]^{\frac{1}{2}}\,. \tag{3.46}$$

The transition $b \to s\nu\bar{\nu}$ can be analogously constrained from the decay $B^+ \to K^+\nu\bar{\nu}$. To extract a limit on the Z' coupling g_{bs} in the presence of left-handed lepton couplings, we will again need the Z' contribution to the branching ratio of this decay [215]. First, we can parametrize any contribution to this process in an EFT approach by the two operators

$$\mathcal{O}_{B^0}^{L/R} = (\bar{s}\gamma_\mu P_{L/R} b)(\bar{\nu}\gamma^\mu(1-\gamma_5)\nu)\,. \tag{3.47}$$

As for kaons, the leading-order SM contributions are coming from electroweak loop diagrams, which therefore are only involving left-handed fermions. The corresponding Wilson coefficient for the SM contributions has been calculated in [215] to

$$C_{\mathrm{SM}}^L = -\frac{e^2\,G_F}{\sqrt{2}\,\pi^2\,\sin(\theta_W)^2}X_t\,, \qquad\qquad X_t = 1.469 \pm 0.017\,, \tag{3.48}$$

with θ_W denoting the Weinberg angle. The leading-order contribution coming from the exchange of a Z' as shown in Fig. 3.6 yields the Wilson coefficients

$$C_{Z'}^{L/R} = \frac{2\sqrt{2}\,\pi^2\,g_{bs}^{L/R}\,g_{\ell_i\ell_j}^L}{e^2\,V_{tb}V_{ts}^*\,M_{Z'}^2}\,. \tag{3.49}$$

[8]Since no detection of this process has been made and the resulting bounds are within regions that are already excluded we simply use the experimental limit on the branching ratio for our estimate.

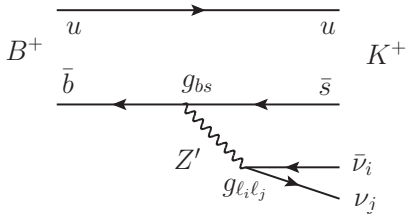

Figure 3.6: Z' contribution to the decay $B^+ \to K^+\nu\bar{\nu}$.

Defining the differential branching fractions for the process as

$$\frac{\mathrm{d}\,\mathrm{BR}(B^+ \to K^+\nu\bar{\nu})}{\mathrm{d}q^2} \equiv \mathcal{B}_K\,, \tag{3.50}$$

one finds for the ratio [215]

$$\mathcal{R}_K = \frac{\mathcal{B}_K}{\mathcal{B}_K^{SM}} = (1-2\eta)\epsilon^2\,, \tag{3.51}$$

with the model-independent quantities

$$\epsilon = \frac{\sqrt{|C^L|^2+|C^R|^2}}{|C^L_{\mathrm{SM}}|}\,, \qquad\qquad \eta = \frac{-\mathrm{Re}(C^L\,C^{R^*})}{|C^L|^2+|C^R|^2}\,. \tag{3.52}$$

From the constraint that $\mathcal{R}_K \leq 4.3$ [215], we can derive a limit on the quark coupling as

$$|g^R_{bs}| \leq \frac{\alpha\,|V_{tb}V^*_{ts}|\sqrt{2\,\mathcal{R}_K}\,M^2_{Z'}}{\pi(1+\rho_q)\;|g^L_{\ell_i\ell_j}|}\;|C^L_{\mathrm{SM}}|\,. \tag{3.53}$$

The corresponding limits from B^0 decays in the bd sector are depicted by the black dotted lines in the upper right panels of Figs. 3.14 to 3.16. The limits from B^+ decays in the bs sector are depicted by the black dotted lines in the upper left panels of Figs. 3.14 to 3.16. As was the case for the limits due to kaons decaying into neutrinos, the corresponding limits from B mesons are only valid if we allow for left- instead of right-handed lepton couplings $g^L_{\ell_i\ell_j}$. The neutrino limits in the B-meson sector are not quite as strong as for the kaons. Nevertheless, for the B_s meson (i.e. in the bs sector) the neutrino limits for non-zero $g^L_{e\tau}$ and $g^L_{\mu\tau}$ coupling exclude close to all regions in parameter space testable at ATLAS and CMS. For non-zero $g^L_{e\mu}$ coupling and generally for B_d mesons (i.e. in the bd sector) the neutrino limits are comparable to those from meson decay into charged leptons. Nevertheless, as can be seen from Figs. 3.14 to 3.16 in the direction of both small quark and lepton couplings the ATLAS limits are more stringent.

3.3.4 Lepton decays

An important leptonic constraint which also involves neutrinos is due to charged lepton decays. As for the meson decays to neutrinos, this constraint applies only to Z' bosons with couplings to left-handed leptons. As this process involves only leptons, the limits

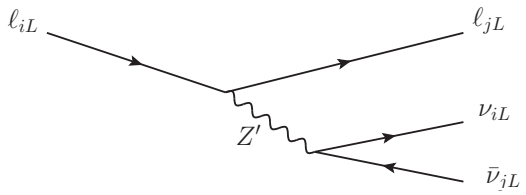

Figure 3.7: Diagrams of the lepton decay $\ell_i \to \ell_j \, \nu_i \, \bar{\nu}_j$. The same diagram also exists for right-handed charged leptons and for the lepton flavor-violating decays $\ell_i \to \ell_j \, \nu_j \, \bar{\nu}_i$, where the neutrino flavors are interchanged.

only depend on the leptonic couplings and will therefore correspond to vertical lines in the plots.

In the SM the decay $\ell_{iL} \to \ell_{jL} \, \nu_{iL} \, \bar{\nu}_{jL}$ is mediated by W boson exchange and does not require flavor-violating couplings. According to the diagram in Fig. 3.7 in our model there is, however, an additional contribution to this decay coming from Z' exchange. This contribution interferes with the SM contribution generated by a W boson exchange. In addition, there are three new decay channels $\ell_{iL} \to \ell_{jL} \, \bar{\nu}_{iL} \, \nu_{jL}$, $\ell_{iR} \to \ell_{jR} \, \nu_{iL} \, \bar{\nu}_{jL} (\bar{\nu}_{iL} \, \nu_{jL})$, which are not allowed in the SM. These channels arise from diagrams as shown in Fig. 3.7 and the ones with neutrino flavors interchanged. Together they modify the SM decay rate [216] into a given lepton plus neutrinos according to,

$$\Gamma_{\ell_i \to \ell_j + \bar{\nu}\nu} = \Gamma^{\rm SM}_{\ell_i \to \ell_j + \bar{\nu}\nu} \left[(1 + x_{ij})^2 + x_{ij}^2 + 2 \, y_{ij}^2 \right] , \tag{3.54}$$

where with g_2 denoting the $SU(2)_L$ coupling constant we have defined

$$x_{ij} = 2 \, \frac{(g^L_{\ell_i \ell_j})^2}{g_2^2} \frac{M_W^2}{M_{Z'}^2}, \qquad\qquad y_{ij} = 2 \, \frac{g^L_{\ell_i \ell_j} \, g^R_{\ell_i \ell_j}}{g_2^2} \frac{M_W^2}{M_{Z'}^2}. \tag{3.55}$$

The first part in Eq. (3.54) is the contribution to the SM-like purely left-handed, non-flavor-violating channel. The second and third part are the non-SM-like chirality-flipped and/or flavor-violating channels. Importantly, we do not distinguish the neutrino species in the measurement of the final state. This is why all the contributions are summed.

As before, we will consider the case of purely left- or right-handed lepton couplings. In the case of purely right-handed couplings we do not get any contribution from the Z' (as due to $g^L_{\ell_i \ell_j} = 0$ also $x_{ij}, y_{ij} = 0$). In the case of purely left-handed couplings the modification of the SM decay rate simplifies to

$$\Gamma_{\ell_i \to \ell_j + \bar{\nu}\nu} = \Gamma^{\rm SM}_{\ell_i \to \ell_j + \bar{\nu}\nu} \left[(1 + x_{ij})^2 + x_{ij}^2 \right] . \tag{3.56}$$

Muon decays

Measurements of the μ lifetime are very precise with a relative uncertainty of the order of 10^{-6} [214]. This suggests very stringent constraints on $x_{\mu e}$. However, the decay of the μ is usually used to determine the Fermi constant G_F. For that reason, this measurement cannot be used again to independently test new physics effects. Therefore, we need an

additional independent measurement to probe the flavor-violating Z' couplings. The β-decay of nucleons is possible only via a charged current and is therefore unaffected by our Z'. However, it contains the CKM matrix element V_{ud} which is usually extracted from those decays. The situation is similar for the decay of kaons which contain the matrix element V_{us}.

Nevertheless, we can extract a limit from this comparison using the following argument. As can be seen from Eq. (3.56) the Z' contribution leads to an increase in the muon decay rate. Using the SM extraction of V_{us} and V_{ud} this would lead to smaller values of these CKM matrix elements. Assuming unitarity for the CKM matrix we can hence constrain $x_{\mu e}$ using the CKM matrix elements determined in the standard way [214],

$$\begin{aligned} 1 - \frac{1}{(1+x_{\mu e})^2 + x_{\mu e}^2} \approx 2\, x_{\mu e} \;&\lesssim\; 1 - (|V_{ud}|^2 + |V_{us}|^2 + |V_{ub}|^2) \\ &\approx\; 1 - (|V_{ud}|^2 + |V_{us}|^2) \approx 0.0005 \pm 0.0005 \lesssim 0.001. \end{aligned} \tag{3.57}$$

On the right hand side we estimate the error by adding the errors for V_{us} and V_{ud} in quadrature and in the next step adding the small deviation from unity.

The resulting limit on $g_{e\mu}^L$ is shown as black vertical dash-dotted line in Fig. 3.14 and again only applies if we take the lepton coupling to be purely left- instead of right-handed. In principle, we could also derive limits from the angular dependence of the decay of polarized muons used to search for right-handed currents in Ref. [217]. However, for these constraints to be effective requires the presence of both left- and right-handed couplings which we do not consider in the lepton sector.

Tau decays

Due to its large mass $m_\tau = 1776.86 \pm 0.12$ MeV [13], the τ-lepton has a much richer decay phenomenology than the muon. In particular, decays into a multitude of hadronic final states are kinematically accessible. In the following we want to discuss the impact of our model on various τ decay modes. We will treat the leptonic and hadronic decay modes separately.

Leptonic mode Due to our choice of allowing only for a single non-zero flavor-changing coupling in the lepton sector, either $g_{e\tau}$ or $g_{\mu\tau}$, a strong constraint on our model can be obtained by comparing the branching ratios of the two channels $\tau \to \mu\bar{\nu}\nu$ and $\tau \to e\bar{\nu}\nu$ [216] within our model (in [218] a comparison with the SM branching ratio is used). In order to illustrate how the corresponding constraint arises, let us for concreteness consider the case of a non-zero $\mu\tau$-coupling first. In the following, we strongly rely on the derivation of this limit in Ref. [216].

A non-zero coupling $g_{\mu\tau}$ leads to an enhancement of the partial decay rate of the process $\tau \to \mu\bar{\nu}\nu$ according to Eq. (3.54). Defining the ratio of the partial decay rates corresponding to $\tau \to \mu\bar{\nu}\nu$ and $\tau \to e\bar{\nu}\nu$,

$$R_{\mu/e} \equiv \frac{\Gamma_{\tau\to\mu\bar{\nu}\nu}}{\Gamma_{\tau\to e\bar{\nu}\nu}}\,, \tag{3.58}$$

we can rewrite Eq. (3.54) as

$$R_{\mu/e} = R_{\mu/e}^{\mathrm{SM}} \left[(1 + x_{\mu\tau})^2 + x_{\mu\tau}^2 + 2\, y_{\mu\tau}^2 \right] . \tag{3.59}$$

Within the SM, the ratio $R_{\mu/e}$ has been very accurately calculated [219] to

$$R_{\mu/e}^{\mathrm{SM}} = 0.972559 \pm 0.000005 . \tag{3.60}$$

For the experimentally determined value, we follow [216, 219] and quote a precise measurement[9] by the BaBar collaboration [222] yielding a value of

$$R_{\mu/e} = 0.9796 \pm 0.0039 . \tag{3.61}$$

This precise measurement is in slight disagreement with the SM prediction and the relative deviation amounts to $1.8\,\sigma$ [219] or

$$\Delta\mathcal{R}_{\mu/e} = \frac{R_{\mu/e}}{R_{\mu/e}^{\mathrm{SM}}} - 1 = 0.0072 \pm 0.0040 . \tag{3.62}$$

By virtue of Eq. (3.59) we can turn this observed deviation into a constraint on our model. Recall that in order for this limit to be present we require a non-zero left-handed lepton coupling $g_{\mu\tau}^L$ (as in the SM neutrinos are purely left-handed). In the general case, where both left- and right-handed lepton couplings are present, we obtain the limit as

$$g_{\mu\tau}^R \leq \frac{g}{2\sqrt{1+\rho_\ell^2}} \frac{M_{Z'}}{M_W} \left[\left(1 + 2\,(1 + \rho_\ell^{-2})\, \Delta\mathcal{R}_{\mu/e} \right)^{\frac{1}{2}} - 1 \right]^{\frac{1}{2}} . \tag{3.63}$$

Next, let us consider the inverse case of non-zero $e\tau$-coupling. In this scenario, the derivation of the limit proceeds analogous to the $\mu\tau$-case, however, using the inverted fraction of branching ratios

$$R_{e/\mu} \equiv \frac{\Gamma_{\tau\to e\bar{\nu}\nu}}{\Gamma_{\tau\to\mu\bar{\nu}\nu}} = \frac{1}{R_{\mu/e}} . \tag{3.64}$$

It is worth noticing that in the case of the inverted fraction $R_{e/\mu}$ the relative deviation of the experimental value from the SM prediction as discussed in Eq. (3.62) becomes negative

$$\Delta\mathcal{R}_{e/\mu} = \frac{R_{e/\mu}}{R_{e/\mu}^{\mathrm{SM}}} - 1 = -0.0072 \pm 0.0040 . \tag{3.65}$$

From Eq. (3.54) we see that structurally the Z' contribution from a non-vanishing $g_{e\tau}$ coupling will always lead to a positive shift in $R_{e/\mu}$. Therefore, the measured fluctuation leading to a negative shift will impose a very stringent bound on $g_{e\tau}$ (cf. Fig. 3.15).

In either case of non-zero lepton coupling $g_{e\tau}$ or $g_{\mu\tau}$, we defined the relative deviation $\Delta\mathcal{R}$ plus the $2\,\sigma$ uncertainty as exclusion bound. The corresponding limits are shown for example in Figs. 3.15 and 3.16 as the vertical black dash-dotted lines. It can be seen that

[9] We want to point out that previously also the ARGUS [220] and CLEO [221] collaboration have determined the branching ratios entering $R_{\mu/e}$. These less precise measurement also enter the PDG world average [214] $R_{\mu/e}^{\mathrm{PDG}} = 0.976 \pm 0.04$.

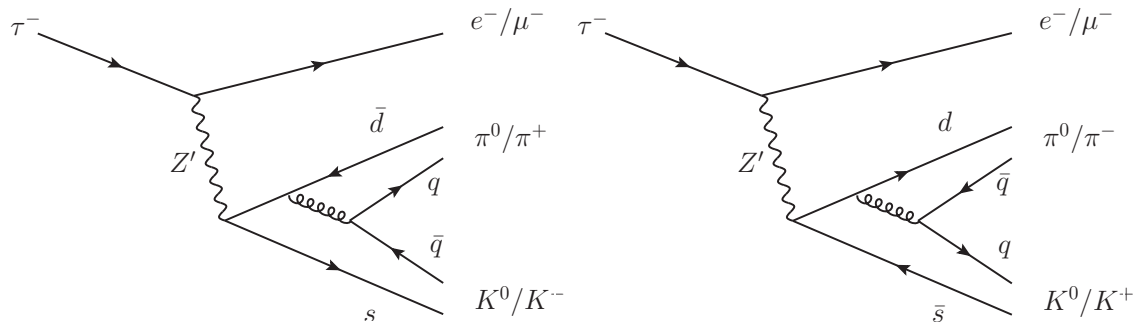

Figure 3.8: Diagrams of a possible signature of a doubly flavor-changing Z' boson with non-zero couplings in the sd and $e\tau/\mu\tau$ sector (q denotes either a d- or a u-quark). The resulting decays are $\tau^\pm \to \ell^\pm (\pi^0 K^0/\pi^\pm K^\mp)$, where $\ell \in \{e, \mu\}$. Only in the sd sector such a semi-leptonic τ decay into a pion and a kaon is kinematically allowed. Especially for a non-zero quark coupling involving a b-quark such a decay is not possible.

leptonic decay modes of the tau yield by far the strongest limits in the $e\tau$ and $\mu\tau$ sectors. They cut far into the region of parameter space testable with multipurpose experiments at the LHC. However, it has to be kept in mind that these limits apply only if we consider purely left- (or mixed) instead of right-handed lepton couplings $g^L_{\ell_i \ell_j}$. In the right-handed case these limits are absent.

If we assume the previously discussed $1.8\,\sigma$ relative deviation in the fraction of branching ratios Eq. (3.62) not to be due to systematics or a fluctuation, we can speculate on a possible new physics origin. In order to justify such speculation, we checked with help of the accurate prediction of $R^{\rm SM}_{\mu/e}$ given in Ref. [219] and the measured tau lifetime that the excess $\Delta\mathcal{R}_{\mu/e}$ is indeed due to the observed value of $\Gamma_{\tau\to\mu\bar{\nu}\nu}$ being significantly higher than its SM prediction. As a matter of fact it has been noticed in previous work [223] that the relative deviation

$$\frac{\Gamma_{\tau\to\mu\bar{\nu}\nu}}{\Gamma^{\rm SM}_{\tau\to\mu\bar{\nu}\nu}} - 1 = (0.69 \pm 0.29)\%\,, \tag{3.66}$$

even amounts to $2.4\,\sigma$. The resulting increase in the total width $\Gamma_{\rm tot}$ of the tau is compatible with the corresponding observed value. Within our Z' model we can fit this excess with a non-zero $g^L_{\mu\tau}$ coupling of $\mathcal{O}(10^{-1})$. We will speculate on such an explanation in Section 3.4.2.

Hadronic mode The search for rare hadronic tau decays opens a unique opportunity for testing our model. In the presence of a non-vanishing g_{sd} and either $g_{e\tau}$ or $g_{\mu\tau}$ coupling[10], the Z' will mediate the decay $\tau^\pm \to \ell^\pm (\pi^0 K^0/\pi^\pm K^\mp)$ with $\ell \in \{e, \mu\}$ due to the diagrams shown in Fig. 3.8. As this mode is not present in the SM, the detection of such a decay would be a smoking gun for a doubly flavor-changing Z'. It should be noted that such a

[10]For a recent example of an explicit model with flavor-violating couplings in the quark sector as well as non-vanishing lepton couplings, motivated by observed anomalies in B decays as well as $(g-2)_\mu$, see [224].

decay is only possible into pions and kaons as decays into B and D mesons are kinematically not allowed.

The corresponding decays into charged meson final states $\tau^- \to \ell^- \pi^\pm K^\mp$ and $\tau^+ \to \ell^+ \pi^\pm K^\mp$ have been searched for at BaBar [225] and Belle [226]. We can derive bounds on the Z' couplings $g_{\ell\tau}$ and g_{sd} from the observed limits on the corresponding branching ratios via the techniques we developed in Section 3.3.3. The relevant operators contributing to these processes are again those of Eqs. (3.28) and (3.29) with corresponding Wilson coefficients given in Eq. (3.30). In order to calculate the branching fraction due to the Z'-induced decay we require the hadronic matrix elements $\langle \pi^+ K^- | (\bar{s}d)_{L/R} | 0 \rangle$, where we have introduced the shorthand $(\bar{s}d)_{L/R} = \bar{s}\,\gamma_\mu P_{L/R} d$. Analogously to Section 3.3.3, we will use isospin symmetry to estimate the matrix element from the observed decay $\tau \to \nu_\tau K^- \pi^0$. The corresponding SM operator for this decay reads

$$\mathcal{O}_{\tau\nu} = (\bar{\nu}_\tau \gamma^\mu P_L \tau)(\bar{s}\,\gamma_\mu P_L u)\,, \tag{3.67}$$

with its Wilson coefficient given by $C_{\tau\nu} = 2\sqrt{2}\,G_F\,V_{us}$. In the following, we assume the electron and muon to be massless, which is justified as $m_e, m_\mu \ll m_\tau$. However, this implies that the outgoing leptons have definite chirality, which leads to distinguishable final states. Therefore, the fraction of branching ratios reads

$$\frac{\Gamma_{\tau^- \to \ell^- \pi^+ K^-}}{\Gamma_{\tau^- \to \nu_\tau \pi^0 K^-}} = \left(\frac{1}{2\sqrt{2}\,G_F\,V_{us}\,M_{Z'}^2} \right)^2 \frac{\left| g_{\ell\tau}^L \langle \ell | (\bar{\ell}\tau)_L | \tau \rangle \right|^2 + \left| g_{\ell\tau}^R \langle \ell | (\bar{\ell}\tau)_R | \tau \rangle \right|^2}{\left| \langle \nu_\tau | (\bar{\nu}_\tau \tau)_L | \tau \rangle \right|^2} \times \frac{\left| g_{sd}^L \langle \pi^+ K^- | (\bar{s}d)_L | 0 \rangle + g_{sd}^R \langle \pi^+ K^- | (\bar{s}d)_R | 0 \rangle \right|^2}{\left| \langle \pi^0 K^- | (\bar{s}u)_L | 0 \rangle \right|^2}\,. \tag{3.68}$$

Treating the leptons as massless translates into $\langle \ell | (\bar{\ell}\tau)_L | \tau \rangle \simeq \langle \nu_\tau | (\bar{\nu}_\tau \tau)_L | \tau \rangle$. Furthermore, we use isospin symmetry to relate the hadronic matrix elements

$$\langle \pi^+ K^- | (\bar{s}d)_L | 0 \rangle \simeq \sqrt{2}\,\langle \pi^0 K^- | (\bar{s}u)_L | 0 \rangle\,. \tag{3.69}$$

As QCD is a non-chiral theory, the same relation holds also with the operator $(\bar{s}d)_L$ replaced by $(\bar{s}d)_R$. With these assumptions we can use Eq. (3.68) to estimate the branching fraction

$$\Gamma_{\tau^- \to \ell^- \pi^+ K^-} \simeq \left(\frac{g_{\ell\tau}^R\, g_{sd}^R}{2\,G_F\,M_{Z'}^2} \right)^2 \frac{(1+\rho_\ell^2)\,|1+\rho_q|^2}{|V_{us}|^2}\,\Gamma^{\text{exp}}_{\tau^- \to \nu_\tau \pi^0 K^-}\,. \tag{3.70}$$

This relation allows us to constrain $g_{\ell\tau}$ and g_{sd} from the limits on $\Gamma_{\tau^- \to \ell\,\pi^+ K^-}$, observed by the Belle collaboration [226],

$$\Gamma_{\tau^- \to e^- \pi^+ K^-} < 5.6 \times 10^{-8}\,, \tag{3.71}$$

$$\Gamma_{\tau^- \to \mu^- \pi^+ K^-} < 16 \times 10^{-8}\,. \tag{3.72}$$

From these constraints, we have derived the corresponding bounds in the $\{sd, e\tau\}$ and $\{sd, \mu\tau\}$ sector. These are shown as the purple areas in the lower left panels of Figs. 3.15 and 3.16. It can be observed that the ATLAS bounds from the 8 TeV dilepton dataset are almost entirely lying within the purple areas. However, the LHC Run II and the HL-LHC scenarios are expected to yield superior limits along the direction of small $g_{\ell\tau}$ and g_{sd}.

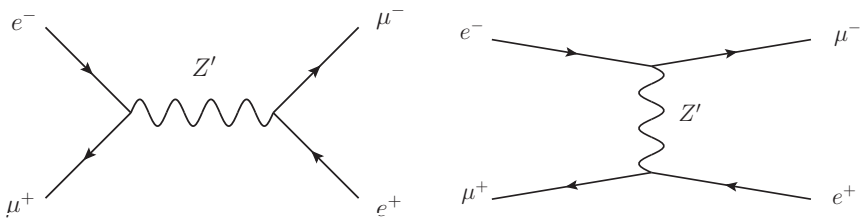

Figure 3.9: Diagrams leading to muonium-antimuonium oscillations from Z' exchange in the case of non-zero $g_{e\mu}$ coupling.

3.3.5 Muonium – antimuonium oscillations

The two leptons e^- and μ^+ can form a hydrogen-like bound state called muonium M. In presence of flavor-changing processes this bound state can oscillate into its conjugate state consisting of $e^+\mu^-$ – the antimuonium $\overline{M}$. The MACS experiment at the Paul Scherrer Institut in Villigen, Switzerland has searched for $M - \overline{M}$ transitions in a muon fixed target experiment. The non-observation of such transitions gives an upper bound for the probability of spontaneous muonium to antimuonium conversion $P_{M\overline{M}} \leq 8.2 \times 10^{-11}$ at 90 % C.L. [227].

In our model we have tree-level contributions to $M - \overline{M}$ transitions from the diagrams depicted in Fig. 3.9. As in the case of meson mixing discussed in Section 3.3.1, these diagrams generate a transition matrix element $\mathcal{M}_{M\overline{M}}$, which induces a mass splitting of the two states [228] as

$$|\Delta M| = 2\,|\mathrm{Re}\,(\mathcal{M}_{M\overline{M}})|\,. \tag{3.73}$$

Following the logic of Section 3.3.1, we can derive the mass splitting of the two bound states in an EFT approach. From our model Lagrangian Eq. (3.2) we obtain the low-energy interaction corresponding to the processes of Fig. 3.9 encoded in the operators

$$\mathcal{O}_{e\mu}^{XY} = (\bar{\mu}\,\gamma^\nu\,P_X\,e)(\bar{\mu}\,\gamma_\nu\,P_Y\,e)\,, \tag{3.74}$$

where $X, Y \in \{L, R\}$ and the corresponding Wilson coefficients are given by

$$C^{XY} = 2\,\frac{g_{e\mu}^X\,g_{e\mu}^Y}{M_{Z'}^2}\,. \tag{3.75}$$

As muonium is a non-relativistic Coulomb bound state, we can calculate the amplitude via a non-relativistic field expansion. The transitions $M - \overline{M}$ can be described by a non-relativistic effective potential $V_{\mathrm{eff}}(\vec{x})$, which we obtain from the Born approximation. Taking into account that the two fermions can either be in a spin singlet or triplet bound state we obtain the two effective potentials

$$V_{\mathrm{singlet}}(\vec{x}) = \;\; 2\,[C^{LL} - 2\,C^{LR} + C^{RR}]\;\delta^{(3)}(\vec{x})\,, \tag{3.76}$$

$$V_{\mathrm{triplet}}(\vec{x}) = -2\,[C^{LL} + 2\,C^{LR} + C^{RR}]\;\delta^{(3)}(\vec{x})\,. \tag{3.77}$$

Assuming the muonium to be in its electronic ground state, we can calculate the mass splitting [228] as

$$|\Delta M| \simeq 2\,\langle\overline{M}|(|\mathrm{Re}\,V_{\mathrm{eff}}(\vec{x})|)|M\rangle = 2\int \mathrm{d}^3x\;\phi^*_{100}(\vec{x})\,|\mathrm{Re}\,V_{\mathrm{eff}}(\vec{x})|\,\phi_{100}(\vec{x}) \tag{3.78}$$

$$= \frac{4}{\pi\,a^3_{M\overline{M}}}\;\left|C^{LL} \mp 2\,C^{LR} + C^{RR}\right|\,, \tag{3.79}$$

with the Bohr radius of the muonium $a_{M\overline{M}} = 1/(\alpha\,m_{\mathrm{red}})$ and the reduced mass $m_{\mathrm{red}} = m_e\,m_\mu/(m_e+m_\mu)$. In order to get in contact with the experiment, we need to know the transition probability $P_{M\overline{M}}$ of an initially prepared muonium atom M to oscillate into $\overline{M}$. Therefore, we need to know the time evolution of the two-state system that is generally obtained by solving the Schrödinger equation [229]

$$i\,\frac{\mathrm{d}}{\mathrm{d}t}\begin{pmatrix}|M(t)\rangle\\ |\overline{M}(t)\rangle\end{pmatrix} = \begin{pmatrix}M - i\frac{\Gamma}{2} & \frac{\Delta M}{2}\\ \frac{\Delta M}{2} & M - i\frac{\Gamma}{2}\end{pmatrix}\begin{pmatrix}|M(t)\rangle\\ |\overline{M}(t)\rangle\end{pmatrix}\,. \tag{3.80}$$

After diagonalizing the Hamiltonian of Eq. (3.80) the time evolution of an initially pure muonium state is found to be given by

$$|M(t)\rangle = \left(\cos\left(\frac{\Delta M}{2}t\right)|M\rangle + i\sin\left(\frac{\Delta M}{2}t\right)|\overline{M}\rangle\right)e^{-\frac{\Gamma}{2}t}\;e^{iMt}\,. \tag{3.81}$$

If the system is mainly in the antimuonium state, it consists of an e^+ and a μ^-. In this case, the muon will decay via $\mu^- \to e^-\,\bar{\nu}_e\,\nu_\mu$ with a highly energetic electron being radiated off. In the reverse case of muonium, the radiated particle instead would be a highly energetic positron. Hence, the measurement principle to detect whether muonium has oscillated into antimuonium is quite straight-forward. Starting from a pure muonium initial state, one searches for highly energetic electrons resulting from the muon decay inside the potential antimuonium bound state. Thus, the search strategy boils down to a counting experiment of outgoing energetic electrons.

We can determine the total number of expected electrons within our model from the integrated partial decay rate of the system into electrons, which is given by the probability of the system being in an antimuonium state multiplied by the muon decay rate. Integration over time yields [230]

$$P_{M\overline{M}} = \int_0^\infty \mathrm{d}t\;\Gamma_\mu\,\sin^2\left(\frac{\Delta M}{2}\,t\right)\,e^{-\Gamma_\mu\,t} = \frac{1}{2\left(\frac{\Gamma_\mu^2}{\Delta M^2}+1\right)}\,. \tag{3.82}$$

Assuming either left- or right-handed lepton couplings this can be directly translated into a limit on the off-diagonal lepton coupling of the Z' as

$$|g^{L/R}_{e\mu}| \leq \frac{1}{S_B}\left[\frac{\pi\,M^2_{Z'}\,\Gamma_\mu}{8\,\alpha^3\,m^3_{\mathrm{red}}}\;\left(\frac{2P_{M\overline{M}}}{1-2P_{M\overline{M}}}\right)^{\frac{1}{2}}\right]^{\frac{1}{2}}\,, \tag{3.83}$$

where $S_B = 0.35$ [228] is a correction factor for the muonium splitting in the magnetic field coming from the $(V\pm A)\times(V\pm A)$ Lorentz structure of the interaction.

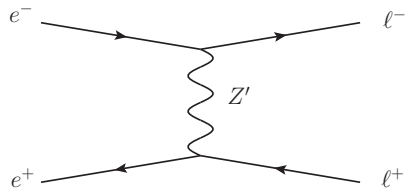

Figure 3.10: Tree-level dilepton production via Z' at LEP, where ℓ is either the μ or the τ.

The resulting limit os illustrated in the plots in Fig. 3.14 by the magenta band. As this limit is purely leptonic, the corresponding bound results in a vertical exclusion line. Due to the very stringent bound on $P_{M\overline{M}}$ [227], this is the strongest limit in the lepton sector alone, if pure right-handed couplings are assumed. In contrast, ATLAS can probe $e\mu$ couplings significantly smaller than those excluded in muonium oscillation experiments. However, this is only true in combination with a same order-of-magnitude quark-sector coupling, while the muonium limits are independent of the quark couplings. Finally, as muonium is a bound state of e^+ and μ^- the $e\tau$ and $\mu\tau$ sectors are completely unaffected by this limit. The corresponding $e\tau$ or $\mu\tau$ bound states would be experimentally very difficult to access as the τ decays very rapidly.

3.3.6 LEP limits

The LEP collider produced a large amount of e^+e^- collisions. Hence, the analyses of $\mu^+\mu^-$ and $\tau^+\tau^-$ final states at LEP offer an experimentally very clean environment to search for lepton-flavor violation. Such final states can be produced from a t-channel Z' exchange within our model for non-zero $g_{e\mu}$ or $g_{e\tau}$ couplings. Hence, we can use the total inclusive cross sections $\sigma(e^+e^- \to \mu^+\mu^-)$ and $\sigma(e^+e^- \to \tau^+\tau^-)$ as measured by the ALEPH collaboration [231] in order to constrain these couplings.

For our analysis we have simulated the total inclusive cross section $\sigma_{Z'}$ for the two processes $e^+e^- \to \mu^+\mu^-$ and $e^+e^- \to \tau^+\tau^-$ with `MadGraph5 v2.3.3` [196] at $\sqrt{s} = 207$ GeV, including the Z' diagram shown in Fig. 3.10. Allowing for an additional hard photon in the final state, we have scanned $\sigma_{Z'}$ over a 2D grid of the lepton couplings $g_{e\mu}$ or $g_{e\tau}$ and the Z' mass $M_{Z'}$. In such a grid search, we can exclude all values of $g_{e\mu}$ and $g_{e\tau}$ which lead to a prediction of the cross section $\sigma_{Z'}$ inconsistent with its experimentally determined value σ_{exp}. We set the corresponding limits by performing a two-sided hypothesis test on the total inclusive cross section. At a given mass $M_{Z'}$, we exclude all coupling values that correspond to a cross section $\sigma \notin [\sigma_{\text{exp}} - 1.96\,\Delta\sigma, \sigma_{\text{exp}} + 1.96\,\Delta\sigma]$, corresponding to a two-sided 95% confidence interval for a Gaussian distribution. In order for this approach to be valid, we must assume that the measured cross section σ_{exp} (i.e the number of signal events) follows a Gaussian distribution. As the experimentally observed total number of events $N_{\mu\mu} = 683$ and $N_{\tau\tau} = 402$ at $\sqrt{s} = 207$ GeV [231] are relatively large, this assumption seems to be justified.

The corresponding limits in Figs. 3.14 and 3.15 are depicted by the golden regions. As was the case for the muonium, these limits are purely leptonic (and therefore correspond

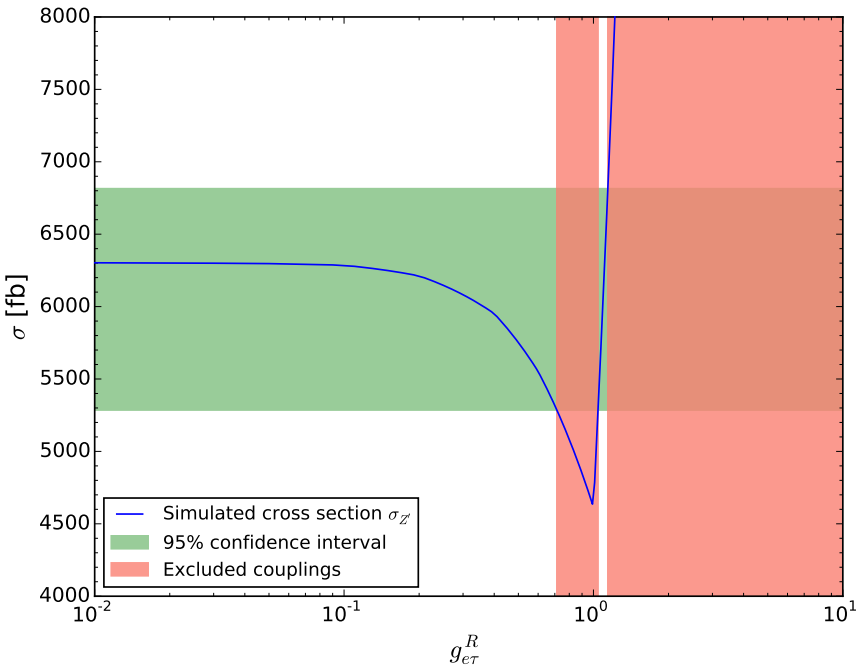

Figure 3.11: The blue curve is the total simulated cross section $\sigma_{Z'}$ for the process $e^+e^- \to \tau^+\tau^-$ at $\sqrt{s} = 207$ GeV. The green band depicts the 95% confidence interval of the measured cross section σ_{exp}. The red area shows the excluded couplings $g^R_{e\tau}$. Figure taken from [170].

to vertical bands in the $g_{qq'} - g_{\ell\ell'}$ plane). As LEP was an electron-positron collider, these limits do not concern the $\mu\tau$ sector. Generally, the LEP limits are weaker than the muonium limits and therefore are only of concern in the $e\tau$ sector (cf. Fig. 3.15) where the muonium limits are not present.

A particular feature of the LEP limits is the gap in the excluded region of parameter space. The origin of this gap can be understood with help of Fig. 3.11. For small couplings $g_{e\ell}$ the total cross section is mainly SM-like and agrees very well with the measurements (i.e. it lies within the 95% confidence interval). For moderate couplings $g_{e\ell} \lesssim 1$ the interference term, which is linear in $g_{e\ell}$ and has negative sign, starts to become important and eventually drives the cross section $\sigma_{Z'}$ below the confidence interval. This leads to the first exclusion band. With increasing couplings $g_{e\ell} > 1$ the pure Z' contribution, which is positive and quadratic in $g_{e\ell}$, starts to dominate and drives the cross section $\sigma_{Z'}$ well above the 95% confidence interval. This leads to the second exclusion band. In between those two regimes we have a transition region where $\sigma_{Z'}$ lies within the 95% confidence interval - the gap in the exclusion region.

3.3.7 Magnetic dipole moments

Two of the most precisely measured quantities in nature are the dimensionless magnetic moments g_e [9] and g_μ [93] of the electron and muon, respectively. The very high precision with which these observables have been determined make g_e and g_μ very sensitive for

possible new physics contributions. Furthermore, special attention has been drawn to the anomalous magnetic moment of the muon $a_\mu = (g_\mu - 2)/2$ in recent years as it exhibits a deviation between theory and experiment of about $3\,\sigma$ [93, 94, 232, 233].

We use this as motivation to study the impact of our flavor-changing Z' boson on the magnetic dipole moments $(g-2)$ of both the electron and muon. In view of the $(g-2)_\mu$ anomaly, we want to assess whether our Z' model can potentially explain the observed deviation similar to earlier work [216, 234–236].

Experimental status

Before analyzing the potential Z' contributions to $(g-2)$ in detail, we will first review the experimental status of the electron and muon anomalous magnetic moment.

We will start the discussion by looking at the determination of the dimensionless magnetic moment g_μ of the muon at the E821 experiment at the Brookhaven Alternating Gradient Synchrotron [237]. The naive SM tree-level calculation, i.e. the Dirac equation, yields for fermions a value of $g = 2$ [238, 239]. Radiative corrections such as higher-order QED processes [240, 241], electroweak loops [242], hadronic vacuum polarization [232, 233] or hadronic light-by-light scattering [243, 244] lead to a shift of the anomalous magnetic moment a_μ. Much interest has been triggered by the findings of the E821 experiment that point towards a mismatch between theory [232, 233] and experiment [93] of up to $\sim 3.6\,\sigma$[11] or

$$\Delta a_\mu = a_\mu^{\text{exp}} - a_\mu^{\text{SM}} = (2.87 \pm 0.80) \times 10^{-9}\,. \tag{3.84}$$

The currently running E989 experiment at Fermilab [96] plans to determine $(g-2)_\mu$ with a factor-of-four improvement in precision. If the central value of the measurement does not change, this will push the total significance of the excess above $5\,\sigma$.

In the case of the electron anomalous magnetic moment the picture is different. As the deviation between theory and experiment [246] only amounts to $\sim 1.3\,\sigma$, or

$$\Delta a_e = a_e^{\text{exp}} - a_e^{\text{SM}} = (-10.5 \pm 8.1) \times 10^{-13}\,, \tag{3.85}$$

the experimental result is in good agreement with the theoretical prediction. The uncertainty in Δa_e is expected to be reduced in the near future, enhancing its potential as a test of new physics. In light of these prospects, we will also investigate the shifts of the anomalous magnetic moment a_e of the electron due to Z' loops.

However, one subtlety that has to be taken into account is the fact that the determination of the fine structure constant α is often deduced from the electron magnetic moment measurement. Hence, in a consistent calculation of a potential new physics contribution to the electron magnetic moment, the used value of α should be determined by another independent measurement, as for example from atom recoil methods with cesium or rubidium atoms [247–250].

Anomalous magnetic moment constraints

At this point we will briefly discuss the calculation of the one-loop Z' contribution to the anomalous magnetic moment a_{f_a} of a fermion f_a due to the diagram of Fig. 3.12.

[11] We note that since the original publication of this work an improved analysis of the hadronic vacuum polarization contribution to a_μ appeared [245] pushing the total deviation to 3.7 σ.

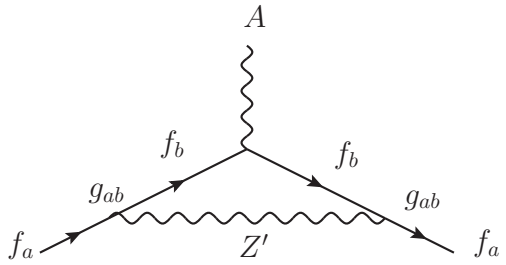

Figure 3.12: Diagram contributing to the anomalous magnetic moment of the fermion f_a due to a Z'-induced loop with two insertions of the flavor-violating coupling g_{ab} and the fermion f_b running in the loop.

Considering the Z' interaction with two generic fermions f_a and f_b,

$$\mathcal{L} = \bar{f}_a \, \gamma^\mu \, \left[g^L_{ab} \, P_L + g^R_{ab} \, P_R \right] f_b \, {Z'}_\mu + h.c. \,, \tag{3.86}$$

we can derive the Z' contribution to a_{f_a} due to f_b running in the loop [251]. Introducing the mass ratios $x_a = m_a/M_{Z'}$ and $x_b = m_b/M_{Z'}$ and the vector and axial-vector couplings $C_V = (g^R_{ab} + g^L_{ab})/2$ and $C_A = (g^R_{ab} - g^L_{ab})/2$, the calculation yields

$$\begin{aligned} a_{f_a}(Z') = -\frac{x_a^2}{8\pi^2} \int_0^1 \mathrm{d}u \Bigg[& u(u-1) \left(2\,(u-2)\,(C_V^2 + C_A^2) + 4\,\frac{x_a}{x_b}\,(C_V^2 - C_A^2) \right) \\ & - u^2\,\frac{x_a}{x_b} \left((x_b - x_a)^2\, C_V^2 - (x_b + x_a)^2\, C_A^2 \right) \\ & + u^2\,(u-1) \left((x_b - x_a)^2\, C_V^2 + (x_b + x_a)^2\, C_A^2 \right) \Bigg] \\ & \times \left[u\left((u-1)\, x_a^2 + x_b^2 \right) + (1-u) \right]^{-1} . \end{aligned} \tag{3.87}$$

Assuming only right-handed couplings (i.e. $C_V = C_A = g^R_{ab}/2$), we can use this relation to turn the observed shift Δa in the electron/muon magnetic moment into a limit on g^R_{ab}.

In order to get a better understanding of the asymptotic behavior of the Z' contribution to the anomalous magnetic moment, let us derive an approximate scaling formula. As we are mostly interested in Z' bosons in the multi-GeV range, we assume $M_{Z'} \gg m_a, m_b$. Therefore, we expand Eq. (3.87) for small ratios x_a and x_b. Keeping only the leading powers yields the approximate formula

$$a_{f_a} \approx \frac{(g^R_{ab})^2}{4\,\pi^2}\, x_a \, \left[x_b \, \rho_\ell - \frac{x_a}{3}\,(1 + \rho_\ell^2) \right] . \tag{3.88}$$

We can now use the shift in the electron magnetic moment Δa_e to constrain the off-diagonal couplings $g_{e\mu}$ and $g_{e\tau}$. From Eq. (3.88) we can see that in the case of purely right-handed lepton couplings ($\rho_\ell = 0$) the Z' contribution to the electron magnetic moment a_e is

suppressed compared to the muon magnetic moment a_μ by the factor

$$\frac{x_e^2}{x_\mu^2} \approx \frac{1}{(200)^2} \sim \mathcal{O}(10^{-5})\,. \tag{3.89}$$

On the other hand, comparing Eq. (3.85) and Eq. (3.84) we see that the uncertainties of Δa_e are smaller by four orders of magnitudes smaller than those of Δa_μ. Combining the smaller uncertainties with the mass suppression, the constraints from Δa_e are thus much weaker than those from Δa_μ. Therefore, Δa_e only plays a role as a constraint for very light Z' bosons[12]. However, for light Z' bosons we obtain rather strong limits from either LEP or muonium-antimuonium oscillation (cf. Figs. 3.14 and 3.15). Therefore, the constraint from Δa_e proves to be always subdominant in our model.

For the $\mu\tau$ sector the situation is more involved. For purely right-handed lepton couplings $g^R_{\mu\tau}$, the Z' contribution to Δa_μ is negative in contrast to the observed positive shift (cf. [216, 236]). As the current deviation between SM prediction and the measured value is greater than $3\,\sigma$ any contribution of such a Z' is ruled out at this level. Therefore, we show exclusions at the 4 and $5\,\sigma$ level in Fig. 3.16 as light and dark cyan bands. These limits are the only purely leptonic constraints in the $\mu\tau$ sector.

Explaining $(g-2)_\mu$

For a suitable chirality structure, the anomalous magnetic moment of the muon can get a positive shift due to radiative corrections from a Z' loop through a non-zero $\mu\tau$-coupling. Such a positive shift can potentially reconcile the experimental value with the theory prediction. A possible explanation of the observed deviation Δa_μ arises in models [234, 252], in which a light Z' boson couples to the (flavor-diagonal) $L_\mu - L_\tau$ current,

$$j_\alpha^{\mu-\tau} = \bar{L}_2\,\gamma_\alpha\,L_2 + \bar{\mu}_R\,\gamma_\alpha\,\mu_R - \bar{L}_3\,\gamma_\alpha\,L_3 - \bar{\tau}_R\,\gamma_\alpha\,\tau_R\,, \tag{3.90}$$

with $L_2 = (\nu_\mu, \mu_L)$ and $L_3 = (\nu_\tau, \tau_L)$. As we will see in Section 4.5.4, in these models neutrino trident production $\nu\,N \to \nu\,\mu^+\mu^-N$ in the Coulomb field of a nucleus N [234–236, 253] rules out an explanation of the $(g-2)_\mu$ tension for heavy Z' of $M_{Z'} \gtrsim$ GeV.

In our model, neutrino trident production is not an issue, however, as it requires flavor-diagonal couplings to μ and τ of the Z' at tree level. As we do not consider flavor-diagonal couplings, the neutrino trident constraints are not applicable to our model. Hence, in our case $(g-2)_\mu$ might still be explained for heavy Z' with a suitable pure $\mu\tau$-coupling [216]. In the future it may be possible to look for flavor-violating trident signals with $e\mu$, $e\tau$ or $\mu\tau$ in the final state at the DUNE [254] and SHiP [255, 256] facilities [257, 258].

An explanation of the observed positive shift Δa_μ of Eq. (3.84) requires thus a positive Z' contribution to a_μ. This is the case when the term in square brackets in Eq. (3.88) is positive[13]. This is a quadratic form in the coupling ratio ρ_ℓ of left- to right-handed

[12] If we assume vector couplings ($\rho_\ell = 1$), the leading term of the contribution to the electron magnetic moment a_e relative to the muon magnetic moment a_μ is suppressed only by a factor $x_e/x_\mu \approx 1/200 \sim \mathcal{O}(10^{-3})$. Furthermore, as the observed shift Δa_e is negative whereas we obtain a positive shift, a_e is a quite strong constraint for a vector coupling scenario.

[13] This approximate relation holds only in the case of heavy Z' bosons with $M_{Z'} \gg m_\tau$.

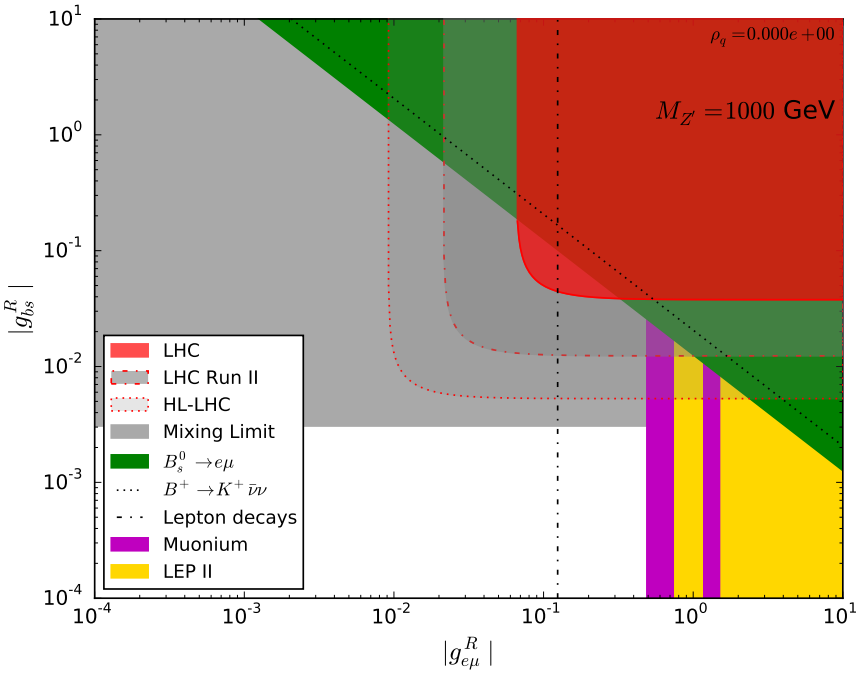

Figure 3.13: The flavor-violating couplings g_{bs}^R and $g_{e\mu}^R$ for a Z' boson of $M_{Z'} = 1000$ GeV with purely right-handed quark couplings ($\rho_q = 0$). In this case, the grey area represents the $B_s^0 - \bar{B}_s^0$ mixing limit. The red area indicates the limit from the ATLAS analysis of the process $pp \to e\mu$ at $\sqrt{s} = 8$ TeV. The red dash-dotted and dashed lines are projections to the LHC Run II and HL-LHC. The green area is the limit coming from the meson decay $B_s^0 \to e\mu$. The gold and magenta areas are purely leptonic limits coming from LEP and muonium oscillation constraints. The black dotted line is the neutrino exclusion limit from $B^+ \to K^+\bar{\nu}\nu$. The dash-dotted line originates from tests of lepton decays. However, these latter two limits only apply for left-handed lepton couplings. Figure adapted from [170].

$\mu\tau$-coupling and is positive only in the interval between its two roots

$$\rho_{\ell,0} = \frac{3}{2}\left[\frac{m_\tau}{m_\mu} \mp \sqrt{\left(\frac{m_\tau}{m_\mu}\right)^2 - \frac{4}{9}}\right] . \tag{3.91}$$

From this formula, we find that the Z' contribution to Δa_μ is positive in the interval $0.02 \lesssim \rho_\ell \lesssim 50.75$, so that there an explanation of the observed $(g-2)_\mu$ excess might be possible. In Section 3.4.2, we will consider two concrete scenarios where such an explanation is realized and discuss the phenomenological implications.

3.4 Results

The goal of this chapter is to investigate the sensitivity of resonance searches with multipurpose detectors at the LHC to flavor violation compared to a large set of flavor observables. In this context, meson mixing typically provides a very stringent bound on flavor-violation

in the quark sector. For example, the constraints on a Z' with $M_{Z'} = 1$ TeV with only non-zero right-handed couplings g^R_{bs} (i.e. $\rho_q = 0$) and $g^R_{e\mu}$ are shown in Fig. 3.13. The grey area shows the limits from $B^0_s - \bar{B}^0_s$ mixing in this case. We can see that this limits excludes all regions of parameter space that can be probed by the current (red area) or future (red dotted and dash-dotted curves) ATLAS limits. This makes searches for flavor violation at multipurpose detectors at the LHC seem unfeasible for a generic model. However, as we have seen in Section 3.3.1, for certain values ρ_0 of the ratio of left- to right-handed quark sector couplings, the limits from meson mixing are subject to cancellation effects.

In the following section, we show exclusion plots for a 1 TeV Z' always for the coupling ratio ρ_0 where the corresponding mixing limit vanishes. For example, from the plot in the upper left panel of Fig. 3.14, we can see that for the scenario with non-zero couplings $\{g_{bs}, g_{e\mu}\}$ just considered, mixing cancellation occurs for $\rho_0 = 0.1276$ with the tolerance $\Delta\rho_- = 0.0006$ and $\Delta\rho_+ = 0.0021$. This means that in this example for $\rho_q \in [0.1270, 0.1297]$, the mixing limit will be less stringent than the ATLAS limit we can set in the regime of large values of $g^R_{e\mu}$.

3.4.1 Benchmark scenario

In this section, we summarize the results of our analysis of the full set of flavor-violating couplings $\{g_{qq'}, g_{\ell\ell'}\}$ with $qq' \in \{sd, bs, bd, cu\}$ and $\ell\ell' \in \{e\mu, e\tau, \mu\tau\}$ exemplified for the benchmark scenario of a Z' boson with a mass of $M_{Z'} = 1$ TeV. Figs. 3.14 to 3.16 show the results in each of the three lepton sectors, $e\mu$, $e\tau$ and $\mu\tau$, respectively.

In the region of parameter space shown here, where meson mixing limits are subject to cancellation effects, the limits from the reinterpreted ATLAS dilepton search (shown as red areas) can exclude previously unprobed parameter space only along the direction of both small quark and lepton sector coupling. The ATLAS limits are generally strongest in the $e\mu$ sector and weakest in the $\mu\tau$ sector. These limits are expected to improve roughly by a factor of ~ 3 in the LHC Run II scenario (illustrated by the red dash-dotted lines) and another additional factor of ~ 2 in the HL-LHC scenario (illustrated by the red dotted lines) in both the quark and lepton sector couplings. For a generic chirality structure of the couplings, however, the ATLAS limits are eclipsed by limits from meson mixing as illustrated in Fig. 3.13.

Meson decays into a pair of charged leptons are sensitive to the product of quark and lepton sector couplings. They lead to moderate constraints of $g_{qq'} g_{\ell\ell'} \lesssim \mathcal{O}(1)$ (depicted by the green areas). Meson decay limits are in general stronger for $e\mu$ final states than for $e\tau$ and $\mu\tau$ final states. Let us note that the limits from meson decays are absent in the cu sector.

For pure quark sector couplings, dijet searches at the LHC (shown as brown areas) can exclude coupling values of $g_{qq'} \lesssim \mathcal{O}(1)$. However, the bs sector is entirely unaffected by these limits. In the lepton sector, LEP resonance searches (gold vertical bands) in dimuon and ditau final states constrain the couplings $g^R_{e\mu}$ and $g^R_{e\tau}$ to values of $\lesssim \mathcal{O}(1)$. In the $e\mu$ sector, an additional more stringent constraint arises from muonium oscillations (magenta vertical band), leading to the bound of $g^R_{e\mu} \lesssim 0.5$. Finally, only the $\mu\tau$ sector receives sizable constraints from the (muon) anomalous magnetic moment due to the large contribution of the heavy tau running in the loop. The 4 and $5\,\sigma$ level exclusion limits

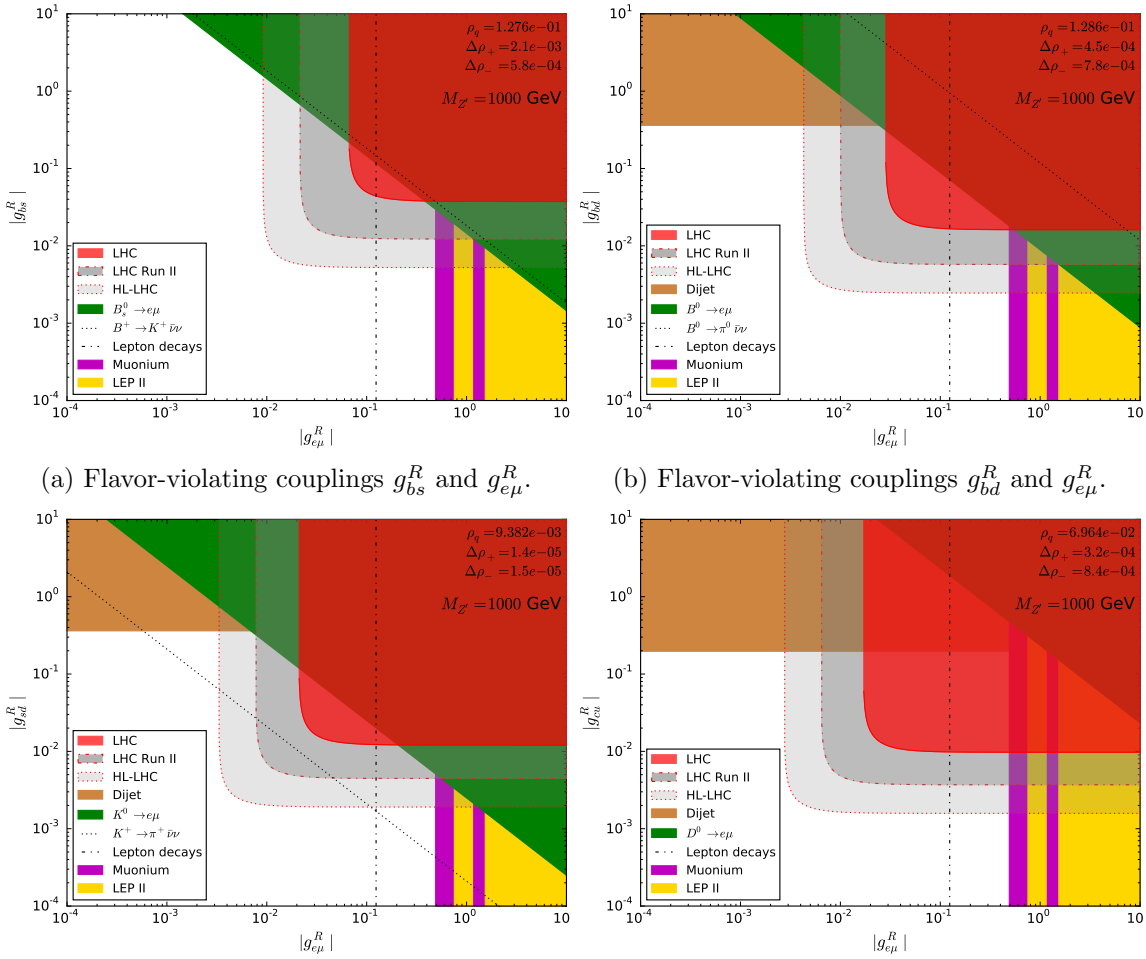

(a) Flavor-violating couplings g_{bs}^R and $g_{e\mu}^R$.

(b) Flavor-violating couplings g_{bd}^R and $g_{e\mu}^R$.

(c) Flavor-violating couplings g_{sd}^R and $g_{e\mu}^R$.

(d) Flavor-violating couplings g_{cu}^R and $g_{e\mu}^R$.

Figure 3.14: Flavor-violating couplings in the $e\mu$ sector for a Z' boson of $M_{Z'} = 1$ TeV. The red areas depict the limits from the ATLAS analysis of the process $pp \to e\mu$ at $\sqrt{s} = 8$ TeV. The red dash-dotted and dashed lines are projections to the LHC Run II and HL-LHC. The brown areas show four-quark contact interaction limits from LHC dijet analyses [193]. The green areas are the limits coming from meson decays into charged leptons. The gold and magenta areas are purely leptonic limits coming from LEP and muonium oscillation constraints. The black dotted lines are meson decay limits into neutrinos and the black dash-dotted line the limits from muon decays. These last two limits, however, apply only for left-handed lepton couplings $g_{e\mu}^L$ instead of $g_{e\mu}^R$. The meson decay limits into neutrinos are absent in the cu sector completely. Figure taken from [170].

of the $(g-2)_\mu$ measurements (depicted by the cyan vertical bands in Fig. 3.16) yield the constraints of $g_{\mu\tau}^R \lesssim 2$ and $g_{\mu\tau}^R \lesssim 3.5$, respectively.

Much more severe constraints arise if we assume that the lepton flavor-violating couplings extend also to the neutrino sector. In this case, decays of the muon and tau lead to strong constraints in the lepton sector. However, as we are concerned with pure SM

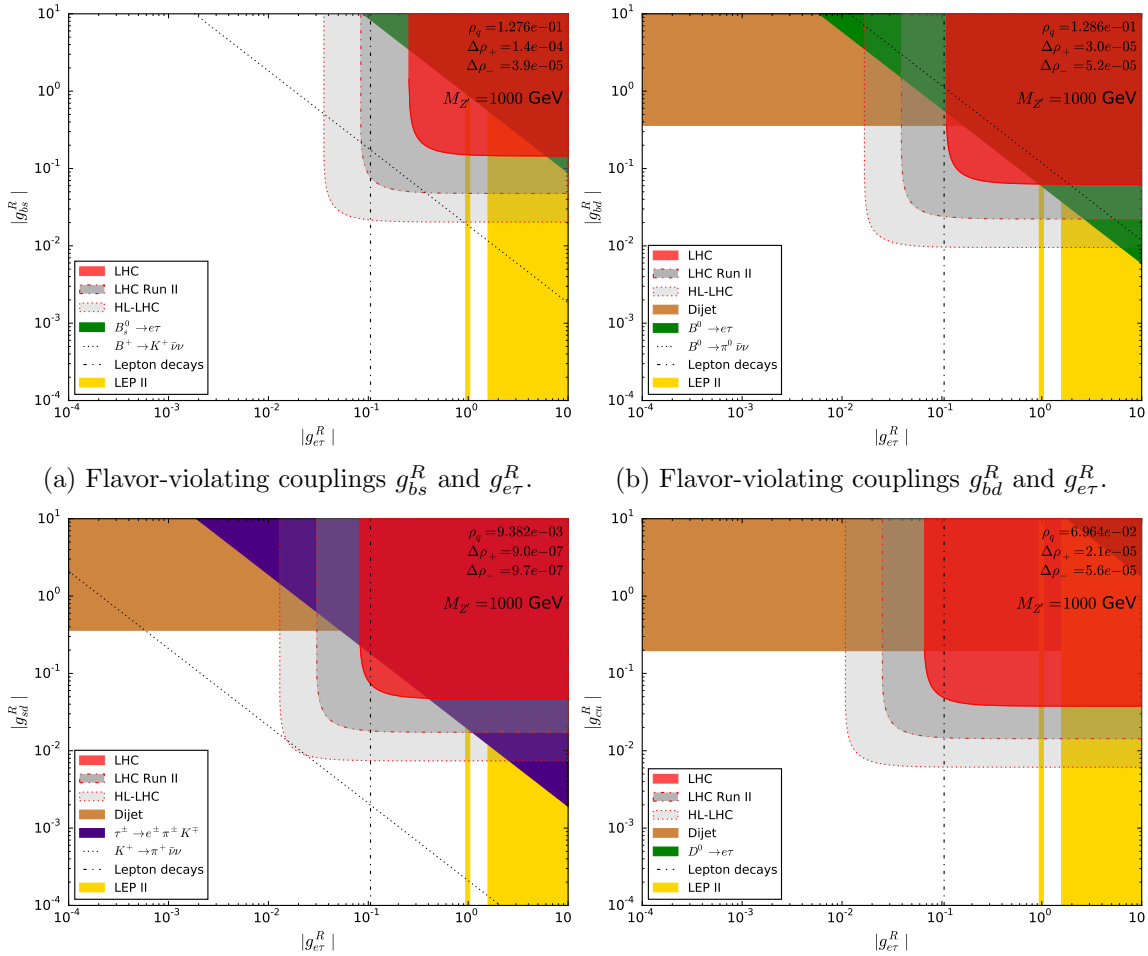

(a) Flavor-violating couplings g_{bs}^R and $g_{e\tau}^R$.

(b) Flavor-violating couplings g_{bd}^R and $g_{e\tau}^R$.

(c) Flavor-violating couplings g_{sd}^R and $g_{e\tau}^R$.

(d) Flavor-violating couplings g_{cu}^R and $g_{e\tau}^R$.

Figure 3.15: Flavor-violating couplings in the $e\tau$ sector for a Z' boson of $M_{Z'} = 1$ TeV. The red areas depict the limits from the ATLAS analysis of the process $pp \to e\tau$ at $\sqrt{s} = 8$ TeV. The red dash-dotted and dashed lines are projections to the LHC Run II and HL-LHC. The brown areas show four-quark contact interaction limits from LHC dijet analyses [193]. The green areas are the limits coming from meson decays into charged leptons. In purple we show the bounds from the rare decay $\tau^- \to e^-\pi^+K^-$ only applicable in the sd sector. The gold areas are purely leptonic limits coming from LEP constraints. The black dotted lines are meson decay limits into neutrinos and the black dash-dotted line the limits from lepton decays. These last two limits, however, apply only for left-handed lepton couplings $g_{e\tau}^L$ instead of $g_{e\tau}^R$. The meson decay limits into neutrinos are absent in the cu sector completely. Figure taken from [170].

neutrino fields, this would require left-handed couplings. The corresponding lepton decay limits are depicted by the black dash-dotted vertical lines and only apply for $g_{\ell\ell'}^R$ replaced by $g_{\ell\ell'}^L$. Similarly, an additional strong constraint would arise in the case of left-handed lepton couplings from semi-hadronic meson decays with neutrinos in the final states (shown

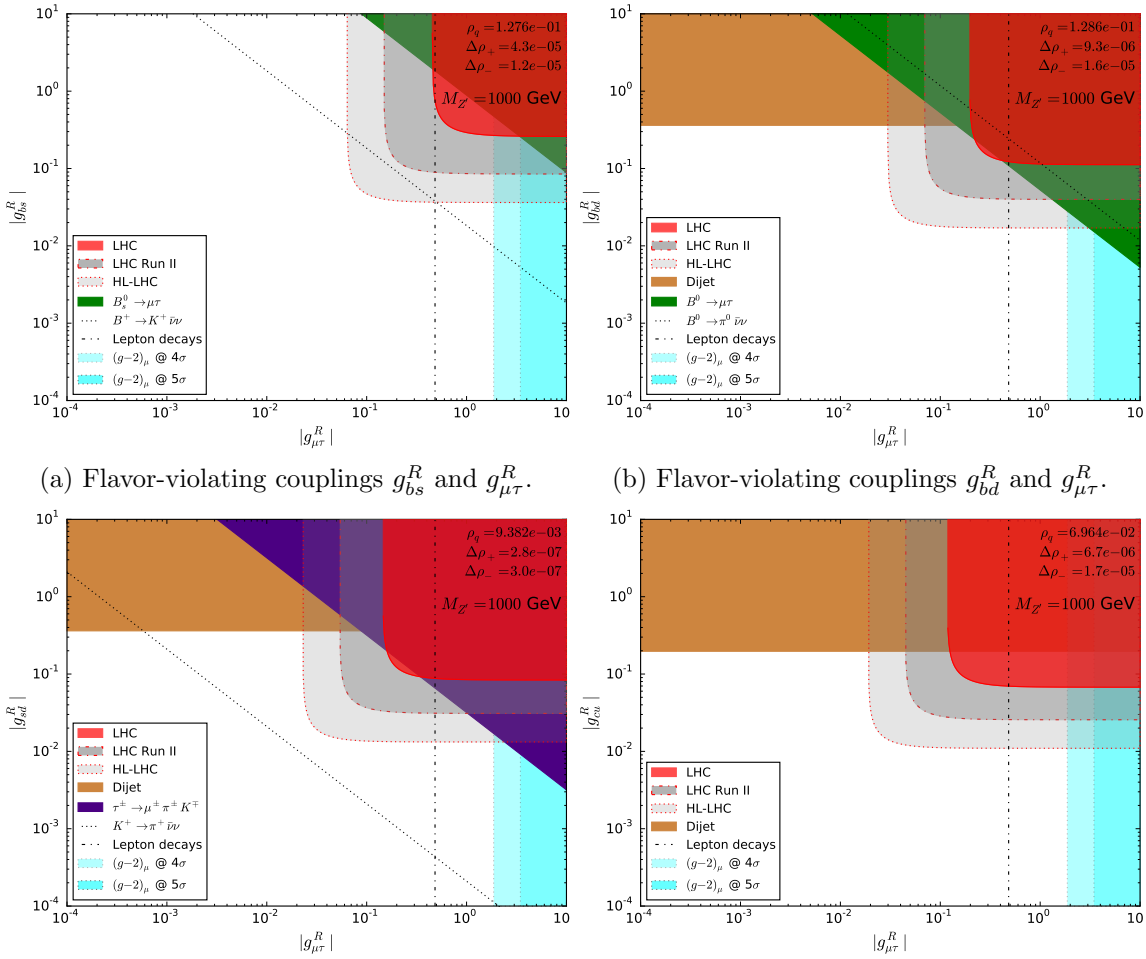

(a) Flavor-violating couplings g^R_{bs} and $g^R_{\mu\tau}$.

(b) Flavor-violating couplings g^R_{bd} and $g^R_{\mu\tau}$.

(c) Flavor-violating couplings g^R_{sd} and $g^R_{\mu\tau}$.

(d) Flavor-violating couplings g^R_{cu} and $g^R_{\mu\tau}$.

Figure 3.16: Flavor-violating couplings in the $\mu\tau$ sector for a Z' boson of $M_{Z'} = 1$ TeV. The red areas depict the limits from the ATLAS analysis of the process $pp \to \mu\tau$ at $\sqrt{s} = 8$ TeV. The red dash-dotted and dashed lines are projections to the LHC Run II and HL-LHC. The brown areas show four-quark contact interaction limits from LHC dijet analyses [193]. The green areas are the limits coming from meson decays into charged leptons. In purple we show the bounds from the rare decay $\tau^- \to \mu^-\pi^+K^-$ only applicable in the *sd* sector. The light and dark cyan areas depict the 4 and 5 σ exclusion bands from Δa_μ. The black dotted lines are meson decay limits into neutrinos and the black dash-dotted line the limits from lepton decays. These last two limits, however, apply only for left-handed lepton couplings $g^L_{\mu\tau}$ instead of $g^R_{\mu\tau}$. The meson decay limits into neutrinos are absent in the *cu* sector completely. Figure taken from [170].

by the black dotted lines). For the peculiar coupling combination $\{g^R_{sd}, g^R_{\mu\tau}\}$ an extra constraint (purple area) emerges from the search for the decay $\tau \to \mu\,\pi^\pm K^\mp$, which can be mediated by the Z' at tree level in this case.

We have performed this analysis for a large range of masses 200 GeV $\leq M_{Z'} \leq$ 2900

GeV. The corresponding exclusion plots can be found under the URL in [198]. The qualitative picture does not change for different masses of the Z' boson. In general, all limits weaken with increasing $M_{Z'}$. Except for the case of direct production at the LHC, the limits typically scale as $g \sim M_{Z'}$. At a given Z' boson mass, the limits tend to be strongest in the $e\mu$ sector and weakest in the $\mu\tau$ sector.

3.4.2 Hints for new physics

In Section 3.3.4, we have argued that the observed excess in the lepton decay ratio $\mathcal{R}_{\mu/e}$ could be due to a new physics effect. From Eqs. (3.55) and (3.59) we see that in order to be able to explain this excess with our Z', we require a non-zero left-handed lepton coupling $g^L_{\mu\tau}$. Simultaneously, we saw in Section 3.3.7 that a positive contribution to Δa_μ is only possible for a $\mu\tau$-coupling with $0.02 \lesssim \rho_\ell \lesssim 50.75$, i.e. non-zero $g^L_{\mu\tau}$.

Realizing that both excesses can only be explained with non-zero $g^L_{\mu\tau}$, we can ask ourselves if it is possible to explain both excesses simultaneously within our Z' model. Therefore, we will consider two possible scenarios that can explain $(g-2)_\mu$. On the one hand side a vector-coupling scenario ($\rho_\ell = 1$) and on the other hand side an optimized scenario, in which the limits from tau decays are weakest while the Z' contribution to a_μ is still positive ($\rho_\ell = 0.053$).

Vector coupling scenario The left panel of Fig. 3.17 shows the $g^R_{bs} - g^R_{\mu\tau}$ plane in a vector-coupling scenario ($\rho_\ell = 1$) for a Z' with a mass of $M_{Z'} = 1$ TeV. First, we notice the absence of a limit from the leptonic meson decay $B^0_s \to \mu\tau$. This can be understood with help of Eq. (3.32), which features a term $|1-\rho_\ell|$ in the denominator and consequently diverges for $\rho_\ell \to 1$. Second, the limit from the meson decay $B^+ \to K^+\bar{\nu}\nu$ in this case becomes unavoidable due to the non-zero left-handed lepton coupling $g^L_{\mu\tau}$. This limit (shown in yellow) is much stronger than the current 8 TeV ATLAS limit (shown in red) and possibly stronger than limits from an LHC Run II scenario (red dash-dotted line). Even a future HL-LHC run could only improve upon this limit along the direction of both small quark and lepton sector couplings. As in this scenario the Z' contribution to a_μ is positive, we can fit the excess Δa_μ. The purple, blue and green bands show the preferred 1, 2 and 3 σ regions of Δa_μ. It is worth noticing that for the example of a Z' boson of $M_{Z'} = 1$ TeV, the excess can naturally be accommodated with $\mathcal{O}(1)$ lepton couplings $g_{\mu\tau}$. However, one has to be careful whether the limits from tau decay rule out such a $(g-2)_\mu$ explanation. At the $2\,\sigma$ level this is indeed the case [216]. We fit the observed deviation $\Delta\mathcal{R}_{\mu/e}$ at the $1\,\sigma$ level. This fit is shown by the black and white hatched area. The observed Δa_μ deviation is still compatible with the τ decay excess within $3\,\sigma$.

Optimized coupling scenario The right panel of Fig. 3.17 shows the $g^R_{bs} - g^R_{\mu\tau}$ plane for a lepton coupling ratio of $\rho_\ell = 0.053$ for a Z' with a mass of $M_{Z'} = 200$ GeV. This scenario is optimized such that for a positive Z' contribution to a_μ the limit from τ decays is weakest. Previously, Altmannshofer *et al.* have shown explicitly in Ref. [216] that for $\rho_\ell = 0.1$ an explanation of Δa_μ is not ruled out by tau decay limits for Z' masses greater

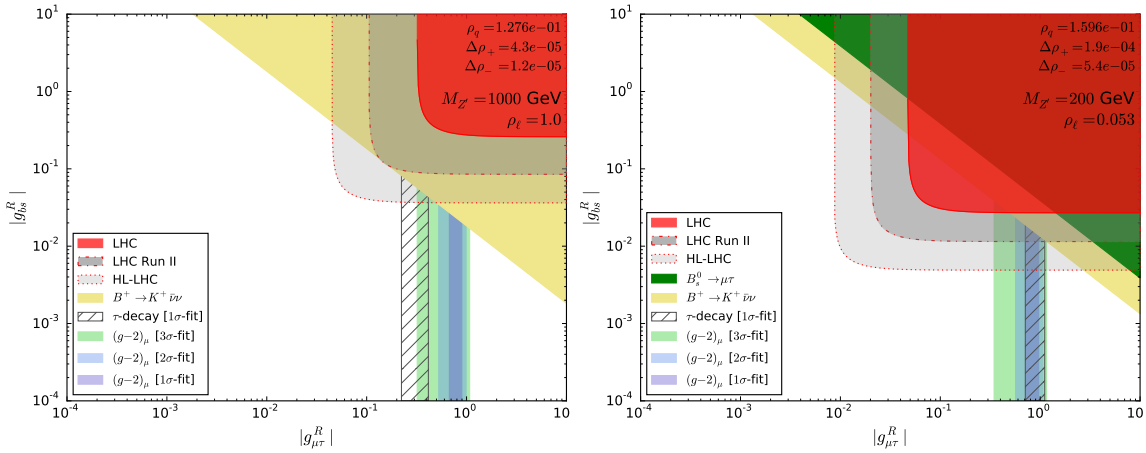

Figure 3.17: The left (right) panel shows the $g^R_{bs} - g^R_{\mu\tau}$ plane for a Z' boson with $M_{Z'} = 1000$ (200) GeV and a lepton coupling ratio of $\rho_\ell = 1.0$ (0.053). The red area indicates the limit from the ATLAS analysis of the process $pp \to \mu\tau$ at $\sqrt{s} = 8$ TeV. The red dash-dotted and dashed lines are projections to the LHC Run II and HL-LHC. The green area represents the excluded region from the leptonic meson decay $B^0_s \to \mu\tau$. The yellow area is the limit from meson decay into neutrinos $B^+ \to K^+\bar{\nu}\nu$. The purple, blue and light green bands are the preferred 1, 2 and 3 σ bands from Δa_μ. The black and white hatched area depicts the preferred 1 σ region of the observed deviation $\Delta\mathcal{R}_{\mu/e} = R_{\mu/e}/R^{\text{SM}}_{\mu/e} - 1$. Figure taken from [170].

than a few GeV. Comparing to the vector coupling scenario we can see that we get a limit from the leptonic meson decay $B^0_s \to \mu\tau$ in this case. In addition, the relative strength of the limit from the meson decay $B^+ \to K^+\bar{\nu}\nu$ to the ATLAS limits is much smaller. This is due to the small fraction $\rho_\ell = 0.053$, which drives the decay into neutrinos. The most important point to notice is that in this scenario the 1 σ fit of the tau decay excess $\Delta\mathcal{R}_{\mu/e}$ lies on top of the 1 σ band of the fit of Δa_μ. Hence, both excesses can be explained simultaneously with a coupling value of $0.7 \lesssim g^R_{\mu\tau} \lesssim 1.0$ for a relatively low mass of $M_{Z'} = 200$ GeV. This effect even persists for small perturbations around $\rho_\ell = 0.053$ roughly in the region $0.03 \lesssim \rho_\ell \lesssim 0.35$. Furthermore, in the right panel of Fig. 3.17 we can see that parameter space relevant for these explanations can already be probed with LHC Run II and HL-LHC data.

Future more precise measurements of the branching fraction of the tau decays $\tau \to \mu\bar{\nu}\nu$ and $\tau \to e\bar{\nu}\nu$, e.g. at the Belle-II experiment [259] as well as the planned factor of four improvement in the precision of $(g-2)_\mu$ in the upcoming E989 experiment at Fermilab [96] can test this interpretation. In addition to the purely leptonic tests, the presence of *sd*-type quark couplings could present an opportunity to test this model in rare tau decays, as discussed in Section 3.3.4. For example, assuming the maximally allowed quark coupling of $g^R_{sd} \approx 3 \times 10^{-3}$ for a 200 GeV Z' discussed in this section yields a branching fraction of $\Gamma_{\tau^- \to \mu^-\pi^+K^-} \approx 9.0 \times 10^{-9}$. This could directly be searched for at Belle-II, which aims at a sensitivity of 1×10^{-9} in branching fraction for 50 ab^{-1} of data [259].

3.5 Conclusions

In this chapter, we have investigated FCNCs in effective Z' models with exclusively flavor-changing interactions, one in the lepton and one in the quark sector. For a generic chirality structure of the Z' interaction, these models are subject to severe constraints from precision tests of flavor violation, in particular from meson mixing. In that sense, the constraints from reinterpreting an ATLAS resonance search in two differently flavored leptons in the final state can be seen as just an independent confirmation of what we already know. However, the strong limits from meson mixing depend on the relative strength of right- and left-handed couplings and there exist small regions of parameter space where they can be evaded. Here, the chirality-independent ATLAS limits take over and become the most sensitive probe of new physics that is weakly coupled. A similar situation arises with limits from mesons and leptons decaying into neutrinos (cf. e.g. [214,215,260,261]). These limits are applicable for left-handed couplings, but can be evaded for purely right-handed ones.

Owing to its coupling to leptons, the Z' boson of these toy models also gives rise to a contribution to the lepton anomalous magnetic moment $(g-2)$. In the case of a non-zero $g_{\mu\tau}$ coupling and a suitable chirality structure, this allows for an explanation of the observed deviation of $(g-2)_\mu$ from the SM expectation. Interestingly, in this scenario $(g-2)_\mu$ and a small excess observed in tau decays into muons and neutrinos can be explained simultaneously (cf. also [216]). This situation is summarized by the plots in Fig. 3.17. In the future, measurements of a Z' decaying into a $\mu\tau$ pair at ATLAS or CMS, or of B decays at LHCb can probe into the region of parameter space relevant for this simultaneous explanation. In particular, a dedicated ATLAS or CMS search at kinematics optimized for a relatively low-mass resonance could be helpful. These experiments can only test part of this interesting region due to their dependence on the quark sector coupling for the Z' production. Hence, it is worthwhile to look for complementary probes relying on the lepton sector couplings only. In this context, the study of tau decays, as can be done e.g. at Belle-II [259], provides for interesting opportunities. For purely leptonic couplings, precision tests of lepton flavor universality in these decays seem particularly promising. In addition, flavor-violating trident production at high intensity experiments like DUNE [254] or SHiP [255, 256] may allow to test this region [257, 258]. Finally, the interplay of these chiral $\mu\tau$-couplings with couplings to the light quarks g_{sd} could provide for smoking-gun signals in rare tau decays into muons and hadrons like e.g. $\tau \to \mu\,\pi^\pm K^\mp$.

Chapter 4

Anomaly-free hidden gauge bosons

The content of this chapter and the related Appendix B corresponds to work done in collaboration with M. Bauer (Durham U., IPPP) and J. Jaeckel (Heidelberg U.) and is published as Ref. [262]. In this work, the author was responsible for recreating the limit calculations of existing beam dump constraints on hidden photons of a secluded $U(1)_X$ and adapting them to the cases of $U(1)_{L_\mu - L_e}$, $U(1)_{L_e - L_\tau}$, $U(1)_{L_\mu - L_\tau}$ and $U(1)_{B-L}$. Furthermore, the author was responsible for adapting the bound on light particles from white dwarf cooling to the gauge bosons considered here. The credit for the discussions concerning the embedding of the $U(1)$ groups into larger symmetries, the flavor structure in the neutrino sector, as well as for the calculation of the Mu3e limits is entitled to M. Bauer. Nearly all results in this chapter, including the plots and tables as well as a significant part of the text, are identical to that in the publication.

4.1 Introduction

Having investigated a set of $U(1)$ toy models with exclusively flavor-violating interactions in Chapter 3, we now want to transition to the study of proper anomaly-free $U(1)$ gauge theories. In this context, we will focus on the well-motivated class of GeV-scale hidden photon models. Starting out from a pure dark, kinetically-mixed $U(1)_X$ model, we will generalize our discussion to a wider class of models under which SM fields are charged.

Models of GeV-mass hidden photons received much popularity in the literature after PAMELA data [30] confirmed previous indications by HEAT [263] and AMS-01 [264] of an excess in the cosmic-ray positron fraction. In particular, Arkani-Hamed et al. [265, 266], in an attempt to explain the positron excess, suggested a framework in which a $\sim$800 GeV weakly-interacting massive particle (WIMP) is charged under a dark gauge group $G_X \supset U(1)_X$ broken at around a GeV. In addition to providing a possible explanation for the large cross section into leptons by Sommerfeld enhancement, this would simultaneously explain the absence of any excess in the anti-proton spectrum. It was soon realized that such scenarios can be naturally realized in weak-scale SUSY breaking [267–272]. The supersymmetric version of the kinetic mixing term reads

$$\mathcal{L} = -\frac{\epsilon_Y}{2} \int \mathrm{d}^2\theta \, W_Y W_X \,, \tag{4.1}$$

where W_Y and W_X are the supersymmetric field strength tensors of hypercharge and the new $U(1)_X$, respectively. This term contains a mixed D-term $\epsilon_Y D_Y D_X$. After EWSB the hypercharge D-term will acquire a VEV proportional to the weak scale $\langle D_Y \rangle \sim \mathcal{O}(v^2)$. This leads to an effective Fayet-Illiopoulos (FI) term $\xi\, D_X$, where $\xi = \epsilon_Y \langle D_Y \rangle$. As the magnitude of kinetic mixing is of the order of $\epsilon_Y = 10^{-4} \dots 10^{-3}$ one obtains typical values of $\xi \sim \mathcal{O}(\mathrm{GeV}^2)$. With this FI term present in the potential, one can find a SUSY vacuum that breaks $U(1)_X$ and therefore leads to a mass of the associated gauge boson of

$$M_X^2 = g_X\, \xi\,, \tag{4.2}$$

which is naturally of $\sim \mathcal{O}(\mathrm{GeV})$.

This construction of SUSY-inspired DM models, containing a light neutral gauge boson that mixes with the SM hypercharge boson, has lead to a wide popularity of such **hidden photon** models [163, 273–275]. Ever since, there has been a strong experimental effort to search for light gauge bosons X_μ of a new dark $U(1)_X$ symmetry mixed with the hypercharge $U(1)_Y$ gauge boson B_μ through the operator [147]

$$\mathcal{L} = -\frac{\epsilon_Y}{2} B_{\mu\nu} X^{\mu\nu}\,, \tag{4.3}$$

connecting the corresponding field strength tensors, $X^{\mu\nu}$ and $B^{\mu\nu}$, respectively.

Going beyond the minimal paradigm of a completely secluded, dark $U(1)_X$ symmetry, there is also the possibility that one of the remaining global symmetries of the SM is gauged. Since only anomaly-free symmetries can be gauged, the number of possible additional gauge groups in the SM without the introduction of additional fermions charged under $SU(3)_C \times SU(2)_L \times U(1)_Y$ is limited. Out of the four independent global symmetries of the SM Lagrangian, $U(1)_B$, $U(1)_{L_e}$, $U(1)_{L_\mu}$, $U(1)_{L_\tau}$ three combinations are anomaly-free without any additional particles, $U(1)_{L_\mu - L_e}$, $U(1)_{L_e - L_\tau}$ and $U(1)_{L_\mu - L_\tau}$ [276–278]. These combinations are theoretically particularly appealing as the corresponding charges of SM fields are integral. The difference between baryon and lepton number $U(1)_{B-L}$ is also anomaly-free if right-handed neutrinos are introduced. Differences between baryon family numbers, e.g. $U(1)_{B_1 - B_3}$ or combinations, e.g. $U(1)_{B_3 - L_\tau}$, are also anomaly-free, but result in an unviable CKM matrix. The addition of right-handed neutrinos allows to reproduce a phenomenologically viable lepton mixing matrix without charged lepton flavor-changing couplings for the $U(1)_{L_\mu - L_\tau}$ gauge group [279].

In the remainder of this chapter, we focus on the four anomaly-free groups, $U(1)_{L_\mu - L_e}$, $U(1)_{L_e - L_\tau}$, $U(1)_{L_\mu - L_\tau}$ and $U(1)_{B-L}$. The phenomenology of a gauge boson of these groups can be very different from that of a secluded hidden photon. For example, at tree level the considered gauge bosons do not couple to the $W^\pm$ gauge bosons. Moreover, the gauge bosons of lepton family number differences $U(1)_{L_i - L_j}$ couple exclusively to the respective charged leptons and neutrinos, but not to baryons. As a consequence, constraints derived for secluded hidden photons with universal couplings do not easily translate into constraints on such additional gauge bosons. As we will see, the neutrino couplings will be of paramount importance for the gauge bosons of the four anomaly-free groups, making them subject to a number of constraints from neutrino experiments.

In the absence of kinetic mixing, constraints on light $U(1)_{B-L}$ gauge bosons have been discussed in [280–284]. The groups $U(1)_{L_\mu - L_e}$, $U(1)_{L_e - L_\tau}$ are considered in [285] and

limits on $U(1)_{L_\mu - L_\tau}$ gauge bosons have been derived in [234, 235, 286–290] (the last two papers take into account kinetic mixing). However, since in all four cases SM fermions are charged under both the new $U(1)$ as well as under hypercharge, a kinetic mixing term between the new gauge boson and the hypercharge boson is automatically induced at the one-loop level, even if $\epsilon_Y = 0$ at tree level. In the case of $U(1)_{L_\mu - L_e}$, $U(1)_{L_e - L_\tau}$, and $U(1)_{L_\mu - L_\tau}$ this mixing term is finite and has significant impact on the experimental sensitivities. We will discuss this mixing in more detail in Section 4.2.

The central aim of this study is to use experimental results and observations that constrain secluded hidden photons to derive limits on $U(1)_{L_\mu - L_e}$, $U(1)_{L_e - L_\tau}$, $U(1)_{L_\mu - L_\tau}$ and $U(1)_{B-L}$ gauge bosons. We use a large set of experiments ranging from beam-dump and fixed target experiments [255, 256, 275, 291–315], e^+e^- colliders [290, 316–329], to lepton precision experiments [250, 330–335]. For $U(1)_{L_\mu - L_e}$, $U(1)_{L_e - L_\tau}$, and $U(1)_{L_\mu - L_\tau}$, we explicitly take into account the unavoidable kinetic mixing generated by the SM particles, that has significant effects on the sensitivities. Technically, where possible and necessary, we recreated the analyses of the experiments thereby making use of more detailed information such as the energy spectrum of the particles in the experiments. In addition, we consider measurements of solar neutrinos with Borexino [289, 336, 337], laboratory neutrino experiments such as, e.g. CHARM-II [338, 339], COHERENT [340, 341] and TEXONO [342], as well as tests of neutrino trident production [234, 343–345]. Furthermore, we include new astrophysical limits from the energy loss of white dwarfs [346]. Looking into the future, we consider projections for planned and proposed experiments for the case of the universal hidden photon, as well as the $U(1)_{L_\mu - L_e}$, $U(1)_{L_e - L_\tau}$, $U(1)_{L_\mu - L_\tau}$ and $U(1)_{B-L}$ gauge boson, respectively. We also discuss the parameter space where the measured deviation in the anomalous magnetic moment of the muon $(g-2)_\mu$ can be explained [164, 235]. In this context, a light $U(1)_{L_\mu - L_\tau}$ gauge boson provides one of the few not yet excluded explanations of $(g-2)_\mu$ [347, 348]. It can further explain the spectrum of the Icecube high-energy neutrino events [349, 350], has the right quantum numbers to explain the hints of lepton flavor non-universality in $R_{K^{(*)}}$ reported by LHCb [234, 351, 352] and might alleviate the tension in the determination of the Hubble constant H_0 [353].

The remaining part of this chapter is organized as follows: First, we introduce the corresponding models of the hidden gauge bosons in Section 4.2 and discuss their phenomenological features. In Sections 4.3 and 4.4 we discuss the strategies employed to recast or rederive existing limits and projections for future experiments. We present the results of our analysis in Section 4.5 and conclude in Section 4.6. In Appendix B we provide additional details: In Appendix B.1 we discuss in detail the rotation to the neutral gauge boson mass eigenstates as well as Higgs interactions. A thorough account of different implementations of beam dump limits as well as a comparison between rescaling limits and recreating the analysis is given in Appendix B.2. Finally, Appendix B.3 provides information on the different experiments constraining the hidden photon parameter space, the relevant processes and couplings.

4.2 Hidden gauge bosons

In order to understand how the different constraints on the universal hidden photon of a secluded $U(1)_X$ are transformed in the scenarios with non-trivial gauge coupling structure,

we will customize our discussion of the physics of a generic $U(1)$ boson of Section 2.3 to the four anomaly-free groups $U(1)_{L_\mu - L_e}$, $U(1)_{L_e - L_\tau}$, $U(1)_{L_\mu - L_\tau}$ and $U(1)_{B-L}$.

In all four cases, the additional gauge boson $\hat{X}_\mu$ is in principle described by the general Lagrangian of Eq. (2.32),

$$\mathcal{L} = \mathcal{L}_{\text{SM}} - \frac{1}{4}\hat{X}_{\mu\nu}\hat{X}^{\mu\nu} - \frac{\epsilon_Y}{2}\hat{B}_{\mu\nu}\hat{X}^{\mu\nu} - \frac{M_X^2}{2}\hat{X}_\mu\hat{X}^\mu - g_x\, j_\mu^x \hat{X}^\mu\,,$$

where $\mathcal{L}_{\text{SM}}$ denotes the SM Lagrangian and $\hat{B}^{\mu\nu}$ and $\hat{X}^{\mu\nu}$ denote the field strength tensors of the hypercharge $U(1)_Y$ and the new $U(1)_X$. The hatted fields indicate that the kinetic terms in Eq. (2.32) are not canonically normalized and the corresponding gauge fields need to be redefined.

The current j_μ^x of the new symmetry depends on the considered gauge group,

$$\begin{aligned}
j_\mu^X &= 0\,, && U(1)_X\,,\\
j_\mu^{i-j} &= \bar{L}_i\gamma_\mu L_i + \bar{\ell}_i\gamma_\mu\ell_i - \bar{L}_j\gamma_\mu L_j - \bar{\ell}_j\gamma_\mu\ell_j\,, && U(1)_{L_i - L_j}\,,\\
j_\mu^{B-L} &= \frac{1}{3}\bar{Q}\gamma_\mu Q + \frac{1}{3}\bar{u}_R\gamma_\mu u_R + \frac{1}{3}\bar{d}_R\gamma_\mu d_R - \bar{L}\gamma_\mu L - \bar{\ell}_R\gamma_\mu\ell_R - \bar{\nu}_R\gamma_\mu\nu_R\,, && U(1)_{B-L}\,,
\end{aligned} \tag{4.4}$$

with $i \neq j = e, \mu, \tau$.

As outlined in Section 4.1, for the case of the secluded hidden photon, GeV-scale masses have been particularly motivated from dark matter considerations. Furthermore, this region was suggested by a (now essentially ruled out) explanation of the $(g-2)_\mu$ anomaly [164]. Consequently, many of the recent experimental activities have been concentrated on this region. This will serve us as a motivation to focus on boson masses in the MeV to multi GeV region in the following. That said, we will see that the explanation of $(g-2)_\mu$ with a weakly-coupled $U(1)_{L_\mu - L_\tau}$ [235] is still viable (cf. Fig. 4.18) in this region. Such masses can arise from a Higgs or a Stückelberg mechanism (cf. Section 2.3.2 for a discussion of these mass generation mechanisms). However, in the former case extra effects due to the additional Higgs boson are likely.

Upon redefining the fields and rotating to the mass eigenstates, the new gauge boson acquires a mixing-induced coupling to the hypercharge current j_μ^Y proportional to ϵ_Y. However, as we are concerned with a light $U(1)_X$ gauge boson (i.e. lighter than the Z boson) and consider small (loop-induced) kinetic mixing ϵ_Y, the interactions of the boson mostly align with those of the SM photon and are suppressed by a factor ϵ_Y. In the case of a secluded $U(1)_X$, i.e. in the absence of a new gauge current $j_\mu^x = 0$, this motivates the name **hidden** or **dark photon** for the mass eigenstate A'_μ of the $U(1)_X$ boson.

For the four gauge groups considered in this chapter, we obtain the interactions of the now unhatted gauge fields and currents after proper normalization and rotation to the mass basis (cf. Appendix B.1),

$$\mathcal{L}_{\text{int}} = \left(e\, j_\mu^{\text{EM}},\ g_Z\, j_\mu^Z,\ g_x\, j_\mu^x\right)\, K\, \begin{pmatrix} A^\mu \\ Z^\mu \\ A'^\mu \end{pmatrix}\,, \tag{4.5}$$

with

$$K = \begin{pmatrix} 1 & 0 & -\epsilon \\ 0 & 1 & 0 \\ 0 & \epsilon \tan\theta_w & 1 \end{pmatrix} + \mathcal{O}(\epsilon\delta, \epsilon^2)\,, \tag{4.6}$$

and where we have defined

$$\epsilon = \epsilon_Y \cos(\theta_w)\,, \qquad \delta = \frac{M_X^2}{M_Z^{\mathrm{SM}\,2}}\,. \tag{4.7}$$

In the general hidden photon scenario of small masses M_X compared to the Z mass and small kinetic mixing, to leading order in ϵ the masses before and after the basis change are equal,

$$M_Z^2 = M_Z^{\mathrm{SM}\,2}(1 + \mathcal{O}(\epsilon^2))\,, \qquad M_{A'}^2 = M_X^2(1 + \mathcal{O}(\epsilon^2))\,. \tag{4.8}$$

The normalization and mass diagonalization procedure also defines the interactions of the new gauge fields with the Higgs boson. This is also detailed in Appendix B.1.

At this point, let us briefly comment on the smallness of the gauge couplings. The smallness of the kinetic mixing parameter ϵ_Y of the hidden photon is naturally suggested if it is loop-induced [147]. However, for the gauge groups we want to consider here the weak interaction strength is directly set by the magnitude of the gauge couplings themselves. Such small gauge couplings arise for example in the context of "LARGE" volume compactifications of string theory [153]. These models naturally suggest gauge couplings in the region

$$\alpha_X = \frac{g_x^2}{4\pi} \sim 10^{-9}, \tag{4.9}$$

but somewhat smaller values are also possible. Nevertheless, this provides a theoretically interesting target area.

4.2.1 Kinetic mixing

Gauge groups such as $U(1)_{L_\mu - L_\tau}$ do not feature direct interactions with the first generation of SM particles that make up most of the ordinary matter and therefore most of the experimental apparatuses that we consider. Hence, the gauge groups that we consider are automatically much harder to probe. Nevertheless, since μ and τ are also charged under the electromagnetic $U(1)$ (or hypercharge, respectively), there exists an unavoidable kinetic mixing of the gauge bosons at the loop level. This allows us to probe these gauge groups also in experiments with first generation particles. By the same token, this enables us to test the purely leptonic gauge groups in experiments utilizing baryons. Let us now consider the loop-induced kinetic mixing, which we discussed for a generic $U(1)$ extension in Section 2.3.1, in more detail for the four explicit examples of $U(1)_{L_\mu - L_e}$, $U(1)_{L_e - L_\tau}$, $U(1)_{L_\mu - L_\tau}$ and $U(1)_{B-L}$.

If the abelian extension of the SM gauge group in Eq. (4.4) is not embedded in a non-abelian gauge group, kinetic mixing can be induced by a new fundamental parameter ϵ_Y. Kinetic mixing between non-abelian and abelian gauge groups is not possible at the

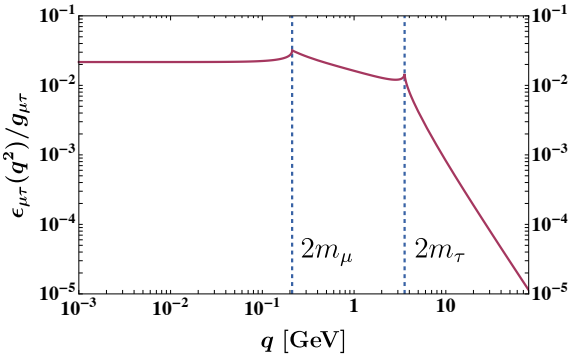

Figure 4.1: Ratio of the loop-induced kinetic mixing $\epsilon_{\mu\tau}(q^2)$ to the $U(1)_{L_\mu - L_\tau}$ gauge coupling $g_{\mu\tau}$ as a function of the momentum q flowing through the loop. The two vertical dashed lines show the resonance values $q = 2m_\mu$ and $q = 2m_\tau$, where the two muons and taus in the loop in Fig. 2.1 can go on shell.

renormalizable level[1]. However, if the extra abelian factor results from the breaking of a non-abelian gauge group, e.g. $SU(N) \to U(1)$, at some high scale, loop effects mediated by fields charged under both the new $U(1)$ and $U(1)_Y$ induce kinetic mixing in the broken phase. For the example of $U(1)_{L_\mu - L_\tau}$, the diagram shown in Fig. 2.1 with the fermion ψ being either L_2, L_3, μ_R or τ_R induces kinetic mixing. This can be calculated from replacing the same fields for ψ_L, ψ_R in Eq. (2.34)[2]

$$\epsilon_{\mu\tau}(q^2) = -\frac{e\, g_{\mu\tau}}{4\pi^2} \int_0^1 dx\, x(x-1) \left[3 \log\left(\frac{m_\mu^2 + q^2 x(x-1)}{m_\tau^2 + q^2 x(x-1)} \right) + \log\left(\frac{m_{\nu_2}^2 + q^2 x(x-1)}{m_{\nu_3}^2 + q^2 x(x-1)} \right) \right], \tag{4.10}$$

where q^2 is the transferred momentum and $g_{\mu\tau}$ the gauge coupling of $U(1)_{L_\mu - L_\tau}$. The same result holds for $U(1)_{L_\mu - L_e}$ and $U(1)_{L_e - L_\tau}$ with the obvious replacements. For large momentum transfer $q^2 \gg m_\tau^2$, this mixing parameter is power-suppressed $\epsilon_{\mu\tau} \propto m_\mu^2/q^2 - m_\tau^2/q^2$, whereas for low momentum transfer $q^2 \ll m_\mu^2$, the mixing can become relevant $\epsilon_{\mu\tau} \propto \log(m_\mu^2/m_\tau^2)$. These features are clearly visible in Fig. 4.1, where we have plotted the ratio $\epsilon_{\mu\tau}(q^2)/g_{\mu\tau}$ showing the hierarchy between the gauge coupling and the loop-induced kinetic mixing. Since this mixing for the gauge groups of lepton-family number differences is finite, we take it into account when we present the constraints on the corresponding gauge bosons in Section 4.5.

As an interesting theoretical feature, we note that the finiteness of Eq. (4.10) is not guaranteed by the fact that the symmetry is anomaly-free alone. In addition, it implies that the group of gauged lepton-family number difference $U(1)_{L_\mu - L_\tau}$ can be embedded into a larger group $\mathcal{G}_{L_\mu - L_\tau}$ that does not contain the SM. The breaking of $\mathcal{G}_{L_\mu - L_\tau}$ to

[1] Beyond the renormalizable level, kinetic mixing can arise from higher-dimensional operators involving the symmetry breaking Higgs fields, see, e.g. [354]. The loop effects discussed in the following can be viewed as generating such operators when integrating out fields.

[2] Note that if $q^2 \gg m_\nu^2 \approx \mathcal{O}(\text{meV}^2)$ (which will be the case for all processes considered in this chapter) the second logarithm in Eq. (4.10) can be neglected and the induced kinetic mixing $\epsilon_{\mu\tau}(q^2)$ is well approximated by keeping only the first logarithm in Eq. (4.10).

$U(1)_{L_\mu - L_\tau}$ does not induce mixing between the corresponding neutral gauge boson and the hypercharge gauge boson (and analogous for $U(1)_{L_e - L_\tau}$ and $U(1)_{L_\mu - L_e}$). Hence, one can construct a UV completion with a gauge group $\mathcal{G}_{\rm SM}$ containing the SM and the gauge group $\mathcal{G}_{L_\mu - L_\tau}$ containing $U(1)_{L_\mu - L_\tau}$, such that

$$\begin{array}{ccc} \mathcal{G}_{\rm SM} & \times & \mathcal{G}_{L_\mu - L_\tau} \\ \downarrow & & \downarrow \\ SU(3)_C \times SU(2)_L \times U(1)_Y & \times & U(1)_{L_\mu - L_\tau} \end{array} .$$

This is for example not possible in the case of an embedding of the $U(1)_{B-L}$ gauge group which we discuss below. As a consequence, neither the scalar that breaks $\mathcal{G}_{L_\mu - L_\tau} \to U(1)_{L_\mu - L_\tau}$ nor the scalar responsible for giving the $U(1)_{L_\mu - L_\tau}$ gauge boson a mass necessarily contributes to the loop-induced mixing $\epsilon_{\mu\tau}$. A straightforward way to embed $U(1)_{L_\mu - L_\tau}$ is to choose $\mathcal{G}_{L_\mu - L_\tau} = SU(2)_{L_\mu - L_\tau}$, and break it to the gauge boson corresponding to the third generator, which determines the couplings to the doublets (L_2, L_3) through $\sigma_3 = \mathrm{diag}(1, -1)$ [278, 279].

For $U(1)_{B-L}$, the result of the one-loop calculation from replacing the charged fields in Eq. (2.34) is not finite and its magnitude still depends on the choice of the renormalization scale μ. This implies that the gauge couplings of $U(1)_Y$ and those of a possible non-abelian embedding of $SU(N)_{B-L} \supset U(1)_{B-L}$ cannot be independent. Similar to the situation of the loop-induced kinetic mixing between the photon and the Z boson in the SM [355], the renormalization scale dependence of three parameters – the two wavefunctions for the $U(1)_{B-L}$ and hypercharge boson as well as $\epsilon(\mu)$ – need to be absorbed by the field renormalizations of the two original fields in the unbroken phase. We can therefore not determine the kinetic mixing parameter $\epsilon_{B-L}(\mu)$ unambiguously. However, invoking the order of magnitude estimate Eq. (2.35), we can deduce the rough coupling hierarchy

$$\frac{\epsilon_{B-L}(q^2)}{g_{B-L}} \approx \underbrace{\frac{g_1}{4\pi^2}}_{0.009} \sum_\psi Y_\psi (B-L)_\psi \underbrace{\log\left(\frac{m_\psi^2}{\mu^2}\right)}_{1\ldots 10} \sim 10^{-1} \ldots 10^{-2} , \tag{4.11}$$

for $q^2 \ll \mu^2$. That said, since all SM fermions ψ relevant to the experiments and observations we consider carry $\mathcal{O}(1)$ $B-L$ charge, the effect of the kinetic mixing is subdominant compared to the $B-L$ gauge interaction. Hence, we neglect it when we present the constraints on g_{B-L} and $M_{A'}$ in Section 4.5.

For completeness, let us note that in the case of a completely secluded $U(1)_X$, where all SM fermions are uncharged under the new symmetry, kinetic mixing is not generated within the SM. Instead, additional BSM fermions are necessary to generate contributions at the one-loop level.

4.2.2 Flavor structure

Both a secluded $U(1)_X$ and the $U(1)_{B-L}$ gauge boson couple universally to all SM quark flavors and lepton flavors, and hence lead to flavor-conserving vertices. In the case of a gauged lepton number difference, this is less obvious. Since the couplings to leptons are

non-universal, flavor changing vertices can in principle arise upon rotating the leptons from the interaction to the mass eigenbasis, as was outlined in Section 2.3.4. However, for gauged lepton-family number differences, the lepton Yukawa couplings which respect this symmetry are diagonal already in the interaction eigenbasis

$$\begin{aligned}\mathcal{L}_Y = &- \begin{pmatrix}\bar{e}_L & \bar{\mu}_L & \bar{\tau}_L\end{pmatrix} \begin{pmatrix} y_e & 0 & 0 \\ 0 & y_\mu & 0 \\ 0 & 0 & y_\tau \end{pmatrix} \begin{pmatrix} e_R \\ \mu_R \\ \tau_R \end{pmatrix} H \\ &- \begin{pmatrix}\bar{\nu}_e & \bar{\nu}_\mu & \bar{\nu}_\tau\end{pmatrix} \begin{pmatrix} y_{\nu_e} & 0 & 0 \\ 0 & y_{\nu_\mu} & 0 \\ 0 & 0 & y_{\nu_\tau} \end{pmatrix} \begin{pmatrix} N_1 \\ N_2 \\ N_3 \end{pmatrix} \tilde{H} + \text{h.c.}\,, \end{aligned} \tag{4.12}$$

where we have included three right-handed neutrinos N_1, N_2, N_3 that are singlets apart from lepton family number charges, and H denotes the SM Higgs boson. As a result, the couplings of the A' gauge boson to leptons are diagonal. This Lagrangian also produces a diagonal lepton mixing matrix. However, both Majorana mass terms of the type of Eq. (2.25), which respect the lepton family symmetry, and mass terms induced by the scalar S, which gives mass to the A' gauge boson, contribute to the neutrino mass term

$$\mathcal{L}_\mathcal{M} = -\frac{1}{2} N_i^T \mathcal{C}^{-1} \big(\mathcal{M}_R\big)_{ij} N_j\,. \tag{4.13}$$

The texture of the full mass matrix $\mathcal{M}_R$ depends on the gauge group and the charge Q_S of the scalar S under this group,

$$\begin{array}{cccc} & U(1)_{L_\mu - L_e} & U(1)_{L_e - L_\tau} & U(1)_{L_\mu - L_\tau} \\ \mathcal{M}_R^{|Q_S|=1} & \begin{pmatrix} 0 & m & M \\ m & 0 & M \\ M & M & m \end{pmatrix} & \begin{pmatrix} 0 & M & m \\ M & m & M \\ m & M & 0 \end{pmatrix} & \begin{pmatrix} m & M & M \\ M & 0 & m \\ M & m & 0 \end{pmatrix} \\ \mathcal{M}_R^{|Q_S|=2} & \begin{pmatrix} M & m & 0 \\ m & M & 0 \\ 0 & 0 & m \end{pmatrix} & \begin{pmatrix} M & 0 & m \\ 0 & m & 0 \\ m & 0 & M \end{pmatrix} & \begin{pmatrix} m & 0 & 0 \\ 0 & M & m \\ 0 & m & M \end{pmatrix} \end{array}\,, \tag{4.14}$$

where we have fixed the magnitude of the charge of the leptons to $|Q_\ell| = 1$ and for charges of the scalar S other than $|Q_S| = 1, 2$ one obtains the above textures with $M \to 0$. Here, m is the Majorana scale that can be fully independent of the mass scale induced by the vacuum expectation value of $M \propto \langle S \rangle = M_{A'}^2/(2 g_x^2 Q_S^2)$. For the hierarchy $m \gg M, v$, the texture $\mathcal{M}_R^{|Q_S|=1}$ for $U(1)_{L_\mu - L_\tau}$ has been discussed in detail in [279] and we refrain from a discussion of the phenomenology in the neutrino sector here. The texture $\mathcal{M}_R^{|Q_S|=1}$ for $U(1)_{L_\mu - L_\tau}$ is strongly preferred by the structure of the neutrino mixing matrix and compatible with the global fit to the leptonic CP phase [351, 356, 357].

In addition, the A' boson acquires lepton-flavor violating couplings to neutrinos, but not to charged leptons. Notice that the introduction of right-handed neutrinos does not introduce additional contributions to the kinetic mixing in Eq. (4.10). Flavor changing couplings arise only at the one-loop level for all three gauge structures, $U(1)_X$, $U(1)_{B-L}$, and $U(1)_{L_\mu - L_e}, U(1)_{L_e - L_\tau}, U(1)_{L_\mu - L_\tau}$ considered here.

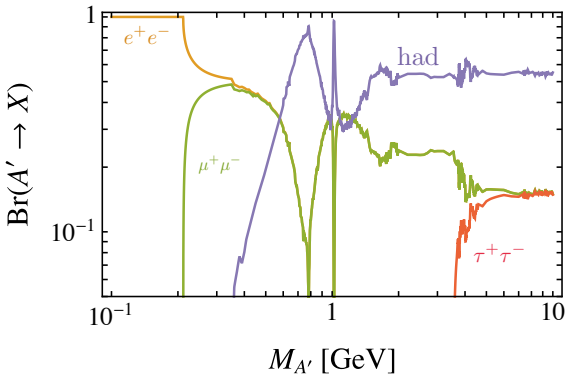

Figure 4.2: Branching ratios for the gauge bosons of a secluded $U(1)_X$ gauge group mixing with the SM hypercharge gauge boson. See text for details. Figure taken from [262].

4.2.3 Decay widths and branching ratios

A crucial ingredient for computing hidden photon limits from experimental observations are the hidden photon decay widths and branching ratios. The decay widths for the gauge boson of a secluded $U(1)_X$ are completely determined by mixing with the hypercharge gauge boson. For a final state of charged SM leptons, the decay width is straightforwardly computed by replacing the coupling of a (massive) photon by $\alpha \to \alpha\epsilon^2$. Decays into hadrons can be determined in a data-driven approach by taking advantage of measurements of the ratio between the production cross section of hadronic final states and muon pairs in e^+e^- collisions, $R(s) = \sigma(e^+e^- \to \text{hadrons})/\sigma(e^+e^- \to \mu^+\mu^-)$ [357, 358]. The hadronic decay width is then given by

$$\Gamma(A' \to \text{hadrons}) = \epsilon^2\, \Gamma(\gamma^* \to \mu^+\mu^-)\, R(M_{A'}^2) \qquad \text{for} \quad U(1)_X\,, \tag{4.14}$$

where $\Gamma(\gamma^* \to \mu^+\mu^-)$ is the partial decay width for a virtual SM photon of mass $M_{A'}$. We show the results in Fig. 4.2.

For gauge bosons of lepton family-number differences, decays into hadronic final states are also only possible through kinetic mixing, and can be determined analogously to the universal gauge boson,

$$\Gamma(A' \to \text{hadrons}) = \epsilon_{\mu\tau}^2(M_{A'}^2)\, \Gamma(\gamma^* \to \mu^+\mu^-)\, R(M_{A'}^2)\,, \qquad \text{for} \quad U(1)_{L_\mu - L_\tau}\,, \tag{4.15}$$

where the kinetic mixing parameter is given by Eq. (4.10) and the obvious replacements hold for $U(1)_{L_\mu - L_e}$ and $U(1)_{L_e - L_\tau}$. The partial decay width into the leptons charged under the corresponding gauge group can be directly deduced from Eqs. (4.4) and (B.9). The respective uncharged lepton family can only couple through kinetic mixing with the photon. The branching ratios for the gauge boson of a gauged lepton family number difference are shown in Fig. 4.3. Hadronic decays are suppressed in all cases and the different shape of $\Gamma(A' \to \text{hadronic})$ in the case of $U(1)_{L_\mu - L_e}$ can be explained by the approximate power suppression in the mixing $\epsilon_{\mu e}(M_{A'}^2) \approx (m_\mu^2 - m_e^2)/M_{A'}^2$ for $M_{A'} > m_\mu$.

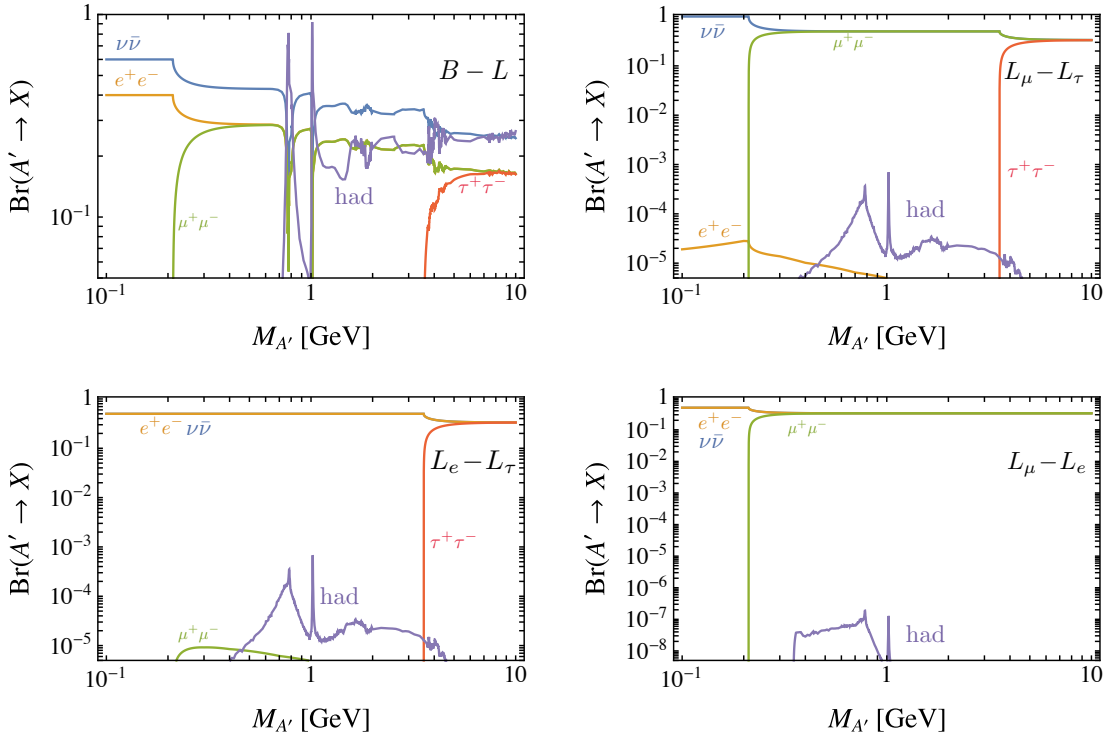

Figure 4.3: Branching ratios for the gauge bosons of a $U(1)_{B-L}$ (upper left), $U(1)_{L_\mu - L_\tau}$ (upper right), $U(1)_{L_e - L_\tau}$ (lower left) and $U(1)_{L_\mu - L_e}$ (lower right) gauge group. In the lower two panels, the branching ratio into neutrinos is indistinguishable from Br$(A' \to e^+e^-)$. See text for details. Figure taken from [262].

For a $U(1)_{B-L}$ gauge boson, we take advantage of the analysis in [284], where the couplings are computed using a data-driven method based on vector-meson dominance (VMD) for masses $M_{A'}$ below the QCD scale. The flavor-universal charges lead to an absence of $A' - \rho$ mixing. Therefore, hadronic decays only open up once the much narrower ω-resonance turns on at $m_\omega = 782$ MeV, and below that scale, the leptonic decay rates dominate as is evident from the upper left panel of Fig. 4.3. For masses of the A' gauge boson above the QCD scale, the vector dominance model breaks down at around $M'_A \gtrsim 1.65$ GeV [284]. We rescale the R-ratio with the $B - L$ charges above this value,

$$\Gamma(A' \to \text{hadrons}) = \frac{\sum_q \Gamma(A' \to q\bar{q})}{\sum_q \Gamma(\gamma^* \to q\bar{q})} \Gamma(\gamma^* \to \mu^+\mu^-)\, R(M^2_{A'})\,, \qquad \text{for} \quad U(1)_{B-L}\,, \quad (4.16)$$

in which the sum extends over all quarks with masses $m_q < M_{A'}/2$. This matching is good, given the expected precision of the VMD method of about $10\% - 20\%$ [284].

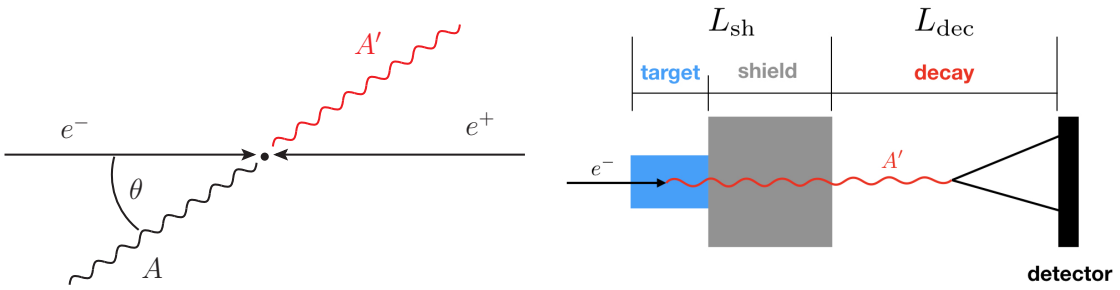

Figure 4.4: (Left) Simplistic sketch of hidden photon production in an e^+e^- collider. (Right) Schematic of hidden photon production in an electron beam dump experiment like SLAC E137. Figure adapted from [262].

4.3 Collider versus beam dump searches

In the following two sections, we will give a thorough account of how limits on hidden photons of a secluded $U(1)_X$ transfer to the gauge bosons of the four anomaly-free symmetries $U(1)_{L_\mu - L_e}$, $U(1)_{L_e - L_\tau}$, $U(1)_{L_\mu - L_\tau}$ and $U(1)_{B-L}$. We will summarize the scalings of he various constraints for these four groups compared to the $U(1)_X$ case in Tables B.2 and B.3.

Let us begin our discussion by reminding ourselves that in the simple case of a secluded $U(1)_X$ the hidden photon A' couples only to the electromagnetic current j_μ^{EM} suppressed by the kinetic mixing parameter ϵ, as discussed in Section 4.2. When we ask ourselves how to search for such an A', it seems natural to look for them in experiments where we expect a high number of electromagnetic interactions to take place. Two natural choices to search for GeV-scale hidden photons are collider experiments on the one side and beam dump or fixed target experiments on the other side [359]. In order to get an intuition of their respective sensitivity to hidden photons, we will perform a very naive comparison of these two types of experiments in the following.

4.3.1 Naive comparison of sensitivities

For simplicity, we will restrict our naive discussion to the case of e^+e^- colliders and electron beam dump experiments at this stage. Much of the following discussion is adapted from [360] and we refer the reader to this reference for a more thorough treatment.

In an e^+e^- collider, an electron and positron beam of N_e particles per bunch each are collided head on. In the hard interaction, a hidden photon A' is produced predominantly from radiative return [361] in association with a photon A. The corresponding diagram of this process is shown in the left panel of Fig. 4.8. Due to momentum conservation, the photon and hidden photon are leaving the interaction point back to back in an angle θ with the beam axis. This situation is shown in the left panel of Fig. 4.4. In the beam dump case, an electron beam of again N_e particles per bunch is typically dumped onto a target of some material ${}^A_Z X$ with atomic weight A and high atomic number Z. The electrons impinging on the target typically undergo multiple scatterings with the target nuclei. During these electron-nucleon scatterings, hidden photons can be produced from Bremsstrahlung as

shown in the diagram in the left panel of Fig. 4.5. If the kinetic mixing parameter ϵ is small, the produced A' has a significant lifetime and interacts weakly enough to pass the shielding following the target unhindered. As shown in the right panel of Fig. 4.4, the A' can decay back into SM particles in an open decay volume behind the shielding – leading to the typical signature of a very displaced vertex.

Let us estimate the collected luminosity in the two situations just discussed. In each bunch crossing in an e^+e^- collider with beam cross section $\mathcal{A}_b$, each of the N_e particles in the electron bunch has N_e potential scatterers in the positron bunch. In a beam dump the situation is a bit more subtle. In this case, the number of scatterers for the incoming N_e electrons is given by the total number n_N of nuclei per unit area of the target plus shielding of length $L_{\rm sh} = L_{\rm target} + L_{\rm shield}$. We can determine n_N from the number density of the shielding $n_{\rm sh} = N_0\,\rho_{\rm sh}/A$ times the absorber length $L_{\rm sh}$, where $N_0 \approx 10^{23}$ mole^{-1} denotes Avogadro's number and $\rho_{\rm sh}$ is the density of the absorber. Put together, we can estimate the collected luminosities per bunch of N_e particles to

$$\mathscr{L}^{\rm coll} \approx \frac{N_e^2}{\mathcal{A}_b}\,, \qquad\qquad \mathscr{L}^{\rm bd} \approx N_e \frac{N_0\,\rho_{\rm sh}\,L_{\rm sh}}{A}\,. \tag{4.17}$$

Parametrically, we can estimate that the luminosity in a beam dump experiment per N_e electrons is larger by a factor of

$$\frac{\mathscr{L}^{\rm bd}}{\mathscr{L}^{\rm coll}} \approx \frac{N_0\,\rho_{\rm sh}\,L_{\rm sh}\,\mathcal{A}_b}{A\,N_e} \approx \mathcal{O}(10^6)\,, \tag{4.18}$$

for typical values of the quantities featuring. In realistic setups, beam dump experiments collect around $\mathcal{O}(\text{ab}^{-1})$ of data per day [274], while e^+e^- collider experiments collect the same amount of data in a decade [362, 363]. For the same beam time, this is still an enhancement factor of $\mathcal{O}(10^3)$ in the collected luminosity.

In order to set this number into perspective, we also need to know the approximate hidden photon production cross section $\sigma_{A'}$ in both experiments. We will postpone a detailed analysis of the cross sections for hidden photon production in radiative return $\sigma_{A'}^{\rm coll}$ to Section 4.3.3 and in electron-nucleon Bremsstrahlung $\sigma_{A'}^{\rm bd}$ to Section 4.3.2. Hence, we will simply quote their approximate scalings [273, 275],

$$\sigma_{A'}^{\rm coll} \propto \frac{\alpha^2\,\epsilon^2}{E_{\rm CM}^2}\,, \qquad\qquad \sigma_{A'}^{\rm bd} \propto \frac{\alpha^3\,Z^2\,\epsilon^2}{M_{A'}^2}\,, \tag{4.19}$$

where we have neglected a mild log-depndence on the mass $M_{A'}$ in the second term (cf. [275]). For a typical scenario, where $\epsilon \sim 10^{-4}$, $M_{A'} \sim 50$ MeV and a collider energy of $E_{\rm CM} \sim 1$ GeV, we find the order of magnitude of the cross sections roughly to be $\sigma_{A'}^{\rm coll} \sim \mathcal{O}(\text{fb})$ and $\sigma_{A'}^{\rm bd} \sim \mathcal{O}(\text{pb})$ [360].

In summary, we have seen that beam dump experiments not only have a largely enhanced luminosity compared to colliders, but also typically feature significantly higher A' production cross sections. The latter is mainly due to the Z^2 enhancement with the atomic number Z. This makes beam dumps prime laboratories for hidden photon searches. With their high luminosities they are particularly suited to search for hidden photons with small kinetic mixings ϵ. Colliders on the other hand, are sensitive in the complimentary

Experiment	${}^{\mathrm{A}}_{\mathrm{Z}}\mathrm{X}$	E_0[GeV]	L_{sh}[m]	L_{dec}[m]	N_{in}	N_{obs}	$N_{95\%}$
CHARM	${}^{63.55}_{29}\mathrm{Cu}$	400	480	35	2.4×10^{18}	0	3
E137	${}^{26.98}_{13}\mathrm{Al}$	20	179	204	1.87×10^{20}	0	3
E141	${}^{183.84}_{74}\mathrm{W}$	9	0.12	35	2×10^{15}	1126^{+1312}_{-1126}	3419
E774	${}^{183.84}_{74}\mathrm{W}$	275	0.3	2	5.2×10^{9}	0^{+9}_{-0}	18
LSND	$\mathrm{H_2O}$	0.8	25.85	8.3	9.2×10^{22}	25	50
Orsay	${}^{183.84}_{74}\mathrm{W}$	1.6	1	2	2×10^{16}	0	3
U70/NuCal	${}^{55.85}_{26}\mathrm{Fe}$	68.6	64	23	1.71×10^{18}	5	7.1/4.5
SHiP	${}^{183.84}_{74}\mathrm{W}$	400	60	50	2×10^{20}	0	10
SeaQuest	${}^{55.85}_{26}\mathrm{Fe}$	120	5	0.95	1.44×10^{18}	0	3
FASER	${}^{1}_{1}\mathrm{H}$	9×10^7	390	10	2.3×10^{16}	0	3

Table 4.1: Material constants and specifications for the different beam dump experiments looking for very displaced vertices. Future experiments are indicated by grey shading. For the FASER setup we have assumed a run at $\sqrt{s} = 13$ TeV with 300 fb^{-1} of data.

region of rather large mixings ϵ, where beam dumps typically lose their sensitivity due to the very short A' lifetimes. In the following section we will analyze the collider and beam dump search strategies in detail to understand how the corresponding hidden photon limits translate to the cases of $U(1)_{L_\mu - L_e}, U(1)_{L_e - L_\tau}, U(1)_{L_\mu - L_\tau}$ and $U(1)_{B-L}$.

4.3.2 Beam dump and fixed target experiments

As we have just argued from our naive sensitivity estimates, beam dump and fixed target experiments provide the best sensitivity to hidden photons of a secluded $U(1)_X$ with masses $M_{A'} \lesssim 1$ GeV for almost the complete range of kinetic mixing parameters ϵ. In this section, we want to discuss how those experiments can constrain the hidden photon parameter space. This will help us to understand how the existing limits and projections for future experiments change for $U(1)_{L_\mu - L_e}, U(1)_{L_e - L_\tau}, U(1)_{L_\mu - L_\tau}$, and $U(1)_{B-L}$ gauge bosons. The material constants and specifications of the beam dump and fixed target experiments we take into account are collected in Table 4.1.

Electron beam dump experiments

In electron beam dump experiments such as SLAC E137, SLAC E141 [275, 292, 293, 304], Fermilab E774 [294] and Orsay [295], hidden photons can be produced in the Bremsstrahlung process shown on the left hand side of Fig. 4.5. They subsequently travel

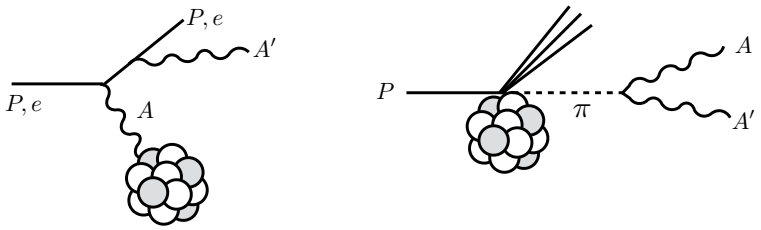

Figure 4.5: Hidden photon production through Bremsstrahlung (left) and meson production (right) in beam dump experiments.

through a shielding material before decaying as sketched in the right panel of Fig. 4.4 and explained in the last section. A pedagogical step-by-step derivation of all the relevant formulae to describe the hidden photon Bremstrahlung process is given in [360]. We will refrain from repeating the entire detailed discussion here and only summarize the most important formulae we used for the derivation of our limits.

The number N of hidden photon decays registered by a detector in an electron beam dump experiment is, in principle, given by the number $N_{A'}$ of produced A', the probability $P_{\rm dec}$ of the A' to decay within the fiducial volume and the branching ratio $\mathrm{Br}_{\rm det}$ of decays into detectable final states. Schematically, this can be written as

$$N = N_{A'}\ P_{\rm dec}\ \mathrm{Br}_{\rm det} = N_e\ \sigma_{A'}\, n_{\rm sh}\, L_{\rm sh}\ P_{\rm dec}\ \mathrm{Br}_{\rm det}\,, \tag{4.20}$$

where $\sigma_{A'}$ is the total A' production cross section, $n_{\rm sh}$ the particle density in the shielding and $L_{\rm sh} = L_{\rm target} + L_{\rm shield}$ the length of the shielding.

In the Weizsäcker-Williams approximation, the differential hidden photon production cross section [275] is given by

$$\frac{d\sigma}{dx_e} = 4\alpha^3\epsilon^2\xi\,\sqrt{1-\frac{M_{A'}^2}{E_0^2}}\,\frac{1-x_e+\frac{x_e^2}{3}}{M_{A'}^2\frac{1-x_e}{x_e}+m_e^2 x_e}\,, \tag{4.21}$$

where $x_e = E_{A'}/E_e$ is the fraction of the lab frame energy of the incoming electrons carried away by the hidden photon and in which ξ denotes the effective photon flux. The flux ξ is a function of the beam energy, the atomic and mass numbers Z and A of the material and the hidden photon mass $M_{A'}$ [364, 365]. It is given by

$$\xi(E_e, M_{A'}, Z, A) = \int_{t_{\rm min}}^{t_{\rm max}} dt \frac{t-t_{\rm min}}{t^2}\, G_2(t)\,, \tag{4.22}$$

with the virtuality $t = -q^2$ of the photon exchanged between the electron and the nucleon and the electric form factor $G_2(t)$.

In a beam dump experiment consisting of a shield of length $L_{\rm sh}$ and an open decay volume of length $L_{\rm dec}$, the probability that a produced hidden photon decays within the

fiducial decay volume is given by

$$P_{\rm dec} = e^{-\frac{L_{\rm sh}}{\ell_{A'}}} \left(1 - e^{-\frac{L_{\rm dec}}{\ell_{A'}}}\right) . \tag{4.23}$$

We see that the decay probability depends crucially on the hidden photon decay length in the lab frame

$$\ell_{A'} = \frac{\beta\gamma}{\Gamma_{\rm tot}} = \beta \frac{E_{A'}}{M_{A'}} \frac{1}{\Gamma_{\rm tot}} , \tag{4.24}$$

with the relativistic boost factor γ, the velocity β and the total hidden photon decay width $\Gamma_{\rm tot}$. This is where a lot of the model dependence of the resulting limits originates from due to the appearance of the total hidden photon width $\Gamma_{\rm tot}$.

Putting everything together, we are now able to derive the total number of detectable hidden photon decays. In the example of a dielectron final state, the number of electron events produced from hidden photon decays in an electron beam dump experiment with an incident electron beam of N_e electrons and energy E_0 is given by [275, 293]

$$\begin{aligned} N = N_e \frac{N_0 X_0}{A} \int_{M_{A'}}^{E_0 - m_e} dE_{A'} \int_{E_{A'}+m_e}^{E_0} dE_e \int_0^{\rho\, L_{\rm sh}/X_0} dt \Bigg[I_e(E_0, E_e, t) \frac{1}{E_e} \frac{d\sigma}{dx_e}\Big|_{x_e = \frac{E_{A'}}{E_e}} \\ \times e^{-\frac{L_{\rm sh}}{\ell_{A'}}} \left(1 - e^{-\frac{L_{\rm dec}}{\ell_{A'}}}\right) \Bigg] {\rm Br}(A' \to e^+ e^-) , \end{aligned} \tag{4.25}$$

where X_0 denotes the unit radiation length of the target material. The function $I_e(E_0, E_e, t)$ [366, 367], which is given in its general form as

$$I_e(E_0, E_e, t) = \frac{1}{E_0} \frac{\left[\ln\left(\frac{E_0}{E_e}\right)\right]^{\frac{4}{3}t - 1}}{\Gamma(\frac{4}{3}t)} , \tag{4.26}$$

describes the distribution of the energy E_e of the incoming electrons after having passed through t radiation lengths of material [368]. By virtue of Eq. (4.25), we can finally determine a limit on the mixing parameter ϵ for a given hidden photon mass $M_{A'}$ from the experimentally observed 95% C.L. limit on N.

Note that if the radiation length and the decay length are comparable the decay probability $\propto \exp(-L_{\rm sh}/\ell_{A'})$ depends on the position t (expressed in radiation lengths) where the A' is produced. We keep the full dependence in computing the limits in these cases. There is also a geometric factor depending on the detector shape and size as well as the angular distributions of the gauge bosons considered here. We neglect this factor for electron beam dumps, which in the case of the secluded hidden photon amounts to a correction of at most 10% [360]. Efficiency factors for the experimental reconstruction and experimental cuts are not included in Eq. (4.25) but applied when we compute the constraints. Details on the exact numerical derivation of our beam dump limits are further outlined in Appendix B.2.

In adapting the bounds from searches for universal hidden photons to gauge bosons of $U(1)_{B-L}$ and the groups of lepton-family number differences, we replace the branching

ratios by the values computed in Section 4.2.3 and compute the corresponding average decay length from the respective total width $\Gamma_{\rm tot}$. In the differential cross section Eq. (4.21), the couplings are replaced by

$$\alpha^3\epsilon^2 \quad \to \quad \begin{cases} \alpha^2\alpha_{\mu e}\,, & \text{for} \quad U(1)_{L_\mu - L_e}\,, \\ \alpha^2\alpha_{e\tau}\,, & \text{for} \quad U(1)_{L_e - L_\tau}\,, \\ \alpha^2\alpha_{\mu\tau}\,\epsilon_{\mu\tau}(M_{A'})^2\,, & \text{for} \quad U(1)_{L_\mu - L_\tau}\,, \\ \alpha^2\alpha_{B-L}\,, & \text{for} \quad U(1)_{B-L}\,, \end{cases} \tag{4.27}$$

where $\alpha_{ij} = g_{ij}^2/(4\pi)$ and g_{ij} denotes the gauge coupling of $U(1)_{L_i-L_j}$, and $\alpha_{B-L} = g_{B-L}^2/(4\pi)$. In writing Eq. (4.27) the fact that the $B-L$ charge of electrons is -1 has already been accounted for.

Looking at Eq. (4.27) it is clear that the electron beam dump constraints are expected to be important for $U(1)_{L_\mu-L_e}, U(1)_{L_e-L_\tau}$ and $U(1)_{B-L}$ gauge bosons, whereas for the $U(1)_{L_\mu-L_\tau}$ gauge boson the constraints are expected to be strongly attenuated. In contrast, experiments with muon beams would be particularly relevant for searches of $U(1)_{L_\mu-L_\tau}$ gauge boson. We comment on such a possibility below in the context of fixed target experiments.

Electron (and future muon) fixed target experiments

In addition to the beam dumps discussed above, we also consider fixed target experiments [300] such as APEX [303], A1/MAMI [301, 309], HPS [310], NA64 [315], VEPP-3 [306] and DarkLight [307, 311]. In these experiments production typically also proceeds via Bremsstrahlung. However, the signal is not a very displaced vertex, but rather kinematic features such as, e.g. a resonance bump in the invariant mass spectrum. This arises for example when the produced on-shell hidden photon decays into a pair of electrons.

Most of the above experiments search for visible decay products (e, μ). They target the region where the hidden photon decays promptly. This eliminates all the non-trivial geometric dependencies discussed above for the beam dumps. To recast the limits, we need to keep the product of production cross section times branching ratio constant. We do this by using the branching ratios computed in Section 4.2.3 for the decay and for the production the replacements given in Eq. (4.27).

NA64, VEPP-3 and the invisible mode of DarkLight measure missing energy. This provides two search regions. The first is for prompt decays into invisible particles and the second is an essentially stable hidden photon. In the parameter region where these experiments provide sensitivity to the gauge groups considered here, we can assume prompt decays into neutrinos that are effectively invisible. We can then rescale as above but using the neutrino branching ratios from Section 4.2.3.[3] As it turns out, for DarkLight the visible mode [311] is more sensitive for the gauge bosons considered here.

A future modified version of NA64 utilizing the upgraded muon beam at the CERN SPS delivering up to 10^{12} muons on target has been proposed [290, 322]. Employing the

[3] Any hidden photon that does not decay would also be considered invisible and therefore only increase the signal. Hence, our estimate is conservative.

same search strategy for missing energy, this NA64μ setup will be able to set much more severe bounds, especially in the case of $U(1)_{L_\mu - L_\tau}$.

Proton beam dump experiments

In proton beam dump experiments, such as CHARM [291], LSND [297] and U70/NuCal [302,308], as well as fixed-target experiments, such as SINDRUM I [296], NA48/2 [312], and the future SeaQuest [313, 314] and SHiP facilities [255, 256], hidden photons are produced in Bremsstrahlung as well as in meson decays produced in proton collisions with the target material. Similarly, the proposed experiment FASER [369] searching for very displaced hidden photon decays at the LHC is making use of these production mechanisms. Other proposed experiments searching for long-lived particles (LLPs) at LHC are MATHUSLA [370, 371] and CodexB [372]. We expect them to have sensitivity in a similar region. While clearly important, calculating their precise sensitivities requires a detailed study beyond the scope of this work. We therefore will showcase the projected FASER limits as a representative for this class of newly proposed experiments searching for LLPs at the LHC.

The Bremsstrahlung production of hidden photons in proton beam dump experiments is similar to the electron Bremsstrahlung process just discussed. The main difference is that the cross section for proton collisions with the target material is usually determined experimentally. The number of expected events for N_P incoming protons with initial energy E_P can then be written as

$$N = N_P \int_{M_{A'}}^{E_P - M_P} dE_{A'} \frac{1}{E_P} \frac{\sigma_{PA}(2M_P(E_P - E_{A'}))}{\sigma_{PA}(2M_P E_P)} \int_0^{p^2_{\perp,\max}} \omega_{A'P}(p_\perp^2) dp_\perp^2 \times e^{-\frac{L_{\rm sh}}{\ell_{A'}}} \left(1 - e^{-\frac{L_{\rm dec}}{\ell_{A'}}}\right) \mathrm{Br}(A' \to e^+e^-)\,, \quad (4.28)$$

where $\omega_{A'P}(p_\perp^2)$ is a weighting function relating the cross section of the $2 \to 3$ process $\sigma(P + A \to P + A + A')$ to the hadronic cross section σ_{PA} of the process $P + A \to P + A$, where A denotes the mass number of the target nucleus. This takes into account the splitting $P \to P + A'$ in the initial state. The ratio $\sigma_{PA}(2M_P(E_P - E_{A'}))/\sigma_{PA}(2M_P E_P)$ relates the hadronic scattering cross section $\sigma(P\,A \to P\,A)$ at the reduced center-of-mass energy after radiation of the A'-boson to the one evaluated at the initial center-of-mass energy. Explicit expressions for these functions can be found in [308]. The hadronic cross section σ_{PA} is linked to the inelastic proton-proton cross section by a function $f(A)$ via $\sigma_{PA} = f(A)\,\sigma_{PP}$, which however drops out in the ratio in Eq. (4.28). The proton-proton cross section σ_{PP} can then be extracted from experimental data [373, 374][4].

The upper limit of the integral over the momentum component perpendicular to the beam axis in Eq. (4.28) is in principle given by $p^2_{\perp,\max} = \max(E_P^2, E_{A'}^2)$ in the approximation of an elastic emission $P \to P + A'$. In practice it is, however, constrained by the largest value for which the fit to the form factors going into the cross section σ_{PP} is reliable.

[4]There is also a constraint for $M_{A'} < 2m_e$ from hidden photon conversion in the detector material, which is however not relevant for the masses we consider [308].

In full analogy to the case of Bremsstrahlung in electron beam dump and fixed-target experiments, it follows that the gauge coupling in $\omega_{A'P}(p_\perp^2) \propto \alpha\,\epsilon^2$ is replaced by

$$\alpha\epsilon^2 \quad \to \quad \begin{cases} \alpha_{\mu e}\,\epsilon_{\mu e}(M_{A'})^2\,, & \text{for} \quad U(1)_{L_\mu - L_e}\,, \\ \alpha_{e\tau}\,\epsilon_{e\tau}(M_{A'})^2\,, & \text{for} \quad U(1)_{L_e - L_\tau}\,, \\ \alpha_{\mu\tau}\,\epsilon_{\mu\tau}(M_{A'})^2\,, & \text{for} \quad U(1)_{L_\mu - L_\tau}\,, \\ \alpha_{B-L}\,, & \text{for} \quad U(1)_{B-L}\,, \end{cases} \tag{4.29}$$

which is suppressed for all flavors of gauged lepton family numbers, and the $B-L$ charge of the proton has been implicitly accounted for. In addition, as we have seen for the case of electron beam dumps, the branching ratios $\mathrm{Br}(A' \to X)$ as well as the decay length $\ell_{A'}$ are model-dependent and have to be adjusted to each case.

An additional source of hidden photons in proton beam dump experiments are decays of mesons M produced in collisions of protons with the target material, as depicted on the right-hand side of Fig. 4.5. For a secluded hidden photon, the number of expected events is given by [302]

$$N = \frac{N_P}{\sigma(PP \to X)} \int_{-1}^{1} dx_F \int_0^{p_{\perp,\mathrm{max}}^2} dp_\perp^2\, A^{\alpha(x_F)}\, \frac{d\sigma(PP \to MX)}{dx_F dp_\perp^2} \mathrm{Br}(M \to A'\gamma) \\ \times\, e^{-\frac{L_{\mathrm{sh}}}{\ell_{A'}}} \left(1 - e^{-\frac{L_{\mathrm{dec}}}{\ell_{A'}}}\right) \mathrm{Br}(A' \to e^+e^-)\,, \tag{4.30}$$

where x_F denotes the Feynman-x variable and $A^{\alpha(x_F)} = \sigma(PN \to MX)/\sigma(PP \to MX)$, with the mass number A of the nuclei N of the target material. Typically, the mesons contributing dominantly to the signal are the pseudo-scalars $M = \pi^0, \eta, \eta'$, which have a large cross section into photons. For example, the differential meson production cross section in proton-nucleon collisions have been measured in [375, 376] at 70 and 400 GeV, respectively.

The cross section is normalized to the total inclusive cross section $\sigma(PP \to X)$, which itself depends on the center-of-mass energy. As before, the decay length and branching ratios of A' depend on the underlying gauge group, and

$$\mathrm{Br}(M \to A'\gamma) = 2\epsilon^2 \left(1 - \frac{M_{A'}^2}{M_M^2}\right)^3 \mathrm{Br}(M \to \gamma\gamma)\,, \tag{4.31}$$

for a secluded hidden photon. For the $U(1)_{L_\mu - L_e}$, $U(1)_{L_e - L_\tau}$and $U(1)_{L_\mu - L_\tau}$ gauge groups, the corresponding expressions follow with the replacements

$$\alpha\epsilon^2 \quad \to \quad \begin{cases} \alpha_{\mu e}\,\epsilon_{\mu e}(M_{A'})^2\,, & \text{for} \quad U(1)_{L_\mu - L_e}\,, \\ \alpha_{e\tau}\,\epsilon_{e\tau}(M_{A'})^2\,, & \text{for} \quad U(1)_{L_e - L_\tau}\,, \\ \alpha_{\mu\tau}\,\epsilon_{\mu\tau}(M_{A'})^2\,, & \text{for} \quad U(1)_{L_\mu - L_\tau}\,. \end{cases} \tag{4.32}$$

For $U(1)_{B-L}$, there is a contribution to $\mathrm{Br}(\pi^0 \to A'\gamma)$ from kinetic mixing (which we neglect), as well as a contribution from the mixed electromagnetic-$B-L$ anomaly (cf. Fig. 4.6)

$$\mathcal{L} = \frac{e\, g_{B-L}}{16\pi^2\, f_\pi} \mathrm{Tr}\left[\sigma^3 Q Q_{B-L}\right]\, F_{\mu\nu}\tilde{F}'^{\mu\nu}\pi^0\,, \tag{4.33}$$

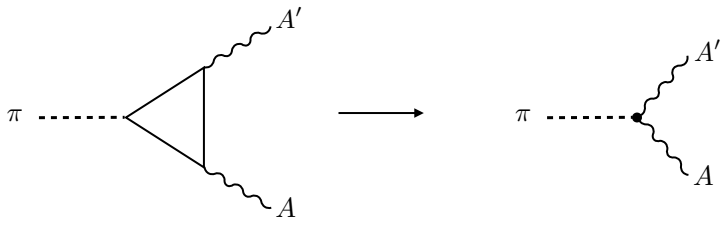

Figure 4.6: Anomalous coupling of a photon and a hidden photon to a pion.

where $\sigma^3 = \text{diag}(1,-1)$, $Q = \text{diag}(2/3,-1/3)$, $Q_{B-L} = \text{diag}(1/3,1/3)$, $\tilde{F}'^{\mu\nu} = 1/2\,\epsilon^{\mu\nu\alpha\beta}F'_{\alpha\beta}$ and f_π is the pion decay constant. Since $\text{Tr}[\sigma^3 Q Q_{B-L}] = \text{Tr}[\sigma^3 Q^2] = 1$ (including a color factor of 3), the branching ratio of pseudo-scalar mesons decaying into a photon and a $U(1)_{B-L}$ gauge boson follows from Eq. (4.31) by the replacement

$$\alpha\epsilon^2 \quad \to \quad \alpha_{B-L}\,, \quad \text{for} \quad U(1)_{B-L}\,. \tag{4.34}$$

This result can be recovered in the VMD approach neglecting mass differences between the vector gauge bosons [284].[5]

4.3.3 Collider experiments

As discussed in Section 4.3.1, a complementary way to search for hidden photons is provided by collider experiments. In this context, hidden photon searches have been conducted at the LHC by ATLAS and CMS [321], as well as by LHCb [324, 325, 328], and at e^+e^- colliders with BaBar [316, 323], Belle [317, 326], KLOE [318, 319, 327, 377] and BESIII [378–380].

Hadron colliders

At the LHC, hidden photons can be produced directly through Drell-Yan production or through the decay of heavy resonances, e.g. $H \to ZA'$ [321]. Feynman diagrams for these processes are shown on the left hand side and in the center of Fig. 4.7.

Limits from Drell-Yan production of hidden photons can be obtained for masses $M_A^2 > (12\text{ GeV})^2$. This cut suppresses backgrounds in the $q\bar{q}$-spectrum from hadronic resonances. The production cross section for an on-shell A' for a given quark initial state can be brought into the usual form

$$\sigma(q\bar{q} \to A') = \frac{12\pi}{M_{A'}^2}\,\text{Br}(A' \to q\bar{q})\,. \tag{4.35}$$

Production of hidden photons in Higgs decays are further constrained by the mass of the hidden gauge boson, with the Higgs decay width given in Eq. (B.10) (see Appendix B.1). For the decays $H \to \gamma A'$, there is no mass suppression $\propto M_{A'}^2/M_Z^2$, but the partial decay

[5] The branching ratio $\text{Br}(M \to A'A') = \mathcal{O}(\epsilon(M_{A'})^4)$ in the case of $U(1)_{L_\mu - L_\tau}$, $U(1)_{L_\mu - L_e}$ and $U(1)_{L_e - L_\tau}$, and vanishes identically for $U(1)_{B-L}$ in the absence of kinetic mixing, because $\text{Tr}[\sigma^3] = 0$.

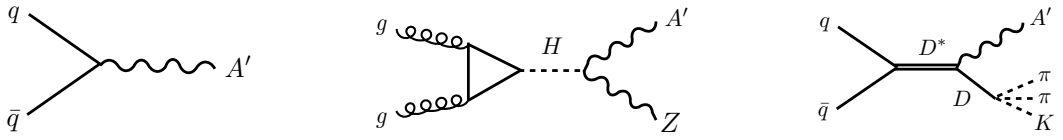

Figure 4.7: Diagrams for the production of hidden photons at hadron colliders. Drell-Yan production (left), Higgs decays (center) and excited meson decays (right).

width is loop-suppressed. Note that Higgs decays into hidden gauge bosons at tree-level are only possible for a non-zero kinetic mixing parameter, which we assume to vanish in the case of $U(1)_{B-L}$ and to be strongly suppressed for $U(1)_{L_\mu - L_e}$, $U(1)_{L_e - L_\tau}$ and $U(1)_{L_\mu - L_\tau}$, because of the power-suppression of $\epsilon(M_{A'}^2) \approx m_\ell^2/M_{A'}^2$ as argued in Section 4.2.1.

Another way to produce a hidden photon is by taking advantage of the large production cross section of heavy, excited mesons at LHCb. When such excited mesons decay into their respective ground state, they radiate a photon. In the presence of kinetic mixing the analogous process with the photon replaced by an A' leads to hidden photon production, as illustrated on the right of Fig. 4.7. The authors of [324] proposed a search through the neutral rare charm meson decay $D^* \to DA'$, for which the $\mathrm{Br}(D^* \to D\gamma) \approx 35\%$ is particularly large, because the mass difference $\Delta M_D = M_{D^*} - M_D = 142.12 \pm 0.07$ MeV leads to a phase space suppression of $\mathrm{Br}(D^* \to D\pi^0) \approx 65\%$. The latter also contributes to the signal through subsequent pion decays $\pi^0 \to \gamma A'$. For secluded $U(1)_X$ gauge bosons and a given luminosity $\mathscr{L}_{\mathrm{LHCb}}$ the number of hidden photons produced from such D^* decays is therefore given by

$$N_{A'} = \mathscr{L}_{\mathrm{LHCb}}\, \sigma_{D*}^{\mathrm{prod}} \Bigg[\mathrm{Br}(D^* \to D\gamma)\, \epsilon^2 \left(1 - \frac{M_{A'}^2}{\Delta M_D^2}\right)^{\frac{3}{2}} + \mathrm{Br}(D^* \to D\pi^0)\, \mathrm{Br}(\pi^0 \to \gamma\gamma)\, 2\epsilon^2 \left(1 - \frac{M_{A'}^2}{M_{\pi^0}^2}\right)^2 \Bigg], \quad (4.36)$$

where $\sigma_{D^*}^{\mathrm{prod}} = \sigma(pp \to D^* + X)$ denotes the D^* production cross section. For the $U(1)_{L_\mu - L_e}$, $U(1)_{L_e - L_\tau}$, $U(1)_{L_\mu - L_\tau}$ and $U(1)_{B-L}$ gauge groups, the kinetic mixing factors ϵ^2 in Eq. (4.36) are replaced by

$$\alpha\epsilon^2 \quad \to \quad \begin{cases} \alpha_{\mu e}\, \epsilon_{\mu e}(M_{A'})^2\,, & \text{for} \quad U(1)_{L_\mu - L_e}\,, \\ \alpha_{e\tau}\, \epsilon_{e\tau}(M_{A'})^2\,, & \text{for} \quad U(1)_{L_e - L_\tau}\,, \\ \alpha_{\mu\tau}\, \epsilon_{\mu\tau}(M_{A'})^2\,, & \text{for} \quad U(1)_{L_\mu - L_\tau}\,, \\ \alpha_{B-L}/4\,, & \text{for} \quad U(1)_{B-L} \text{ and } \mathrm{Br}(D^* \to D\gamma)\,, \\ \alpha_{B-L}\,, & \text{for} \quad U(1)_{B-L} \text{ and } \mathrm{Br}(D^* \to D\pi^0)\,. \end{cases} \quad (4.37)$$

A note on LHCb displaced searches The simple coupling rescaling procedure of Eq. (4.37) is only applicable to limits obtained from searches of prompt decays. However, the authors of [324] have also proposed a search for displaced A' decays in $D^* \to D\gamma$

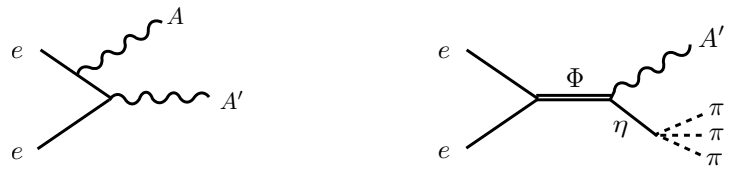

Figure 4.8: Diagrams for the different production mechanisms of hidden photons at e^+e^- colliders: Radiative return (left) and meson decays (right).

transitions. The derivation of these limits proceeds in analogy to the calculation of meson decay induced beam dump limits described in Section 4.3.2. This, however, demands knowledge of the D^* production spectra. To our knowledge, these spectra have not yet been measured for LHC energies of $\sqrt{s} = 13$ TeV and the Monte Carlo generated spectra used in the calculations in [324] have not been published. To obtain rigorous constraints from $D^* \to D\gamma$ transitions to the gauge groups discussed in this work, such Monte Carlo simulations of the D^* production spectra are required. This is, however, beyond the scope of this work and will be left for future studies.

e^+e^- colliders

At e^+e^- colliders, hidden gauge bosons are produced through radiative return or again through heavy meson decay. Feynman diagrams for the corresponding processes are shown in Fig. 4.8. In the latter case, the decay widths $\Gamma(\Phi \to \eta A')$ of the Φ-meson can be obtained in full analogy to the $D^* \to DA'$ case as the initial state for the production of the intermediate mesons plays no role. In the case of radiative return, the differential production cross section for the $U(1)_X$ gauge boson is given by [273]

$$\frac{d\sigma(e^+e^- \to \gamma A')}{d\cos\theta} = \frac{2\pi\alpha^2\epsilon^2}{s}\left(1 - \frac{M_{A'}^2}{s}\right)\frac{1 + \cos^2\theta + \frac{4M_{A'}^2 s}{(s-M_{A'}^2)^2}}{1 - \cos^2\theta}\,, \tag{4.38}$$

where θ is the angle of the photon momentum with the beam axis (cf. left panel of Fig. 4.4). The production cross section for gauged lepton-family number differences and $U(1)_{B-L}$ follows from Eq. (4.38) with the replacements

$$\alpha^2\epsilon^2 \quad \to \quad \begin{cases} \alpha\alpha_{\mu e}\,, & \text{for} \quad U(1)_{L_\mu - L_e}\,, \\ \alpha\alpha_{e\tau}\,, & \text{for} \quad U(1)_{L_e - L_\tau}\,, \\ \alpha\alpha_{\mu\tau}\,\epsilon_{\mu\tau}(M_{A'})^2\,, & \text{for} \quad U(1)_{L_\mu - L_\tau}\,, \\ \alpha\alpha_{B-L}\,, & \text{for} \quad U(1)_{B-L}\,, \end{cases} \tag{4.39}$$

making this channel particularly relevant for all gauge groups apart from $U(1)_{L_\mu - L_\tau}$.

For the experiments BaBar [316, 323], Belle [317, 326], KLOE [318, 319, 327, 377] and BESIII [378–380], the decays are prompt for all relevant regions. Again we use the relevant branching fractions from Section 4.2.3. As our hidden photons also feature invisible decays into neutrinos, they can additionally be searched for in a mono photon (or mono-Φ)

search [329]. Due to the lower SM background, the mono-photon searches can allow for more stringent limits than searches for $e^+e^- \to \gamma A' \to \gamma \ell^+ \ell^-$ [381].

4.4 Indirect probes for hidden photons

In the previous section, we studied in detail how hidden photons can be produced at colliders or beam bump facilities and what the relevant search strategies are. However, hidden photons also can enter physical observables in more subtle ways. In the following, we therefore want to discuss a selection of more indirect probes for hidden photons and argue that they have important consequences for the hidden photon parameter space.

4.4.1 Rare muon and tau decays and Mu3e

Experiments designed to search for lepton flavor violation are in principle well-suited to constrain the gauge groups we consider here, which all feature gauge couplings to leptons. However, since none of the gauge bosons we consider have flavor-changing neutral couplings, decays of the type $\mu^+ \to e^+e^-e^+$ or $\tau^+ \to \mu^+e^-e^+$, etc., are not mediated at tree-level.

More promising channels are the rare muon and tau decays into charged and neutral leptons, $\mu^+ \to e^+\nu_e\bar{\nu}_\mu A'(\to e^+e^-)$ or $\tau^+ \to e^+\nu_e\bar{\nu}_\tau A'(\to e^+e^-)$. In presence of new gauge bosons, these decays can be mediated by processes of the type as shown in Fig. 4.9. However, these rare lepton decays are already present within the SM via the processes, $\mu^+ \to e^+\nu_e\bar{\nu}_\mu\gamma^*(\to e^+e^-)$ or $\tau^+ \to e^+\nu_e\bar{\nu}_\tau\gamma^*(\to e^+e^-)$, etc. The most precise measurements of these decays have been performed by the SINDRUM [330] and CLEO collaborations [331], constraining the branching ratios to

$$\mathrm{Br}(\mu^- \to e^-e^+e^-\nu_e\nu_\mu) = (3.4 \pm 0.4) \times 10^{-5}\,, \tag{4.40}$$

$$\mathrm{Br}(\tau \to e\ e^+e^-\nu_e\nu_\tau) = (2.8 \pm 1.5) \times 10^{-5}\,, \tag{4.41}$$

$$\mathrm{Br}(\tau \to \mu\ e^+e^-\nu_\tau\nu_\mu) \leq 3.2 \times 10^{-5}\,. \tag{4.42}$$

Below the muon threshold, the SM background can be reduced by requiring the hidden photon to be on-shell. The future Mu3e experiment will probe $10^{15} - 10^{16}$ muon decays, providing three to four orders of magnitude more muons than SINDRUM [334]. Projections for the expected limits from a search by the Mu3e experiment for secluded hidden photons contributing to the process $\mu^- \to e^-e^+e^-\nu_e\nu_\mu$ have been computed in [335]. These limits take advantage of a resonance in the invariant e^+e^- mass spectrum and are relevant for all gauge groups we consider.

For the example of $U(1)_{L_\mu - L_\tau}$, the relevant diagrams are shown in Fig. 4.9. Depending on the gauge group, there are also diagrams in which the hidden photon is radiated from the electron leg, the electron-neutrino leg or from the $W^\pm$-propagator. The latter is suppressed with respect to inital- and final-state radiation by $m_\mu^2/M_W^2 \approx 10^{-6}$ and can be neglected. Initial- and final-state radiation scale differently for the different gauge groups, due to the lepton-family specific couplings. We have implemented the models in `Feynrules` [195] and used `MadGraph5` [196] to compute the branching ratio $\mathrm{Br}(\mu^+ \to e^+\nu_e\bar{\nu}_\mu A')$ for the different gauge groups we consider, taking the appropriate scaling of initial and final-state radiation

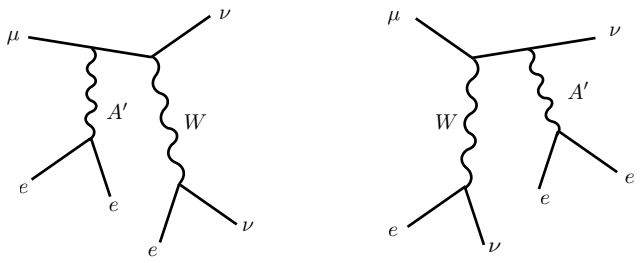

Figure 4.9: Diagram contributing to the $\mu^+ \to e^- e^+ e^- \nu_\mu \bar{\nu}_e$ signal mediated by the exchange of A'.

processes into account. We have scanned the parameter space in the coupling-mass plane and rescaled the limits [335] to derive projected limits for a future Mu3e search.

Similarly, tau decays can provide limits on gauge bosons with couplings to taus and electrons. To the best of our knowledge, no search for a resonance in rare leptonic tau decays $\tau \to e\nu_e\nu_\tau A'$ has been performed. We produced the corresponding branching ratio with `MadGraph5` and estimated the current and future reach, assuming a sensitivity comparable to the error on the $\mathrm{Br}(\tau \to e\ e^+e^-\nu_e\nu_\tau)$ measurement by CLEO and the projected improvement by Belle II [382]. The current and projected limits are rather weak. In the case of either a $U(1)_X$ or $U(1)_{B-L}$ gauge boson, current (future) searches for tau decays probe values of $\epsilon^2 \lesssim 5 \times 10^{-4}$ (5×10^{-5}) and $\alpha_{B-L}/\alpha \lesssim 5 \times 10^{-4}$ (5×10^{-5}), respectively. For a $U(1)_{L_e-L_\tau}$ gauge boson, the current (projected) limits are slightly better, constraining $\alpha_{e-\tau}/\alpha \lesssim 3 \times 10^{-4}$ (3×10^{-5}). Nevertheless, these constraints are not competitive with the other constraints discussed in this section. The loop-induced contribution of a $U(1)_{L_\mu-L_\tau}$ gauge boson to the decay $\tau \to \mu\bar{\nu}_\mu\nu_\tau$ has been considered in [234] in order to address the deviation in the measured $\mathrm{Br}(\tau \to \mu\nu_\tau\bar{\nu}_\mu)$ compared to the SM prediction. For masses of $M_{A'} < 10$ GeV an explanation of this deviation requires a coupling of $\alpha_{\mu-\tau}/\alpha \approx 10^{-2}$, which is safely excluded.

4.4.2 Limits from neutrino experiments

A crucial feature of the four gauge groups $U(1)_{L_\mu-L_e}$, $U(1)_{L_e-L_\tau}$, $U(1)_{L_\mu-L_\tau}$ and $U(1)_{B-L}$ setting them apart from the universal secluded $U(1)_X$ are the gauge couplings to neutrinos of the associated gauge bosons. In this section, we will investigate how these couplings can help to probe these models.

Neutrino trident production

The neutrino trident process $\nu N \to \nu N\, \mu^+\mu^-$ has been identified as an important probe for the gauge couplings of the $U(1)_{L_\mu-L_\tau}$ gauge boson [235]. The current best limit has been obtained by combining the measurements of the CHARM-II collaboration [343], the CCFR collaboration [344], and the NuTeV collaboration [345]. These experiments

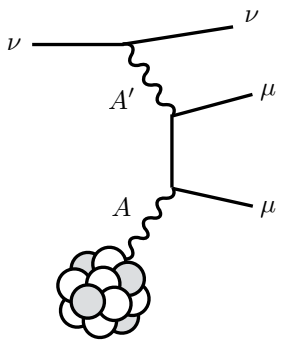

Figure 4.10: Diagram for neutrino trident production of muons.

utilized ν_μ ($\bar{\nu}_\mu$) beams dumped on different target materials to search for neutrino trident production. The weighted average of their respective limits normalized to the SM value is given by

$$\frac{\sigma(\nu_\mu N \to \nu_\mu N\, \mu^+\mu^-)}{\sigma_{\rm SM}(\nu_\mu N \to \nu_\mu N\, \mu^+\mu^-))} = 0.83 \pm 0.18\,. \tag{4.43}$$

In Fig. 4.10, we show the prototypical diagram due to A' exchange contributing to this process. For the $U(1)_{L_\mu - L_\tau}$, $U(1)_{L_\mu - L_e}$ and $U(1)_{B-L}$ gauge bosons, the A' contribution to muon-neutrino trident production is not suppressed. The potential contribution from a $U(1)_X$ or a $U(1)_{L_e - L_\tau}$ gauge boson is completely negligible, because the coupling to the muon neutrino only arises through mixing with the Z.

In principle, there is an additional diagram for $U(1)_{L_\mu - L_e}$ and $U(1)_{B-L}$ gauge bosons from incoming electron-neutrinos, but both the wide-band neutrino beam at CERN (CHARM-II) and Fermilab (CCFR/NuTeV) produce 2-3 orders of magnitude more muon- than electron-neutrinos and we can safely neglect this contribution [383, 384]. Hence, we can directly adopt the limits from [235]. In the future, these limits can be improved by measurements of the neutrino trident production cross section at LBNE [235], with the INGRID detector at T2K [289], and by measurements of atmospheric neutrino trident production with Cherenkov telescopes [385].

Borexino

Borexino is a liquid scintillator experiment measuring neutrinos scattering off electrons [336]. The original goal of this experiment was to measure the neutrino-electron scattering rate of solar electron-neutrinos reaching earth in order to determine the survival probability P_{ee} in neutrino oscillations. However, this measurement can also be used to probe non-standard interactions (NSI) between the neutrinos and the target. The resulting constraints are irrelevant for hidden photons with suppressed couplings to neutrinos, but relevant for any other gauge group we consider.

Using the fact that solar electron neutrinos will oscillate also into ν_μ and ν_τ, we can use the Borexino measurements to constrain the A' interactions with neutrinos. Limits

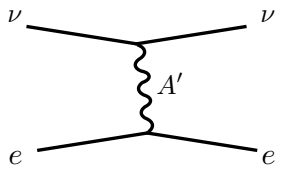

Figure 4.11: Neutrino-electron scattering via A' exchange.

for the $U(1)_{B-L}$ gauge boson have been derived in [337] and generalized to the case of $U(1)_{L_\mu - L_\tau}$ gauge bosons in [289]. We adopt the method of [289] and rescale the constraints on $U(1)_{B-L}$ bosons as

$$\alpha_{B-L}^2 \to \begin{cases} \left[\sum_{i,j=1}^3 f_i \left|(U^\dagger Q_{\mu e} U)_{ij}\right|^2\right]^{1/2} \alpha_{\mu e}^2 \,, & \text{for} \quad U(1)_{L_\mu - L_e} \,, \\ \left[\sum_{i,j=1}^3 f_i \left|(U^\dagger Q_{e\tau} U)_{ij}\right|^2\right]^{1/2} \alpha_{e\tau}^2 \,, & \text{for} \quad U(1)_{L_e - L_\tau} \,, \\ \left[\sum_{i,j=1}^3 f_i \left|(U^\dagger Q_{\mu\tau} U)_{ij}\right|^2\right]^{1/2} \alpha\, \alpha_{\mu\tau}\, \epsilon_{\mu\tau}(q^2) \,, & \text{for} \quad U(1)_{L_\mu - L_\tau} \,, \end{cases} \tag{4.44}$$

in which f_1, f_2 and f_3 denote the fraction of the corresponding mass eigenstates of ^{7}Be neutrinos at the earth [386], U is the lepton mixing matrix and $Q_{\mu\tau} = \mathrm{diag}(0, 1, -1)$, $Q_{\mu e} = \mathrm{diag}(1, 0, -1)$ and $Q_{e\tau} = \mathrm{diag}(1, 0, -1)$ are the neutrino coupling matrices. Mixing suppressed contributions have been omitted.

TEXONO

The TEXONO collaboration has measured the elastic $\bar{\nu}_e - e^-$ scattering cross section at the Kuo-Sheng Nuclear Power Reactor with a CsI(TI) scintillating crystal array [342]. The detector is located at a distance of 28 m from the reactor core such that the flux of incoming neutrinos can be assumed to be pure $\bar{\nu}_e$.

The experimentally determined $\bar{\nu}_e - e^-$ scattering spectrum can be used to constrain extra scattering due to the exchange of a new light A' boson from the diagram depicted in Fig. 4.11. This has been done in [282, 387] for the case of a gauged $U(1)_{B-L}$ with a particular emphasis on interference effects of the A' with the SM. The determined limit on the gauge coupling g_{B-L} directly applies to the case of $U(1)_{L_\mu - L_e}$ and $U(1)_{L_e - L_\tau}$, where the first generation of leptons also carries a charge of $|Q_{L_e}| = 1$.

COHERENT

Another sensitive laboratory for neutrino interactions is provided by coherent elastic neutrino-nucleus scattering (CEνNS). The high sensitivity of CEνNS to NSI induced by BSM physics [340] makes it a powerful probe of the neutrino couplings of the hidden photons considered in this work. The enhancement in the sensitivity to neutrino-nucleus scattering is achieved by relatively low-energy neutrinos (typically $E_\nu \lesssim 50$ MeV), which have a wavelength comparable to the size of the nucleus. This induces an N^2 enhancement

in the cross section, where N denotes the number of neutrons in the nucleus, due to the coherent scattering off the full nucleus rather than a single nucleon.

The COHERENT experiment has measured this process for the first time [341]. The detector consisted of a CsI target that is exposed to neutrinos from decays of secondary pions, which were produced from a proton beam dumped into a mercury fixed target. The observed signal has been used in [388] to set limits on a secluded hidden photon as well as on a $U(1)_{L_\mu - L_\tau}$ gauge boson. Furthermore, a future accelerator setup with a COHERENT-like detector consisting of a NaI/Ar target and an assumed total exposure of 10 t×yr has been used to derive projected sensitivities.

Charm-II

The CHARM-II detector has been exposed to the wide band neutrino beam at CERN in order to study $\nu_\mu(\bar{\nu}_\mu)e^-$ scattering. The CHARM-II collaboration has published both the measured total number of scattering events [338] as well as the differential cross section [339].

In [282, 387] these results have been used to set a limit on the coupling constant g_{B-L} of a gauged $U(1)_{B-L}$, again taking into account interference effects. However, from the experimental publications, the exact neutrino fluxes seem to be unknown and the SM prediction of the differential cross section given in [339] appears to have been determined by a shape fit. Therefore, we are in doubt whether a rigorous calculation of the neutrino rate R at CHARM-II is possible and whether the χ^2-fit used for limit determination in [282] is applicable. Noting this, we will show the corresponding limits by a dashed line assuming the correct neutrino flux was used for limit calculation.

In the cases of $U(1)_{L_\mu - L_e}$ and $U(1)_{L_\mu - L_\tau}$ (for $U(1)_{L_e - L_\tau}$ no tree-level coupling to ν_μ exists), first and second generation leptons carry opposite charges under the new group. Thus, the interference term changes sign relative to the $U(1)_{B-L}$ case and the full interference-sensitive limit cannot be obtained by rescaling. Therefore, we extract an upper bound on the change in cross section $\Delta\sigma_{\text{lim}}$ from the limits on g_{B-L} in [282], which have been provided for the case of only taking into account pure A' contributions (no interference). We use this bound $\Delta\sigma_{\text{lim}}$ to set limits on g_{ij} where constructive interference is expected ($\nu_\mu e^-$ scattering for both $U(1)_{L_\mu - L_e}$ and $U(1)_{L_\mu - L_\tau}$). A full analysis accounting for interference should yield stronger bounds. We will leave such an analysis for future work and simply apply our more conservative rescaling strategy.

Neutrino matter effects and Super-Kamiokande

It has been argued that new leptonic forces modify the matter potentials relevant for neutrino oscillations [285]. If the matter effects are changed due to new physics this should be visible in neutrino oscillations. The water Cherenkov detector Super-Kamiokande (Super-K) provides a strong limit on the difference between the matter potential for ν_μ and ν_τ, $|\epsilon_{\mu\mu} - \epsilon_{\tau\tau}| < 0.147$ [389–391][6].

[6] Note, that here $\epsilon_{\mu\mu}$ and $\epsilon_{\tau\tau}$ quantify the interaction strength between muon and tau neutrinos [389–391], not to be confused with the loop-induced mixing parameters $\epsilon_{\mu\tau}, \epsilon_{\mu e}$ and $\epsilon_{e\tau}$ defined in Eq. (4.10).

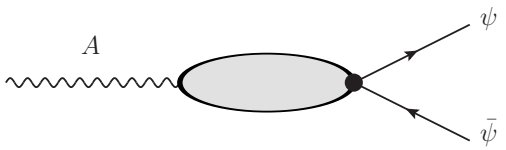

Figure 4.12: In-medium plasmon decays into a pair of fermions $\bar{\psi}\psi$ due to the longitudinal polarization of the photon mediated by coherent oscillations of the electromagnetic medium.

In the region of GeV-mass hidden photons A', the matter effects are given by,

$$|\epsilon_{\mu\mu} - \epsilon_{\tau\tau}| = \begin{cases} \frac{4\pi\alpha_{\mu e}}{\sqrt{2}G_F M_{A'}^2} & \text{for} \quad U(1)_{L_\mu - L_e} \\ \frac{4\pi\alpha_{e\tau}}{\sqrt{2}G_F M_{A'}^2} & \text{for} \quad U(1)_{L_e - L_\tau}, \\ 0 & \text{for} \quad U(1)_{L_\mu - L_\tau}, \\ 0 & \text{for} \quad U(1)_{B-L}. \end{cases} \tag{4.45}$$

For the latter two groups the measurement is insensitive because there is no difference in the matter effects for the two considered neutrino species.

The authors of [285] also consider a potential measurement at the future Deep Underground Neutrino Experiment (DUNE) [392] that could improve the limits into the $|\epsilon_{\mu\mu} - \epsilon_{\tau\tau}| \sim 0.01$ range, which we will use for a projection of the DUNE sensitivity.

4.4.3 Astrophyscial and cosmological probes

We will conclude our discussion of hidden photon limits by considering astrophysical and cosmological probes. Due to their relatively light mass and their interactions with light species (electrons, neutrinos, etc.), the hidden gauge bosons considered in this work might play an important role in stellar cooling processes and during the evolution of the early universe. Constraints potentially arise from the impact of hidden photons on the cooling of white dwarfs [346], big bang nucleosynthesis (BBN) [393], supernovae neutrino bursts as well as cosmic microwave background anisotropies.

White dwarf cooling

The most relevant astrophysical constraints for the parameter space we consider arise from White Dwarf (WD) cooling, which is measured by observing variations of the WD luminosity function. The WD luminosity function has been very well measured for a wide range of bolometric magnitudes of WD stars [394–396] and hence can be used to derive bounds on extra cooling contributions due to new physics.

The cooling of WDs proceeds mainly via photons and neutrinos. The nuclei inside a WD can be considered as approximately forming a classical Boltzmann gas. Most of the WD's thermal energy is stored in this classical gas and in particular for colder WDs the main source of energy loss is due to photon emission in the surface layer [346]. However, for hotter WDs a second cooling process becomes important, which is due to neutrino pair

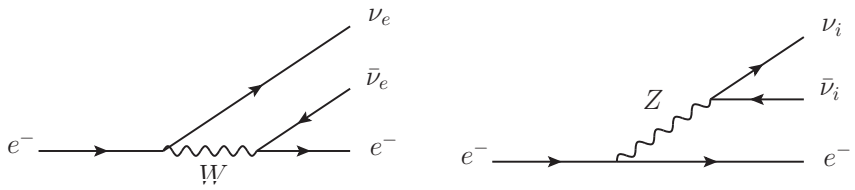

Figure 4.13: SM electroweak processes contributing to in-medium plasmon decay.

production in the so-called **plasmon decay** of the photon [397] within the stellar medium. Due to energy-momentum conservation, a photon cannot decay into a pair of fermions in vacuum. In the stellar medium, however, the propagating photon is accompanied by a coherent oscillation of electrons. This surrounding cloud of coherently oscillating electron effectively induces a longitudinal polarization for the photon, which allows it to decay. This plasmon decay is depicted in Fig. 4.12.

In order to describe the corresponding contribution to the WD luminosity function, we have to take into account interactions of electrons with neutrinos. At the relatively low WD core temperatures of $\mathcal{O}(\text{keV})$, we can perform the analysis in an EFT approach. The relevant operator is then given by

$$O_{\text{WD}} = (\bar{\nu}\gamma_\mu P_L \nu)(\bar{e}\gamma_\mu e)\,. \tag{4.46}$$

Within the SM this operator is generated by electroweak interactions of electrons with neutrinos as depicted in Fig. 4.13. The hidden gauge bosons discussed in this chapter will induce an additional contribution to plasmon decay due to the diagram shown in the right panel of Fig. 4.13 with the Z replaced by an A'.

As the neutrino cooling contribution of the SM to the WD luminosity function agrees very well with observations, we can use this to derive a constraint on the hidden photon contribution to neutrino cooling. In Ref. [346], the corresponding limit on extra neutrino cooling is reported as a limit on the Wilson coefficient C_{WD} of the operator in Eq. (4.46). This limit amounts to

$$\frac{1.12\times10^{-5}}{\text{GeV}^2} < C_{\text{WD}} < \frac{4.50\times10^{-3}}{\text{GeV}^2}\,, \tag{4.47}$$

in which the upper limit corresponds to an interaction strength that leads to a trapping of the neutrinos, which therefore effectively do not contribute to the cooling of the WD. Note that the trapping requires a sizable interaction with electrons and the above upper limit is probably quite conservative.

For a secluded hidden photon, the contribution to the Wilson coefficient C_{WD} is strongly suppressed, because a coupling to neutrinos only arises through mixing with the Z boson,

$$C_{\text{WD}} = \frac{4\pi}{M_{A'}^2}\,\alpha\epsilon\,\delta = \frac{4\pi}{M_Z^2}\,\alpha\epsilon\,, \qquad \text{for} \quad U(1)_X\,. \tag{4.48}$$

For the $U(1)_{B-L}$ and $U(1)_{L_\mu-L_e}$, $U(1)_{L_e-L_\tau}$, $U(1)_{L_\mu-L_\tau}$ gauge groups, however, the contributions to the Wilson coefficient can become important for small masses and sizable

couplings,

$$C_{\mathrm{WD}} = \begin{cases} \dfrac{8\pi}{3M_{A'}^2}\,\alpha_{\mu e}\,, & \text{for} \quad U(1)_{L_\mu - L_e}\,, \\ \dfrac{8\pi}{3M_{A'}^2}\,\alpha_{e\tau}\,, & \text{for} \quad U(1)_{L_e - L_\tau}\,, \\ \dfrac{8\pi}{3M_{A'}^2}\,\alpha_{\mu\tau}\,\epsilon_{\mu\tau}(M_{A'}^2)\,, & \text{for} \quad U(1)_{L_\mu - L_\tau}\,, \\ \dfrac{4\pi}{M_{A'}^2}\,\alpha_{B-L}\,, & \text{for} \quad U(1)_{B-L}\,. \end{cases} \tag{4.49}$$

Big bang nucleosynthesis

When the early universe cooled down below a temperature of $T \lesssim \mathcal{O}(1)$ MeV, BBN set in and first light elements formed. From comparing simulations of late-time relic abundances of light nuclei to the observed values, constraints on the amount of extra dark radiation during BBN have been derived, limiting the number of effective degrees of freedom N_{eff} [398–400].

In principle, hidden photons can contribute to N_{eff} in two ways. If the A' itself is still relativistic at the time of BBN, it would directly contribute with $\Delta N_{\mathrm{eff}} = 3 \times 4/7 \simeq 1.7$ to N_{eff}. However, once $T \lesssim M_{A'}$ the A' become non-relativistic and their number density is suppressed by a Boltzmann factor $\sim \exp(-M_{A'}/T)$. As we only consider masses of $M_{A'} > 1$ MeV, our hidden photons are non-relativistic during BBN and this contribution is strongly suppressed. The second possibility of how the hidden photons can contribute to N_{eff} is via couplings to neutrinos. For the case of $U(1)_{L_\mu - L_\tau}$, the A' gauge boson will stay in equilibrium with ν_τ and ν_μ in the early universe. Once the A' becomes non-relativistic, it transfers its entropy to the neutrinos. If this happens close to or during BBN this provides additional energy to these relativistic neutrinos and leads to an increase in the effective number of degrees of freedom N_{eff} at BBN [286].

In principle, a similar effect is present also for the other gauge groups with neutrino couplings. However, in this case also couplings to the electron and electron neutrino exist. A robust limit would require a more detailed analysis which we leave for future work.

A note on supernova limits

Limits on hidden photons from the observation of the neutrino burst from the supernova explosion SN1987A have been discussed in a number of papers [275, 401–406] and in principle constrain very low couplings[7] (mostly for the secluded case[8]). However, there seem to be significant differences in the limits obtained by different collaborations. While there is clear need and motivation for further investigations, this is beyond the scope of this work. Furthermore, the very low coupling regime constrained by supernova bounds is not the focus of this work. We therefore prefer not to show any limit and instead refer the reader to the corresponding literature.

[7] For strong constraints at much lower masses see e.g. [407–410].

[8] A limit for B-L has been given in [406] but in the region of interest to us it is based on the hidden photon limit.

4.5 Results

After having discussed the various sources of constraints on hidden gauge bosons in detail, we want to present the results for the four anomaly-free gauge groups $U(1)_{B-L}$, $U(1)_{L_\mu - L_e}$, $U(1)_{L_e - L_\tau}$ and $U(1)_{L_\mu - L_\tau}$ in the following section. For our analyses, we have considered gauge bosons in the mass range of 1 MeV to 80 GeV and coupling constants of 10^{-2} to 10^{-9}. Our main results are summarized in Figs. 4.15 to 4.18, showing exclusion contours for the four different groups. For each of the considered gauge groups we show two plots. One with the existing limits and another one with the planned and future experiments overlaid.

For comparison we show the usual secluded hidden photon case $U(1)_X$ in Fig. 4.14. For sizable values of the kinetic mixing parameter $\epsilon \gtrsim 10^{-3}$, limits from searches for prompt decays of hidden photons A' exist over the whole mass range considered here. Most of these bounds are due to collider searches, which are mainly sensitive in the large-coupling region as discussed in Section 4.3.1. Together with the bounds derived from measurements of the electron anomalous magnetic moment $(g-2)_e$ (shown in yellow), these prompt searches exclude all parameter space relevant for an explanation of the excess in $(g-2)_\mu$ (depicted by the red band) in the secluded $U(1)_X$ case. The possible contributions of a neutral gauge boson to the anomalous magnetic moments of leptons has been discussed in detail in Section 3.3.7. The corresponding limits for the hidden gauge bosons discussed in this chapter can be obtained from Eq. (3.87) with the obvious replacements of the couplings and masses.

In the low-mass and low-mixing region, limits from beam dump and fixed target experiments have high sensitivity as discussed in Section 4.3.1 and exclude a large region of parameter space. The sharp cutoff in the U70 limits at the pion threshold $M_{A'} \sim m_\pi$ is expected, as in the derivation of these limits A' production from pion decay has been considered. The isolated islands in parameter space from dimuon resonance searches at LHCb make use of cm-length displaced decays within the LHCb detector [325, 328]. This search provides a promising strategy to bridge the gap in sensitivity to parameter space between the bounds from classical beam dump and collider searches. This is also emphasized by the projections for displaced hidden photon in inclusive dimuon final states and in D^* decays shown in the lower panel of Fig. 4.14. Note the features in the projected SHiP reach in Fig. 4.14; similar to the U70 limits, for hidden photons with masses above the pion threshold, the production through pion decays shuts off and the sensitivity for small gauge couplings is decreased. The dips in sensitivity for masses of $M_{A'} \sim \mathcal{O}(1)$ GeV correspond to hadronic resonances, which increase sensitivity for small gauge couplings and decrease it for sizable gauge couplings, as the hidden photon becomes short-lived.

Finally, let us note that the very low-ϵ region not testable at beam dump experiments should be subject to constraints from energy loss due to neutrinos in supernova explosions as discussed in Section 4.4.3. However, due to the ongoing discussions on the correct derivation of these limits, we refrain from showing them here. Furthermore, this very low-coupling region is not the focus of this work.

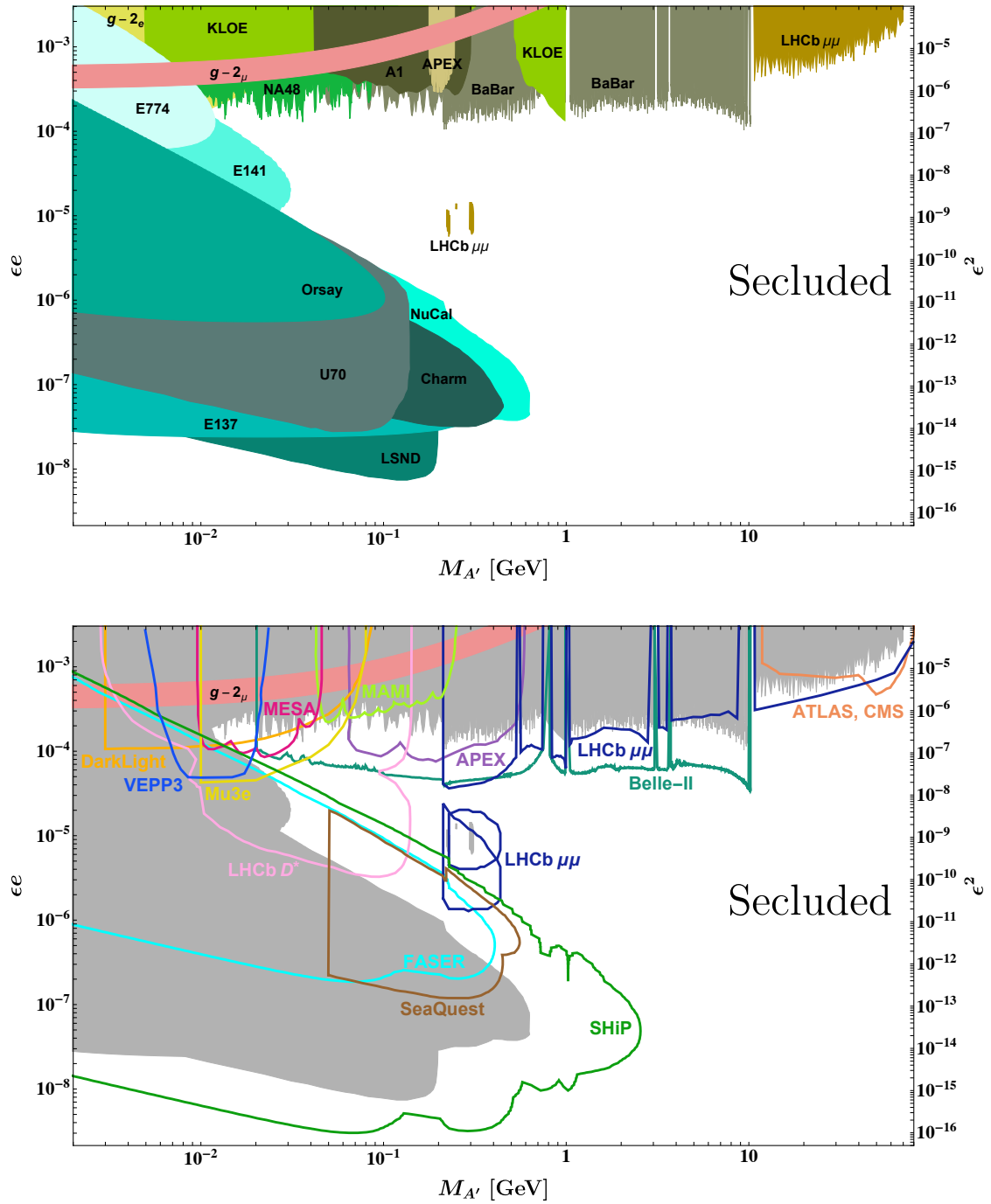

Figure 4.14: Constraints from current (upper panel) and future (lower panel) experiments on a secluded $U(1)_X$ gauge boson with kinetic mixing parameter ϵ. The red band shows the $2\,\sigma$ preferred region for $(g-2)_\mu$. The grey area in the lower plot show the current limits. Additional constraints from supernova cooling are not shown (see Section 4.4.3). Figure adapted from [262].

4.5.1 $U(1)_{B-L}$

Let us now consider each of the different gauge groups $U(1)_{B-L}$, $U(1)_{L_\mu - L_e}$, $U(1)_{L_e - L_\tau}$ and $U(1)_{L_\mu - L_\tau}$ and discuss the similarities and changes of the corresponding limits with respect to the case of a secluded $U(1)_X$ hidden photon. For a further detailed discussion of the calculation of beam dump limits in this work and how they are related to the recasted limits, we refer to Appendix B.2.

In the case of $U(1)_{B-L}$, the beam dump, fixed target and collider limits are very similar to the case of a secluded hidden photon. In particular, an explanation of the excess in the muon anomalous magnetic moment $(g-2)_\mu$ is safely excluded by the existing constraints. We note that the limit from CHARM and the LHCb displaced searches are absent because we lacked sufficient information to adequately reproduce these limits, not because there is a physics reason that makes these searches insensitive. However, the CHARM region is mostly covered by other experiments as one can also see from the rescaling done in [284].

The most notable difference to the $U(1)_X$ case arises from the coupling to neutrinos. This makes the $U(1)_{B-L}$ gauge boson additionally testable in a variety of neutrino experiments strongly constraining the 10 to 100 MeV mass region. These bounds close the gap in parameter space between beam dump and collider limits for small hidden photon masses. Interestingly, these limits from neutrino experiments cover already all parameter space that can be probed in the future with DarkLight, VEPP-3, Mu3e, MESA and MAMI.

The couplings of the hidden gauge boson to neutrinos also lead to constraints from the cooling of white dwarfs. However, these are subdominant in the case of $U(1)_{B-L}$ and do not excluded any previously unprobed region of parameter space. Furthermore, searches for invisible decays of hidden photons can test the neutrino couplings. For example, the BaBar invisible search (shown in light blue in the upper panel of Fig. 4.15) can close the gaps in the searches for visible final states due to hadronic resonances. Similarly, the Belle-II mono-photon plus missing energy search will be able to exclude couplings of $g_{B-L} \lesssim 2 \times 10^{-5}$ over a large range of hidden photon masses.

In general, the most promising future probes are the beam dumps SHiP and SeaQuest and the collider experiments Belle-II, LHCb and FASER (a similar reach is expected for the future proposed experiments CodexB and MATHUSLA). Due to the tree-level couplings of the $U(1)_{B-L}$ gauge boson to hadrons, SHiP has a similar sensitivity as in the case of a secluded $U(1)_X$. It can be further noted that the SHiP reach exposes the same characteristic features as in the $U(1)_X$ like the shutting off of the A' production from meson decay above the η-meson threshold or the pronounced bump at the φ-resonance.

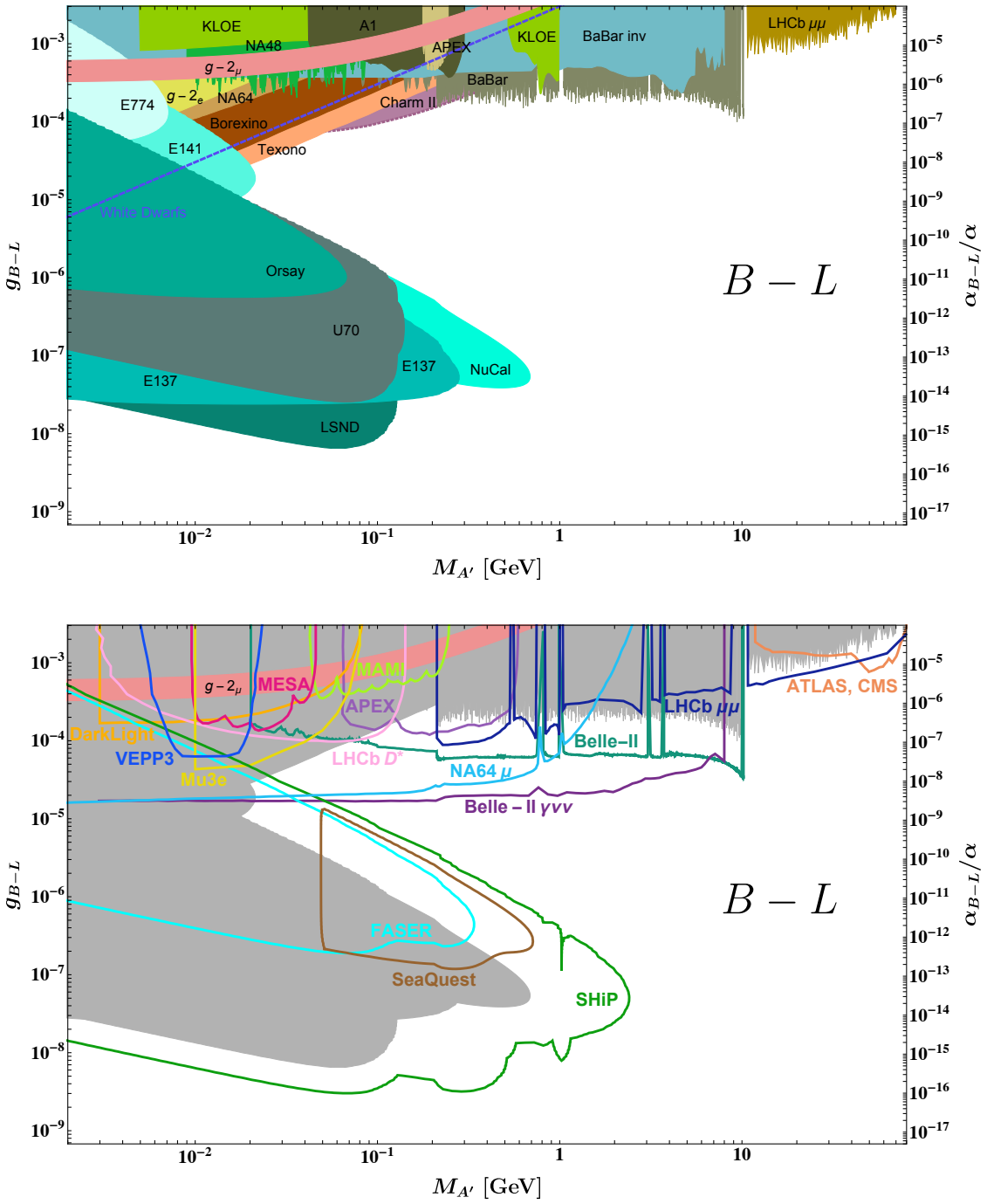

Figure 4.15: Constraints from current (upper panel) and future (lower panel) experiments on a $U(1)_{B-L}$ gauge boson with gauge coupling $g_{B-L} \equiv \epsilon\, e$. The red band shows the $2\,\sigma$ preferred region for $(g-2)_\mu$. The grey area in the lower plot show the current limits. Additional constraints from supernova cooling and BBN are not shown (see Section 4.4.3). Figure taken from [262].

4.5.2 $U(1)_{L_\mu - L_e}$

For the gauge group $U(1)_{L_\mu - L_e}$, as well as for the other two groups of lepton-family number differences $U(1)_{L_e - L_\tau}$ and $U(1)_{L_\mu - L_\tau}$, one main difference to both the case of $U(1)_X$ and $U(1)_{B-L}$ is the weakening of all limits from hadronic collider, beam dump and fixed target experiments. This is due to the fact that the hidden gauge bosons of the groups $U(1)_{L_i - L_j}$ only interact with hadrons via loop-suppressed kinetic mixing. This is most prominently illustrated for the example of the limit from meson decay production of the A' at the proton beam dump experiment NuCal. For both the cases of $U(1)_X$ and $U(1)_{B-L}$ the corresponding limit has the largest mass reach of all beam dump and fixed target limits. However, for $U(1)_{L_\mu - L_e}$ this limit is drastically weakened and is largely superseded by the limits from the electron beam dumps Orsay and E137. Hence, we see that electron beam dumps are much more favorable to explore very small couplings in this case. In general, the upper boundaries of the beam dump limits are significantly less affected, because these boundaries arises from the premature decay of the produced hidden gauge bosons in the shielding. It therefore mostly depends on the total decay width and is less sensitive to the details of the production mechanism. In order to increase the sensitivity towards larger couplings, a favorable geometry is more important.

It is further noteworthy that the limits from LHCb dimuon resonance searches for rather large boson masses are completely absent due to the loop-suppressed Drell-Yan production of A's at the LHC. In the high-mass region 10 GeV $\lesssim M_{A'} \lesssim M_Z$, limits from a dimuon resonance search in a four-muon final state at CMS [411] take over at much larger couplings. These limits are depicted by the dark orange area in the inset plot in the upper panel of Fig. 4.16. In this context, one can see that for $U(1)_{L_\mu - L_e}$ an explanation of the excess in $(g-2)_\mu$ is excluded over the entire mass range considered here.

As is the case for $U(1)_{B-L}$, interactions of the associated hidden gauge boson with neutrinos lead to additional strong constraints. Especially strong constraints arise from Super-K [285] due to the non-universal coupling of neutrinos to matter that modify the neutrino oscillations. Furthermore, constraints on the elastic electron-neutrino scattering cross section at TEXONO [282] lead to a strong bound. The neutrino bounds again help to excluded parameter space between the collider and beam dump limits.

From the lower panel of Fig. 4.16, we can see that of the future proposed beam dump experiments only SHiP will have some sensitivity to this scenario (in the region where it benefits from a suitable geometry and a high boost factor). However, a dedicated run of NA64 with a muon beam could help to exclude large parts of parameter space. The reach for small couplings in SHiP and NA64μ is slightly diminished above the pion and the muon threshold, respectively. Furthermore, both a search for visible as well as invisible (mono-photon) final states at Belle-II will potentially lead to strong constraints. In the neutrino sector, measurements of neutrino oscillation at DUNE might improve the current bounds.

Finally, let us mention that mainly due to the strong limits from neutrino interactions, the future experiments DarkLight, VEPP-3, Mu3e, MESA and MAMI as well as FASER will not be able to probe any previously unconstrained parameter space.

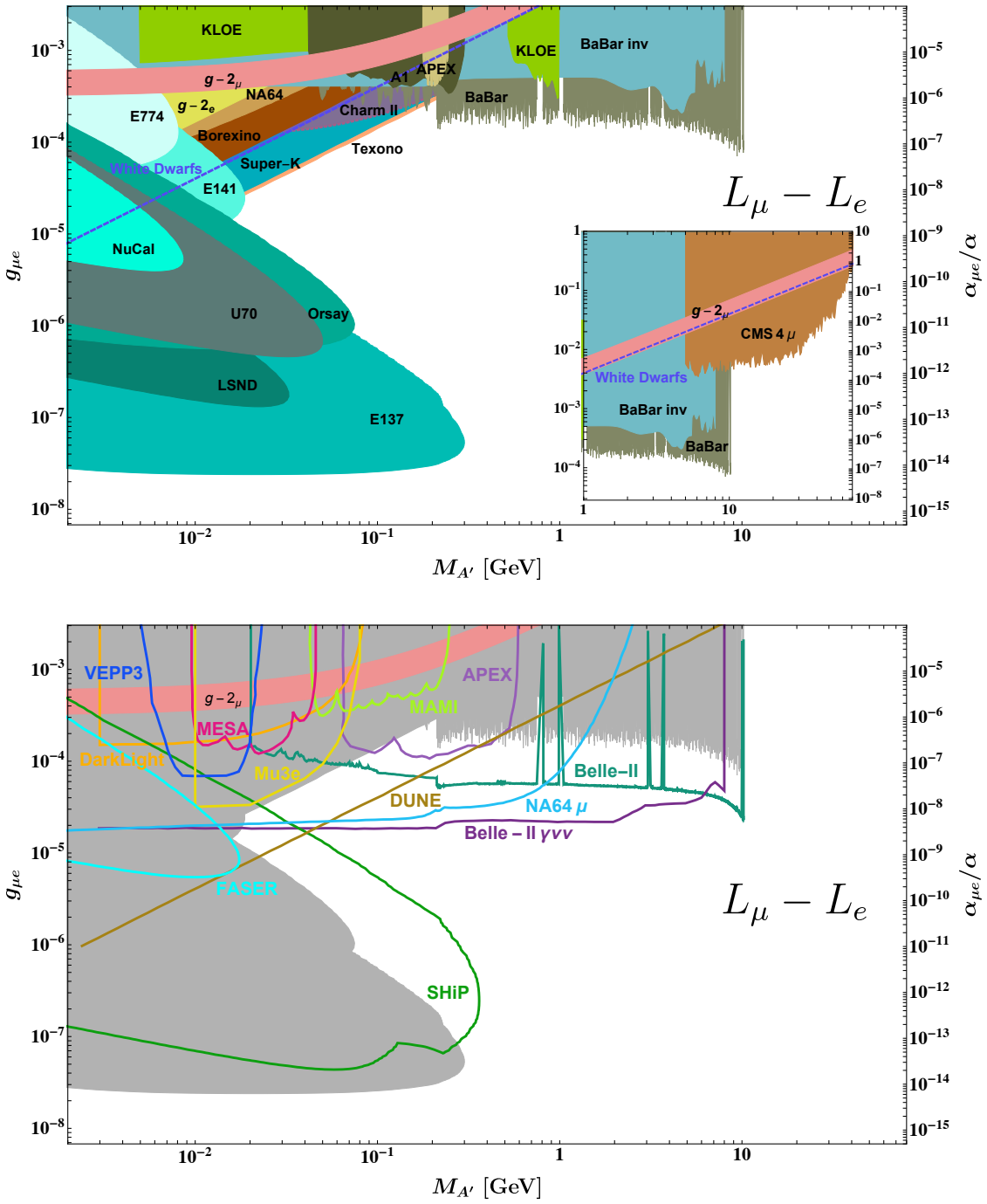

Figure 4.16: Constraints from current (upper panel) and future (lower panel) experiments on a $U(1)_{L_\mu - L_e}$ gauge boson with gauge coupling $g_{\mu-e} = \epsilon\, e$. The red band shows the $2\,\sigma$ preferred region for $(g-2)_\mu$. The grey area in the lower plot show the current limits. Additional constraints from supernova cooling and BBN are not shown (see Section 4.4.3). Figure adapted from [262].

4.5.3 $U(1)_{L_e-L_\tau}$

For $U(1)_{L_e-L_\tau}$ the situation is very similar to that of $U(1)_{L_\mu-L_e}$. The most notable difference is the absence of gauge couplings of the A' to muons. Hence, it can only interact with muons via loop-suppressed kinetic mixing. As a consequence, the high-mass KLOE limit based on a muon channel as well as the CMS four-muon limit are irrelevant in this scenario. Similarly, the future dedicated muon run of NA64 will not be able to probe this case. Let us also note that the gauge boson of a $U(1)_{L_e-L_\tau}$ does not contribute significantly to $(g-2)_\mu$ due to its suppressed muon-couplings. Consequently, the red $(g-2)_\mu$ bands are absent in the plots in Fig. 4.17.

In addition to SHiP, APEX, Belle-II and DUNE, the proposed FASER experiment gains some sensitivity compared to the $U(1)_{L_\mu-L_e}$ case. This is because above the threshold for the heavier of the two leptons, i.e. the muon in case of $U(1)_{L_\mu-L_e}$, the kinetic mixing is suppressed as it evolves towards zero at large momenta. For $U(1)_{L_e-L_\tau}$ this happens only above the tau mass. Therefore the mixing is larger in the relevant region.

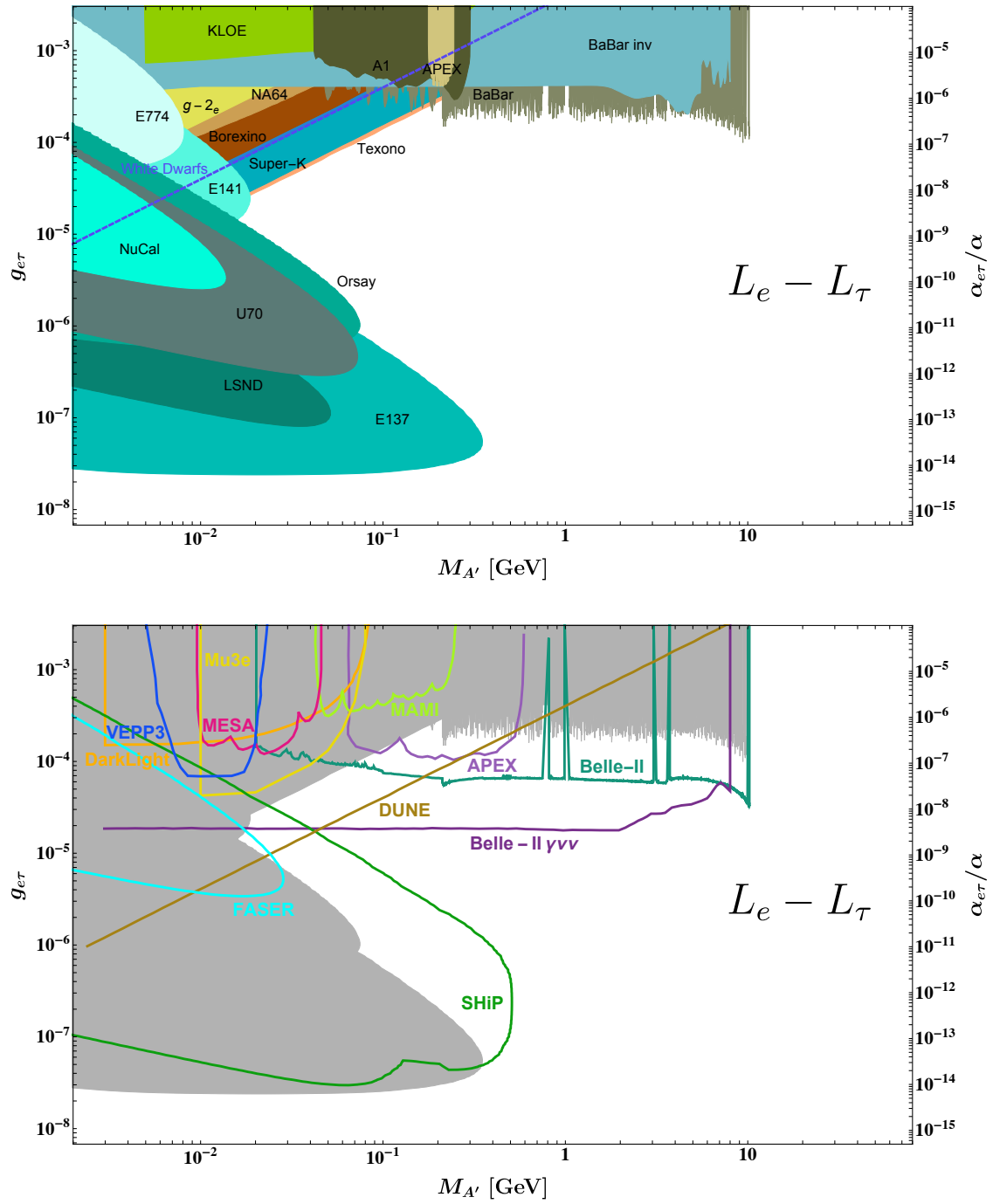

Figure 4.17: Constraints from current (upper panel) and future (lower panel) experiments on a $U(1)_{L_e-L_\tau}$ gauge boson with gauge coupling $g_{e-\tau} = \epsilon\, e$. The grey area in the lower plot show the current limits. Additional constraints from supernova cooling and BBN are not shown (see Section 4.4.3). Figure taken from [262].

4.5.4 $U(1)_{L_\mu - L_\tau}$

Let us finally discuss the limits on the hidden gauge boson in the case of $U(1)_{L_\mu - L_\tau}$. This group exhibits the biggest changes compared to the case of pure kinetic mixing in a secluded $U(1)_X$. The reason why most of the usual hidden photon searches lose sensitivity in this case is the fact that the associate gauge boson only has loop-suppressed couplings to hadrons and electrons. As almost all ordinary matter (and so also the experimental apparatuses) are composed of protons, neutrons and electrons, it is genuinely hard to produce and detect the $U(1)_{L_\mu - L_\tau}$ boson. In this context, we can immediately see that except for a very small region of parameter space excluded by E137 there are no constraints from beam dump or fixed target experiments at all. By the same token, the strong limits from resonance searches in collider experiments like Babar and LHCb are attenuated.

Instead, the search for the boson $U(1)_{L_\mu - L_\tau}$ requires some special experimental setups and observational strategies. The current best limits arise from experiments and observations that involve at most one kinetic mixing factor $\epsilon_{\mu\tau}$. In the high mass region $M_{A'} \gtrsim 2m_\mu$, the strongest constraints arise from dimuon resonance searches in four-muon final states at BaBar and CMS. This process is sensitive to the $U(1)_{L_\mu - L_\tau}$ case as the boson is radiated from one muon leg and decays into an additional pair of muons. Hence, it only involves gauge couplings and is therefore not loop-suppressed.

Below the dimuon threshold, one of the leading constraints originates from neutrino trident production (NTP) observed at CHARM-II, CCFR and NuTeV discussed in Section 4.4.2. The corresponding limit is shown by the dark blue area in the upper panel of Fig. 4.18. In addition, there is a strong constraint from elastic scattering of solar neutrinos measured with Borexino (brown area) as well as the BBN limit from [286].[9]

Most importantly, we note that there is still room for an explanation of the $(g-2)_\mu$ anomaly [235][10] as can be seen in the inset plot in the upper panel of Fig. 4.18. In particular, we notice that the white dwarf limit derived in Section 4.4.3 excludes part of this previously unconstrained region, where $(g-2)_\mu$ can be explained.

The fact that in this scenario an explanation of the excess in the muon anomalous magnetic moment $(g-2)_\mu$ is still possible, makes the $U(1)_{L_\mu - L_\tau}$ gauge boson a particularly attractive target for future experimental searches. The future fixed target experiment SHiP will cover a large region of the parameter space, but it will not reach the area suggested by $(g-2)_\mu$ excess. The additional region of projected SHiP sensitivity for $M_{A'} > 2m_\mu$ is a consequence of high statistics and the unsuppressed $\mathrm{Br}(A' \to \mu^+\mu^-)$. However, the $(g-2)_\mu$ area will be probed by coherent neutrino-nucleus scattering at COHERENT [388], and most decisively by the proposed muon run of NA64μ [290, 322].

[9] For this limit we show the coupling range displayed in [286] as solid. For weaker couplings the region is hatched. A determination of the decoupling of the gauge boson in the early universe would require a more sophisticated analysis.

[10] For similar discussions of explaining $(g-2)_\mu$ in the context of flavor-changing couplings, we refer to Chapter 3 and [170, 216].

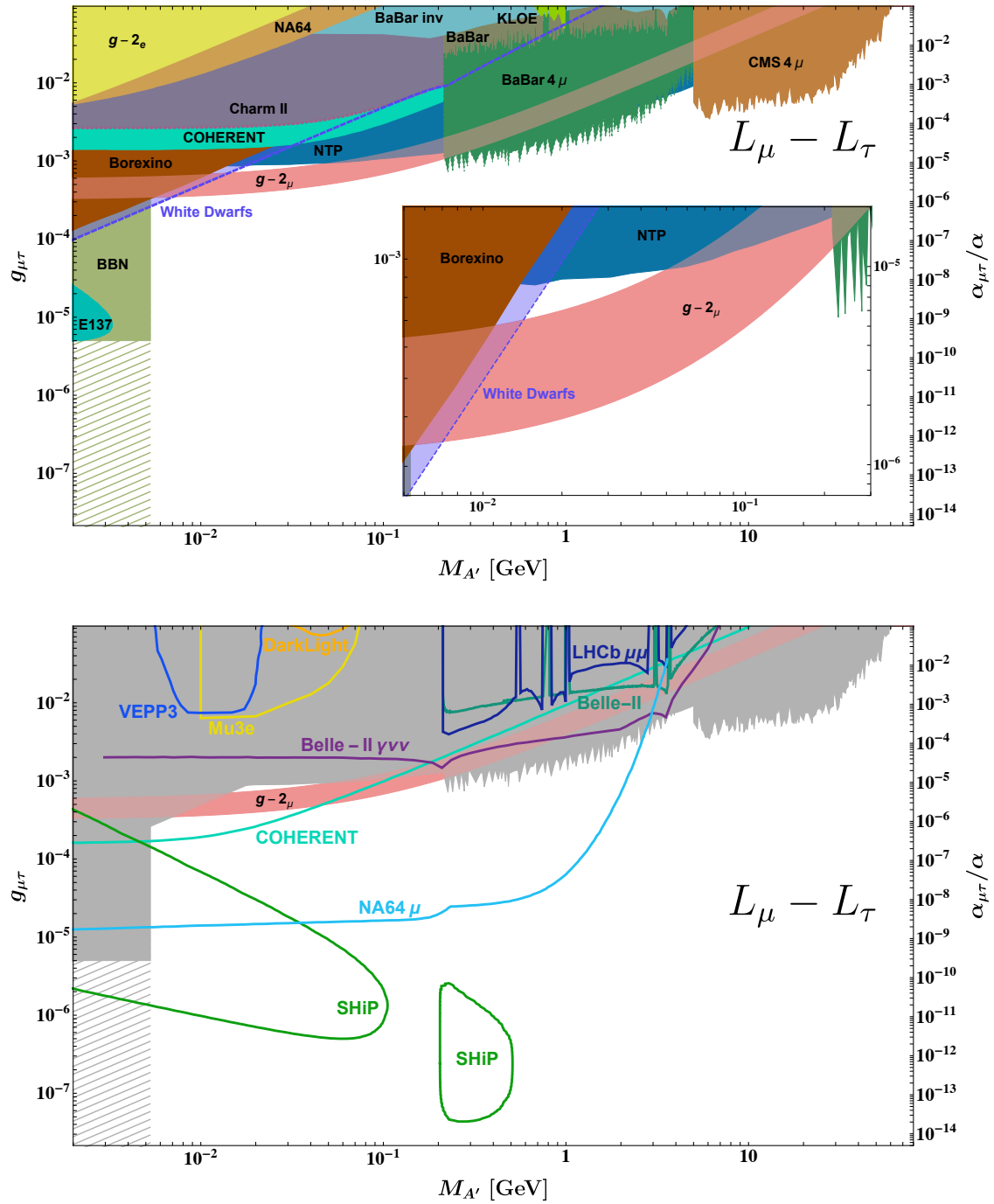

Figure 4.18: Constraints from current (upper panel) and future (lower panel) experiments on a $U(1)_{L_\mu - L_\tau}$ gauge boson with gauge coupling $g_{\mu-\tau} = \epsilon\, e$. The red band shows the $2\,\sigma$ preferred region for $(g-2)_\mu$. The grey area in the lower plot show the current limits. Additional constraints from supernova cooling are not shown (see Section 4.4.3). Figure adapted from [262].

4.6 Conclusions

In this chapter, we have investigated and collected phenomenological constraints on weakly coupled gauge bosons of the anomaly-free gauge groups $U(1)_{B-L}$, $U(1)_{L_\mu - L_\tau}$, $U(1)_{L_\mu - L_e}$ and $U(1)_{L_e - L_\tau}$. For this purpose, we have considered a wide variety of constraints from laboratory experiments as well as astrophysical and cosmological observations. We also provide a survey of future planned and proposed experiments. Our main results are summarized in Figs. 4.15 to 4.18.

Important constraints can be translated from experiments and observations limiting hidden photons interacting only via kinetic mixing (see Fig. 4.14 and cf. also [284]). However, there are also a number of significant differences as well as special features that need to be taken into account.

- All the gauge bosons considered in this analysis interact with neutrinos. This makes them amenable to experiments and observations from neutrino physics, which results in important additional constraints. The reactor experiments TEXONO and Super-K provide the leading constraints for a sizable part of the parameter space in the case of $U(1)_{B-L}$, $U(1)_{L_\mu - L_e}$ and $U(1)_{L_e - L_\tau}$. DUNE has the potential to significantly increase these limits for $U(1)_{L_\mu - L_e}$ and $U(1)_{L_e - L_\tau}$. Limits from white dwarf cooling, which have not been considered before, provide the leading constraint for a $U(1)_{L_\mu - L_\tau}$ in the low mass region, which is slightly better than the Borexino limit. Moreover, a future high-exposure run of COHERENT will probe substantial parts of the $(g-2)_\mu$ explanation.

- The gauge bosons of purely leptonic gauge groups interact with hadrons only via kinetic mixing. This kinetic mixing is automatically generated by the SM particles, and is finite. Taking this mixing into account, those gauge bosons can also be tested in experiments with protons and other hadrons, providing limits previously not considered.

- A gauge boson of $U(1)_{L_\mu - L_\tau}$ has direct interactions only with the second and third generation leptons. Again the loop-generated kinetic mixing becomes important, but the corresponding limits are generally weaker. This shows a clear need for experiments that directly use muons or taus. Particularly since this gauge group still allows for a viable explanation of the $(g-2)_\mu$ anomaly.

Going beyond the existing experiments, we can look towards a bright future. Proposed experiments like SHiP, SeaQuest, LHCb, CodexB, FASER, MATHUSLA, Belle-II, a muon run of NA64, Mu3e as well as neutrino experiments such as DUNE and COHERENT, will explore large and interesting areas of parameter space and thereby provide many opportunities for a discovery.

Chapter 5

Exploring the dark matter connection of hidden photons

The content of this chapter corresponds to work done in a previous study that is published as Ref. [412]. In this context, we have extended previous work by considering a vector-like fermion χ charged under a $U(1)_{L_\mu - L_\tau}$ symmetry instead of a dark $U(1)_X$. Building on our own results of Ref. [262], we consider the full set of constraints on the associated hidden gauge boson in addition to the bounds on the DM particle χ. Nearly all results in this chapter, including the plots and tables as well as a significant part of the text, are identical to that in the publication.

5.1 Introduction

One of the most fundamental shortcomings of the SM is the absence of a viable candidate for DM. However, we know today that the fraction of the energy density of the universe attributed to non-luminous DM is approximately five times higher than the one due to ordinary baryonic matter. Historically, the observed discrepancy in the velocity distribution of galaxies in the coma cluster, which motivated Zwicky in 1933 [413] to speculate on the presence of a large fraction of DM, was the first of a series of experimental evidences for DM. Today we have ample evidence for the existence of DM from galaxy rotation curves [414–418], gravitational lensing [419–421], temperature fluctuations in the CMB [21, 422, 423] or baryon acoustic oscillations [424]. However, even in light of the recent determination of the cosmic DM relic abundance with unprecedented accuracy to $\Omega_{\rm DM} h^2 = 0.120 \pm 0.001$ [21], the true nature of DM remains unknown.

Pinning down the exact properties of DM has hence inspired a myriad of particle physics models. One class of particularly well-studied DM candidates are WIMPs (see [425] for a recent review). Lately, rather stringent bounds on heavy WIMPs [62, 68, 426] have lead to increased interest in the (sub-)GeV mass range [427–433], where many of the strong constraints can be evaded. One such class of models is that of a dark sector charged under a new, secluded $U(1)_X$ symmetry. In these models, dark sector particles are only coupled to the SM via kinetic mixing of the new dark gauge boson with the SM hypercharge boson [156, 265, 434–436].

As we have seen in Chapter 4, considering the case of a gauged $U(1)_{L_\mu - L_\tau}$ symmetry instead of a purely secluded dark $U(1)_X$, the $\sim 4\,\sigma$ excess of the anomalous muon magnetic moment $(g-2)_\mu$ observed at the BNL E821 experiment [93, 94, 232, 233] can still be explained. This leads us to the interesting question, whether this excess could be the imprint of new physics with a possible link to DM. In this chapter, we hence study an extension of the $U(1)_{L_\mu - L_\tau}$ model considered in Chapter 4 by adding a (vector-like) Dirac fermion χ charged under the new symmetry as a candidate for DM. Making the DM particle χ transform under a non-chiral representation of $U(1)_{L_\mu - L_\tau}$ cancels all potential gauge anomalies. The fact that χ is charged under $U(1)_{L_\mu - L_\tau}$ instead of a dark $U(1)_X$ will have important consequences for the DM phenomenology. In such a model, the DM particle couples mainly to muons, taus and neutrinos, but only via loop-suppressed kinetic mixing to electrons and hadrons. In particular, this means that the DM freeze-out abundance is primarily set when χ falls out of chemical equilibrium with the neutrinos. Typical DM direct detection bounds are drastically weakened in this model as they rely on elastic DM-electron and -nucleon scattering, which are both loop-suppressed.

In the literature, DM charged under a $U(1)_{L_\mu - L_\tau}$ symmetry has been studied for heavy (weak-scale) WIMPs [352, 437–442]. However, in this chapter we explore the MeV mass range. The purpose of this work is to show that there the $(g-2)_\mu$ anomaly [235, 252, 347, 443] and the observed DM relic abundance $\Omega_{\rm DM} h^2$ can *simultaneously* be explained. This is not possible in the simple secluded dark sector scenario.

A similar scenario has been considered earlier in Ref. [444]. However, this approach differs in three crucial aspects: *i*) As was done in Chapter 4, we fully take into account unavoidable loop-induced kinetic mixing $-\epsilon_Y/2\,\hat{B}_{\mu\nu}\hat{X}^{\mu\nu}$ of the new gauge boson with the SM hypercharge boson. *ii*) While the scenario explaining the EDGES anomaly presented in [444] requires a charge hierarchy of at least $\mathcal{O}(10^2)$, we do not impose any charge hierarchies larger than already present in the SM (i.e. $\mathcal{O}(10)$). Instead we focus on the case of $Q_\chi = 1$. *iii*) We include and calculate the full set of constraints on the associated hidden photon A' previously discussed in Chapter 4.

In the remainder of this chapter, we first introduce the model in Section 5.2 and discuss its chemical and kinetic decoupling from the SM plasma in the early universe. In Sections 5.3 and 5.4, we study constraints on the DM particle χ from astrophysical and cosmological observations, as well as from laboratory experiments. In Section 5.5, we briefly outline the impact of the DM particle on the hidden photon constraints considered in Chapter 4. Finally, we present the results of our analysis and conclude in Section 5.6.

5.2 Adding dark matter in a $U(1)_{L_\mu - L_\tau}$ model

Starting out from the minimal anomaly-free setup of an extra $U(1)_{L_\mu - L_\tau}$ symmetry treated in Chapter 4, we add a new SM-singlet fermion χ that transforms under a non-chiral representation of the new symmetry. Hence, under the full gauge symmetry $SU(3)_C \times SU(2)_L \times U(1)_Y \times U(1)_{L_\mu - L_\tau}$, both the left- and the right-handed components of the vector-like field χ transform as

$$\chi_{L/R} \sim (\mathbf{1}, \mathbf{1}, 0, Q_\chi)\,. \tag{5.1}$$

As the left- and right-handed chiral components of a fermion always contribute with opposite sign to the anomaly coefficients of mixed and pure gauge anomalies, the addition of such a vector-like fermion will preserve anomaly cancellation in the $U(1)_{L_\mu - L_\tau}$ model independent of the choice of Q_χ. The full Lagrangian of this model is then given by Eq. (2.32) extended by the interaction and mass term[1] of the new field χ,

$$\mathcal{L}_\chi = -g_{\mu\tau} Q_\chi \; \bar{\chi}\gamma_\mu \chi \; \hat{X}^\mu - m_\chi \bar{\chi}\chi \,. \tag{5.2}$$

As χ is only charged under $U(1)_{L_\mu - L_\tau}$ and not under $U(1)_Y$, it does not contribute to the loop-induced kinetic mixing $\epsilon_{\mu\tau}(q^2)$ of Eq. (4.10) (cf. also the discussion in Section 2.3.1). Analogously to Chapter 4, we are interested in the light regime $M_{A'} < M_Z$, where the hidden photon will only decay into fermionic final states with the partial decay widths given in Eq. (B.9). In this chapter, we take $m_\chi < M_{A'}/2$ so that the hidden photon has an additional decay mode into a $\bar{\chi}\chi$ final state. Compared to the hidden photon width $\Gamma_{A',0}$ in the minimal setup of Chapter 4, the total width is increased by the $\bar{\chi}\chi$ contribution $\Gamma_{A'} = \Gamma_{A',0} + \Gamma_{A'\to\bar{\chi}\chi}$. The additional $\bar{\chi}\chi$ channel will also increase the invisible branching fraction of the A', making this scenario more sensitive to invisible searches.

5.2.1 Thermally averaged cross section

In order to study the DM phenomenology of the extra fermion χ, we will require knowledge of the thermally averaged DM annihilation cross section $\langle\sigma v\rangle$. In the following we will derive an approximate expression for $\langle\sigma v\rangle$ in the case of $m_\chi \ll M_{A'}$. We will discuss the limits of applicability of this approximate relation and also introduce the general expression.

Velocity expansion

For our model we can derive approximate expressions for the thermally averaged annihilation cross section by performing a low velocity expansion $\sigma v_{\text{rel}} = a_{\text{rel}} + b_{\text{rel}}\, v_{\text{rel}}^2 + ...$ A step-by-step prescription of how to obtain the corresponding expansion coefficients has been given in [446]. Keeping only the leading term a_{rel} (as the annihilation processes proceed via s-wave scattering) we find the approximate expression

$$\langle\sigma v\rangle_{\chi\bar{\chi}\to f\bar{f}} = g_{fA'}^2\, g_{\mu\tau}^2 Q_\chi^2\, \frac{N_c^f}{2\,\pi} \sqrt{1 - \frac{m_f^2}{m_\chi^2}}\; \frac{2m_\chi^2 + m_f^2}{\left(M_{A'}^2 - 4m_\chi^2\right)^2 + \Gamma_{A'}^2 M_{A'}^2}\,, \tag{5.3}$$

where N_c^f denotes the color factor of the final state and the coupling of the A' to the final state fermion f in the mass basis is given by

$$g_{fA'} = \begin{cases} g_{\mu\tau}\, Q_f\,, & \text{for fermions charged under } U(1)_{L_\mu - L_\tau}\,, \\ \epsilon_{\mu\tau}(q^2)\, e\, Q_f^{\text{EM}}\,, & \text{for fermions coupling via kinetic mixing}\,. \end{cases} \tag{5.4}$$

[1] In this chapter we are not studying explicitly the scalar breaking of the $U(1)_{L_\mu - L_\tau}$ and hence treat m_χ and $M_{A'}$ as effectively free parameters. For studies of the impact of the extra scalar in hidden photon models see e.g. [434, 445].

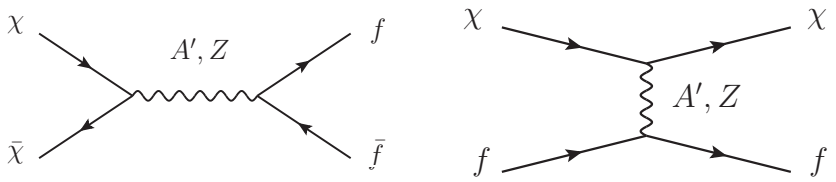

Figure 5.1: Feynman diagrams of processes relevant for early universe cosmology. (Left) DM annihilation into a $f\bar{f}$ final state relevant for setting the freeze-out relic abundance. (Right) Elastic scattering of the DM particle χ off the SM fermion f responsible for keeping the DM and SM sector in kinetic equilibrium.

Note that in order to obtain the expression for DM annihilation into massless left-handed neutrinos, the expression in Eq. (5.3) has to be divided by a factor of 2 due to the missing right-handed component.

The above expression Eq. (5.3) is a good approximation of the thermally average DM annihilation cross section as long as the DM mass lies well below the A' mass pole $m_\chi \ll M_{A'}/2$. However, in this chapter we will be interested in exploring the near-resonance region $m_\chi \lesssim M_{A'}/2$ as this is phenomenologically particularly appealing. In [447] it has been shown that some care has to be taken when using the velocity expansion in the thermal average near a pole in the cross section. Hence, we will have to calculate the exact thermal average whenever we are interested in the near-resonance scenario.

Full thermal average

The full thermal average of the DM annihilation cross section can be calculated following [448] from the expression

$$\langle\sigma v\rangle_{\rm CM} = \frac{x}{2\,[K_1^2(x)+K_2^2(x)]}\int_2^\infty \mathrm{d}z\,\sigma(z^2 m_\chi^2)(z^2-4)z^2\,K_1(zx)\,, \tag{5.5}$$

where $x = m_\chi/T$ and $z = \sqrt{s}/m_\chi$ and $K_n(x)$ are the modified Bessel functions of the second kind.

The general cross section of the process $\chi\bar{\chi}\to f\bar{f}$ shown in the left panel of Fig. 5.1 can be expressed as

$$\sigma_{A'}(s) = g_{fA'}^2\,g_{\mu\tau}^2 Q_\chi^2\,\frac{N_c^f}{12\,\pi}\sqrt{\frac{s-4m_f^2}{s-4m_\chi^2}}\,\frac{s^2+2\,(m_\chi^2+m_f^2)\,s+4\,m_\chi^2\,m_f^2}{s\,\left((s-M_{A'}^2)^2+\Gamma_{A'}^2 M_{A'}^2\right)}\,, \tag{5.6}$$

with $g_{fA'}$ as in Eq. (5.4). In principle, there are also contributions to the cross section from Z-mediation and the interference term. These contributions are, however, generically suppressed by at least a factor of $\epsilon_{\mu\tau}/g_{\mu\tau}\times M_{A'}^2/M_Z^2$ relative to the A' contribution and therefore may safely be neglected below the Z resonance.

Kinetic decoupling

As we will later be interested in calculating the thermally averaged annihilation cross section $\langle\sigma v\rangle$ at the time of recombination we will have to track the temperature T_χ of the

DM gas after chemical decoupling (i.e. **freeze-out**) during the evolution of the universe. After chemical decoupling elastic scattering processes as depicted in the right panel of Fig. 5.1 will still energetically equilibrate the DM with the SM sector. Therefore, the DM gas will still be in local thermal equilibrium with the SM plasma and essentially track the plasma temperature T [449]. Only after elastic scattering has become inefficient the two sectors are kinetically decoupled and the temperature of the DM gas will evolve as that of non-relativistic matter. In [450] the functional form of the DM temperature evolution $T_\chi(T)$ has been derived from first principles. Approximating the zero-momentum elastic scattering amplitude $|\mathcal{M}|^2_{t=0} \propto c_n(\omega/m_\chi)^n$ by the leading power n of the energy ω of the scattered heat bath particle and the corresponding expansion coefficient c_n, one finds

$$\frac{T_\chi}{T} = \left\{ 1 - \frac{z^{1/(n+2)}}{n+2} \exp(z) \Gamma[-(n+2)^{-1}, z] \right\}_{z=\frac{a}{n+2}\left(\frac{T}{m_\chi}\right)^{n+2}} , \tag{5.7}$$

where Γ is the incomplete Gamma function and the parameter a is defined as

$$a = \sum_f \left(\frac{5}{2(2\pi)^9 g_\star} \right)^{\frac{1}{2}} g^f_{\mathrm{SM}} c_n \, N^+_{n+3} \, \frac{M_{Pl}}{m_\chi} , \tag{5.8}$$

with the functional form of N^+_{n+j} given in Appendix B of [450]. The sum runs over all scattering partners f with g^f_{SM} internal degrees of freedom and $g_\star$ denotes the heat bath relativistic degrees of freedom [451]. By means of Eq. (5.7), the temperature at kinetic decoupling T_{kd} is finally found to be

$$\frac{T_{\mathrm{kd}}}{m_\chi} = \left(\left(\frac{a}{n+2} \right)^{1/(n+2)} \Gamma\left[\frac{n+1}{n+2} \right] \right)^{-1} . \tag{5.9}$$

For details on the derivation of kinetic decoupling and the evolution of the DM temperature we refer the reader to [450].

With this formalism at hand and the low energy behavior of the elastic DM-SM scattering amplitudes given by

$$c^f_{n=0} = g^2_{fA'} \, g^2_{\mu\tau} Q^2_\chi \, \frac{4 N^f_c \, m^4_f}{M^4_{A'} + \Gamma^2_{A'} M^2_{A'}} , \qquad \text{for massive fermions } f , \tag{5.10}$$

$$c^f_{n=2} = g^4_{\mu\tau} Q^2_\chi \, \frac{8 m^4_\chi}{M^4_{A'} + \Gamma^2_{A'} M^2_{A'}} , \qquad \text{for massless neutrinos } \nu , \tag{5.11}$$

we can track the evolution of the DM temperature down to kinetic decoupling and below.

5.2.2 Relic abundance

As we want the new vector-like fermion χ to play the role of DM, we will have to calculate its relic abundance Ω_χ in the universe today. In the model under study here, the DM-SM interactions are sizable enough for the gas of DM particles χ to have been in chemical (and kinetic) equilibrium with the SM heat bath in the early universe. In the following, we will summarize how this condition can lead to a non-zero DM relic abundance from freeze-out of equilibrium annihilation processes.

Boltzmann equation

Kinetic theory tells us that the evolution of phase-space density $f(\vec{p},\vec{x},t)$ of a particle species is in general governed by the Boltzmann equation (BE),

$$L[f] = C[f]\,, \tag{5.12}$$

where the left-hand side is the Liouville operator [452]

$$L[f] = \left(\frac{\partial}{\partial t} + \frac{\vec{p}}{m}\cdot\nabla_{\vec{x}} + \vec{F}\cdot\nabla_{\vec{p}}\right) f\,, \tag{5.13}$$

describing the total net rate of f. The right-hand side of the BE is the collision term describing the loss and gain of particles due to interactions with other particle species.
In a homogeneous and isotropic Friedmann-Lemaître-Robertson-Walker (FLRW) background it is reasonable to assume that the particle distribution function will, however, only depend on t and E, so that $f = f(t,E)$. Then the Liouville operator simplifies to

$$L[f] = \frac{\partial f}{\partial t} - H\frac{|\vec{p}|^2}{E}\frac{\partial f}{\partial t}\,, \tag{5.14}$$

where $H = \dot{a}/a$ is the Hubble expansion rate and a denotes the scale factor of the universe. Ultimately, we are not interested in the phase-space distribution $f(t,E)$ of the DM but rather in its number density

$$n = \int f(t,E)\frac{g_\chi \mathrm{d}^3p}{(2\pi)^3}\,, \tag{5.15}$$

with g_χ denoting the number of spin degrees of freedom of the particle χ. We can derive a BE for n by integrating Eq. (5.12) over the DM momentum. The integrated Liouville operator reads

$$\int L[f]\frac{g_\chi \mathrm{d}^3p}{(2\pi)^3} = \dot{n} + 3Hn\,. \tag{5.16}$$

Integration over the collision term will leave us only with the inelastic contributions [448] from $\chi\bar{\chi} \leftrightarrows f\bar{f}$ processes as shown in the left diagram of Fig. 5.1. We can then write the integrated collision term for the annihilation of two particles, 1 and 2, into two others, 3 and 4, as

$$\int C[f_1]\frac{g_\chi \mathrm{d}^3p}{(2\pi)^3} = \sum_{\text{spins}}\int \Big[f_1 f_2(1\pm f_3)(1\pm f_4)|\mathcal{M}_{\chi\bar{\chi}\to f\bar{f}}|^2 - f_3 f_4(1\pm f_1)(1\pm f_2)|\mathcal{M}_{f\bar{f}\to\chi\bar{\chi}}|^2\Big] \times (2\pi)^4\delta^{(4)}(P_i - P_f)\prod_{i=1}^{4}\frac{\mathrm{d}^3p_i}{(2\pi)^3 2E_i}\,. \tag{5.17}$$

With the two expressions Eqs. (5.16) and (5.17) at hand, we can derive a very elegant equation for the DM number density n_χ under the assumption that the created SM products $f\bar{f}$ go quickly into equilibrium with the SM bath and by using unitarity and the principle of detailed balance in equilibrium (cf. Ref [448] for a detailed derivation). If one

further substitutes the definition of the cross section in the collision term, the BE for n_χ finally reads

$$\dot{n}_\chi + 3Hn_\chi = -\frac{\langle\sigma v\rangle}{2}(n_\chi^2 - n_{\chi,\mathrm{eq}}^2)\,. \tag{5.18}$$

However, in writing Eq. (5.18) we have to take care of treating the decrease in number density caused by the expansion of the universe, which is manifest in the term proportional to the Hubble expansion H. In defining the quantity $Y = n/s$, where $s = S/a^3$ is the entropy density of the universe, we can go into the comoving frame and treat the Hubble expansion implicitly. Here, we assume absence of entropy production $\dot{S} = 0$. If we then change from our time variable t to $x = m_\chi/T$, with the photon temperature T, the BE can very elegantly be written as

$$\frac{\mathrm{d}Y}{\mathrm{d}x} = -\left(\frac{45}{\pi}G\right)^{-\frac{1}{2}} \frac{g_\star^{1/2} m_\chi}{x^2}\frac{\langle\sigma v\rangle}{2}\left(Y^2 - Y_{\mathrm{eq}}^2\right)\,, \tag{5.19}$$

where G is the gravitational constant and $g_\star$ denotes the effective degrees of freedom of the universe [451].

Freeze-out

At the temperature x_f, when the interaction rate $\Gamma = n\,\langle\sigma v\rangle$ drops below the Hubble rate H, the right-hand side of Eq. (5.19) becomes negligible. Thus, the density Y does not change anymore and becomes approximately constant. On the other side, the equilibrium density is given by [453]

$$Y_{\mathrm{eq}} = \frac{45}{2\pi^4}\left(\frac{\pi}{8}\right)^{\frac{1}{2}} \frac{g_\chi}{g_s}\, x^{\frac{3}{2}}\, e^{-x}\,, \tag{5.20}$$

where g_s denotes the number of entropy degrees of freedom. From this expression it becomes clear that the equilibrium density falls off exponentially with increasing temperature x. However, we just saw that for $x > x_f$ the density Y remains constant and cannot track the equilibrium density anymore. Hence, the density Y falls out of equilibrium and **freezes out**.

In order to obtain this freeze-out density for our DM candidate χ, we have implemented our model in `Feynrules` [195]. We then use the program package `MadDM` v.3.0 [454] to solve the differential equation Eq. (5.19) numerically to obtain the freeze-out temperature x_f and density Y_f at chemical decoupling. From these values the asymptotic DM density Y_0 at present time can be found from

$$\frac{1}{Y_0} = \frac{1}{Y_f} + \left(\frac{45}{\pi}G\right)^{-\frac{1}{2}} \int_{x_f}^{x_0} \frac{g_\star^{1/2} m_\chi}{x^2}\frac{\langle\sigma v\rangle}{2}\,\mathrm{d}x\,. \tag{5.21}$$

Finally, the present-day relic abundance of the DM particle χ can be obtained from the present-time density Y_0 via

$$\Omega_\chi = \frac{\rho_\chi}{\rho_{\mathrm{crit}}} = 8\pi G\,\frac{m_\chi s_0 Y_0}{3H_0^2}\,, \tag{5.22}$$

where quantities with subscript zero refer to their present-time values.

5.3 Astrophysical and cosmological constraints

With the discussion of the relevant tools to compute thermally averaged cross sections, as well as the chemical and kinetic decoupling of χ in the previous section, we are now ready to study the phenomenology of the DM particle χ charged under $U(1)_{L_\mu - L_\tau}$. In the following section, we will discuss constraints on the DM parameter space arising from various astrophysical and cosmological observations. the results of our analysis of these constraints are summarized in Figs. 5.5 to 5.7 in Section 5.6.

5.3.1 Big bang nucleosynthesis

In the early universe, weak interactions kept neutrons and protons in chemical equilibrium via the reactions $n + \nu \leftrightarrows p + e^-$ and $n + e^+ \leftrightarrows p + \bar{\nu}$. However, once the temperature of the primordial plasma dropped below $\mathcal{O}(1)$ MeV, weak interactions became inefficient, neutrons and protons fell out of chemical equilibrium and the neutron-to-proton ratio froze out [455]. Only then neutrons and protons started binding together and formed light elements - the big bang nucleosynthesis (BBN).

The epoch when weak interactions became inefficient is mainly controlled by the expansion rate of the universe in the radiation domination era,

$$H^2 = \frac{8\pi G}{3}\,\rho_R\,. \tag{5.23}$$

Here, G again refers to the gravitational constant and the energy density stored in radiation can be written as

$$\rho_R = \rho_\gamma \left[1 + \frac{7}{8}\left(\frac{T_\nu^0}{T_\gamma}\right) N_{\text{eff}}\right]\,, \tag{5.24}$$

where ρ_γ is the photon energy density, T_ν^0 and T_γ denote the neutrino and photon temperatures, respectively, and N_{eff} are the effective number of neutrinos.

In Section 4.4.3, we have discussed how the presence of a light neutrino-coupled hidden photon A' affects N_{eff} during BBN. We will now consider the impact of a light DM candidate coupled to neutrinos. In the model studied here, the fermionic WIMP χ with g_χ internal degrees of freedom is kept in thermal equilibrium with neutrinos via the A'-mediated interactions. In this case, the effective number of neutrinos can be parametrized as [456]

$$N_{\text{eff}}(y_\nu) = \left(\frac{T_\nu^0}{T_\gamma}\right)^{-4}\left(\frac{T_\nu}{T_\gamma}\right)^4 \left[N_\nu + \frac{g_\chi}{2} I(y_\nu)\right]\,, \tag{5.25}$$

where we have defined $y_\nu = m_\chi / T_\nu$, and T_ν^0 and N_ν refer to the temperature and number of neutrinos in the SM. In this scenario, the neutrino-to-photon temperature ratio can be expressed as

$$\frac{T_\nu}{T_\gamma} = \left(\frac{T_\nu^0}{T_\gamma}\right)\left[\frac{N_\nu + \frac{g_\chi}{2} F(y_\nu|_{T_D})}{N_\nu + \frac{g_\chi}{2} F(y_\nu)}\right]^{\frac{1}{3}}\,, \tag{5.26}$$

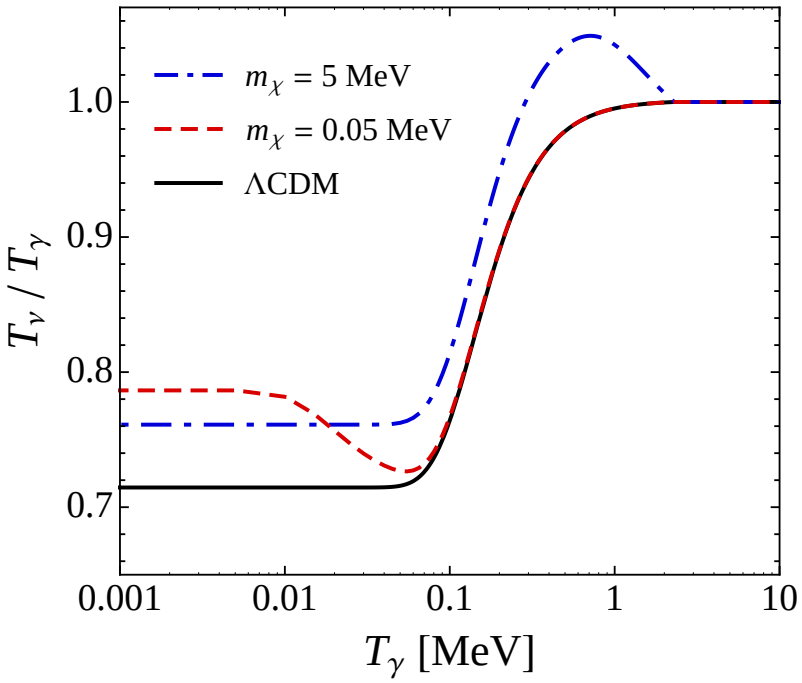

Figure 5.2: Evolution of the temperature ratio T_ν/T_γ with the photon temperature T_γ. The black solid lines shows the evolution in the standard cold DM cosmology (ΛCDM). The red and the blue line assume a (Majorana) DM particle in equilibrium with neutrinos. For a DM mass of $m_\chi = 5$ MeV (blue line), thermal decoupling of the DM gas from the neutrinos happens partly during BBN and part of the reheating energy can be transferred to the photons. For $m_\chi = 0.05$ MeV (red line), decoupling happens fully after BBN and DM only reheats the neutrinos. Figure taken from [456].

with the integrals

$$I(y) = \frac{120}{7\pi^4}\int_y^\infty \mathrm{d}\xi \frac{\xi^2\sqrt{\xi^2-y^2}}{e^\xi+1}\,, \tag{5.27}$$

$$F(y) = \frac{30}{7\pi^4}\int_y^\infty \mathrm{d}\xi \frac{(4\xi^2-y^2)\sqrt{\xi^2-y^2}}{e^\xi+1}\,, \tag{5.28}$$

and the neutrino decoupling temperature T_D.

In general, the extra particle χ will reheat the neutrino gas when χ becomes non-relativistic at a temperature $T \sim m_\chi$ and thus lead to a higher neutrino-to-photon ratio T_ν/T_γ than in the SM. If χ becomes non-relativistic before neutrino decoupling at temperatures $T_\gamma > T_D$ part of the reheating will take place when photons and neutrinos are still in equilibrium and hence the photon will also be partially reheated [456]. This leads to a moderate increase in the final T_ν/T_γ (cf. e.g. blue line in Fig. 5.2).

However, as illustrated by the red line in Fig. 5.2, if the reheating takes place fully after neutrino decoupling the final T_ν/T_γ will have significantly increased. This increase in the temperature ratio will in return lead to an elevated N_{eff} and therefore to a higher energy

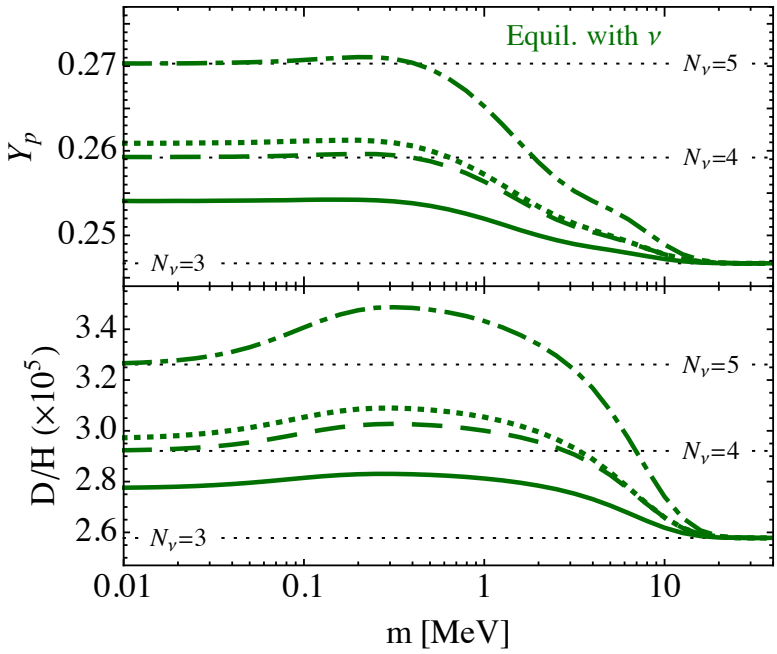

Figure 5.3: Variations of the relic ^{4}He abundance Y_p and the deuterium-to-hydrogen ratio D/H with the mass of the DM particle m_χ. The green solid and dotted lines show the scenario of the DM particle being a real or complex scalar, and the green dashed and dash-dotted lines of being a Majorana or Dirac (this work) fermion, respectively. The horizontal black dotted lines illustrate the predicted abundances for N_ν equivalent (massless) neutrinos. Figure taken from [457].

density ρ_R, as can be seen from Eqs. (5.24) and (5.25). As a consequence of the thus increased Hubble expansion rate (cf. Eq. (5.23)), the weak interactions maintaining chemical equilibrium between neutrons and protons will become inefficient earlier and hence the neutron-to-proton ratio will freeze out earlier. This will lead to a higher neutron abundance at BBN. These additional neutrons will be efficiently synthesized into stable ^{4}He and in turn will lead to an increase in the observed helium relic abundance Y_p. On similar grounds, an increased expansion rate of the universe will also lead to an earlier freeze-out of processes depleting the created deuterium abundance. A measurable consequence of this will be an elevated deuterium-to-hydrogen ratio D/H in the late-time universe. Both these effects are nicely summarized by the plots in Fig. 5.3.

These expected deviations from their respective SM predictions have been confronted with first results from the Planck satellite [458] for extra light Dirac fermions in [457,459]. The analysis of [459] excludes extra light fermions χ with masses below

$$m_\chi \lesssim 9.28 \text{ MeV}\,, \tag{5.29}$$

assuming that χ has been in thermal equilibrium with the neutrinos all throughout BBN.

This constraint can not be applied anymore once the DM particle starts to decouple kinetically from the neutrino gas at BBN temperatures of $T_\gamma^{\rm BBN} \approx 1$ MeV. Therefore, we

have scanned the decoupling temperature $T_{\rm kd}$ of χ as a function of the coupling constant $g_{\mu\tau}$ for $m_\chi \leq 9.28$ MeV by use of Eq. (5.9) and only plotted the limit in the region where $T_{\rm kd}(g_{\mu\tau}) \leq T_\nu^{\rm BBN}$.

5.3.2 Cosmic microwave background

The cosmic microwave background (CMB) radiation formed at the time of last scattering of photons, before they decoupled from the primordial plasma. However, as the photon gas did not decouple instantaneously but rather during some finite period, the surface of last scattering has a finite width (in time). A significant increase in the post-recombination ionization of the plasma due to DM decays would in turn lead to extra free electrons and photons broadening this last scattering surface. Such a broadening would modify the temperature and polarization power spectra of the CMB [460] and hence should be visible in measurements of these spectra with e.g. the WMAP [461] or Planck [462] satellite.

In order to use this to constrain the interactions of the DM particle χ, we have to quantify the energy of the DM decays that proceeds into the plasma. The amount of additional energy released per unit volume [463] is given by

$$\frac{{\rm d}E}{{\rm d}t\,{\rm d}V}(z) = 2g\rho_{\rm crit}^2 c^2 \Omega_c (1+z)^6 P_{\rm ann}(z)\,, \tag{5.30}$$

with the model-dependent DM annihilation parameter

$$P_{\rm ann}(z) = f(z)\frac{\langle\sigma v\rangle}{m_\chi}\,. \tag{5.31}$$

Here, $f(z)$ is a redshift-dependent efficiency factor characterizing the fraction of rest-mass energy released into the gas. This has been calculated for the case of electrons and photons in [463, 464] for several models via DM cascade decays into stable particles. However, as current CMB data is only sensitive to energy injection during a rather narrow range of redshifts, $z \sim 1000 - 600$, one can neglect the redshift dependence and take $f_{\rm eff}$ to be constant over the time that the CMB formed. For electron and photon final states these constant coefficients have been calculated in [465] as a function of energy. Using these, a mass-dependent effective efficiency factor quantizing the amount of energy proceeding into photons and positrons can be derived,

$$f_{\rm eff}(m_\chi) = \frac{1}{2m_\chi}\int_0^{m_\chi} E\,dE\left[2\,f_{\rm eff}^{e^+e^-}(E)\,\frac{dN_{e^+}}{dE} + f_{\rm eff}^{\gamma}(E)\frac{dN_\gamma}{dE}\right]\,, \tag{5.32}$$

where dN_{e^+}/dE and dN_γ/dE are the positron and photon spectra, respectively. In [465] these coefficients have been provided for various annihilation channels down to DM masses of $\mathcal{O}$(GeV).

The annihilation parameter has been recently constrained to

$$P_{\rm ann} < 3.5\times10^{-28}\ {\rm cm}^3 s^{-1}\ {\rm GeV}^{-1}\,, \tag{5.33}$$

by the very precise measurement of the CMB angular temperature and polarization power spectrum with the Planck satellite [21]. This constitutes an improvement of the limit of

about 17% over previous results [466]. For $m_\chi > 5$ GeV we have used this bound together with the effective efficiency factors $f_{\rm eff}$ provided in [465] to robustly constrain $\langle\sigma v\rangle$ by virtue of Eq. (5.31).

However, these efficiency factors have been calculated only for $m_\chi \gtrsim 5$ GeV in [465]. As we are mainly interested in MeV-scale DM, we will apply the somewhat conservative bound of $\langle\sigma v\rangle/m_\chi < 5.1\times10^{-27}{\rm cm}^3 s^{-1}{\rm GeV}$ derived in [467] for $m_\chi \lesssim 5$ GeV. Taking into account the recent 17% improvement of the Planck limit this bound reduces to

$$\frac{\langle\sigma v\rangle}{m_\chi} < 4.35\times10^{-27}{\rm cm}^3 s^{-1}{\rm GeV}^{-1}\,, \tag{5.34}$$

as the annihilation parameter $P_{\rm ann}$ is linear in $\langle\sigma v\rangle$.

5.3.3 Dwarf spheroidal galaxies

Dwarf spheroidal galaxies in our local group expose rather significant DM densities [468]. These objects of high DM densities are therefore of particular interest in the study of DM annihilations. Typically, pairs of DM particles can annihilate into SM particles as shown in the left panel of Fig. 5.1. These decay products usually further decay down in cascades into stable electrons, positrons and photons. If the DM particle is assumed to be a WIMP it can typically produce highly energetic gamma rays due to its high mass. These products can in turn be searched for in gamma ray telescopes.

Given a model of DM, we can determine the spectrum of gamma ray photons dN_γ/dE from its different decay channels

$$\frac{dN_\gamma}{dE} = \sum_f {\rm Br}_f \frac{dN_\gamma^f}{dE}\,, \tag{5.35}$$

where ${\rm Br}_f$ is the branching fraction of the DM annihilation into final state f and dN_γ^f/dE the corresponding yield of gamma ray photons. Before we can use the gamma ray photon yield within dwarf galaxies as a constraint on the DM particle, we still need to know the exact DM density of a given dwarf galaxy.

It has been demonstrated by use of N-body simulations that the DM densities of spheroidal galaxies independent of their halo mass are well described by a Navarro-Frenk-White (NFW) profile [469]

$$\frac{\rho_{\rm DM}(r)}{\rho_{\rm crit}} = \frac{\delta_c}{(r/r_s)(1+r/r_s)^2}\,, \tag{5.36}$$

where r_s is some scale radius, δ_c is a characteristic density and $\rho_{\rm crit} = 3H^2/8\pi G$ is the critical density for closure. With this knowledge of the local DM density $\rho_{\rm DM}(r)$ of dwarf spheroidal galaxies, the flux of gamma ray photons observed in a solid angle $\Delta\Omega$ at the Fermi Large Area Telescope (Fermi-LAT) is given by [470]

$$\phi_s(\Delta\Omega) = \underbrace{\frac{1}{4\pi}\frac{\langle\sigma v\rangle}{2m_{\rm DM}^2}\int_{E_{\rm min}}^{E_{\rm max}}\frac{{\rm d}N_\gamma}{{\rm d}E}\,{\rm d}E_\gamma}_{\text{particle physics}} \times \underbrace{\int_{\Delta\Omega}\int_{l.o.s}\rho_{\rm DM}(r)^2 {\rm d}l{\rm d}\Omega'}_{J-\text{factor}}\,. \tag{5.37}$$

The second term is the line of sight integral through the DM distribution, the so-called J-factor, and only depends on astrophysics. These J-factors have been well studied in the literature for the Milky Way dwarf galaxies and can be extracted from e.g. [471]. Therefore, provided knowledge of the differential photon yield per DM annihilation $\mathrm{d}N_\gamma/\mathrm{d}E$ one can place stringent limits on $\langle\sigma v\rangle$ from the different DM annihilation channels. By making use of Eq. (5.37), this has been done for individual final states of DM annihilations in [470,472].

5.3.4 Cosmic ray positron flux

The Cosmic Ray (CR) positron fraction has been accurately measured at the international space station with the AMS-02 detector [33, 34]. The findings of the AMS-02 experiment exhibit a rise in the positron spectrum at energies above ~ 10 GeV. This confirms earlier hints found by PAMELA [30] and Fermi-LAT [32]. While there is still an ongoing debate on whether nearby pulsars could efficiently source enough high energy positrons to explain this rise in the positron spectrum [473,474], typical sources of CR positrons are supernova explosions accelerating the Interstellar Medium (ISM) or inelastic scatterings of primary CR charged particles like protons and nuclei with the ISM [475].

An alternative explanation of the observed rise in the positron fraction could be due to annihilations and decays of DM particles as was argued for example in [265,266]. Typically, in such models the DM particle is a rather heavy WIMP ($m_{\mathrm{DM}} \sim \mathcal{O}(100)$ GeV) coupled to a GeV-mass mediator, which would naturally lead to enhanced annihilation cross sections into leptonic final states while suppressing hadronic ones. In this chapter, however, we rather want to use the high accuracy measurement of the positron fraction at AMS-02 to constrain the various annihilation channels of the light DM particle χ. In that sense, CR positrons are a complementary astrophysical probe to gamma ray photons in the study of DM interactions.

Positrons injected by DM annihilations can be described by the source term

$$Q_{\mathrm{DM}} = \frac{1}{2}\langle\sigma v\rangle \left(\frac{\rho_\chi}{m_\chi}\right)^2 \sum_f \mathrm{Br}_f \frac{dN^f_{e^+}}{dE}\,, \tag{5.38}$$

where $dN^f_{e^+}/dE$ denotes the produced positron spectrum from an $\bar{f}f$ final state in analogy to the gamma ray spectrum of Eq. (5.35). The AMS-02 data has been used in [467] to set an upper limit on $\langle\sigma v\rangle$ for different single final-state annihilations. As the DM particle χ studied in this chapter annihilates into e^+e^- pairs only via kinetic-mixing suppressed interactions, dominant positron injection results mainly from secondary leptonic decays of τ^+ and μ^+ of the corresponding dilepton final state. From the analysis of [467], we find that the most stringent bound is set from secondary positron injection originating from the muonic DM annihilation final state. The resulting constraint on the DM annihilation cross section into muons is shown by the brown line in Figs. 5.5 to 5.7.

5.3.5 Cosmic neutrino fluxes

To conclude the section of astrophysical and cosmological probes, we will investigate the potential observational impact of DM interactions with neutrinos. If the DM particle χ is indeed charged under a local $U(1)_{L_\mu - L_\tau}$ gauge group, it necessarily interacts with

neutrinos either via annihilation (cf. left diagram of Fig. 5.1) or elastic scattering (cf. right diagram of Fig. 5.1). In this chapter, we are considering DM candidates with $\mathcal{O}(\text{MeV})$ masses, such that annihilations of the DM particles into a pair of tau- or muon-neutrinos is kinematically always possible. In fact as the DM particle is significantly heavier than neutrinos $m_\chi \gg m_\nu$, these annihilations will create a pair of monochromatic neutrinos with exactly the energy of the DM mass $E_\nu = m_\chi$.

We can utilize such DM-neutrino interactions as a possible DM detection signal. Assuming that DM annihilation in the Milky Way halo produce such pairs of neutrinos, in analogy to Eq. (5.37) we obtain a corresponding differential neutrino flux at earth of

$$\frac{d\phi}{dE_\nu} = R_i \, \frac{\langle \sigma v \rangle}{2 m_{\text{DM}}^2} \, \delta(E_\nu - m_\chi) \times \int_{\Delta\Omega} \int_{l.o.s} \rho_{\text{DM}}(r)^2 \mathrm{d}l \mathrm{d}\Omega' \,, \tag{5.39}$$

where the factor

$$R_i \approx \begin{cases} 1/5 \,, & \text{for } \nu_e \,, \\ 2/5 \,, & \text{for } \nu_\nu, \nu_\tau \,, \end{cases} \tag{5.40}$$

accounts for the flavor ratios of the neutrinos due to oscillation between production and detection [476].

One way to search for these neutrinos produced in DM annihilations in detectors is to search for inverse beta decay, where a $\bar{\nu}_e$ scatters off a free proton within the fiducial volume of the detector and produces a free neutron and positron. In particular, the low-threshold search for supernova relic neutrinos at the Super-Kamiokande water Cherenkov detector was used to look for positrons in the energy range $18 - 82$ MeV. This data has been reinterpreted to set limits on the thermally averaged cross section of DM particles with dominant neutrino interactions [477, 478]. We will show the corresponding limit in our exclusion plots in Section 5.6.

Using a projected improvement in the fiducial detector volume of a factor of ~ 25 and a background reduction of a factor of ~ 5 due to 0.1% of gadolinium doping of the water detector, the sensitivity of the planned Hyper-Kamiokande experiment to DM-induced neutrino fluxes has been explored in Ref. [479]. We have used the results of this study in order to derive a projected limit on the DM particle χ studied here.

5.4 Laboratory constraints

Complementary to the indirect search for cosmic signals as remnants of DM interactions, hypothetical couplings of the DM to SM particles are put to the test in laboratory direct detection experiments. In this section, we will discuss the sensitivity of electron and nucleon scattering experiments on a DM particle χ carrying charge under $U(1)_{L_\mu - L_\tau}$.

5.4.1 Nuclear scattering

One of the first strategies to search for DM interactions was to search for the nuclear recoil from elastic DM-nucleus scattering [480]. The differential rate of recoils in such a direct

detection experiment can be parametrized [481] as

$$\frac{dR}{dE_{\rm nr}} = \frac{\sigma_N\,\rho_\chi}{2m_\chi\,\mu_{\chi N}^2}\;F(q)^2\int_{v_{\rm min}}^{\infty}\frac{f(v)}{v}dv\,, \tag{5.41}$$

where σ_N is the elastic DM-nucleus scattering cross section, ρ_χ denotes the local DM density, $\mu_{\chi N} = m_\chi m_N/(m_\chi + m_N)$ is the DM-nucleus reduced mass and $F(q)$ denotes a form factor accounting for the finite size of the nucleus. The function $f(v)$ describes the distribution of the DM speed relative to the detector and $v_{\rm min} = (m_N E_{\rm nr}/2\mu_{\chi N}^2)^{1/2}$ is the minimum speed of the DM particle to result in a recoil $E_{\rm nr}$ [482]. The recoil energy per scattering depends quadratically on the momentum transfer q,

$$E_{\rm nr} = \frac{q^2}{2m_N}\,. \tag{5.42}$$

Similar to the hidden photon case of a secluded $U(1)_X$, kinetic mixing of the hypercharge boson with the $U(1)_{L_\mu - L_\tau}$ gauge boson induces a non-zero elastic DM-nucleus scattering cross section [483],

$$\sigma_N = \frac{1}{\pi}g_{\mu\tau}^2\,\epsilon_{\mu\tau}^2(q^2)\mu_{\chi N}^2\left|\frac{f_N^{(A')}}{M_{A'}^2} - \frac{\sin\theta_W\,f_N^{(Z)}}{M_Z^2 - M_{A'}^2}\right|^2\,, \tag{5.43}$$

where

$$f_N^{(X)} = \frac{1}{A}\Big(Z\,(2g_{uX} + g_{dX}) + (A - Z)\,(g_{uX} + 2g_{dX})\Big)\,. \tag{5.44}$$

Here, A and Z refer to mass and atomic number of the nucleus and $g_{qX} = g_{qX_L} + g_{qX_R}$ denotes the sum of the chiral couplings [439] of the quark q to the boson $X = (A', Z)$ in the mass basis. In models of gauged lepton-family number differences with kinetic mixing, as e.g. $U(1)_{L_\mu - L_\tau}$, these couplings read to leading power in the kinetic-mixing parameter $\epsilon_{\mu\tau}$ and the mass parameter δ defined in Eq. (4.7)

$$g_{qZ_{L/R}} = g_Z\left(T_3 - \sin(\theta_W)^2\,Q_{\rm EM}\right), \tag{5.45}$$

$$g_{qA'_{L/R}} = -g_Z\,\tan\theta_W\,\epsilon_{\mu\tau}(q^2)\,Q_{\rm EM}\big(1 - \sin(\theta_W)^2\big) + \mathcal{O}(\epsilon_{\mu\tau}\,\delta)\,. \tag{5.46}$$

In direct detection experiments the recoil spectrum of the target nuclei is then measured and utilized to constrain induced recoils from an elastic DM-nucleus cross section σ_N.

The current best such limit on the DM-nucleon scattering cross section comes from the 1 t×yr exposure dataset of the XENON1T experiment [68]. The XENON detector is a time projection chamber consisting of a cylindrical tank filled with 3.2 t of liquid xenon (LXe) instrumented above and below by arrays of photomultiplier tubes. The active volume is further defined by a cathode and a gate electrode, which provide a drift field for ionized electrons. With this setup, XENON is able to measure the nuclear recoil both from ionized electrons and prompt scintillation photons, which are generated from the relaxation of the electrons of the excited xenon atoms back into their ground state.

The typical momentum transfer of a cold DM particle with $v \sim 10^{-3}$ producing such nuclear recoil signals is to good approximation given by $q \sim m_{\rm DM} v$. In the case of MeV-mass light DM, then the typical recoil energy of a nucleus with $m_N \sim 10$ GeV scales as [484]

$$E_N = \frac{q^2}{2\, m_N} \approx 1 \text{ eV } \left(\frac{m_{\rm DM}}{100 \text{ MeV}}\right)^2 \left(\frac{10 \text{ GeV}}{m_N}\right) . \tag{5.47}$$

However, typical setups searching for elastic DM-nucleon interactions, like liquid xenon detectors, have $\mathcal{O}$(keV) thresholds [485]. These lie significantly above the typical light DM recoil energies. Consequently, nuclear scattering experiments are mainly sensitive to WIMPs with masses of $m_\chi \sim$ few 10 GeV. Nevertheless, with the experimental sensitivity expected to improve over the coming years, we can employ nuclear scattering techniques to probe light WIMP scenarios from the high-mass end of the spectrum.

In this spirit, we use the XENON1T limit on σ_N to constrain the parameter space of the DM particle χ. The proposed DARWIN experiment will follow a similar design concept as XENON and due to its planned total amount of 50 t of LXe will be able to probe even smaller cross sections [486]. In our analysis we will include projections for the expected DARWIN sensitivity.

5.4.2 Electron scattering

In canonical WIMP models with DM particles of weak-scale masses, direct detection of elastic DM-nucleus scattering quite severely constrain the WIMP parameter space. Even in the case of pure leptophilic DM that only interacts with electrons but not with quarks, the DM-nucleus interactions induced at one- and two-loop will impose more stringent bounds than those from direct detection of DM-electron scattering [487]. However, nuclear scattering loses all its sensitivity for sub-GeV DM candidates as discussed in the previous section, and we need to explore complementary strategies to search for these particles in direct detection experiments. Considering instead elastic DM-electron scattering, there are mainly two atomic processes that seem promising in detecting light DM interactions:

- **Electron ionization**. If the DM particle scatters off an electron bound in an atom in the detector target material, this might ionize the electron and kick it out of the atom. The corresponding signal would be individual electrons, which could be observed [488]. A particularly promising way to test this is in semiconductor materials. There the electron only has to be excited to the conduction band and then can induce a secondary signal from drifting and scattering due to an applied electric field [489].

- **Electronic excitation**. Similarly, if the scattered electron is not kicked out of the atom, but rather excited to a higher electronic level, it can emit a secondary photon from de-excitation [490]. Such DM-induced photon emission can potentially be detected from the scintillation light of e.g. xenon detectors [491].

In order to use these electronic processes to constrain potential DM-electron interactions, we have to calculate the corresponding scattering cross section. In a model-independent

way we can parametrize a reference cross section for DM-electron scattering as [484]

$$\bar{\sigma}_e = \frac{\mu_{\chi e}^2}{16\,\pi\,m_\chi^2\,m_e^2}\;\overline{|\mathcal{M}_{\chi e}(q)|^2}\,\Big|_{q^2=\alpha^2 m_e^2}\;\times\;|F_{\rm DM}(q)|^2\,, \tag{5.48}$$

where $\overline{|\mathcal{M}_{\chi e}(q)|^2}$ denotes the spin-averaged DM-electron scattering matrix element, $F_{\rm DM}(q)$ is a DM from factor and $q = \alpha m_e$ is a momentum transfer appropriate for atomic processes. For our model of a DM particle χ charged under a $U(1)_{L_\mu - L_\tau}$, kinetic mixing of the associated hidden photon A' with the SM photon leads to a non-zero elastic DM-electron scattering. In our case of $M_{A'} > m_e$, the DM form factor is found to be $F_{\rm DM}(q) = 1$ and the relevant scattering cross section reads

$$\bar{\sigma}_e = \frac{16\,\pi\,\mu_{\chi e}^2 \alpha\,\epsilon_{\mu\tau}^2(q^2)\,\alpha_{\mu\tau}}{(m_{A'}^2 + \alpha^2 m_e^2)^2}\,, \tag{5.49}$$

where $\mu_{\chi e}$ denotes the electron-DM reduced mass. The typical momentum transfer in DM-electron scatterings will be of $q \sim \mathcal{O}(\alpha\, m_e) \ll m_\mu, m_\tau$ [489]. Hence, the kinetic mixing will be constant in the relevant kinematic region,

$$\epsilon_{\mu\tau}(q \ll m_\mu, m_\tau) \approx -\frac{e\,g_{\mu\tau}}{4\pi^2}\;\log\left(\frac{m_\mu}{m_\tau}\right)\,. \tag{5.50}$$

One way to test this DM-electron scattering cross section is in ionization in the silicon and germanium crystal detectors of the future SuperCDMS SNOLAB experiment [492]. In [489] it has been pointed out that making use of both the measurement of phonon and ionization energy deposited in the crystal one can distinguish nuclear from electron recoil signals. This allows SuperCDMS to search specifically for DM-electron scattering events and put quite stringent constraints on the DM-electron scattering cross section for MeV-scale DM. However, as in our model the DM particle χ interacts with electrons only via loop-induced kinetic mixing, SuperCDMS will not be able to test unconstrained parameter space.

5.5 Hidden photon constraints

The model of a light vector-like DM particle χ discussed here is based on an extension of the minimal model of anomaly-free gauged $U(1)_{L_\mu - L_\tau}$ symmetry studied in Chapter 4. As such, this model is still subject to all the constraints on the associated hidden gauge boson A' discussed in Chapter 4. Hence, in order to obtain a complete picture of the phenomenology of this model we also have to take into account the effects of the DM particle χ on the hidden photon observables.

As we discussed briefly in Section 5.2, adding an extra DM fermion χ with mass $m_\chi < M_{A'}/2$ will lead to an increase of the hidden photon width due to the extra decay channel $A' \to \chi\bar{\chi}$. At a fixed hidden photon mass $M_{A'}$ and coupling constant $g_{\mu\tau}$, the increased width will reduce the A' lifetime compared to the minimal case. This means that the hidden photon will decay faster and therefore can in principle shift the sensitivity of beam dump experiments towards smaller coupling values at a given mass. However,

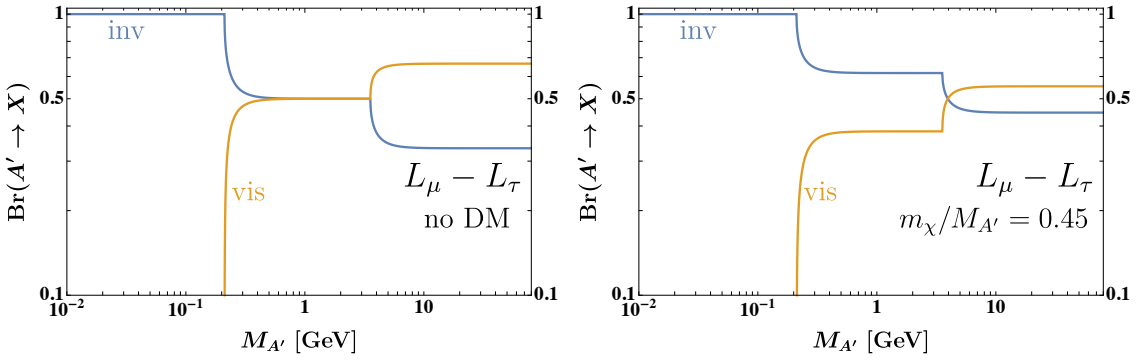

Figure 5.4: Branching ratio of the $U(1)_{L_\mu - L_\tau}$ boson into visible and invisible final states. (Left) The branching ratios in the minimal model without DM. In this case the invisible final state is given by the neutrinos ν_μ and ν_τ. The visible final states consists mainly of muons and taus. (Right) The branching ratios with a vector-like DM particle χ with mass ratio $m_\chi/M_{A'} = 0.45$ and charge $Q_\chi = 1$. In this case the invisible final state also contains the DM χ.

due to the additional decay channel into DM particles, the overall branching fraction into invisible final states will increase compared to the minimal case. This is illustrated by the two plot in Fig. 5.4. In the left panel we show the visible and invisible final states in the minimal model without DM. The right panel shows the case with DM. It is clearly visible that compared to the minimal model, here the invisible final states dominate the hidden photon decays below the ditau threshold. In general, this makes searches for invisible decays of the A' more sensitive to DM scenario and decreases the sensitivity of visible searches.

With this discussion in mind, we will consider all constraints on the hidden photon discussed in Chapter 4 in our analysis. To re-derive the limits for the DM scenario, we have to replace the hidden photon width $\Gamma_{A'}$ and the branching ratios with the corresponding expressions taking into account the presence of the new particle χ. In general, we will thus expect limits derived from visible searches to weaken and those from invisible searches to become more stringent. Finally, we will expect no effect on limits from e.g. elastic neutrino scattering measurements or white dwarf cooling that test the couplings themselves, but are insensitive to the A' branching fractions and total width.

5.6 Results

In the following section we present and discuss the results of our analysis of the combined hidden photon and DM parameter space in a model of gauged $L_\mu - L_\tau$ number. In our study of this model, we have fixed the ratio of the DM mass to the hidden photon mass $m_\chi/M_{A'}$. This allows us to present constraints on the model both from DM and hidden photon searches in the $g_{\mu\tau} - M_{A'}$ plane. This way of presenting the limits is particularly suited to see the interplay and complementarity of DM and hidden photon searches on the parameter space of this model. While in the literature models of fermionic DM coupled to a vector mediator are usually studied in an off-resonance scenario of $m_\chi/M_{A'} = 1/3$,

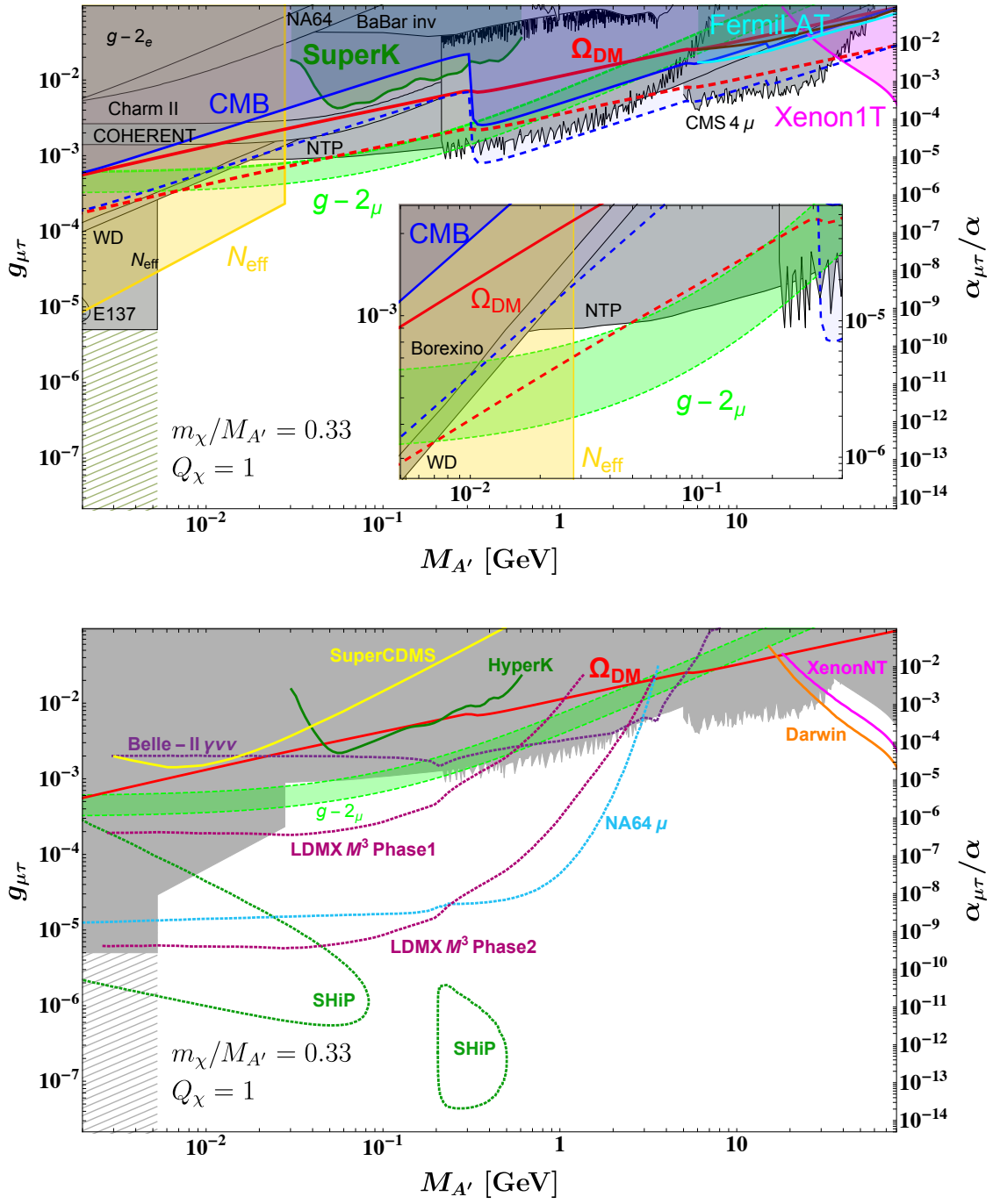

Figure 5.5: Current (upper panel) and future (lower panel) constraints on the combined parameter space of a $U(1)_{L_\mu - L_\tau}$ gauge boson and vector-like fermion of charge $Q_\chi = 1$ for $m_\chi/M_{A'} = 0.33$. Figure taken from [412].

one central goal of this chapter is to investigate how the phenomenology of such a model changes in the near-resonance region. In Fig. 5.5 we show the limits of our analysis in the Standard Benchmark (SB) scenario of $m_\chi/M_{A'} = 0.33$. For comparison, we have performed a second analysis in a Near-Resonance (NR) scenario with $m_\chi/M_{A'} = 0.45$ and a DM charge of $Q_\chi = 1$. The corresponding NR limits are shown in Fig. 5.6.

The greyscale contours (dotted lines) in the upper (lower) panels of Figs. 5.5 and 5.6 show current (projected) hidden photon constraints that were discussed in detail in Chapter 4. The constraints from white dwarf cooling (WD), neutrino trident production (NTP), and elastic neutrino scattering experiments (Borexino, COHERENT, CharmII) are completely unaffected by the presence of the DM particle χ. This is due to the fact that the corresponding observables directly probe the couplings of the hidden photon A' to SM particle (electrons, muons, neutrinos), but are not sensitive to the A' width or branching ratio, where the effect of χ would show up. Hence, the corresponding limits in both the SB and NR scenario are exactly the same as in the minimal $U(1)_{L_\mu - L_\tau}$ model discussed in Section 4.5.4.

Constraints from searches of visible decays (e.g. BaBar/CMS 4μ, SHiP, etc.) are generally weakened due to the reduced visible branching fraction of the A' as discussed in Section 5.5. Conversely, constraints from invisible searches (e.g. NA64 μ, LDMX M^3) become more stringent as the decay into a pair of DM particle contributes to the invisible final state. If the mass of the DM particle χ is close to resonance $m_\chi \approx M_{A'}/2$ both effects are less pronounced as the decay $A' \to \chi\bar{\chi}$ becomes phase-space suppressed.

The colored contours (solid lines) in the upper (lower) panels of Figs. 5.5 and 5.6 represent current (projected) limits from DM searches. While at low masses the most stringent limit is due to constraints on N_{eff} at BBN (yellow), the high-mass region is most constrained by the Xenon1T (magenta) limit on kinetic-mixing induced DM-nucleon scattering. In the intermediate mass region between the N_{eff} and Xenon1T limits, a combination of measurements of gamma rays at Fermi-LAT (cyan), positron fluxes at AMS-02 (brown) and energy injection into the CMB (blue) at Planck yield the most constraining limit on the DM particle χ. However, in this intermediate region the most stringent constraints on the model come from hidden photon searches in four-muon final states at BaBar and CMS, as well as the NTP limit on A'. Furthermore, we see that the projected limits from DM-electron scattering at SuperCDMS (yellow line), as well as the future expected bounds from cosmic neutrinos observed at Hyper-Kamiokande (green line) will not be able to test previously unprobed parameter space.

The red curve represents points in parameter space where the relic abundance of the particle χ accounts for all of the DM, $\Omega_\chi = \Omega_{\text{DM}}$. Points above the red curve, i.e. larger couplings at a given DM mass m_χ, correspond to regions where χ is a subcomponent of DM, $\Omega_\chi < \Omega_{\text{DM}}$. This can be made intuitively plausible, as lager couplings lead to a more efficient DM annihilation process during freeze-out. This kept the DM longer in chemical equilibrium with the SM sector in the early universe, such that freeze-out happened later and lead to a smaller relic abundance.

First, we note that in the SB scenario an explanation of Ω_{DM} is ruled out in the entire mass range considered here if the DM carries unit charge $Q_\chi = 1$. Only by increasing the charge of χ to $Q_\chi = 10$, the DM relic abundance can be explained in the range

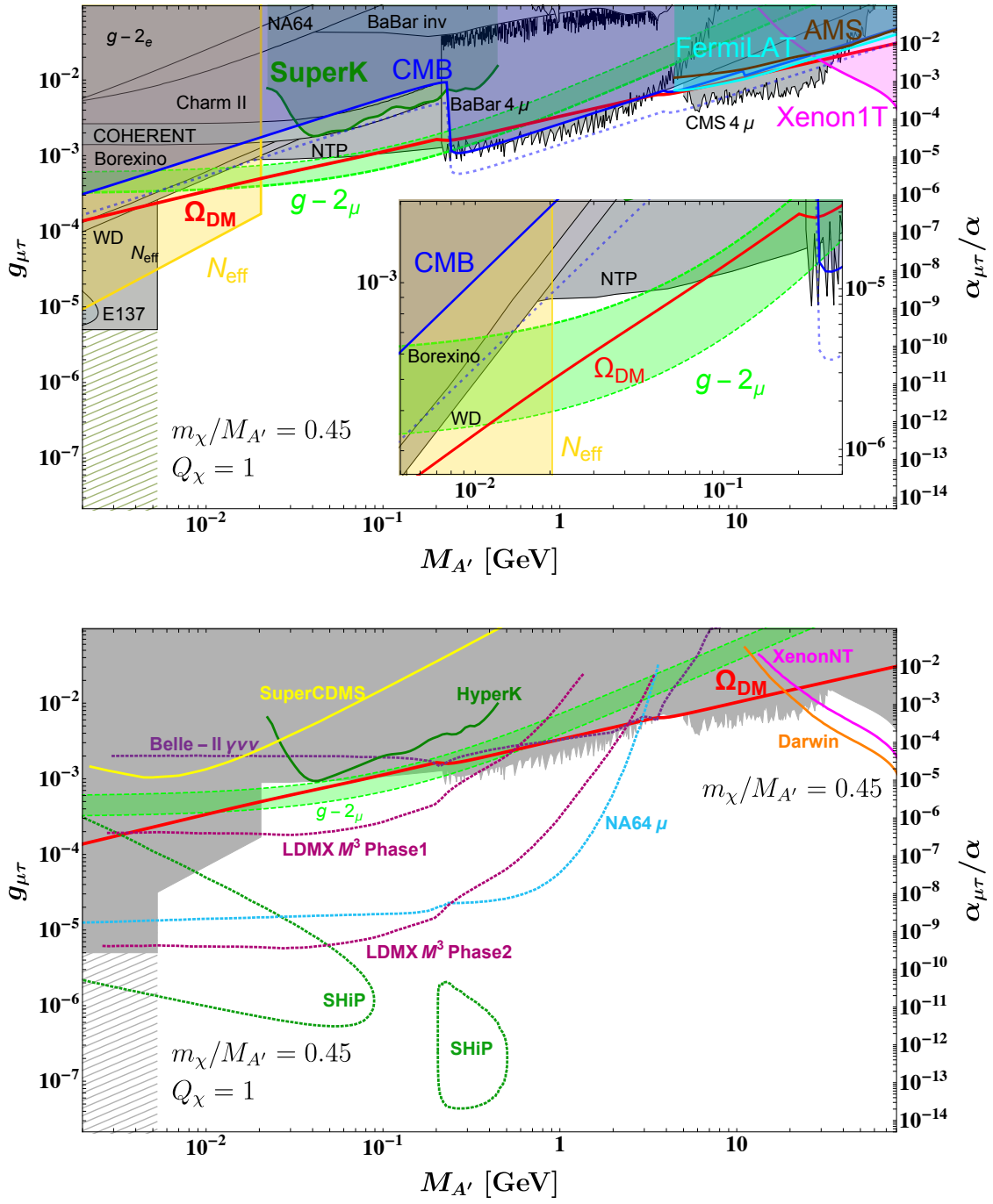

Figure 5.6: Current (upper panel) and future (lower panel) constraints on the combined parameter space of a $U(1)_{L_\mu - L_\tau}$ gauge boson and vector-like fermion of charge $Q_\chi = 1$ for $m_\chi/M_{A'} = 0.45$. Figure taken from [412].

$28 \lesssim M_{A'} \lesssim 50$ MeV. For this situation the corresponding relic density and the CMB bound are shown by the dashed red and blue curves in the upper panel of Fig. 5.5.

On the other hand, in the NR scenario we can accommodate an explanation of $\Omega_{\rm DM}$ in the range of $20 \lesssim M_{A'} \lesssim 85$ MeV with unit DM charge[2] (see inset plot in the upper panel of Fig. 5.6). Interestingly, the entire region where χ can account for the whole DM relic abundance allows for a simultaneous explanation of the $(g-2)_\mu$ anomaly (the green band corresponds to the preferred 2σ region). This region is consistent with the latest bounds from DM energy injection into the CMB. In particular, it is even unaffected by the theoretically maximum possible CMB bound (dotted blue in the upper panel of Fig. 5.6) obtained from assuming that visible DM annihilation products inject all of their energy into the CMB. From the lower panel of Fig. 5.6, we can see that this particularly interesting low-mass region will be testable at the future muon beam experiments NA64μ [290] and LDMX M^3 [444, 493].

Finally, to study the effect of different DM charges on the phenomenology of this model, we have performed an addition analysis for the NR scenario with $Q_\chi = 3$. The corresponding exclusion plot is shown in Fig. 5.7. In this case, due to the relatively high partial width into $\chi\bar{\chi}$ final states, the branching fraction of the hidden photon into visible final states is significantly decreased. As a consequence the limit from the four-muon resonance search by CMS [411] drastically weakens. While in the case of $Q_\chi = 1$ the DM relic abundance could not be explained for masses of $M_{A'} \gtrsim 85$ MeV, the weakening of the CMS limit opens up a window for a high-mass explanation of $\Omega_{\rm DM}$ in the region of $16.5 \lesssim M_{A'} \lesssim 30$ GeV[3] for charges of $Q_\chi = 3$ or higher (see Fig. 5.7). Interestingly, this region grows upon increasing the ratio $m_\chi/M_{A'}$ up to $m_\chi = M_{A'}/2$. The reason that $\Omega_{\rm DM}$ is still viable below the model-independent lower bound on the DM mass of $m_\chi \gtrsim 20$ GeV (cf. Ref. [467]) is twofold: first, the particle χ has a sizable invisible annihilation branching fraction into neutrinos, which do not leave any imprint on the CMB in this mass range [467]. Second, the Fermi-LAT bound we applied is conservative in the sense that we have used a single final-state limit on $\langle\sigma v\rangle$ obtained for 100% branching fraction into taus. In the inset plot of Fig. 5.7, we show projections of future direct detection experiments for the NR scenario with $Q_\chi = 3$. We can see that the high-mass region where $\Omega_{\rm DM}$ is explained can be tested by the future XenonNT (magenta line) [494] and Darwin (orange line) experiments [486].

In summary, our analysis showed that in the SB scenario, often considered in the literature, an explanation of the DM relic abundance $\Omega_{\rm DM}$ is excluded in the whole MeV to a few GeV DM mass range for unit charges $Q_\chi = 1$. However, in the NR scenario of $m_\chi/M_{A'} = 0.45$, the DM relic abundance $\Omega_{\rm DM}h^2$ and the observed excess in the muon anomalous magnetic moment $(g-2)_\mu$ can simultaneously be explained in the mass range of $20 \lesssim M_{A'} \lesssim 85$ MeV. In particular, future muon beam dump facilities like NA64μ and LDMX M^3 will be essential for putting such an explanation to the test.

[2] We note that for mass ratios $m_\chi/M_{A'} < m_\chi^{\rm BBN}/2m_\mu \approx 0.044$ an explanation of $(g-2)_\mu$ is excluded by the $N_{\rm eff}$ bound.

[3] In the intermediate-mass region of $3 \lesssim M_{A'} \lesssim 5$ GeV the DM relic abundance $\Omega_{\rm DM}$ is also not yet excluded. However, this is most probably an artifact of our conservative estimate of the CMB bound below $m_\chi = 5$ GeV [467] explained in Section 5.3.2.

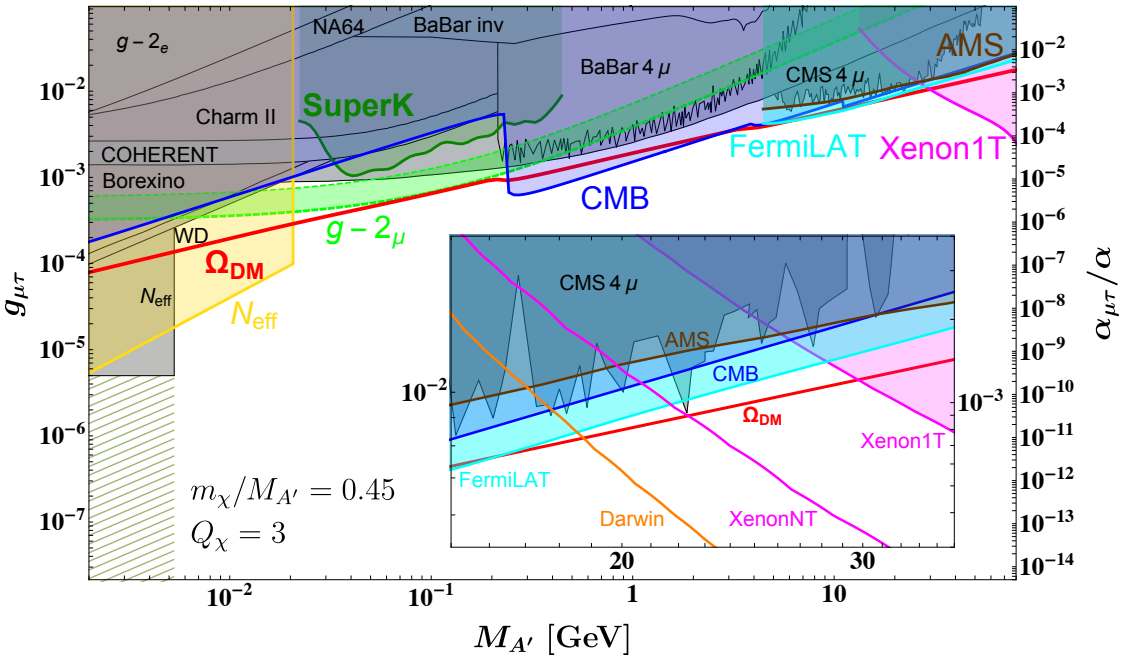

Figure 5.7: Same as upper panel of Fig. 5.6, but for $Q_\chi = 3$. Figure taken from [412].

For higher values of the DM charge of $Q_\chi \gtrsim 3$ there might be still some room for an explanation of $\Omega_{\rm DM}$ in the region of $16.5 \lesssim M_{A'} \lesssim 30$ GeV, which eventually will be tested by direct DM-nucleus scattering at XenonNT and Darwin.

Chapter 6

Conclusions

As the quest for new physics continues, thorough phenomenological studies making use of the full complementarity of astrophysical, cosmological and particle physics observations will become more and more important. These will be essential for identifying interesting directions in BSM theories or, in turn, to rule them out. Asking the question of how new physics could be incorporated into the well-established SM in a consistent way, one can identify the dimension-four portal interactions as being of special relevance.

With the vector portal interaction serving as a starting point, we started out in this thesis to investigate the phenomenology of extra abelian gauge symmetries as simple models of a (possibly) more fundamental, UV-complete BSM theory. Such models of extra $U(1)$ symmetries are theoretically well-motivated from various UV completions of the SM like string or GUT models. Depending on the concrete realization of these models, the low-energy phenomenology of the associated gauge bosons can drastically alter. This calls for a systematic study of such models at various energy scales, potentially giving us deeper insight into the underlying UV theory.

In the first part of this thesis in Chapter 3, we studied an effective $U(1)$ model of a heavy Z' mediator (i.e. $M_{Z'} > M_Z$) with exclusively flavor-changing couplings. In this scenario, we investigated in a systematic way the effect of combined leptonic and hadronic Z'-induced FCNCs. In this context, meson mixing as well as rare meson decays are particularly sensitive to such flavor-changing effects. For the leptonic couplings, flavored lepton decays, LEP measurements and muonium oscillations are sensitive probes.

We found that for a generic chirality structure of the Z' couplings, meson mixing quite severely constrains off-diagonal quark couplings. However, we could show that these constraints are attenuated by cancellation effects for certain chirality structures. In the cases where cancellation occurs, resonance searches in different-flavor dilepton final states at the LHC can impose strong bounds on the combined parameter space of lepton and quark flavor-changing couplings.

In the lepton sector, the case of a non-zero flavor-changing coupling in the $\mu\tau$ sector proved particularly interesting. For suited chirality, this allows for an explanation of the excess in the anomalous magnetic moment of the muon $(g-2)_\mu$. Furthermore, it can help to explain the tension in the observed tau decay ratio into muons over electrons compared to its SM expectation.

For the future, we have identified the tau decay channels $\tau^\pm \to \ell^\pm (\pi^0 K^0 / \pi^\pm K^\mp)$ as particularly promising for the study of simultaneous lepton and quark flavor changing-couplings.

Going to smaller mediator masses, MeV-scale hidden photons A' as the associated gauge boson of a secluded $U(1)_X$ symmetry with purely kinetic mixing induced couplings to the SM have been particularly well-studied in the literature. In Chapter 4, we have collected and where necessary reanalyzed constraints on such hidden photons. Most hidden photon constraints either originate from beam dump and fixed target experiments sensitive to small couplings and masses, or from collider experiments, which can constrain large to moderate couplings over a very large range of masses. We used these previous studies and applied them to a broader class of hidden gauge bosons of anomaly-free $U(1)$ symmetries under which SM particles are allowed to carry charge. In this context, we focussed on the four groups $U(1)_{B-L}$, $U(1)_{L_\mu - L_e}$, $U(1)_{L_e - L_\tau}$ and $U(1)_{L_\mu - L_\tau}$, which are anomaly-free with the SM field content.

Most prominently, these groups differ from the minimal secluded hidden photon case in their gauge couplings to neutrinos. These help to probe the usually unconstrained region of parameter space for moderate hidden photon masses at couplings which are too small to yield a signal at colliders, but too large for the hidden photon to decay within the fiducial volume of beam dump experiments. In this context, the most relevant neutrino experiments are Super-Kamiokande and TEXONO, and in the future COHERENT and DUNE. The groups of lepton-family number differences $U(1)_{L_\mu - L_e}$, $U(1)_{L_e - L_\tau}$ and $U(1)_{L_\mu - L_\tau}$ are generally difficult to probe at experiments that use hadronic production of the A', due to the loop-suppressed kinetic mixing induced coupling to hadrons.

The hidden photon of the group $U(1)_{L_\mu - L_\tau}$ is particularly difficult to probe as it only has loop-suppressed couplings to both hadrons and electrons. In particular, this still leaves room for an explanation of the $(g-2)_\mu$ excess. We demonstrated that constraints from white dwarf cooling can rule out part of the relevant parameter space.

In an extension of this phenomenologically appealing $U(1)_{L_\mu - L_\tau}$ model by a fermionic, vector-like DM candidate χ, we studied the combined DM and hidden photon constraints on the corresponding parameter space in Chapter 5. For this study we considered a multitude of DM probes ranging from the number of effective neutrinos N_{eff} at BBN over cosmic fluxes of photons, positrons and neutrinos to direct detection experiments. Our results show that in the standard benchmark considered in the literature of a mass ratio of $m_\chi / M_{A'} = 1/3$, the particle χ cannot explain the observed relic DM abundance Ω_{DM} with unit charges $Q_\chi = 1$. However, in scenarios where the DM particle is close to resonance $m_\chi \lesssim M_{A'}/2$, a simultaneous explanation of the relic abundance Ω_{DM} and the muon anomalous magnetic moment $(g-2)_\mu$ is possible. This makes the $U(1)_{L_\mu - L_\tau}$ scenario of particular interest for future searches. The relevant region of parameter space where Ω_{DM} and $(g-2)_\mu$ are explained can be probed in the future with dedicated muon runs of e.g. NA64 and LDMX.

Motivated by the renormalizable vector portal interaction, we started out to study a number of general $U(1)$ extensions of the SM. We saw that such models of extra $U(1)$ symmetries can have a very rich phenomenology and typically are testable at a large variety

of different experiments. Particular coupling choices make such extra $U(1)$ symmetries attractive candidates for explaining the $(g-2)_\mu$ excess. If the upcoming results of the currently running E989 experiment at Fermilab should confirm the $(g-2)_\mu$ excess at the $5\,\sigma$ level this will make future searches of the $U(1)$ bosons all the more important as independent tests of new physics.

From a bottom-up perspective, it is important to systematically scrutinize consistent extensions of the SM as possible windows on new physics. While in this context the vector portal motivates the study of $U(1)$ models, universality dictates complementary investigations of e.g. extended scalar sectors or sterile neutrinos as motivated by the Higgs and neutrino portals, respectively. Conversely, top-down approaches trying to UV-complete the SM, like e.g. string theory or grand unification, provide an independent strategy of constructing consistent theories for new physics. Experimentally challenging the predictions of such consistent models for new physics, we might hope to close down on the true nature of BSM physics in the future.

Acknowledgements

At the end of my doctoral studies, it is time to thank many great people for their support through out all the years. I am really grateful to every single one of them and want to use these acknowledgements to express my gratitude. If I should have forgotten anybody this is entirely due to my lack of sleep and not because they are less important.

First of all, I want to take this opportunity to thank my PhD advisor Joerg Jaeckel. I am very grateful to him for having accepted me as a PhD student and for having given me the opportunity to work on a couple of fun physics projects with him. Throughout the tree years of my PhD, I always enjoyed the physics discussions with him, which were always a source of inspiration. I keep being impressed with his ability of "naively" estimating about any physical effect on one sheet of white paper. I want to especially thank him for the freedom he provided me with in shaping our research projects, which helped to educate my independent thinking and ultimately lead to my first single-authored publication. Finally, I am really grateful for the opportunities he provided me with to conduct research abroad at the University of Washington in Seattle, USA and at KIAS in Seoul, Republic of Korea.

Next, I want to thank Martin Bauer for his great support and incentive during our joint research project. He kept me motivated throughout the whole project with his enthusiastic way of discussing physics. I am particularly grateful for all his good advice, not only concerning physics, but also on career choices. I am therefore really looking forward to working together with him as a PostDoc in Durham.

I am also very grateful to Tilman Plehn for his support throughout all my Heidelberg years, not only by accepting me into the RTG "Particle Physics Beyond the Standard Model", but also for adopting me as a member of his group. Apart from constantly reminding me of the uttermost importance of my work, this thesis and $U(1)$ physics in general, he was also always ready to give insightful advice on life itself. Furthermore, I always enjoyed discussing physics with him and I am looking forward to finally work on our joint dark matter project. Last but not least, I want to thank him for the good times in the ITP trombone quartet.

Let me also thank Susanne Westhoff for stimulating discussions on dark matter and flavor physics, as well as for agreeing to referee this thesis. In this context, I also want to thank Björn Malte Schäfer and Stephanie Hansmann-Menzemer for completing my examination committee.

At this stage, I want to acknowledge support from the research training group "Particle Physics Beyond the Standard Model" (GRK 1940) for the full three years of my PhD. I also want to thank Svende Braun for an enjoyable and smooth two years that we shared the office of the RTG student representatives.

At this point, I want to give a big thank-you to everybody who helped to proofread this thesis. I am very indebted to Gonzalo Alonso Álvarez, Martin Bauer, Sebastian Bruggisser, Anastasiia Filimonova, and especially to Anke Biekötter and Sebastian Schenk, who went almost through the whole thesis and even sacrificed part of their easter holidays to help me finish this. I also want to thank Jennifer Thompson for helping me with the command of the English language. If this document is any readable it is mainly due to the effort of my proof readers. Let me also thank Anja Butter for providing me with some last minute medication and LaTeX templates that I desperately needed to finish this thesis. Finally, everybody who finds some typos gets to keep them.

Throughout the time I spent at the Institute for Theoretical Physics in Heidelberg during my master's and PhD, I got to know a whole lot of great people. Instead of listing them here all by name, I want to collectively thank the whole Pheno group for making my time here so enjoyable. I have plenty of good memories of the many "ice cream days", group barbecues, institute parties, as well as field trips to Wurst- and Weihnachtsmarkt or a fine day of Bosseln in the Neuenheimer Feld. In this context, I want to explicitly thank Gonzalo Alonso Álvarez, Marco Bellagente, Anke Biekötter, Johann Brehmer, Anja Butter, Anastasiia Filimonova, Peter Reimitz, Torben Schell, Sebastian Schenk and Ramon Winterhalder for suffering through (part of) their PhD with me.

I am also thankful for the good times I had with the CORE4 – be it in one of the many coffee breaks or a weekend trip to Hamburg. A very special thanks goes to my academic brother Sebastian Schenk for completing his civil service with me in Korea and for always being there to discuss physics or life, either over coffee or beer!

Before concluding, I want to thank all my friends and family to whom I am very indebted for their great support over all the years, who built me up again when I was down. Finally, I am really grateful to Mirjam Gölz for always being there for me – in the good and in the bad times – and for her infinite patience and positive attitude towards life!

Appendix A

Higher order effects and Monte Carlo details

A.1 Higher order effects in cancellation

In Section 3.3.1 we have discussed meson mixing limits in the context of a new Z' boson with exclusively flavor violating couplings defined by the Lagrangian in Eq. (3.2). We saw that the relevant operators inducing meson mixing are generated at tree level in such a model. Furthermore, we argued that there are solutions of the coupling ratio ρ_q for which the mixing exactly cancel. In the following we will investigate higher-order effects contributing to mixing and its impact on the cancellation.

A.1.1 NLO effects

Electroweak loop-diagrams as shown in Fig. A.1 give rise to corrections of the Wilson coefficients C_i of the four-quark operators in Eqs. (3.17) to (3.19). Let us define the Wilson coefficients of the corresponding operators as

$$C_1^{\mathrm{VLL}} = \frac{\left(g^L_{q_i q_j}\right)^2}{M^2_{Z'}} R_1^{\mathrm{VLL}}(\mu)\,, \tag{A.1}$$

$$C_1^{\mathrm{VRR}} = \frac{\left(g^R_{q_i q_j}\right)^2}{M^2_{Z'}} R_1^{\mathrm{VRR}}(\mu)\,, \tag{A.2}$$

$$C_1^{\mathrm{LR}} = \frac{g^L_{q_i q_j}\, g^R_{q_i q_j}}{M^2_{Z'}} R_1^{\mathrm{LR}}(\mu)\,. \tag{A.3}$$

In the following we study the various corrections to these coefficients C_i. There are three independent one-loop contributions we take into account. Apart from the processes shown in Fig. A.1 we also consider these diagrams with the Z replaced by a SM Higgs or an additional Z' (only the right diagram).

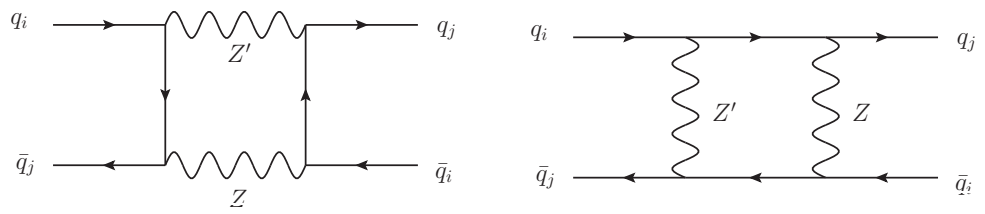

Figure A.1: One-loop mixing diagram giving rise to higher order corrections of the four-quark operators Eqs. (3.17) to (3.19). The same diagrams exist also with the Z replaced by a Higgs boson. A third correction comes from the right diagram with the Z exchanged by a second Z'.

Higgs loop contribution

First, we will consider a SM Higgs h as the additional boson in the loop. The important feature of the Higgs is that it flips the chirality of the fermion at the vertex. Therefore, the Higgs introduces operator mixing in the sense that the Higgs correction to the Wilson coefficient of e.g. operator $\mathcal{O}_1^{\mathrm{VLL}}$ will be proportional to $\mathcal{O}_1^{\mathrm{LR}}$. A short calculation of the contributions from the one-loop diagrams in Fig. A.1 with the Z replaced by the Higgs leads to the estimate

$$\delta C_i^{(h)} \sim \frac{1}{8\pi^2}\ \frac{m_q^2}{v^2}\ \log\left(\frac{M_h}{M_{Z'}}\right) C_j\ \sim\ 10^{-7}\ C_j\,, \tag{A.4}$$

where we have used $m_q = 1$ GeV and $M_{Z'} = 1$ TeV to obtain the last relation. Hence, operator mixing due to NLO Higgs exchange is an effect roughly of the order of 10^{-7} and therefore much too small to be of any concern as will become clear in the following.

Z loop contribution

Next, we consider the Z contributions due to the diagrams of Fig. A.1 as is. Structurally, the coupling of the Z and Z' are the same, so we do not introduce any mixing amongst operators of the kind $\delta C_i \propto C_j$. Analogously, an order of magnitude estimate yields for the correction to the Wilson coefficients

$$\delta C_i^{(Z)} \sim\ \frac{1}{2\pi^2}\ (g_q^Z)^2\ \log\left(\frac{M_Z}{M_{Z'}}\right)\ C_i\ \sim\ 10^{-3}\ C_i\,, \tag{A.5}$$

where we have assumed for the coupling of the quark to the Z a conservative value of $g_q^Z = 0.1$ and $M_{Z'} = 1$ TeV to obtain the last relation. The correction due to the Z loop is much larger than the Higgs contribution. We further note that the correction of the Wilson coefficient is proportional to the Wilson coefficient itself due to the absence of operator mixing. This implies that the correction will be universal for all Wilson coefficients and hence only shift the value of cancellation solution ρ_0 and tolerance interval I_0.

Z' loop contribution

Finally, we consider the case of a pure Z'-induced loop diagram. In this case only the right diagram of Fig. A.1 will contribute to generic meson mixing. The diagram on the left only

contributes for mesons consisting of a quark-antiquark pair of the same flavor. As before we can estimate the order of magnitude of the correction to the Wilson coefficients

$$\delta C_i^{(Z')} \sim \frac{1}{4\pi^2} (g_{qq'}^{Z'})^2 C_i \sim 10^{-2} (g_{qq'}^{Z'})^2 C_i . \tag{A.6}$$

This contribution is in the same ballpark as the Z contribution, but it introduces higher powers of the Z' coupling. This changes the structure of Eq. (3.21) fundamentally and could possibly destroy the cancellation effect.

A.1.2 Numerical stability of cancellation

We will now examine whether the correction due to a Z' loop can spoil the cancellation solution ρ_q. As the correction is of the order of $\delta C_i/C_i \sim 10^{-2}$ we will assume that the exact cancellation solution can be approximated by a perturbation series

$$\rho = \rho_0 + \delta\rho + \text{higher orders} . \tag{A.7}$$

As we have just seen, the Wilson coefficients at one-loop level due to Z' corrections schematically read

$$C_i^{(Z')} \sim \left(1 + \frac{1}{4\,\pi^2}\, g^2\right) C_i . \tag{A.8}$$

Hence the full cancellation equation at one-loop level becomes

$$\begin{aligned} 0 = &\left[C_1^{\text{VLL}} P_1^{\text{VLL}} (1+\rho_q^2) + \left(C_1^{\text{LR}} P_1^{\text{LR}} + C_2^{\text{LR}} P_2^{\text{LR}}\right) \rho_q\right] g_R^2 \quad \leftarrow \text{tree-level relation} \\ &+ \frac{1}{4\pi^2}\left[C_1^{\text{VLL}} P_1^{\text{VLL}} (1+\rho_q^4) + C_1^{\text{LR}} P_1^{\text{LR}} \rho_q^2\right] g_R^4 . \qquad \leftarrow \text{1-loop correction} \end{aligned} \tag{A.9}$$

If we then define the tree-level and one-loop terms as

$$f(\rho_q) = \left[C_1^{\text{VLL}} P_1^{\text{VLL}} (1+\rho_q^2) + \left(C_1^{\text{LR}} P_1^{\text{LR}} + C_2^{\text{LR}} P_2^{\text{LR}}\right) \rho_q\right] g_R^2 , \tag{A.10}$$

$$h(\rho_q) = \frac{1}{4\pi^2}\left[C_1^{\text{VLL}} P_1^{\text{VLL}} (1+\rho_q^4) + C_1^{\text{LR}} P_1^{\text{LR}} \rho_q^2\right] g_R^4 , \tag{A.11}$$

we find for the correction to the cancellation solution from perturbation theory

$$\delta\rho = -\frac{h(\rho_0)}{f'(\rho_0) + h'(\rho_0)} . \tag{A.12}$$

We checked these Z' corrections for the B_d, B_s, D and K mesons. In all cases the corrections are reasonably small for typical values of the quark coupling $g_{qq'}^R \lesssim 1$. Especially, we find that the ratio $\delta\rho/\rho_0 < 1$ for all coupling combinations $\{qq', \ell\ell'\}$. We can calculate by the same method the correction on the tolerance $\delta(\Delta\rho)$. We find that this is generally much smaller than the tolerance itself $\delta(\Delta\rho)/\Delta\rho \ll 1$ and therefore negligible. Hence, we obtain a mere shift of the cancellation solution ρ_0 and its tolerance interval I_0. Therefore, the cancellation solution ρ_0 is stable against higher order corrections and persists beyond the tree level.

However it should be noted that in the $\mu\tau$ sector and for high masses in the $e\tau$ sector the ratio of the shift to the tolerance $\delta\rho/\Delta\rho$ can be greater than 1. This is not a problem, as the cancellation solution still persists. It merely means that the shifted cancellation ρ can lie outside of its original tolerance interval I_0. This is an artifact of the extremely small tolerance intervals, which we observe in those channels.

A.2 Monte Carlo simulation details

In this section we want to summarize important parameters we used for the determination of the simulated cross section σ_{MC} for the process $pp \to Z' \to \ell\ell'$.

In Table A.1 we have summarized the values of the mass-dependent K-factors encoding NNLO contributions to the different final states.

$M_{Z'}$[GeV]	500	550	600	650	700	750	800	1000	1200	2000
$K_{e\mu}$	1.449	1.447	1.414	1.436	1.427	1.423	1.480	1.494	1.501	1.602
$K_{e\tau}$	1.355	1.313	1.379	1.428	1.351	1.391	1.424	1.455	1.483	1.510
$K_{\mu\tau}$	1.444	1.421	1.428	1.429	1.483	1.511	1.506	1.510	1.525	1.661

Table A.1: NNLO K-factors from SSM Z'

In Table A.2 we find the efficiencies allowing to translate the Monte Carlo result into post-detector cross sections.

$M_{Z'}$[GeV]	$(A \times \epsilon)_{e\mu}$	$(A \times \epsilon)_{e\tau}$	$(A \times \epsilon)_{\mu\tau}$
500	0.374	0.109	0.083
550	0.380	0.116	0.086
600	0.389	0.117	0.086
650	0.401	0.122	0.090
700	0.403	0.118	0.094
750	0.410	0.123	0.091
800	0.416	0.122	0.090
900	0.428	0.116	0.098
1000	0.440	0.115	0.095
1100	0.441	0.117	0.103
1200	0.441	0.118	0.098
1400	0.449	0.119	0.096
1600	0.445	0.119	0.099
1800	0.431	0.114	0.096
2000	0.415	0.109	0.089
2200	0.386	0.104	0.082
2500	0.358	0.093	0.071
3000	0.283	0.069	0.053

Table A.2: Acceptance times efficiency from SSM Z'.

Appendix B

Hidden gauge bosons: mass eigenstates and experimental signatures

B.1 Rotation to hidden photon mass eigenstate

In Section 2.3.3 we outlined the procedure of canonical normalization of the weak neutral boson fields and the diagonalization of their mass matrix $\mathcal{M}$ for the case of a generic $U(1)_X$ extension of the SM. If we consider the hidden photon case of small kinetic mixing ϵ_Y and light boson mass $M_X \ll M_Z$, we can simplify these relations in order to enhance our physical intuition.

As in the general case, we first canonically normalize the boson fields via Eqs. (2.45) and (2.46). Then the diagonalization of the mass matrix $\mathcal{M}$ of the canonically normalized fields (B_μ, W^3_μ, X_μ)[1] proceeds through a combination of two block-diagonal rotations with the weak mixing angle θ_w and an additional angle ξ,

$$R_1(\xi) R_2(\theta_w)\, \mathcal{M}^2\, R_2(\theta_w)^T R_1(\xi)^T = \mathrm{diag}\,(M_A^2, M_Z^2, M_{A'}^2)\,, \tag{B.1}$$

where (A_μ, Z_μ, A'_μ) denote the photon, Z and hidden photon mass eigenstates. The rotation matrices $R_1(\xi)$ and $R_2(\theta_w)$ are those defined in Eq. (2.48). However, in the hidden photon case, the second rotation angle is given to good approximation by the relation

$$\tan 2\xi = \frac{2\epsilon_Y \sin\theta_w}{1-\delta} + \mathcal{O}(\epsilon_Y^2)\,. \tag{B.2}$$

Here we have defined $\delta = M_X^2/M_Z^{\mathrm{SM}\,2}$ and $M_Z^{\mathrm{SM}} = g_Z\, v/2$ is the mass of the Z-boson in the SM. In the hidden photon approximation, we then find the mass eigenvalues given by

[1] We denote gauge bosons in the non-orthogonal basis by hatted fields and define the neutral gauge bosons in the electroweak symmetric phase by (B_μ, W^3_μ, X_μ) and in the electroweak broken phase by (A_μ, Z_μ, A'_μ).

$M_A^2 = 0$ as it should be and

$$M_Z^2 = M_Z^{\mathrm{SM}\,2}\big(1 + \epsilon_Y^2 \sin^2\theta_w(1+2\delta)\big) + \mathcal{O}(\delta^2\epsilon_Y^2)\,, \tag{B.3}$$

$$M_{A'}^2 = M_X^2\big(1 + \epsilon_Y^2(1 - \sin^2\,\theta_w(1+\delta))\big) + \mathcal{O}(\delta^2\epsilon_Y^2)\,. \tag{B.4}$$

Couplings between the gauge boson mass eigenstates A_μ, Z_μ and A'_μ and the fermion currents are then given by

$$\big(e\,j_\mu^{\mathrm{EM}},\; g_Z\,j_\mu^Z,\; g_x\,j_\mu^x\big)\begin{pmatrix}\hat{A}^\mu\\ \hat{Z}^\mu\\ \hat{A}'^\mu\end{pmatrix} = \big(e\,j_\mu^{\mathrm{EM}},\; g_Z\,j_\mu^Z,\; g_x\,j_\mu^x\big)\;K\;\begin{pmatrix}A^\mu\\ Z^\mu\\ A'^\mu\end{pmatrix}\,, \tag{B.5}$$

with

$$\begin{aligned} K = \big[R_1(\xi)R_2(\theta_w)G^{-1}(\epsilon_Y)R_2(\theta_w)^{-1}\big]^{-1} &= \begin{pmatrix}1 & 0 & -\epsilon_Y\cos\theta_w\\ 0 & 1 & 0\\ 0 & \epsilon_Y\sin\theta_w & 1\end{pmatrix} + \mathcal{O}(\epsilon_Y\delta,\epsilon_Y^2)\\ &= \begin{pmatrix}1 & 0 & -\epsilon\\ 0 & 1 & 0\\ 0 & \epsilon\tan\theta_w & 1\end{pmatrix} + \mathcal{O}(\epsilon\delta,\epsilon^2)\,, \end{aligned} \tag{B.6}$$

where in the second line we have introduced $\epsilon \equiv \epsilon_Y\cos\theta_w$. Couplings of the massless photon are protected by the unbroken electromagnetic gauge symmetry $U(1)_{\mathrm{EM}}$. The new gauge boson X couples to leading order in ϵ to the electromagnetic current [152, 495] so that the full interaction Lagrangian of the hidden photon mass state A' reads

$$\mathcal{L}_{\mathrm{int}} = \big(g_x\,j_\mu^x - e\epsilon\,j_\mu^{\mathrm{EM}}\big)\;A'^\mu\,. \tag{B.7}$$

For a secluded $U(1)_X$ with $j_\mu^x = 0$, the gauge boson has couplings to the SM only through kinetic mixing proportional to ej_μ^{EM}, which motivates the name **hidden photon**.

The leading terms in ϵ of the $A'W^+W^-$ coupling follow from replacing the photon by $A \to A - \epsilon A'$ in the AW^+W^- vertex. Couplings of the new gauge boson A' to the Z-current only appear at $\mathcal{O}(\delta\epsilon)$ and can be obtained by replacing $Z \to Z - \epsilon\delta\tan\theta_w A'$. As a consequence, couplings of the physical Higgs boson h to the new gauge boson are further suppressed,

$$\mathcal{L} \supset \frac{M_Z^{\mathrm{SM}\,2}}{2v}\,(A_\mu, Z_\mu, A'_\mu)\begin{pmatrix}0 & 0 & 0\\ 0 & 1 & -\epsilon\tan\theta_w\,\delta\\ 0 & -\epsilon\tan\theta_w\,\delta & \epsilon^2\tan^2\theta_w\,\delta^2\end{pmatrix}\,h\,\begin{pmatrix}A^\mu\\ Z^\mu\\ A'^\mu\end{pmatrix}\,, \tag{B.8}$$

where we have only kept the leading terms in the $\epsilon\delta$-expansion for each element.

These couplings determine the decay modes of the A' boson for a given mass $M_{A'}$. We assume $M_{A'} \ll M_Z$ such that only fermionic decay modes are relevant with a natural hierarchy between couplings to fermions from j_μ^x and mixing-induced couplings,

$$\Gamma(A' \to f\bar{f}) = \frac{M_{A'}}{24\pi}C_f\sqrt{1-\frac{4m_f^2}{M_{A'}^2}}\left[(g_L^2+g_R^2)\Big(1-\frac{m_f^2}{M_{A'}^2}\Big) + 6\frac{m_f^2}{M_{A'}^2}g_Lg_R\right]\,, \tag{B.9}$$

where $C_f = 3(1)$ for quarks (leptons) is a color factor and the couplings can be determined by matching the currents in Eq. (B.5) to $j_\mu = \bar{f}\gamma_\mu(g_L P_L + g_R P_R)f$ with projectors $P_{R/L} = \frac{1}{2}(1 \pm \gamma_5)$. Another phenomenological consequence are the exotic Higgs decays $h \to ZA'$ and $h \to A'A'$,

$$\Gamma(h \to A'Z) = \frac{1}{16\pi}\epsilon^2 \tan^2\theta_w \frac{M_h^3}{v^2}\frac{M_{A'}^2}{M_Z^2}\left(1 - \frac{M_Z^2}{M_h^2}\right), \tag{B.10}$$

$$\Gamma(h \to A'A') = \frac{1}{32\pi}\epsilon^4 \tan^4\theta_w \frac{M_h^3}{v^2}\frac{M_{A'}^4}{M_Z^4}, \tag{B.11}$$

where we have neglected higher order corrections in $\delta\epsilon$ and $M_{A'}^2/M_h^2$. Due to the suppression of the decay widths with factors of ϵ^2 and $M_{A'}^2/M_h^2$, Higgs decays do not provide relevant constraints, if the only coupling between the Higgs and the hidden gauge boson is mediated by the kinetic mixing term.

B.2 Beam dump limit calculation

In this Appendix we want to illustrate a prototypical limit calculation for beam dump experiments. For concreteness, we will consider the electron beam dump experiment E137 operated at SLAC in the 1980s.

The E137 setup is schematically shown in the right panel of Fig. 4.4. A total of $N_e \sim 1.87 \times 10^{20}$ electrons with momentum $p = 20$ GeV have been dumped onto an aluminum target followed by 200 m of rock, which served as shielding. In the target material the incoming electrons interact with the nuclei and lose energy via Bremsstrahlung. The hidden photon of a secluded $U(1)_X$ has the same coupling to the electron as the photon, only suppressed by the mixing parameter ϵ. Hence, it can also be produced in a Bremsstrahlung process. The total number of produced A' decaying visibly within the detector volume is described by Eq. (4.25). During the full data taking period no signal events have been observed in the E137 detector [293]. According to Poisson statistics, we can therefore exclude any point in model parameter space predicting more than $N_{95} = 3$ observed events at 95 % C.L..

B.2.1 Bjorken implementation

For the beam dump experiment E137, limits on hidden photons A' have been first calculated by Bjorken *et al.* [275] for e^+e^- final states. The expected number of events has been calculated via Eq. (4.25) with the approximate differential cross section given in Eq. (4.21) (which includes an erroneous factor of 2 in [275] that has been corrected in [304]). For the full details of this calculation we refer the reader to the Appendices A - C of [275].

We have implemented the full calculation of Bjorken *et al.* in `MATHEMATICA` [496], which we will refer to as ***Bjorken implementation***. In order to derive limits we have discretized the 2D parameter space of the $M_{A'} - \epsilon^2$ plane into a finely-grained grid and calculated the expected number of hidden photon induced events N at each grid point. The expected number of events normalized to the 95% C.L. limit N/N_{95} are depicted in Fig. B.1. The edge of the outermost blue contour gives our limit.

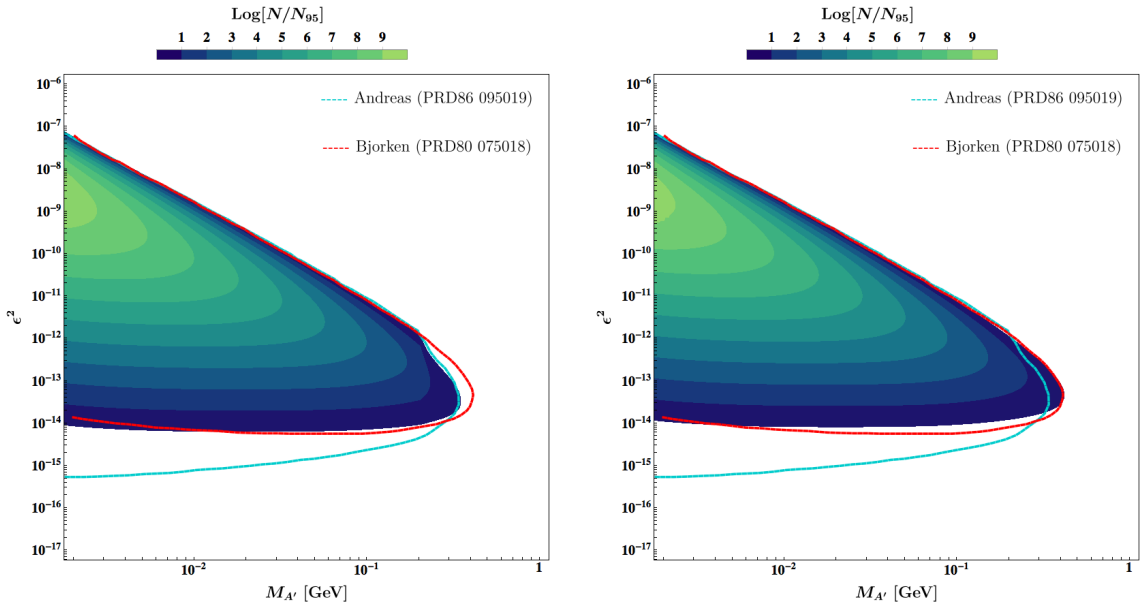

Figure B.1: Expected number of events normalized to the 95% C.L. limit N/N_{95} for a secluded hidden photon A' at the SLAC E137 experiment obtained from the ***Bjorken implementation*** as a function of the mixing parameter ϵ^2 and the mass $M_{A'}$. The red (Bjorken) and cyan (Andreas) lines show the exclusion contours calculated in [275] and in [304], respectively. Left: Including the full A' width, in particular also the partial width into muons. Right: Only including the partial width of the A' into electrons, assuming $N_{95} = 10$ and including the extra factor of 2. Figure taken from [262].

The left panel shows the results of the *Bjorken implementation* including the full A' width, which is described in detail in Section 4.2.3. This includes in particular the partial width into muons that becomes equal in size to the one into electrons for $M_{A'} \gtrsim 2m_\mu$. In Fig. B.1 we compare the limit we obtained from the *Bjorken implementation* to those derived by Bjorken *et al.* [275] and Andreas *et al.* [304] (for details see Appendix B.2.2), which we will refer to as the Bjorken and Andreas limit, respectively. We see that our limit aligns perfectly with the Andreas limit in the high-ϵ^2 domain, where it also shows the exact same threshold behavior at $M_{A'} \sim 2m_\mu$. But we can reconstruct the Bjorken limit nearly exactly (within the limits of numerical integration and discretization) if we only take into account the partial width of the A' into electrons, assume 10 events as exclusion bound as done by Bjorken *et al.* and include the erroneous extra factor of 2.

However, for a secluded hidden photon a muon coupling with the same strength as of the electron coupling is unavoidable. Hence, the limits for E137 derived by Bjorken *et al.*, seemingly neglecting the partial width into muons, rather overestimate the hidden photon mass reach. This is not an issue for the E141 and E774 limits as the mass reach is well below the dimuon threshold.

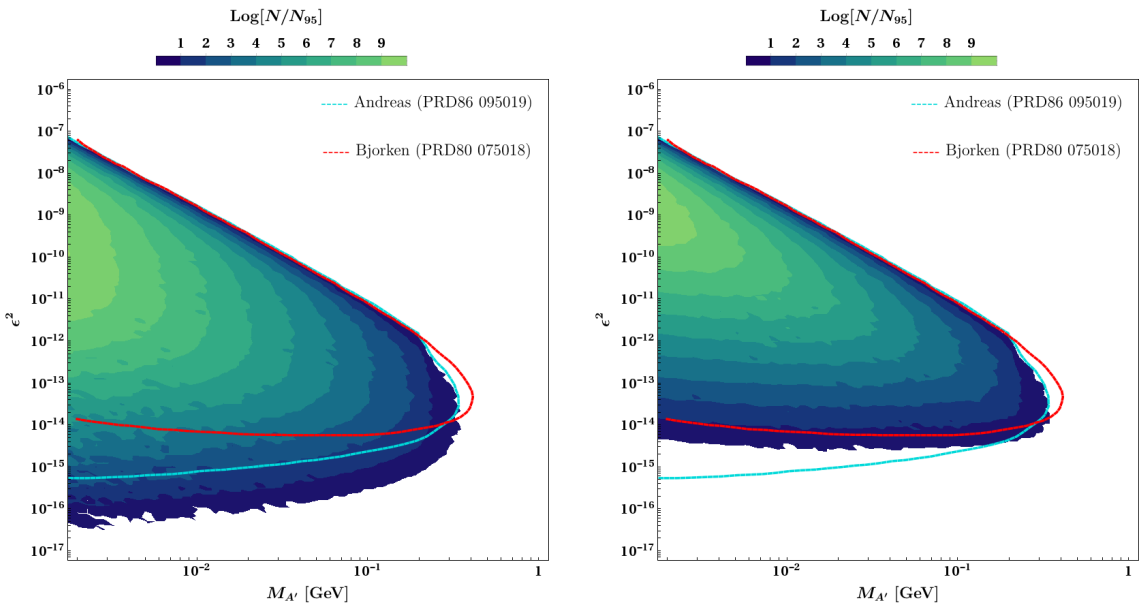

Figure B.2: Expected number of events normalized to the 95% C.L. limit N/N_{95} for a secluded hidden photon A' at the SLAC E137 experiment obtained from the ***Andreas implementation*** as a function of the mixing parameter ϵ^2 and the mass $M_{A'}$. The red (Bjorken) and cyan (Andreas) lines show the exclusion contours calculated in [275] and in [304], respectively. Left: Using the hidden photon mass as minimum A' energy $E_{A'}^{\min} = M_{A'}$. Right: Including the experimental minimum cutoff energy $E_{A'}^{\min} = E_{\text{cut}}$.

B.2.2 Andreas implementation

Improving on the analysis of Bjorken *et al.*, the hidden photon limits from E137 have been rederived in a more rigorous treatment by Andreas *et al.* [304]. The approximate differential cross section Eq. (4.21) has been corrected. But in particular, a full-fletched Monte Carlo simulation of the A' decays including detector geometry has been done and for the limit determination the full energy dependence of the differential cross section has been taken into account. A very thorough account of the many important details of this calculation can be found in Chapter 3 and Appendix B of [360].

Again we have implemented the full calculation in `MATHEMATICA`, which we will refer to as ***Andreas implementation***. As before we have discretized the parameter space and calculated the expected number of hidden photon induced events N at each point. The expected number of events from the *Andreas implementation* normalized to the 95% C.L. limit N/N_{95} are depicted in Fig. B.2.

The left panel shows the results of the *Andreas implementation* using $E_{A'}^{\min} = M_{A'}$ in Eq. (4.25) for the minimum energy of the produced A', as suggested in [304]. This is a sensible choice as it corresponds to an A' produced on shell in the lab frame, which can then resonantly decay into electrons. Such an A' can be looked for in a dielectron resonance search in the experiment. This choice explains the mass-dependent behavior of the low-ϵ^2 domain both of the Andreas and our derived limit (The fact that our limit is

excluding even smaller ϵ^2 is mainly due to our lack of a full Monte Carlo simulation of the A' decay geometry).

To see this explicitly, let us note that the lower boundary of the beam dump limit is reached when the A' has a typical decay length that is much larger than the experimental setup $\ell_{A'} \gg L_{\rm sh}, L_{\rm sh}$. In this case, we can expand the hidden photon decay probability as

$$P_{\rm dec} \;=\; e^{-\frac{L_{\rm sh}}{\ell_{A'}}}\left(1 - e^{-\frac{L_{\rm dec}}{\ell_{A'}}}\right) \;\approx\; \frac{L_{\rm dec}}{\ell_{A'}} \;\propto\; L_{\rm dec}\,\frac{M_{A'}^2\,\alpha\,\epsilon^2}{E_{A'}}\,. \tag{B.12}$$

Combined with the estimate for the beam dump cross section in Eqs. (A15) and (A16) of Ref. [275],

$$\sigma \propto \frac{\alpha^3\,\epsilon^2\,Z^2}{M_{A'}^2}\,, \tag{B.13}$$

we see that the leading powers of $M_{A'}^2$ cancel in the calculation of the expected number of hidden photon events

$$N \propto \int_{E_{A'}^{\rm min}}^{E_0} dE_{A'}\,\sigma_{A'}\,P_{\rm dec}(E_{A'})\,. \tag{B.14}$$

If we use the hidden photon mass as the lower integration limit $E_{A'}^{\rm min} = M_{A'}$ in Eq. (B.14), as done in [304], the lower boundary of the beam dump limit has an explicit dependence on $M_{A'}$. This is shown in the left panel of Fig. B.2. From Eqs. (B.12) to (B.14) we can see that in this regime the total number of events scales with ϵ^4 and therefore has a quite steep fall-off, such that the lower boundary is mainly statistics limited. There still might be a residual logarithmic dependence of N on the mass $M_{A'}$ coming from the integration of $dE_{A'}/E_{A'}$.

However, the experimental analysis searching for resonant dielectron events applied a cut of $E_{\rm cut} = 3$ GeV to their data [293]. Implementing this experimental cut as $E_{A'}^{\rm min} = E_{\rm cut}$ the *Andreas implementation* yields the results in the right panel of Fig. B.2. We see that we recover the horizontal scaling (i.e. no mass dependence) of the low-ϵ^2 domain, which is present in the Bjorken limit (again we expect the overshooting of our exclusion contour in this domain to be fixed by including Monte Carlo simulated geometric acceptances). This is what we expect from Eq. (B.14). With a constant minimum energy $E_{\rm cut} \gg M_{A'}$ the exponent only scales with ϵ^4 and shows no mass dependence anymore.

In summary, it seems likely that Andreas *et al.* have not included experimental cuts on the minimum energy of the observed events. This would mean that the limit deduced for E137 by Andreas *et al.* is too optimistic in the low-ϵ^2 domain. This issue also persists for the derived limits for E141, E774 and Orsay as all the relevant analyses include energy cuts (cf. Table B.1).

B.2.3 Towards more accurate limits

We have seen that both the limits derived by Andreas *et al.* and Bjorken *et al.* can possibly be refined in certain aspects. We therefore adopted the improved approximate equations derived in [304] with the inclusion of the experimental energy cut for the calculation of electron beam dump limits in this work. Further improvements could be obtained from a full calculation of these limits as outlined in [360] with the implementation of the energy cuts and a full Monte Carlo simulated detector acceptance.

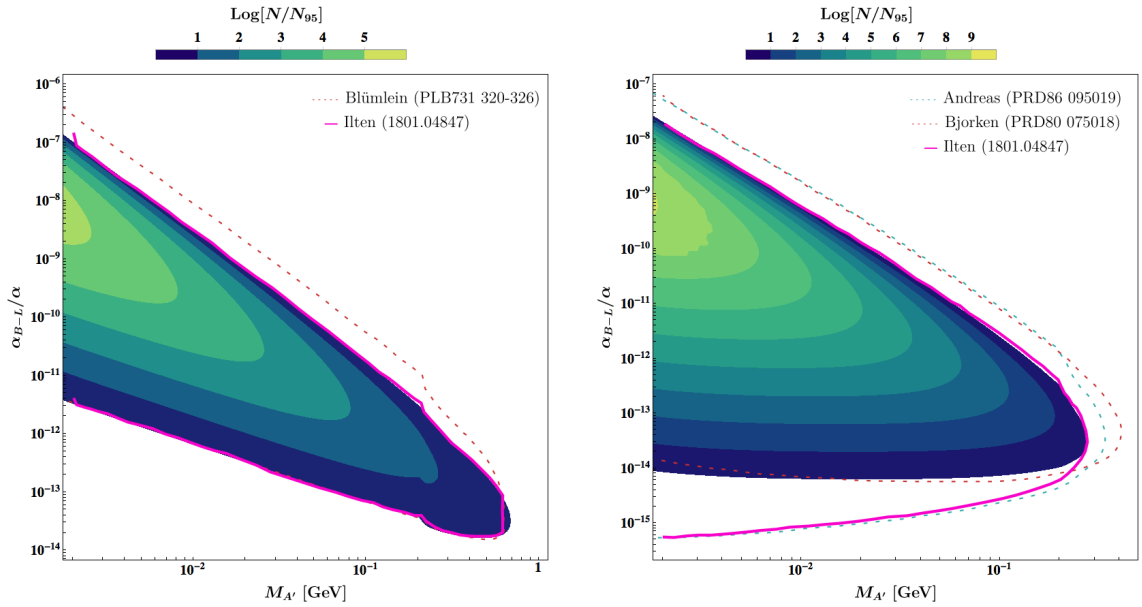

Figure B.3: Comparison of beam bump limits for the $U(1)_{B-L}$ gauge boson calculated in this work to the recasted limits of Ref. [284] for the two beam dump experiments **NuCal** (left) and **E137** (right). The calculated limits are given by the border of the outermost dark blue contour. The recasted limits are depicted by the pink solid lines. (Left) The red dashed line shows the respective NuCal limit for the secluded hidden photon. (Right) The red and cyan dashed lines show the respective E137 limits for the secluded hidden photons discussed previously. Figure taken from [262].

Experiment	E137	E141	E774	Orsay
E_{cut} [GeV]	3	4.5	27.5	0.75

Table B.1: Cuts on the minimum event energy used in the analyses of E137 [293], E141 [292], E774 [294] and Orsay [295].

B.2.4 A note on recasting beam dump limits

In previous work, Ilten *et al.* have presented a framework for recasting limits on hidden photons in Ref. [284]. In particular, they have recasted existing limits on a secluded hidden photon to the $U(1)_{B-L}$ gauge boson by use of their recasting framework. In Fig. B.3 we compare these recasted limits to those derived in this work from the full calculation for the case of $U(1)_{B-L}$.

In the left panel we show the limits obtained from the NuCal proton beam bump experiment. The recasted limits of [284] match those obtained from the full calculation over a large range of masses. However, the full calculation improves the mass reach of the $U(1)_{B-L}$ limit, which is due to the higher relative branching fraction into leptons for

A' masses of the order of the ω mass. The full calculation excludes A' masses of up to 688 MeV compared to 624 MeV for the recasted limits. In the right panel, the limits obtained from E137 are shown. In the high-α_{B-L} domain the recasted limits match those derived in this work quite well. However, it seems that the limits derived in [284] are based on the analysis in [304] and therefore exhibit the same mass scaling in the low-α_{B-L} domain as the Andreas limits. This is the main reason for the different behavior at small couplings. The same holds for the recasted electron beam dump limits of E141, E774 and Orsay.

Overall, our comparison shows that the recasted limits [284] match a full implementation to a good level (if they have been derived with the same implementation of the beam dump event calculation). Yet a full implementation provides quantitative improvements and increased confidence in the results.

B.3 Relevant processes and couplings for the different experiments

Experiment		Process	$B-L$	$L_\mu - L_e$	$L_e - L_\tau$	$L_\mu - L_\tau$
E137, E141, E774, Orsay, APEX, A1/MAMI	prod	e-Bremsstrahlung	$-g_{B-L}$	$-g_{\mu e}$	$g_{e\tau}$	$e\,\epsilon_{\mu\tau}(q^2)$
	det	$A' \to ee$	$-g_{B-L}$	$-g_{\mu e}$	$g_{e\tau}$	$e\,\epsilon_{\mu\tau}(q^2)$
CHARM	prod	η/η'-decay	g_{B-L}	$e\,\epsilon_{\mu e}(q^2)$	$e\,\epsilon_{e\tau}(q^2)$	$e\,\epsilon_{\mu\tau}(q^2)$
	det	$A' \to ee$	$-g_{B-L}$	$-g_{\mu e}$	$g_{e\tau}$	$e\,\epsilon_{\mu\tau}(q^2)$
LSND, NA48/2	prod	π^0-decay	g_{B-L}	$e\,\epsilon_{\mu e}(q^2)$	$e\,\epsilon_{e\tau}(q^2)$	$e\,\epsilon_{\mu\tau}(q^2)$
	det	$A' \to ee$	$-g_{B-L}$	$-g_{\mu e}$	$g_{e\tau}$	$e\,\epsilon_{\mu\tau}(q^2)$
U70/NuCal	prod	π^0-decay	g_{B-L}	$e\,\epsilon_{\mu e}(q^2)$	$e\,\epsilon_{e\tau}(q^2)$	$e\,\epsilon_{\mu\tau}(q^2)$
	prod	p-Bremsstrahlung	g_{B-L}	$e\,\epsilon_{\mu e}(q^2)$	$e\,\epsilon_{e\tau}(q^2)$	$e\,\epsilon_{\mu\tau}(q^2)$
	det	$A' \to ee$	$-g_{B-L}$	$-g_{\mu e}$	$g_{e\tau}$	$e\,\epsilon_{\mu\tau}(q^2)$
	det	$A' \to \mu\mu$	$-g_{B-L}$	$g_{\mu e}$	$e\,\epsilon_{e\tau}(q^2)$	$g_{\mu\tau}$
DarkLight	prod	e-Bremsstrahlung	$-g_{B-L}$	$-g_{\mu e}$	$g_{e\tau}$	$e\,\epsilon_{\mu\tau}(q^2)$
	det	$A' \to ee$	$-g_{B-L}$	$-g_{\mu e}$	$g_{e\tau}$	$e\,\epsilon_{\mu\tau}(q^2)$
	det	$A' \to$ inv	$-g_{B-L}$	$g_{\mu e}$	$g_{e\tau}$	$g_{\mu\tau}$
NA64	prod	e-Bremsstrahlung	$-g_{B-L}$	$-g_{\mu e}$	$g_{e\tau}$	$e\,\epsilon_{\mu\tau}(q^2)$
	prod	μ-Bremsstrahlung	$-g_{B-L}$	$g_{\mu e}$	$e\,\epsilon_{e\tau}(q^2)$	$g_{\mu\tau}$
	det	$A' \to$ inv	$-g_{B-L}$	$g_{\mu e}$	$g_{e\tau}$	$g_{\mu\tau}$
Mu3e	prod	μ-Bremsstrahlung	$-g_{B-L}$	$g_{\mu e}$	$e\,\epsilon_{e\tau}(q^2)$	$g_{\mu\tau}$
	det	$A' \to ee$	$-g_{B-L}$	$-g_{\mu e}$	$g_{e\tau}$	$e\,\epsilon_{\mu\tau}(q^2)$

Experiment		**Process**	$\boldsymbol{B-L}$	$\boldsymbol{L_\mu - L_e}$	$\boldsymbol{L_e - L_\tau}$	$\boldsymbol{L_\mu - L_\tau}$
FASER, SeaQuest, SHiP	prod	$\pi^0/\eta/\eta'$-decay	g_{B-L}	$e\,\epsilon_{\mu e}(q^2)$	$e\,\epsilon_{e\tau}(q^2)$	$e\,\epsilon_{\mu\tau}(q^2)$
	prod	p-Bremsstrahlung	g_{B-L}	$e\,\epsilon_{\mu e}(q^2)$	$e\,\epsilon_{e\tau}(q^2)$	$e\,\epsilon_{\mu\tau}(q^2)$
	det	$A' \to ee$	$-g_{B-L}$	$-g_{\mu e}$	$g_{e\tau}$	$e\,\epsilon_{\mu\tau}(q^2)$
	det	$A' \to \mu\mu$	$-g_{B-L}$	$g_{\mu e}$	$e\,\epsilon_{e\tau}(q^2)$	$g_{\mu\tau}$
VEPP-3	prod	$e^+e^- \to \gamma A'$	$-g_{B-L}$	$-g_{\mu e}$	$g_{e\tau}$	$e\,\epsilon_{\mu\tau}(q^2)$
	det	$A' \to$ inv	$-g_{B-L}$	$g_{\mu e}$	$g_{e\tau}$	$g_{\mu\tau}$
KLOE	prod	$e^+e^- \to \gamma A'$	$-g_{B-L}$	$-g_{\mu e}$	$g_{e\tau}$	$e\,\epsilon_{\mu\tau}(q^2)$
	det	$A' \to \mu\mu$	$-g_{B-L}$	$g_{\mu e}$	$e\,\epsilon_{e\tau}(q^2)$	$g_{\mu\tau}$
	det	$A' \to \pi^+\pi^-$	$\frac{1}{3}g_{B-L}$	$e\,\epsilon_{\mu e}(q^2)$	$e\,\epsilon_{e\tau}(q^2)$	$e\,\epsilon_{\mu\tau}(q^2)$
BaBar, Belle-II	prod	$e^+e^- \to \gamma A'$	$-g_{B-L}$	$-g_{\mu e}$	$g_{e\tau}$	$e\,\epsilon_{\mu\tau}(q^2)$
	det	$A' \to \mu\mu$	$-g_{B-L}$	$g_{\mu e}$	$e\,\epsilon_{e\tau}(q^2)$	$g_{\mu\tau}$
	det	$A' \to ee$	$-g_{B-L}$	$-g_{\mu e}$	$g_{e\tau}$	$e\,\epsilon_{\mu\tau}(q^2)$
LHCb	prod	$\pi^0/\eta/\eta'$-decay	g_{B-L}	$e\,\epsilon_{\mu e}(q^2)$	$e\,\epsilon_{e\tau}(q^2)$	$e\,\epsilon_{\mu\tau}(q^2)$
	prod	D^*-decay	0	$e\,\epsilon_{\mu e}(q^2)$	$e\,\epsilon_{e\tau}(q^2)$	$e\,\epsilon_{\mu\tau}(q^2)$
	prod	p-Bremsstrahlung	g_{B-L}	$e\,\epsilon_{\mu e}(q^2)$	$e\,\epsilon_{e\tau}(q^2)$	$e\,\epsilon_{\mu\tau}(q^2)$
	det	$A' \to \mu\mu$	$-g_{B-L}$	$g_{\mu e}$	$e\,\epsilon_{e\tau}(q^2)$	$g_{\mu\tau}$
	det	$A' \to ee$	$-g_{B-L}$	$-g_{\mu e}$	$g_{e\tau}$	$e\,\epsilon_{\mu\tau}(q^2)$
ATLAS, CMS	prod	Drell-Yan	$\frac{1}{3}\,g_{B-L}$	$e\,\epsilon_{\mu e}(q^2)$	$e\,\epsilon_{e\tau}(q^2)$	$e\,\epsilon_{\mu\tau}(q^2)$
	det	$A' \to \mu\mu$	$-g_{B-L}$	$g_{\mu e}$	$e\,\epsilon_{e\tau}(q^2)$	$g_{\mu\tau}$
	det	$A' \to ee$	$-g_{B-L}$	$-g_{\mu e}$	$g_{e\tau}$	$e\,\epsilon_{\mu\tau}(q^2)$

Table B.2: Coupling strengths for the different gauge groups relevant for the production (prod) and detection (det) of hidden photons in experiments discussed in this work compared to the universal $e\,\epsilon\,Q_{\rm EM}$ coupling of the secluded hidden photon.

Experiment	**Process**	$\boldsymbol{B-L}$	$\boldsymbol{L_\mu - L_e}$	$\boldsymbol{L_e - L_\tau}$	$\boldsymbol{L_\mu - L_\tau}$
Borexino	$\nu\, e^- \to \nu\, e^-$	g_{B-L}^2	$g_{\mu e}^2$	$g_{e\tau}^2$	$e\, g_{\mu\tau}\, \epsilon_{\mu\tau}(q^2)$
Charm-II	$\nu_\mu\, e^- \to \nu_\mu\, e^-$	g_{B-L}^2	$-g_{\mu e}^2$	0	$e\, g_{\mu\tau}\, \epsilon_{\mu\tau}(q^2)$
	$\bar{\nu}_\mu\, e^- \to \bar{\nu}_\mu\, e^-$	$-g_{B-L}^2$	$g_{\mu e}^2$	0	$-e\, g_{\mu\tau}\, \epsilon_{\mu\tau}(q^2)$
Texono	$\bar{\nu}_e\, e^- \to \bar{\nu}_e\, e^-$	$-g_{B-L}^2$	$-g_{\mu e}^2$	$-e\, g_{e\tau}\, \epsilon_{e\tau}(q^2)$	0
DUNE, Super-K	$\nu_{\mu/\tau} e^-$	0	$g_{\mu e}^2$	$g_{e\tau}^2$	0
Charm-II, CCFR, NuTeV	$\nu Z \to \nu\mu\mu Z$	g_{B-L}^2	$g_{\mu e}^2$	0	$g_{\mu\tau}^2$

Table B.3: Coupling strengths for the different gauge groups relevant at neutrino experiments. Note that the hidden photon of a secluded $U(1)_X$ does not have any neutrino couplings and therefore is not constrained by these experiments.

Bibliography

[1] M. Born, W. Heisenberg and P. Jordan, *Zur Quantenmechanik. II.*, *Z. Phys.* **35** (1926) 557–615.

[2] P. A. M. Dirac, *Quantum theory of emission and absorption of radiation*, *Proc. Roy. Soc. Lond.* **A114** (1927) 243.

[3] P. Jordan and E. P. Wigner, *About the Pauli exclusion principle*, *Z. Phys.* **47** (1928) 631–651.

[4] W. Heisenberg and W. Pauli, *On Quantum Field Theory. (In German)*, *Z. Phys.* **56** (1929) 1–61.

[5] W. Heisenberg and W. Pauli, *On Quantum Field Theory. 2. (In German)*, *Z. Phys.* **59** (1930) 168–190.

[6] S. L. Glashow, *Partial Symmetries of Weak Interactions*, *Nucl. Phys.* **22** (1961) 579–588.

[7] S. Weinberg, *A Model of Leptons*, *Phys. Rev. Lett.* **19** (1967) 1264–1266.

[8] A. Salam, *Weak and Electromagnetic Interactions*, *Conf. Proc.* **C680519** (1968) 367–377.

[9] D. Hanneke, S. Fogwell and G. Gabrielse, *New Measurement of the Electron Magnetic Moment and the Fine Structure Constant*, *Phys. Rev. Lett.* **100** (2008) 120801, [0801.1134].

[10] D. Hanneke, S. F. Hoogerheide and G. Gabrielse, *Cavity Control of a Single-Electron Quantum Cyclotron: Measuring the Electron Magnetic Moment*, *Phys. Rev.* **A83** (2011) 052122, [1009.4831].

[11] ATLAS collaboration, G. Aad et al., *Observation of a new particle in the search for the Standard Model Higgs boson with the ATLAS detector at the LHC*, *Phys. Lett.* **B716** (2012) 1–29, [1207.7214].

[12] CMS collaboration, S. Chatrchyan et al., *Observation of a new boson at a mass of 125 GeV with the CMS experiment at the LHC*, *Phys. Lett.* **B716** (2012) 30–61, [1207.7235].

[13] Particle Data Group collaboration, M. Tanabashi et al., *Review of Particle Physics*, *Phys. Rev.* **D98** (2018) 030001.

[14] R. N. Cahn, *The Eighteen arbitrary parameters of the standard model in your everyday life*, *Rev. Mod. Phys.* **68** (1996) 951–960.

[15] M. P. Bronstein, *Kvantovanie gravitatsionnykh voln [Quantization of gravitational waves]*, *Sov. Phys. JETP* **6** (dec, 1936) 195.

[16] M. P. Bronstein, *Quantentheorie schwacher Gravitationsfelder*, *Phys. Z. Sowjetunion* **2-3** (1936) 140–157.

[17] J. A. Wheeler, *Geons*, *Phys. Rev.* **97** (1955) 511–536.

[18] J. D. Wells, *Lectures on Higgs Boson Physics in the Standard Model and Beyond*, in *39th British Universities Summer School in Theoretical Elementary Particle Physics (BUSSTEPP 2009) Liverpool, United Kingdom, August 24-September 4, 2009*, 2009. 0909.4541.

[19] J. Polchinski, *Effective field theory and the Fermi surface*, in *Proceedings, Theoretical Advanced Study Institute (TASI 92): From Black Holes and Strings to Particles: Boulder, USA, June 1-26, 1992*, pp. 0235–276, 1992. hep-th/9210046.

[20] G. F. Giudice, *Naturally Speaking: The Naturalness Criterion and Physics at the LHC*, 0801.2562.

[21] Planck collaboration, N. Aghanim et al., *Planck 2018 results. VI. Cosmological parameters*, 1807.06209.

[22] A. D. Sakharov, *Violation of CP Invariance, C asymmetry, and baryon asymmetry of the universe*, *Pisma Zh. Eksp. Teor. Fiz.* **5** (1967) 32–35.

[23] J. M. Cline, *Baryogenesis*, in *Les Houches Summer School - Session 86: Particle Physics and Cosmology: The Fabric of Spacetime Les Houches, France, July 31-August 25, 2006*, 2006. hep-ph/0609145.

[24] K. Kajantie, M. Laine, K. Rummukainen and M. E. Shaposhnikov, *Is there a hot electroweak phase transition at $m_H \gtrsim m_W$?*, *Phys. Rev. Lett.* **77** (1996) 2887–2890, [hep-ph/9605288].

[25] Z. Fodor, F. Csikor, J. Heitger, Y. Aoki and A. Ukawa, *End point of the electroweak phase transition*, in *Strong and electroweak matter '98. Proceedings, Conference, SEWM'98, Copenhagen, Denmark, December 2-5, 1998*, pp. 190–195, 1998. hep-ph/9901307.

[26] G. R. Farrar and M. E. Shaposhnikov, *Baryon asymmetry of the universe in the minimal Standard Model*, *Phys. Rev. Lett.* **70** (1993) 2833–2836, [hep-ph/9305274].

[27] G. R. Farrar and M. E. Shaposhnikov, *Baryon asymmetry of the universe in the standard electroweak theory*, *Phys. Rev.* **D50** (1994) 774, [hep-ph/9305275].

[28] M. B. Gavela, P. Hernandez, J. Orloff and O. Pene, *Standard model CP violation and baryon asymmetry*, *Mod. Phys. Lett.* **A9** (1994) 795–810, [hep-ph/9312215].

[29] P. Huet and E. Sather, *Electroweak baryogenesis and standard model CP violation*, *Phys. Rev.* **D51** (1995) 379–394, [hep-ph/9404302].

[30] PAMELA collaboration, O. Adriani et al., *An anomalous positron abundance in cosmic rays with energies 1.5-100 GeV*, *Nature* **458** (2009) 607–609, [0810.4995].

[31] PAMELA collaboration, O. Adriani et al., *Cosmic-Ray Positron Energy Spectrum Measured by PAMELA*, *Phys. Rev. Lett.* **111** (2013) 081102, [1308.0133].

[32] Fermi-LAT collaboration, M. Ackermann et al., *Measurement of separate cosmic-ray electron and positron spectra with the Fermi Large Area Telescope*, *Phys. Rev. Lett.* **108** (2012) 011103, [1109.0521].

[33] AMS collaboration, M. Aguilar et al., *Electron and Positron Fluxes in Primary Cosmic Rays Measured with the Alpha Magnetic Spectrometer on the International Space Station*, *Phys. Rev. Lett.* **113** (2014) 121102.

[34] AMS collaboration, L. Accardo et al., *High Statistics Measurement of the Positron Fraction in Primary Cosmic Rays of 0.5–500 GeV with the Alpha Magnetic Spectrometer on the International Space Station*, *Phys. Rev. Lett.* **113** (2014) 121101.

[35] I. V. Moskalenko and A. W. Strong, *Production and propagation of cosmic ray positrons and electrons*, *Astrophys. J.* **493** (1998) 694–707, [astro-ph/9710124].

[36] P. Blasi, *The origin of the positron excess in cosmic rays*, *Phys. Rev. Lett.* **103** (2009) 051104, [0903.2794].

[37] I. Cholis, L. Goodenough, D. Hooper, M. Simet and N. Weiner, *High Energy Positrons From Annihilating Dark Matter*, *Phys. Rev.* **D80** (2009) 123511, [0809.1683].

[38] L. Bergstrom, T. Bringmann and J. Edsjo, *New Positron Spectral Features from Supersymmetric Dark Matter - a Way to Explain the PAMELA Data?*, *Phys. Rev.* **D78** (2008) 103520, [0808.3725].

[39] K. M. Zurek, *Multi-Component Dark Matter*, *Phys. Rev.* **D79** (2009) 115002, [0811.4429].

[40] R. Harnik and G. D. Kribs, *An Effective Theory of Dirac Dark Matter*, *Phys. Rev.* **D79** (2009) 095007, [0810.5557].

[41] M. Cirelli and A. Strumia, *Minimal Dark Matter predictions and the PAMELA positron excess*, *PoS* **IDM2008** (2008) 089, [0808.3867].

[42] Fermi-LAT collaboration, M. Ajello et al., *Fermi-LAT Observations of High-Energy γ-Ray Emission Toward the Galactic Center*, *Astrophys. J.* **819** (2016) 44, [1511.02938].

[43] L. Goodenough and D. Hooper, *Possible Evidence For Dark Matter Annihilation In The Inner Milky Way From The Fermi Gamma Ray Space Telescope*, 0910.2998.

[44] D. Hooper and L. Goodenough, *Dark Matter Annihilation in The Galactic Center As Seen by the Fermi Gamma Ray Space Telescope*, *Phys. Lett.* **B697** (2011) 412–428, [1010.2752].

[45] D. Hooper and T. Linden, *On The Origin Of The Gamma Rays From The Galactic Center*, *Phys. Rev.* **D84** (2011) 123005, [1110.0006].

[46] K. N. Abazajian and M. Kaplinghat, *Detection of a Gamma-Ray Source in the Galactic Center Consistent with Extended Emission from Dark Matter Annihilation and Concentrated Astrophysical Emission*, *Phys. Rev.* **D86** (2012) 083511, [1207.6047].

[47] C. Gordon and O. Macias, *Dark Matter and Pulsar Model Constraints from Galactic Center Fermi-LAT Gamma Ray Observations*, *Phys. Rev.* **D88** (2013) 083521, [1306.5725].

[48] D. Hooper and T. R. Slatyer, *Two Emission Mechanisms in the Fermi Bubbles: A Possible Signal of Annihilating Dark Matter*, *Phys. Dark Univ.* **2** (2013) 118–138, [1302.6589].

[49] W.-C. Huang, A. Urbano and W. Xue, *Fermi Bubbles under Dark Matter Scrutiny. Part I: Astrophysical Analysis*, 1307.6862.

[50] F. Calore, I. Cholis and C. Weniger, *Background Model Systematics for the Fermi GeV Excess*, *JCAP* **1503** (2015) 038, [1409.0042].

[51] R. Bartels, S. Krishnamurthy and C. Weniger, *Strong support for the millisecond pulsar origin of the Galactic center GeV excess*, *Phys. Rev. Lett.* **116** (2016) 051102, [1506.05104].

[52] S. K. Lee, M. Lisanti, B. R. Safdi, T. R. Slatyer and W. Xue, *Evidence for Unresolved γ-Ray Point Sources in the Inner Galaxy*, *Phys. Rev. Lett.* **116** (2016) 051103, [1506.05124].

[53] R. Bernabei et al., *Final model independent result of DAMA/LIBRA-phase1*, *Eur. Phys. J.* **C73** (2013) 2648, [1308.5109].

[54] R. Bernabei et al., *First Model Independent Results from DAMA/LIBRA–Phase2*, *Universe* **4** (2018) 116, [1805.10486].

[55] K. Blum, *DAMA vs. the annually modulated muon background*, 1110.0857.

[56] J. Pradler, B. Singh and I. Yavin, *On an unverified nuclear decay and its role in the DAMA experiment*, *Phys. Lett.* **B720** (2013) 399–404, [1210.5501].

[57] J. Pradler and I. Yavin, *Addendum to 'On an unverified nuclear decay and its role in the DAMA experiment"*, *Phys. Lett.* **B723** (2013) 168–171, [1210.7548].

[58] J. H. Davis, *Fitting the annual modulation in DAMA with neutrons from muons and neutrinos*, *Phys. Rev. Lett.* **113** (2014) 081302, [1407.1052].

[59] R. Bernabei et al., *No role for neutrons, muons and solar neutrinos in the DAMA annual modulation results*, *Eur. Phys. J.* **C74** (2014) 3196, [1409.3516].

[60] J. Klinger and V. A. Kudryavtsev, *Muon-induced neutrons do not explain the DAMA data*, *Phys. Rev. Lett.* **114** (2015) 151301, [1503.07225].

[61] EDELWEISS collaboration, L. Hehn et al., *Improved EDELWEISS-III sensitivity for low-mass WIMPs using a profile likelihood approach*, *Eur. Phys. J.* **C76** (2016) 548, [1607.03367].

[62] PandaX-II collaboration, X. Cui et al., *Dark Matter Results From 54-Ton-Day Exposure of PandaX-II Experiment*, *Phys. Rev. Lett.* **119** (2017) 181302, [1708.06917].

[63] PICO collaboration, C. Amole et al., *Dark Matter Search Results from the PICO-60 C_3F_8 Bubble Chamber*, *Phys. Rev. Lett.* **118** (2017) 251301, [1702.07666].

[64] DarkSide collaboration, P. Agnes et al., *Low-Mass Dark Matter Search with the DarkSide-50 Experiment*, *Phys. Rev. Lett.* **121** (2018) 081307, [1802.06994].

[65] DarkSide collaboration, P. Agnes et al., *DarkSide-50 532-day Dark Matter Search with Low-Radioactivity Argon*, *Phys. Rev.* **D98** (2018) 102006, [1802.07198].

[66] LUX collaboration, D. S. Akerib et al., *Search for annual and diurnal rate modulations in the LUX experiment*, *Phys. Rev.* **D98** (2018) 062005, [1807.07113].

[67] SuperCDMS collaboration, R. Agnese et al., *Low-mass dark matter search with CDMSlite*, *Phys. Rev.* **D97** (2018) 022002, [1707.01632].

[68] XENON collaboration, E. Aprile et al., *Dark Matter Search Results from a One Ton-Year Exposure of XENON1T*, *Phys. Rev. Lett.* **121** (2018) 111302, [1805.12562].

[69] SuperCDMS collaboration, R. Agnese et al., *Results from the Super Cryogenic Dark Matter Search Experiment at Soudan*, *Phys. Rev. Lett.* **120** (2018) 061802, [1708.08869].

[70] SuperCDMS collaboration, R. Agnese et al., *Search for Low-Mass Dark Matter with CDMSlite Using a Profile Likelihood Fit*, *Phys. Rev.* **D99** (2019) 062001, [1808.09098].

[71] CRESST collaboration, A. H. Abdelhameed et al., *First results from the CRESST-III low-mass dark matter program*, 1904.00498.

[72] F. Kahlhoefer, F. Reindl, K. Schäffner, K. Schmidt-Hoberg and S. Wild, *Model-independent comparison of annual modulation and total rate with direct detection experiments*, *JCAP* **1805** (2018) 074, [1802.10175].

[73] LHCb collaboration, R. Aaij et al., *Test of lepton universality using $B^+ \to K^+\ell^+\ell^-$ decays*, *Phys. Rev. Lett.* **113** (2014) 151601, [1406.6482].

[74] LHCb collaboration, R. Aaij et al., *Test of lepton universality with $B^0 \to K^{*0}\ell^+\ell^-$ decays*, *JHEP* **08** (2017) 055, [1705.05802].

[75] C. Bobeth, G. Hiller and G. Piranishvili, *Angular distributions of $\bar{B} \to \bar{K}\ell^+\ell^-$ decays*, *JHEP* **12** (2007) 040, [0709.4174].

[76] N. Serra, R. Silva Coutinho and D. van Dyk, *Measuring the breaking of lepton flavor universality in $B \to K^*\ell^+\ell^-$*, *Phys. Rev.* **D95** (2017) 035029, [1610.08761].

[77] B. Capdevila, A. Crivellin, S. Descotes-Genon, J. Matias and J. Virto, *Patterns of New Physics in $b \to s\ell^+\ell^-$ transitions in the light of recent data*, *JHEP* **01** (2018) 093, [1704.05340].

[78] W. Altmannshofer, P. Stangl and D. M. Straub, *Interpreting Hints for Lepton Flavor Universality Violation*, *Phys. Rev.* **D96** (2017) 055008, [1704.05435].

[79] G. D'Amico, M. Nardecchia, P. Panci, F. Sannino, A. Strumia, R. Torre et al., *Flavour anomalies after the R_{K^*} measurement*, *JHEP* **09** (2017) 010, [1704.05438].

[80] G. Hiller and I. Nisandzic, *R_K and R_{K^*} beyond the standard model*, *Phys. Rev.* **D96** (2017) 035003, [1704.05444].

[81] L.-S. Geng, B. Grinstein, S. Jäger, J. Martin Camalich, X.-L. Ren and R.-X. Shi, *Towards the discovery of new physics with lepton-universality ratios of $b \to s\ell\ell$ decays*, *Phys. Rev.* **D96** (2017) 093006, [1704.05446].

[82] M. Ciuchini, A. M. Coutinho, M. Fedele, E. Franco, A. Paul, L. Silvestrini et al., *On Flavourful Easter eggs for New Physics hunger and Lepton Flavour Universality violation*, *Eur. Phys. J.* **C77** (2017) 688, [1704.05447].

[83] A. Celis, J. Fuentes-Martin, A. Vicente and J. Virto, *Gauge-invariant implications of the LHCb measurements on lepton-flavor nonuniversality*, *Phys. Rev.* **D96** (2017) 035026, [1704.05672].

[84] BaBar collaboration, J. P. Lees et al., *Measurement of an Excess of $\bar{B} \to D^{(*)}\tau^-\bar{\nu}_\tau$ Decays and Implications for Charged Higgs Bosons*, *Phys. Rev.* **D88** (2013) 072012, [1303.0571].

[85] Belle collaboration, M. Huschle et al., *Measurement of the branching ratio of $\bar{B} \to D^{(*)}\tau^-\bar{\nu}_\tau$ relative to $\bar{B} \to D^{(*)}\ell^-\bar{\nu}_\ell$ decays with hadronic tagging at Belle*, *Phys. Rev.* **D92** (2015) 072014, [1507.03233].

[86] LHCb collaboration, R. Aaij et al., *Measurement of the ratio of branching fractions $\mathcal{B}(\bar{B}^0 \to D^{*+}\tau^-\bar{\nu}_\tau)/\mathcal{B}(\bar{B}^0 \to D^{*+}\mu^-\bar{\nu}_\mu)$*, *Phys. Rev. Lett.* **115** (2015) 111803, [1506.08614].

[87] A. Abdesselam et al., *Measurement of the τ lepton polarization in the decay $\bar{B} \to D^* \tau^- \bar{\nu}_\tau$*, 1608.06391.

[88] HFLAV collaboration, Y. Amhis et al., *Averages of b-hadron, c-hadron, and τ-lepton properties as of summer 2016*, *Eur. Phys. J.* **C77** (2017) 895, [1612.07233].

[89] F. U. Bernlochner, Z. Ligeti, M. Papucci and D. J. Robinson, *Combined analysis of semileptonic B decays to D and D^*: $R(D^{(*)})$, $|V_{cb}|$, and new physics*, *Phys. Rev.* **D95** (2017) 115008, [1703.05330].

[90] D. Bigi, P. Gambino and S. Schacht, *$R(D^*)$, $|V_{cb}|$, and the Heavy Quark Symmetry relations between form factors*, *JHEP* **11** (2017) 061, [1707.09509].

[91] Muon g-2 collaboration, G. W. Bennett et al., *Measurement of the positive muon anomalous magnetic moment to 0.7 ppm*, *Phys. Rev. Lett.* **89** (2002) 101804, [hep-ex/0208001].

[92] Muon g-2 collaboration, G. W. Bennett et al., *Measurement of the negative muon anomalous magnetic moment to 0.7 ppm*, *Phys. Rev. Lett.* **92** (2004) 161802, [hep-ex/0401008].

[93] Muon g-2 collaboration, G. W. Bennett et al., *Final Report of the Muon E821 Anomalous Magnetic Moment Measurement at BNL*, *Phys. Rev.* **D73** (2006) 072003, [hep-ex/0602035].

[94] F. Jegerlehner and A. Nyffeler, *The Muon g-2*, *Phys. Rept.* **477** (2009) 1–110, [0902.3360].

[95] J. P. Miller, E. de Rafael, B. L. Roberts and D. Stöckinger, *Muon (g-2): Experiment and Theory*, *Ann. Rev. Nucl. Part. Sci.* **62** (2012) 237–264.

[96] Muon g-2 collaboration, J. Grange et al., *Muon (g-2) Technical Design Report*, 1501.06858.

[97] Muon g-2 collaboration, J. L. Holzbauer, *The Muon g-2 Experiment Overview and Status*, *PoS* **NuFact2017** (2018) 116, [1712.05980].

[98] J. R. Ellis, *The Superstring: Theory of Everything, or of Nothing?*, *Nature* **323** (1986) 595–598.

[99] P. A. M. Dirac, *The fundamental equations of quantum mechanics*, *Proc. Roy. Soc. Lond.* **A109** (1925) 642–653.

[100] M. Srednicki, *Quantum field theory*. Cambridge University Press, 2007.

[101] S. Weinberg, *The Quantum theory of fields. Vol. 1: Foundations*. Cambridge University Press, 1995.

[102] M. E. Peskin and D. V. Schroeder, *An Introduction to quantum field theory*. Addison-Wesley, Reading, USA, 1995.

[103] M. D. Schwartz, *Quantum Field Theory and the Standard Model*. Cambridge University Press, 2014.

[104] A. V. Manohar, *Effective field theories*, *Lect. Notes Phys.* **479** (1997) 311–362, [hep-ph/9606222].

[105] D. B. Kaplan, *Five lectures on effective field theory*, 2005. nucl-th/0510023.

[106] B. Patt and F. Wilczek, *Higgs-field portal into hidden sectors*, hep-ph/0605188.

[107] V. Silveira and A. Zee, *SCALAR PHANTOMS*, *Phys. Lett.* **161B** (1985) 136–140.

[108] D. O'Connell, M. J. Ramsey-Musolf and M. B. Wise, *Minimal Extension of the Standard Model Scalar Sector*, *Phys. Rev.* **D75** (2007) 037701, [hep-ph/0611014].

[109] J. Choi and R. R. Volkas, *Real Higgs singlet and the electroweak phase transition in the Standard Model*, *Phys. Lett.* **B317** (1993) 385–391, [hep-ph/9308234].

[110] S. W. Ham, Y. S. Jeong and S. K. Oh, *Electroweak phase transition in an extension of the standard model with a real Higgs singlet*, *J. Phys.* **G31** (2005) 857–871, [hep-ph/0411352].

[111] R. M. Schabinger and J. D. Wells, *A Minimal spontaneously broken hidden sector and its impact on Higgs boson physics at the large hadron collider*, *Phys. Rev.* **D72** (2005) 093007, [hep-ph/0509209].

[112] J. McDonald, *Gauge singlet scalars as cold dark matter*, *Phys. Rev.* **D50** (1994) 3637–3649, [hep-ph/0702143].

[113] C. P. Burgess, M. Pospelov and T. ter Veldhuis, *The Minimal model of nonbaryonic dark matter: A Singlet scalar*, *Nucl. Phys.* **B619** (2001) 709–728, [hep-ph/0011335].

[114] J. M. Cline, K. Kainulainen, P. Scott and C. Weniger, *Update on scalar singlet dark matter*, *Phys. Rev.* **D88** (2013) 055025, [1306.4710].

[115] ATLAS collaboration, T. A. collaboration, *Combined measurements of Higgs boson production and decay using up to 80 fb^{-1} of proton–proton collision data at $\sqrt{s}$ = 13 TeV collected with the ATLAS experiment*, .

[116] CMS collaboration, A. M. Sirunyan et al., *Combined measurements of Higgs boson couplings in proton-proton collisions at $\sqrt{s}$ = 13 TeV*, *Submitted to: Eur. Phys. J.* (2018) , [1809.10733].

[117] ATLAS collaboration, M. Aaboud et al., *Search for pair production of Higgs bosons in the $b\bar{b}b\bar{b}$ final state using proton-proton collisions at $\sqrt{s} = 13$ TeV with the ATLAS detector*, *JHEP* **01** (2019) 030, [1804.06174].

[118] CMS collaboration, A. M. Sirunyan et al., *Search for heavy resonances decaying into two Higgs bosons or into a Higgs boson and a W or Z boson in proton-proton collisions at 13 TeV*, *JHEP* **01** (2019) 051, [1808.01365].

[119] ATLAS collaboration, M. Aaboud et al., *Combination of searches for heavy resonances decaying into bosonic and leptonic final states using 36 fb^{-1} of proton-proton collision data at $\sqrt{s} = 13$ TeV with the ATLAS detector*, *Phys. Rev.* **D98** (2018) 052008, [1808.02380].

[120] M.-L. Xiao and J.-H. Yu, *Stabilizing electroweak vacuum in a vectorlike fermion model*, *Phys. Rev.* **D90** (2014) 014007, [1404.0681].

[121] A. Falkowski, C. Gross and O. Lebedev, *A second Higgs from the Higgs portal*, *JHEP* **05** (2015) 057, [1502.01361].

[122] DELPHI collaboration, P. Abreu et al., *Search for low mass Higgs bosons produced in Z0 decays*, *Z. Phys.* **C51** (1991) 25–36.

[123] G. Arcadi, A. Djouadi and M. Raidal, *Dark Matter through the Higgs portal*, 1903.03616.

[124] LEP Working Group for Higgs boson searches, ALEPH, DELPHI, L3, OPAL collaboration, R. Barate et al., *Search for the standard model Higgs boson at LEP*, *Phys. Lett.* **B565** (2003) 61–75, [hep-ex/0306033].

[125] A. Boyarsky, O. Ruchayskiy and M. Shaposhnikov, *The Role of sterile neutrinos in cosmology and astrophysics*, *Ann. Rev. Nucl. Part. Sci.* **59** (2009) 191–214, [0901.0011].

[126] K. R. Dienes, E. Dudas and T. Gherghetta, *Neutrino oscillations without neutrino masses or heavy mass scales: A Higher dimensional seesaw mechanism*, *Nucl. Phys.* **B557** (1999) 25, [hep-ph/9811428].

[127] N. Arkani-Hamed, S. Dimopoulos, G. R. Dvali and J. March-Russell, *Neutrino masses from large extra dimensions*, *Phys. Rev.* **D65** (2001) 024032, [hep-ph/9811448].

[128] Y. Grossman and M. Neubert, *Neutrino masses and mixings in nonfactorizable geometry*, *Phys. Lett.* **B474** (2000) 361–371, [hep-ph/9912408].

[129] N. Arkani-Hamed and Y. Grossman, *Light active and sterile neutrinos from compositeness*, *Phys. Lett.* **B459** (1999) 179–182, [hep-ph/9806223].

[130] C. Giunti and C. W. Kim, *Fundamentals of Neutrino Physics and Astrophysics*. Oxford University Press, 2007.

[131] P. Minkowski, *$\mu \to e\gamma$ at a Rate of One Out of 10^9 Muon Decays?*, *Phys. Lett.* **67B** (1977) 421–428.

[132] T. Yanagida, *Horizontal gauge symmetry and masses of neutrinos*, *Conf. Proc.* **C7902131** (1979) 95–99.

[133] P. Ramond, *The Family Group in Grand Unified Theories*, in *International Symposium on Fundamentals of Quantum Theory and Quantum Field Theory Palm Coast, Florida, February 25-March 2, 1979*, pp. 265–280, 1979. hep-ph/9809459.

[134] M. Gell-Mann, P. Ramond and R. Slansky, *Complex Spinors and Unified Theories*, *Conf. Proc.* **C790927** (1979) 315–321, [1306.4669].

[135] R. N. Mohapatra and G. Senjanovic, *Neutrino Mass and Spontaneous Parity Nonconservation*, *Phys. Rev. Lett.* **44** (1980) 912.

[136] G. Lazarides, Q. Shafi and C. Wetterich, *Proton Lifetime and Fermion Masses in an SO(10) Model*, *Nucl. Phys.* **B181** (1981) 287–300.

[137] J. Schechter and J. W. F. Valle, *Neutrino Masses in $SU(2) \bigotimes U(1)$ Theories*, *Phys. Rev.* **D22** (1980) 2227.

[138] T. Yanagida, *Horizontal Symmetry and Masses of Neutrinos*, *Prog. Theor. Phys.* **64** (1980) 1103.

[139] M. Fukugita and T. Yanagida, *Baryogenesis Without Grand Unification*, *Phys. Lett.* **B174** (1986) 45–47.

[140] W. Buchmuller, R. D. Peccei and T. Yanagida, *Leptogenesis as the origin of matter*, *Ann. Rev. Nucl. Part. Sci.* **55** (2005) 311–355, [hep-ph/0502169].

[141] S. Blanchet and P. Di Bari, *The minimal scenario of leptogenesis*, *New J. Phys.* **14** (2012) 125012, [1211.0512].

[142] C. S. Fong, E. Nardi and A. Riotto, *Leptogenesis in the Universe*, *Adv. High Energy Phys.* **2012** (2012) 158303, [1301.3062].

[143] S. Dodelson and L. M. Widrow, *Sterile-neutrinos as dark matter*, *Phys. Rev. Lett.* **72** (1994) 17–20, [hep-ph/9303287].

[144] A. Boyarsky, M. Drewes, T. Lasserre, S. Mertens and O. Ruchayskiy, *Sterile Neutrino Dark Matter*, *Prog. Part. Nucl. Phys.* **104** (2019) 1–45, [1807.07938].

[145] M. Drewes, *The Phenomenology of Right Handed Neutrinos*, *Int. J. Mod. Phys.* **E22** (2013) 1330019, [1303.6912].

[146] L. B. Okun, *LIMITS OF ELECTRODYNAMICS: PARAPHOTONS?*, *Sov. Phys. JETP* **56** (1982) 502.

[147] B. Holdom, *Two U(1)'s and Epsilon Charge Shifts*, *Phys. Lett.* **166B** (1986) 196–198.

[148] R. Essig et al., *Working Group Report: New Light Weakly Coupled Particles*, in *Proceedings, 2013 Community Summer Study on the Future of U.S. Particle Physics: Snowmass on the Mississippi (CSS2013): Minneapolis, MN, USA, July 29-August 6, 2013*, 2013. 1311.0029.

[149] M. Raggi and V. Kozhuharov, *Results and perspectives in dark photon physics*, *Riv. Nuovo Cim.* **38** (2015) 449–505.

[150] P. Galison and A. Manohar, *TWO Z's OR NOT TWO Z's?*, *Phys. Lett.* **136B** (1984) 279–283.

[151] K. S. Babu, C. F. Kolda and J. March-Russell, *Implications of generalized $Z - Z'$ mixing*, *Phys. Rev.* **D57** (1998) 6788–6792, [hep-ph/9710441].

[152] H. Davoudiasl, H.-S. Lee and W. J. Marciano, *'Dark' Z implications for Parity Violation, Rare Meson Decays, and Higgs Physics*, *Phys. Rev.* **D85** (2012) 115019, [1203.2947].

[153] C. P. Burgess, J. P. Conlon, L.-Y. Hung, C. H. Kom, A. Maharana and F. Quevedo, *Continuous Global Symmetries and Hyperweak Interactions in String Compactifications*, *JHEP* **07** (2008) 073, [0805.4037].

[154] M. Cicoli, M. Goodsell, J. Jaeckel and A. Ringwald, *Testing String Vacua in the Lab: From a Hidden CMB to Dark Forces in Flux Compactifications*, *JHEP* **07** (2011) 114, [1103.3705].

[155] L. Ackerman, M. R. Buckley, S. M. Carroll and M. Kamionkowski, *Dark Matter and Dark Radiation*, *Phys. Rev.* **D79** (2009) 023519, [0810.5126].

[156] R. Foot and S. Vagnozzi, *Dissipative hidden sector dark matter*, *Phys. Rev.* **D91** (2015) 023512, [1409.7174].

[157] E. C. G. Stueckelberg, *Interaction energy in electrodynamics and in the field theory of nuclear forces*, *Helv. Phys. Acta* **11** (1938) 225–244.

[158] E. C. G. Stueckelberg, *Interaction forces in electrodynamics and in the field theory of nuclear forces*, *Helv. Phys. Acta* **11** (1938) 299–328.

[159] B. Kors and P. Nath, *A Stueckelberg extension of the standard model*, *Phys. Lett.* **B586** (2004) 366–372, [hep-ph/0402047].

[160] H. Ruegg and M. Ruiz-Altaba, *The Stueckelberg field*, *Int. J. Mod. Phys.* **A19** (2004) 3265–3348, [hep-th/0304245].

[161] B. Kors and P. Nath, *Aspects of the Stueckelberg extension*, *JHEP* **07** (2005) 069, [hep-ph/0503208].

[162] D. Feldman, Z. Liu and P. Nath, *The Stueckelberg Z' Extension with Kinetic Mixing and Milli-Charged Dark Matter From the Hidden Sector*, *Phys. Rev.* **D75** (2007) 115001, [hep-ph/0702123].

[163] B. Batell, M. Pospelov and A. Ritz, *Probing a Secluded U(1) at B-factories*, *Phys. Rev.* **D79** (2009) 115008, [0903.0363].

[164] M. Pospelov, *Secluded U(1) below the weak scale*, *Phys. Rev.* **D80** (2009) 095002, [0811.1030].

[165] M. Ahlers, J. Jaeckel, J. Redondo and A. Ringwald, *Probing Hidden Sector Photons through the Higgs Window*, *Phys. Rev.* **D78** (2008) 075005, [0807.4143].

[166] ALEPH, DELPHI, L3, OPAL, SLD, LEP Electroweak Working Group, SLD Electroweak Group, SLD Heavy Flavour Group collaboration, S. Schael et al., *Precision electroweak measurements on the Z resonance*, *Phys. Rept.* **427** (2006) 257–454, [hep-ex/0509008].

[167] A. Leike, S. Riemann and T. Riemann, *ZZ' mixing in presence of standard weak loop corrections*, hep-ph/9808374.

[168] J. Erler, P. Langacker, S. Munir and E. Rojas, *Improved Constraints on Z' Bosons from Electroweak Precision Data*, *JHEP* **08** (2009) 017, [0906.2435].

[169] S. Descotes-Genon and P. Koppenburg, *The CKM Parameters*, *Ann. Rev. Nucl. Part. Sci.* **67** (2017) 97–127, [1702.08834].

[170] P. Foldenauer and J. Jaeckel, *Purely flavor-changing Z' bosons and where they might hide*, *JHEP* **05** (2017) 010, [1612.07789].

[171] J. C. Pati and A. Salam, *Unified Lepton-Hadron Symmetry and a Gauge Theory of the Basic Interactions*, *Phys. Rev.* **D8** (1973) 1240–1251.

[172] H. Georgi and S. L. Glashow, *Unity of All Elementary Particle Forces*, *Phys. Rev. Lett.* **32** (1974) 438–441.

[173] H. Georgi, H. R. Quinn and S. Weinberg, *Hierarchy of Interactions in Unified Gauge Theories*, *Phys. Rev. Lett.* **33** (1974) 451–454.

[174] M. B. Green and J. H. Schwarz, *Anomaly Cancellation in Supersymmetric D=10 Gauge Theory and Superstring Theory*, *Phys. Lett.* **149B** (1984) 117–122.

[175] R. W. Robinett and J. L. Rosner, *Mass Scales in Grand Unified Theories*, *Phys. Rev.* **D26** (1982) 2396.

[176] J. L. Hewett and T. G. Rizzo, *Low-Energy Phenomenology of Superstring Inspired E(6) Models*, *Phys. Rept.* **183** (1989) 193.

[177] F. Del Aguila, *The Physics of z-prime bosons*, *Acta Phys. Polon.* **B25** (1994) 1317–1336, [hep-ph/9404323].

[178] F. Del Aguila, M. Cvetic and P. Langacker, *Reconstruction of the extended gauge structure from Z-prime observables at future colliders*, *Phys. Rev.* **D52** (1995) 37–43, [hep-ph/9501390].

[179] K. S. Babu, C. F. Kolda and J. March-Russell, *Leptophobic U(1) s and the R(b) - R(c) crisis*, *Phys. Rev.* **D54** (1996) 4635–4647, [hep-ph/9603212].

[180] S. M. Barr and A. Zee, *Calculating the Electron Mass in Terms of Measured Quantities*, *Phys. Rev.* **D17** (1978) 1854.

[181] F. Wilczek and A. Zee, *Horizontal Interaction and Weak Mixing Angles*, *Phys. Rev. Lett.* **42** (1979) 421.

[182] A. Davidson, M. Koca and K. C. Wali, *U(1) as the Minimal Horizontal Gauge Symmetry*, *Phys. Rev. Lett.* **43** (1979) 92.

[183] C. L. Ong, *Adding a Horizontal Gauge Symmetry to the Weinberg-Salam Model: An Eight Quark Model*, *Phys. Rev.* **D19** (1979) 2738.

[184] T. Yanagida, *Horizontal Symmetry and Mass of the Top Quark*, *Phys. Rev.* **D20** (1979) 2986.

[185] R. N. Mohapatra, *Gauge Model for Chiral Symmetry Breaking and Muon electron Mass Ratio*, *Phys. Rev.* **D9** (1974) 3461.

[186] P. Langacker and M. Plumacher, *Flavor changing effects in theories with a heavy Z' boson with family nonuniversal couplings*, *Phys. Rev.* **D62** (2000) 013006, [hep-ph/0001204].

[187] D. Guadagnoli, R. N. Mohapatra and I. Sung, *Gauged Flavor Group with Left-Right Symmetry*, *JHEP* **04** (2011) 093, [1103.4170].

[188] B. Grinstein, M. Redi and G. Villadoro, *Low Scale Flavor Gauge Symmetries*, *JHEP* **11** (2010) 067, [1009.2049].

[189] A. Leike, *The Phenomenology of extra neutral gauge bosons*, *Phys. Rept.* **317** (1999) 143–250, [hep-ph/9805494].

[190] P. Langacker, *The Physics of New U(1)' Gauge Bosons*, *AIP Conf. Proc.* **1200** (2010) 55–63, [0909.3260].

[191] S. F. King, *Flavourful Z' models for $R_{K^{(*)}}$*, *JHEP* **08** (2017) 019, [1706.06100].

[192] A. Falkowski, S. F. King, E. Perdomo and M. Pierre, *Flavourful Z' portal for vector-like neutrino Dark Matter and $R_{K^{(*)}}$*, *JHEP* **08** (2018) 061, [1803.04430].

[193] S. Davidson and S. Descotes-Genon, *Constraining flavoured contact interactions at the LHC*, *JHEP* **05** (2014) 066, [1311.5981].

[194] ATLAS collaboration, G. Aad et al., *Search for a Heavy Neutral Particle Decaying to $e\mu$, $e\tau$, or $\mu\tau$ in pp Collisions at $\sqrt{s} = 8$ TeV with the ATLAS Detector*, *Phys. Rev. Lett.* **115** (2015) 031801, [1503.04430].

[195] A. Alloul, N. D. Christensen, C. Degrande, C. Duhr and B. Fuks, *FeynRules 2.0 - A complete toolbox for tree-level phenomenology*, *Comput. Phys. Commun.* **185** (2014) 2250–2300, [1310.1921].

[196] J. Alwall, R. Frederix, S. Frixione, V. Hirschi, F. Maltoni, O. Mattelaer et al., *The automated computation of tree-level and next-to-leading order differential cross sections, and their matching to parton shower simulations*, *JHEP* **07** (2014) 079, [1405.0301].

[197] T. Sjostrand, S. Mrenna and P. Z. Skands, *A Brief Introduction to PYTHIA 8.1*, *Comput. Phys. Commun.* **178** (2008) 852–867, [0710.3820].

[198] P. Foldenauer and J. Jaeckel, *Exclusion plots for flavor-violating Z' bosons*, http://www.thphys.uni-heidelberg.de/~foldenauer/Zp_limits/ .

[199] ATLAS collaboration, *Search for beyond the Standard Model phenomena in $e\mu$ final states in pp collisions at $\sqrt{s}$ = 13 TeV with the ATLAS detector*, *ATLAS-CONF-2015-072* (2015) .

[200] ATLAS collaboration, M. Aaboud et al., *Search for lepton-flavor violation in different-flavor, high-mass final states in pp collisions at $\sqrt{s} = 13$ TeV with the ATLAS detector*, *Phys. Rev.* **D98** (2018) 092008, [1807.06573].

[201] CMS collaboration, A. M. Sirunyan et al., *Search for lepton-flavor violating decays of heavy resonances and quantum black holes to e? final states in proton-proton collisions at $\sqrt{s} = 13$ TeV*, *JHEP* **04** (2018) 073, [1802.01122].

[202] A. J. Buras and J. Girrbach, *Complete NLO QCD Corrections for Tree Level Delta F = 2 FCNC Processes*, *JHEP* **03** (2012) 052, [1201.1302].

[203] A. J. Buras, M. Misiak and J. Urban, *Two loop QCD anomalous dimensions of flavor changing four quark operators within and beyond the standard model*, *Nucl. Phys.* **B586** (2000) 397–426, [hep-ph/0005183].

[204] R. Babich, N. Garron, C. Hoelbling, J. Howard, L. Lellouch and C. Rebbi, *$K^0 - \bar{K}^0$ mixing beyond the standard model and CP-violating electroweak penguins in quenched QCD with exact chiral symmetry*, *Phys. Rev.* **D74** (2006) 073009, [hep-lat/0605016].

[205] D. Becirevic, V. Gimenez, G. Martinelli, M. Papinutto and J. Reyes, *B parameters of the complete set of matrix elements of delta B = 2 operators from the lattice*, *JHEP* **04** (2002) 025, [hep-lat/0110091].

[206] E. Golowich, J. Hewett, S. Pakvasa and A. A. Petrov, *Implications of D^0 - $\bar{D}^0$ Mixing for New Physics*, *Phys. Rev.* **D76** (2007) 095009, [0705.3650].

[207] UTfit collaboration, http://www.utfit.org.

[208] E. Golowich, J. Hewett, S. Pakvasa and A. A. Petrov, *Relating $\bar{D}^0 - D^0$ Mixing and $D^0 \to \ell^+\ell^-$ with New Physics*, *Phys. Rev.* **D79** (2009) 114030, [0903.2830].

[209] E. Golowich, J. Hewett, S. Pakvasa, A. A. Petrov and G. K. Yeghiyan, *Relating B_s Mixing and $B_s \to \mu^+\mu^-$ with New Physics*, *Phys. Rev.* **D83** (2011) 114017, [1102.0009].

[210] A. J. Buras, *Weak Hamiltonian, CP violation and rare decays*, in *Probing the standard model of particle interactions. Proceedings, Summer School in Theoretical Physics, NATO Advanced Study Institute, 68th session, Les Houches, France, July 28-September 5, 1997. Pt. 1, 2*, pp. 281–539, 1998. hep-ph/9806471.

[211] ETM collaboration, N. Carrasco, P. Dimopoulos, R. Frezzotti, V. Lubicz, G. C. Rossi, S. Simula et al., *ΔS=2 and ΔC=2 bag parameters in the standard model and beyond from N_f=2+1+1 twisted-mass lattice QCD*, *Phys. Rev.* **D92** (2015) 034516, [1505.06639].

[212] E949 collaboration, A. V. Artamonov et al., *New measurement of the $K^+ \to \pi^+ \nu\bar{\nu}$ branching ratio*, *Phys. Rev. Lett.* **101** (2008) 191802, [0808.2459].

[213] A. J. Buras, D. Buttazzo, J. Girrbach-Noe and R. Knegjens, *$K^+ \to \pi^+ \nu\bar{\nu}$ and $K_L \to \pi^0 \nu\bar{\nu}$ in the Standard Model: status and perspectives*, *JHEP* **11** (2015) 033, [1503.02693].

[214] Particle Data Group collaboration, C. Patrignani et al., *Review of Particle Physics*, *Chin. Phys.* **C40** (2016) 100001.

[215] A. J. Buras, J. Girrbach-Noe, C. Niehoff and D. M. Straub, *$B \to K^{(*)} \nu\bar{\nu}$ decays in the Standard Model and beyond*, *JHEP* **02** (2015) 184, [1409.4557].

[216] W. Altmannshofer, C.-Y. Chen, P. S. Bhupal Dev and A. Soni, *Lepton flavor violating Z' explanation of the muon anomalous magnetic moment*, *Phys. Lett.* **B762** (2016) 389–398, [1607.06832].

[217] A. Jodidio et al., *Search for Right-Handed Currents in Muon Decay*, *Phys. Rev.* **D34** (1986) 1967.

[218] R. Foot, X. G. He, H. Lew and R. R. Volkas, *Model for a light Z' boson*, *Phys. Rev.* **D50** (1994) 4571–4580, [hep-ph/9401250].

[219] A. Pich, *Precision Tau Physics*, *Prog. Part. Nucl. Phys.* **75** (2014) 41–85, [1310.7922].

[220] ARGUS collaboration, H. Albrecht et al., *Evidence for the production of the charmed, doubly strange baryon omega(c) in e+ e- annihilation*, *Phys. Lett.* **B288** (1992) 367–372.

[221] CLEO collaboration, A. Anastassov et al., *Experimental test of lepton universality in tau decay*, *Phys. Rev.* **D55** (1997) 2559–2576.

[222] BaBar collaboration, B. Aubert et al., *Measurements of Charged Current Lepton Universality and $|V_{us}|$ using Tau Lepton Decays to $e^- \bar{\nu}_e \nu_\tau$, $\mu^- \bar{\nu}_\mu \nu_\tau$, $\pi^- \nu_\tau$ and $K^- \nu_\tau$*, *Phys. Rev. Lett.* **105** (2010) 051602, [0912.0242].

[223] A. Crivellin, J. Heeck and P. Stoffer, *A perturbed lepton-specific two-Higgs-doublet model facing experimental hints for physics beyond the Standard Model*, *Phys. Rev. Lett.* **116** (2016) 081801, [1507.07567].

[224] E. Coluccio Leskow, G. D'Ambrosio, A. Crivellin and D. Müller, *$(g-2)\mu$, lepton flavor violation, and Z decays with leptoquarks: Correlations and future prospects*, *Phys. Rev.* **D95** (2017) 055018, [1612.06858].

[225] BaBar collaboration, B. Aubert et al., *Search for lepton-flavor and lepton-number violation in the decay $\tau^- \to \ell^\mp h^\pm h'^-$*, *Phys. Rev. Lett.* **95** (2005) 191801, [hep-ex/0506066].

[226] Belle collaboration, Y. Miyazaki et al., *Search for Lepton Flavor and Lepton Number Violating tau Decays into a Lepton and Two Charged Mesons*, *Phys. Lett.* **B682** (2010) 355–362, [0908.3156].

[227] L. Willmann et al., *New bounds from searching for muonium to anti-muonium conversion*, *Phys. Rev. Lett.* **82** (1999) 49–52, [hep-ex/9807011].

[228] T. E. Clark and S. T. Love, *Muonium - anti-muonium oscillations and massive Majorana neutrinos*, *Mod. Phys. Lett.* **A19** (2004) 297–306, [hep-ph/0307264].

[229] U. Nierste, *Three Lectures on Meson Mixing and CKM phenomenology*, in *Heavy quark physics. Proceedings, Helmholtz International School, HQP08, Dubna, Russia, August 11-21, 2008*, pp. 1–38, 2009. 0904.1869.

[230] R. Harnik, J. Kopp and J. Zupan, *Flavor Violating Higgs Decays*, *JHEP* **03** (2013) 026, [1209.1397].

[231] ALEPH collaboration, S. Schael et al., *Fermion pair production in e^+e^- collisions at 189-209-GeV and constraints on physics beyond the standard model*, *Eur. Phys. J.* **C49** (2007) 411–437, [hep-ex/0609051].

[232] M. Davier, A. Hoecker, B. Malaescu and Z. Zhang, *Reevaluation of the Hadronic Contributions to the Muon $g-2$ and to $\alpha(M_Z)$*, *Eur. Phys. J.* **C71** (2011) 1515, [1010.4180].

[233] K. Hagiwara, R. Liao, A. D. Martin, D. Nomura and T. Teubner, *$(g-2)_\mu$ and $\alpha(M_Z^2)$ re-evaluated using new precise data*, *J. Phys.* **G38** (2011) 085003, [1105.3149].

[234] W. Altmannshofer, S. Gori, M. Pospelov and I. Yavin, *Quark flavor transitions in $L_\mu - L_\tau$ models*, *Phys. Rev.* **D89** (2014) 095033, [1403.1269].

[235] W. Altmannshofer, S. Gori, M. Pospelov and I. Yavin, *Neutrino Trident Production: A Powerful Probe of New Physics with Neutrino Beams*, *Phys. Rev. Lett.* **113** (2014) 091801, [1406.2332].

[236] J. Heeck, *Lepton flavor violation with light vector bosons*, *Phys. Lett.* **B758** (2016) 101–105, [1602.03810].

[237] Muon g-2 collaboration, G. W. Bennett et al., *Measurement of the positive muon anomalous magnetic moment to 0.7 ppm*, *Phys. Rev. Lett.* **89** (2002) 101804, [hep-ex/0208001].

[238] P. A. M. Dirac, *The quantum theory of the electron*, *Proc. Roy. Soc. Lond.* **A117** (1928) 610–624.

[239] P. A. M. Dirac, *The Quantum theory of electron. 2.*, *Proc. Roy. Soc. Lond.* **A118** (1928) 351.

[240] T. Aoyama, M. Hayakawa, T. Kinoshita and M. Nio, *Tenth-Order QED Contribution to the Electron g-2 and an Improved Value of the Fine Structure Constant*, *Phys. Rev. Lett.* **109** (2012) 111807, [1205.5368].

[241] T. Aoyama, T. Kinoshita and M. Nio, *Revised and Improved Value of the QED Tenth-Order Electron Anomalous Magnetic Moment*, *Phys. Rev.* **D97** (2018) 036001, [1712.06060].

[242] C. Gnendiger, D. Stöckinger and H. Stöckinger-Kim, *The electroweak contributions to $(g-2)_\mu$ after the Higgs boson mass measurement*, *Phys. Rev.* **D88** (2013) 053005, [1306.5546].

[243] J. Prades, E. de Rafael and A. Vainshtein, *The Hadronic Light-by-Light Scattering Contribution to the Muon and Electron Anomalous Magnetic Moments*, *Adv. Ser. Direct. High Energy Phys.* **20** (2009) 303–317, [0901.0306].

[244] A. Nyffeler, *Precision of a data-driven estimate of hadronic light-by-light scattering in the muon $g-2$: Pseudoscalar-pole contribution*, *Phys. Rev.* **D94** (2016) 053006, [1602.03398].

[245] A. Keshavarzi, D. Nomura and T. Teubner, *Muon $g-2$ and $\alpha(M_Z^2)$: a new data-based analysis*, *Phys. Rev.* **D97** (2018) 114025, [1802.02995].

[246] G. F. Giudice, P. Paradisi and M. Passera, *Testing new physics with the electron g-2*, *JHEP* **11** (2012) 113, [1208.6583].

[247] V. Gerginov, K. Calkins, C. E. Tanner, J. J. McFerran, S. Diddams, A. Bartels et al., *Optical frequency measurements of $6s\ ^2S_{1/2} - 6p\ ^2P_{1/2}$ (D_1) transitions in ^{133}Cs and their impact on the fine-structure constant*, *Phys. Rev.* **A73** (2006) 032504.

[248] P. Clade, E. de Mirandes, M. Cadoret, S. Guellati-Khelifa, C. Schwob, F. Nez et al., *Determination of the Fine Structure Constant Based on Bloch Oscillations of Ultracold Atoms in a Vertical Optical Lattice*, *Phys. Rev. Lett.* **96** (2006) 033001.

[249] M. Cadoret, E. de Mirandes, P. Cladé, F. Nez, L. Julien, F. Biraben et al., *Atom interferometry based on light pulses: Application to the high precision measurement of the ratio h/ m and the determination of the fine structure constant*, *European Physical Journal Special Topics* **172** (Jun, 2009) 121–136, [0809.3177].

[250] R. Bouchendira, P. Clade, S. Guellati-Khelifa, F. Nez and F. Biraben, *New determination of the fine structure constant and test of the quantum electrodynamics*, *Phys. Rev. Lett.* **106** (2011) 080801, [1012.3627].

[251] K. R. Lynch, *A Note on one loop electroweak contributions to g-2: A Companion to BUHEP-01-16*, hep-ph/0108081.

[252] S. Baek, N. G. Deshpande, X. G. He and P. Ko, *Muon anomalous $g-2$ and gauged $L_\mu - L_\tau$ models*, *Phys. Rev.* **D64** (2001) 055006, [hep-ph/0104141].

[253] BaBar collaboration, J. P. Lees et al., *Search for a muonic dark force at BABAR*, *Phys. Rev.* **D94** (2016) 011102, [1606.03501].

[254] DUNE collaboration, R. Acciarri et al., *Long-Baseline Neutrino Facility (LBNF) and Deep Underground Neutrino Experiment (DUNE)*, 1512.06148.

[255] SHiP collaboration, M. Anelli et al., *A facility to Search for Hidden Particles (SHiP) at the CERN SPS*, 1504.04956.

[256] S. Alekhin et al., *A facility to Search for Hidden Particles at the CERN SPS: the SHiP physics case*, *Rept. Prog. Phys.* **79** (2016) 124201, [1504.04855].

[257] G. Magill and R. Plestid, *Neutrino Trident Production at the Intensity Frontier*, *Phys. Rev.* **D95** (2017) 073004, [1612.05642].

[258] J. Heeck, "Private communication."

[259] T. Aushev et al., *Physics at Super B Factory*, 1002.5012.

[260] A. J. Buras, D. Buttazzo and R. Knegjens, *$K \to \pi\nu\overline{\nu}$ and ε'/ε in simplified new physics models*, *JHEP* **11** (2015) 166, [1507.08672].

[261] CLEO collaboration, A. J. Weinstein, *Tau electroweak couplings*, hep-ex/9911002.

[262] M. Bauer, P. Foldenauer and J. Jaeckel, *Hunting All the Hidden Photons*, *JHEP* **07** (2018) 094, [1803.05466].

[263] HEAT collaboration, S. W. Barwick et al., *Measurements of the cosmic ray positron fraction from 1-GeV to 50-GeV*, *Astrophys. J.* **482** (1997) L191–L194, [astro-ph/9703192].

[264] AMS 01 collaboration, M. Aguilar et al., *Cosmic-ray positron fraction measurement from 1 to 30-GeV with AMS-01*, *Phys. Lett.* **B646** (2007) 145–154, [astro-ph/0703154].

[265] N. Arkani-Hamed, D. P. Finkbeiner, T. R. Slatyer and N. Weiner, *A Theory of Dark Matter*, *Phys. Rev.* **D79** (2009) 015014, [0810.0713].

[266] N. Arkani-Hamed and N. Weiner, *LHC Signals for a SuperUnified Theory of Dark Matter*, *JHEP* **12** (2008) 104, [0810.0714].

[267] K. R. Dienes, C. F. Kolda and J. March-Russell, *Kinetic mixing and the supersymmetric gauge hierarchy*, *Nucl. Phys.* **B492** (1997) 104–118, [hep-ph/9610479].

[268] D. Hooper and K. M. Zurek, *A Natural Supersymmetric Model with MeV Dark Matter*, *Phys. Rev.* **D77** (2008) 087302, [0801.3686].

[269] M. Baumgart, C. Cheung, J. T. Ruderman, L.-T. Wang and I. Yavin, *Non-Abelian Dark Sectors and Their Collider Signatures*, *JHEP* **04** (2009) 014, [0901.0283].

[270] C. Cheung, J. T. Ruderman, L.-T. Wang and I. Yavin, *Kinetic Mixing as the Origin of Light Dark Scales*, *Phys. Rev.* **D80** (2009) 035008, [0902.3246].

[271] A. Katz and R. Sundrum, *Breaking the Dark Force*, *JHEP* **06** (2009) 003, [0902.3271].

[272] D. E. Morrissey, D. Poland and K. M. Zurek, *Abelian Hidden Sectors at a GeV*, *JHEP* **07** (2009) 050, [0904.2567].

[273] R. Essig, P. Schuster and N. Toro, *Probing Dark Forces and Light Hidden Sectors at Low-Energy e+e- Colliders*, *Phys. Rev.* **D80** (2009) 015003, [0903.3941].

[274] M. Reece and L.-T. Wang, *Searching for the light dark gauge boson in GeV-scale experiments*, *JHEP* **07** (2009) 051, [0904.1743].

[275] J. D. Bjorken, R. Essig, P. Schuster and N. Toro, *New Fixed-Target Experiments to Search for Dark Gauge Forces*, *Phys. Rev.* **D80** (2009) 075018, [0906.0580].

[276] R. Foot, *New Physics From Electric Charge Quantization?*, *Mod. Phys. Lett.* **A6** (1991) 527–530.

[277] X. G. He, G. C. Joshi, H. Lew and R. R. Volkas, *NEW Z' PHENOMENOLOGY*, *Phys. Rev.* **D43** (1991) 22–24.

[278] X.-G. He, G. C. Joshi, H. Lew and R. R. Volkas, *Simplest Z' model*, *Phys. Rev.* **D44** (1991) 2118–2132.

[279] J. Heeck and W. Rodejohann, *Gauged $L_\mu - L_\tau$ Symmetry at the Electroweak Scale*, *Phys. Rev.* **D84** (2011) 075007, [1107.5238].

[280] J. Kopp, *New signals in dark matter detectors*, *J. Phys. Conf. Ser.* **485** (2014) 012032, [1210.2703].

[281] J. Heeck, *Unbroken $B - L$ symmetry*, *Phys. Lett.* **B739** (2014) 256–262, [1408.6845].

[282] S. Bilmis, I. Turan, T. M. Aliev, M. Deniz, L. Singh and H. T. Wong, *Constraints on Dark Photon from Neutrino-Electron Scattering Experiments*, *Phys. Rev.* **D92** (2015) 033009, [1502.07763].

[283] Y. S. Jeong, C. S. Kim and H.-S. Lee, *Constraints on the $U(1)_L$ gauge boson in a wide mass range*, *Int. J. Mod. Phys.* **A31** (2016) 1650059, [1512.03179].

[284] P. Ilten, Y. Soreq, M. Williams and W. Xue, *Serendipity in dark photon searches*, *JHEP* **06** (2018) 004, [1801.04847].

[285] M. B. Wise and Y. Zhang, *Lepton Flavorful Fifth Force and Depth-dependent Neutrino Matter Interactions*, *JHEP* **06** (2018) 053, [1803.00591].

[286] A. Kamada and H.-B. Yu, *Coherent Propagation of PeV Neutrinos and the Dip in the Neutrino Spectrum at IceCube*, *Phys. Rev.* **D92** (2015) 113004, [1504.00711].

[287] T. Araki, F. Kaneko, T. Ota, J. Sato and T. Shimomura, *MeV scale leptonic force for cosmic neutrino spectrum and muon anomalous magnetic moment*, *Phys. Rev.* **D93** (2016) 013014, [1508.07471].

[288] T. Araki, S. Hoshino, T. Ota, J. Sato and T. Shimomura, *Detecting the $L_\mu - L_\tau$ gauge boson at Belle II*, *Phys. Rev.* **D95** (2017) 055006, [1702.01497].

[289] Y. Kaneta and T. Shimomura, *On the possibility of a search for the $L_\mu - L_\tau$ gauge boson at Belle-II and neutrino beam experiments*, *PTEP* **2017** (2017) 053B04, [1701.00156].

[290] S. N. Gninenko and N. V. Krasnikov, *Probing the muon $g_\mu - 2$ anomaly, $L_\mu - L_\tau$ gauge boson and Dark Matter in dark photon experiments*, *Phys. Lett.* **B783** (2018) 24–28, [1801.10448].

[291] CHARM collaboration, F. Bergsma et al., *A Search for Decays of Heavy Neutrinos in the Mass Range 0.5-GeV to 2.8-GeV*, *Phys. Lett.* **166B** (1986) 473–478.

[292] E. M. Riordan et al., *A Search for Short Lived Axions in an Electron Beam Dump Experiment*, *Phys. Rev. Lett.* **59** (1987) 755.

[293] J. D. Bjorken, S. Ecklund, W. R. Nelson, A. Abashian, C. Church, B. Lu et al., *Search for Neutral Metastable Penetrating Particles Produced in the SLAC Beam Dump*, *Phys. Rev.* **D38** (1988) 3375.

[294] A. Bross, M. Crisler, S. H. Pordes, J. Volk, S. Errede and J. Wrbanek, *A Search for Shortlived Particles Produced in an Electron Beam Dump*, *Phys. Rev. Lett.* **67** (1991) 2942–2945.

[295] M. Davier and H. Nguyen Ngoc, *An Unambiguous Search for a Light Higgs Boson*, *Phys. Lett.* **B229** (1989) 150–155.

[296] SINDRUM I collaboration, R. Meijer Drees et al., *Search for weakly interacting neutral bosons produced in $\pi^- p$ interactions at rest and decaying into e^+e^- pairs.*, *Phys. Rev. Lett.* **68** (1992) 3845–3848.

[297] LSND collaboration, C. Athanassopoulos et al., *Evidence for muon-neutrino —> electron-neutrino oscillations from pion decay in flight neutrinos*, *Phys. Rev.* **C58** (1998) 2489–2511, [nucl-ex/9706006].

[298] LSND collaboration, A. Aguilar-Arevalo et al., *Evidence for neutrino oscillations from the observation of anti-neutrino(electron) appearance in a anti-neutrino(muon) beam*, *Phys. Rev.* **D64** (2001) 112007, [hep-ex/0104049].

[299] R. Essig, R. Harnik, J. Kaplan and N. Toro, *Discovering New Light States at Neutrino Experiments*, *Phys. Rev.* **D82** (2010) 113008, [1008.0636].

[300] R. Essig, P. Schuster, N. Toro and B. Wojtsekhowski, *An Electron Fixed Target Experiment to Search for a New Vector Boson A' Decaying to e+e-*, *JHEP* **02** (2011) 009, [1001.2557].

[301] A1 collaboration, H. Merkel et al., *Search for Light Gauge Bosons of the Dark Sector at the Mainz Microtron*, *Phys. Rev. Lett.* **106** (2011) 251802, [1101.4091].

[302] J. Blumlein and J. Brunner, *New Exclusion Limits for Dark Gauge Forces from Beam-Dump Data*, *Phys. Lett.* **B701** (2011) 155–159, [1104.2747].

[303] APEX collaboration, S. Abrahamyan et al., *Search for a New Gauge Boson in Electron-Nucleus Fixed-Target Scattering by the APEX Experiment*, *Phys. Rev. Lett.* **107** (2011) 191804, [1108.2750].

[304] S. Andreas, C. Niebuhr and A. Ringwald, *New Limits on Hidden Photons from Past Electron Beam Dumps*, *Phys. Rev.* **D86** (2012) 095019, [1209.6083].

[305] S. N. Gninenko, *Constraints on sub-GeV hidden sector gauge bosons from a search for heavy neutrino decays*, *Phys. Lett.* **B713** (2012) 244–248, [1204.3583].

[306] B. Wojtsekhowski, D. Nikolenko and I. Rachek, *Searching for a new force at VEPP-3*, 1207.5089.

[307] Y. Kahn and J. Thaler, *Searching for an invisible A' vector boson with DarkLight*, *Phys. Rev.* **D86** (2012) 115012, [1209.0777].

[308] J. Blümlein and J. Brunner, *New Exclusion Limits on Dark Gauge Forces from Proton Bremsstrahlung in Beam-Dump Data*, *Phys. Lett.* **B731** (2014) 320–326, [1311.3870].

[309] H. Merkel et al., *Search at the Mainz Microtron for Light Massive Gauge Bosons Relevant for the Muon g-2 Anomaly*, *Phys. Rev. Lett.* **112** (2014) 221802, [1404.5502].

[310] M. Battaglieri et al., *The Heavy Photon Search Test Detector*, *Nucl. Instrum. Meth.* **A777** (2015) 91–101, [1406.6115].

[311] J. Balewski et al., *The DarkLight Experiment: A Precision Search for New Physics at Low Energies*, 2014. 1412.4717.

[312] NA48/2 collaboration, J. R. Batley et al., *Search for the dark photon in π^0 decays*, *Phys. Lett.* **B746** (2015) 178–185, [1504.00607].

[313] S. Gardner, R. J. Holt and A. S. Tadepalli, *New Prospects in Fixed Target Searches for Dark Forces with the SeaQuest Experiment at Fermilab*, *Phys. Rev.* **D93** (2016) 115015, [1509.00050].

[314] A. Berlin, S. Gori, P. Schuster and N. Toro, *Dark Sectors at the Fermilab SeaQuest Experiment*, *Phys. Rev.* **D98** (2018) 035011, [1804.00661].

[315] NA64 collaboration, D. Banerjee et al., *Search for invisible decays of sub-GeV dark photons in missing-energy events at the CERN SPS*, *Phys. Rev. Lett.* **118** (2017) 011802, [1610.02988].

[316] BaBar collaboration, B. Aubert et al., *Search for Dimuon Decays of a Light Scalar Boson in Radiative Transitions Upsilon —> gamma A0*, *Phys. Rev. Lett.* **103** (2009) 081803, [0905.4539].

[317] Belle-II collaboration, T. Abe et al., *Belle II Technical Design Report*, 1011.0352.

[318] KLOE-2 collaboration, F. Archilli et al., *Search for a vector gauge boson in ϕ meson decays with the KLOE detector*, *Phys. Lett.* **B706** (2012) 251–255, [1110.0411].

[319] KLOE-2 collaboration, D. Babusci et al., *Limit on the production of a light vector gauge boson in phi meson decays with the KLOE detector*, *Phys. Lett.* **B720** (2013) 111–115, [1210.3927].

[320] KLOE-2 collaboration, D. Babusci et al., *Search for light vector boson production in $e^+e^- \to \mu^+\mu^-\gamma$ interactions with the KLOE experiment*, *Phys. Lett.* **B736** (2014) 459–464, [1404.7772].

[321] D. Curtin, R. Essig, S. Gori and J. Shelton, *Illuminating Dark Photons with High-Energy Colliders*, *JHEP* **02** (2015) 157, [1412.0018].

[322] S. N. Gninenko, N. V. Krasnikov and V. A. Matveev, *Muon g-2 and searches for a new leptophobic sub-GeV dark boson in a missing-energy experiment at CERN*, *Phys. Rev.* **D91** (2015) 095015, [1412.1400].

[323] BaBar collaboration, J. P. Lees et al., *Search for a Dark Photon in e^+e^- Collisions at BaBar*, *Phys. Rev. Lett.* **113** (2014) 201801, [1406.2980].

[324] P. Ilten, J. Thaler, M. Williams and W. Xue, *Dark photons from charm mesons at LHCb*, *Phys. Rev.* **D92** (2015) 115017, [1509.06765].

[325] P. Ilten, Y. Soreq, J. Thaler, M. Williams and W. Xue, *Proposed Inclusive Dark Photon Search at LHCb*, *Phys. Rev. Lett.* **116** (2016) 251803, [1603.08926].

[326] G. Inguglia, *Belle II studies of missing energy decays and searches for dark photon production*, *PoS* **DIS2016** (2016) 263, [1607.02089].

[327] KLOE-2 collaboration, A. Anastasi et al., *Limit on the production of a new vector boson in $e^+e^- \to U\gamma$, $U \to \pi^+\pi^-$ with the KLOE experiment*, *Phys. Lett.* **B757** (2016) 356–361, [1603.06086].

[328] LHCb collaboration, R. Aaij et al., *Search for Dark Photons Produced in 13 TeV pp Collisions*, *Phys. Rev. Lett.* **120** (2018) 061801, [1710.02867].

[329] BaBar collaboration, J. P. Lees et al., *Search for Invisible Decays of a Dark Photon Produced in e^+e^- Collisions at BaBar*, *Phys. Rev. Lett.* **119** (2017) 131804, [1702.03327].

[330] SINDRUM collaboration, W. H. Bertl et al., *Search for the Decay $\mu^+ \to e^+e^+e^-$*, *Nucl. Phys.* **B260** (1985) 1–31.

[331] CLEO collaboration, M. S. Alam et al., *Tau decays into three charged leptons and two neutrinos*, *Phys. Rev. Lett.* **76** (1996) 2637–2641.

[332] H. Davoudiasl, H.-S. Lee and W. J. Marciano, *Dark Side of Higgs Diphoton Decays and Muon g-2*, *Phys. Rev.* **D86** (2012) 095009, [1208.2973].

[333] M. Endo, K. Hamaguchi and G. Mishima, *Constraints on Hidden Photon Models from Electron g-2 and Hydrogen Spectroscopy*, *Phys. Rev.* **D86** (2012) 095029, [1209.2558].

[334] A. Blondel et al., *Research Proposal for an Experiment to Search for the Decay $\mu \to eee$*, 1301.6113.

[335] B. Echenard, R. Essig and Y.-M. Zhong, *Projections for Dark Photon Searches at Mu3e*, *JHEP* **01** (2015) 113, [1411.1770].

[336] G. Bellini et al., *Precision measurement of the 7Be solar neutrino interaction rate in Borexino*, *Phys. Rev. Lett.* **107** (2011) 141302, [1104.1816].

[337] R. Harnik, J. Kopp and P. A. N. Machado, *Exploring nu Signals in Dark Matter Detectors*, *JCAP* **1207** (2012) 026, [1202.6073].

[338] CHARM-II collaboration, P. Vilain et al., *Precision measurement of electroweak parameters from the scattering of muon-neutrinos on electrons*, *Phys. Lett.* **B335** (1994) 246–252.

[339] CHARM-II collaboration, P. Vilain et al., *Measurement of differential cross-sections for muon-neutrino electron scattering*, *Phys. Lett.* **B302** (1993) 351–355.

[340] COHERENT collaboration, D. Akimov et al., *The COHERENT Experiment at the Spallation Neutron Source*, 1509.08702.

[341] COHERENT collaboration, D. Akimov et al., *Observation of Coherent Elastic Neutrino-Nucleus Scattering*, *Science* **357** (2017) 1123–1126, [1708.01294].

[342] TEXONO collaboration, M. Deniz et al., *Measurement of $\bar{\nu}_e$ - Electron Scattering Cross-Section with a CsI(Tl) Scintillating Crystal Array at the Kuo-Sheng Nuclear Power Reactor*, *Phys. Rev.* **D81** (2010) 072001, [0911.1597].

[343] CHARM-II collaboration, D. Geiregat et al., *First observation of neutrino trident production*, *Phys. Lett.* **B245** (1990) 271–275.

[344] CCFR collaboration, S. R. Mishra et al., *Neutrino tridents and W Z interference*, *Phys. Rev. Lett.* **66** (1991) 3117–3120.

[345] NuTeV collaboration, T. Adams et al., *Neutrino trident production from NuTeV*, in *High-energy physics. Proceedings, 29th International Conference, ICHEP'98, Vancouver, Canada, July 23-29, 1998. Vol. 1, 2*, pp. 631–634, 1998. hep-ex/9811012.

[346] H. K. Dreiner, J.-F. Fortin, J. Isern and L. Ubaldi, *White Dwarfs constrain Dark Forces*, *Phys. Rev.* **D88** (2013) 043517, [1303.7232].

[347] E. Ma, D. P. Roy and S. Roy, *Gauged $L_\mu - L_\tau$ with large muon anomalous magnetic moment and the bimaximal mixing of neutrinos*, *Phys. Lett.* **B525** (2002) 101–106, [hep-ph/0110146].

[348] K. Harigaya, T. Igari, M. M. Nojiri, M. Takeuchi and K. Tobe, *Muon g-2 and LHC phenomenology in the $L_\mu - L_\tau$ gauge symmetric model*, *JHEP* **03** (2014) 105, [1311.0870].

[349] T. Araki, F. Kaneko, Y. Konishi, T. Ota, J. Sato and T. Shimomura, *Cosmic neutrino spectrum and the muon anomalous magnetic moment in the gauged $L_\mu - L_\tau$ model*, *Phys. Rev.* **D91** (2015) 037301, [1409.4180].

[350] A. DiFranzo and D. Hooper, *Searching for MeV-Scale Gauge Bosons with IceCube*, *Phys. Rev.* **D92** (2015) 095007, [1507.03015].

[351] A. Crivellin, G. D'Ambrosio and J. Heeck, *Addressing the LHC flavor anomalies with horizontal gauge symmetries*, *Phys. Rev.* **D91** (2015) 075006, [1503.03477].

[352] W. Altmannshofer, S. Gori, S. Profumo and F. S. Queiroz, *Explaining dark matter and B decay anomalies with an $L_\mu - L_\tau$ model*, *JHEP* **12** (2016) 106, [1609.04026].

[353] M. Escudero, D. Hooper, G. Krnjaic and M. Pierre, *Cosmology with a very light L_μ ? L_τ gauge boson*, *JHEP* **03** (2019) 071, [1901.02010].

[354] F. Brummer, J. Jaeckel and V. V. Khoze, *Magnetic Mixing: Electric Minicharges from Magnetic Monopoles*, *JHEP* **06** (2009) 037, [0905.0633].

[355] J. Fleischer, *THE ON-SHELL RENORMALIZATION SCHEME IN THE GWS MODEL*, *Acta Phys. Polon.* **B17** (1986) 897.

[356] T. Araki, J. Heeck and J. Kubo, *Vanishing Minors in the Neutrino Mass Matrix from Abelian Gauge Symmetries*, *JHEP* **07** (2012) 083, [1203.4951].

[357] V. V. Ezhela, S. B. Lugovsky and O. V. Zenin, *Hadronic part of the muon g-2 estimated on the sigma**2003(tot)(e+ e- —> hadrons) evaluated data compilation*, hep-ph/0312114.

[358] Particle Data Group collaboration, C. Patrignani et al., *Review of Particle Physics*, *Chin. Phys.* **C40** (2016) 100001.

[359] P. Foldenauer, *Hidden photons, Student lecture delivered at the research training group 'Particle Physics Beyond the Standard Model':* https://www.thphys.uni-heidelberg.de/∼gk_ppbsm/doku.php?id=students:lectures:ws18_19 (2019) .

[360] S. Andreas, *Light Weakly Interacting Particles: Constraints and Connection to Dark Matter*. PhD thesis, Hamburg U., 2013. DESY-THESIS-2013-024.

[361] M. Karliner, M. Low, J. L. Rosner and L.-T. Wang, *Radiative return capabilities of a high-energy, high-luminosity e^+e^- collider*, *Phys. Rev.* **D92** (2015) 035010, [1503.07209].

[362] Belle collaboration, J. Brodzicka et al., *Physics Achievements from the Belle Experiment*, *PTEP* **2012** (2012) 04D001, [1212.5342].

[363] BaBar collaboration, J. P. Lees et al., *Time-Integrated Luminosity Recorded by the BABAR Detector at the PEP-II e^+e^- Collider*, *Nucl. Instrum. Meth.* **A726** (2013) 203–213, [1301.2703].

[364] K. J. Kim and Y.-S. Tsai, *IMPROVED WEIZSACKER-WILLIAMS METHOD AND ITS APPLICATION TO LEPTON AND W BOSON PAIR PRODUCTION*, *Phys. Rev.* **D8** (1973) 3109.

[365] Y.-S. Tsai, *Pair Production and Bremsstrahlung of Charged Leptons*, *Rev. Mod. Phys.* **46** (1974) 815.

[366] H. Bethe and W. Heitler, *On the Stopping of fast particles and on the creation of positive electrons*, *Proc. Roy. Soc. Lond.* **A146** (1934) 83–112.

[367] Y.-S. Tsai and V. Whitis, *THICK TARGET BREMSSTRAHLUNG AND TARGET CONSIDERATION FOR SECONDARY PARTICLE PRODUCTION BY ELECTRONS*, *Phys. Rev.* **149** (1966) 1248–1257.

[368] L. W. Mo and Y.-S. Tsai, *Radiative Corrections to Elastic and Inelastic e p and mu p Scattering*, *Rev. Mod. Phys.* **41** (1969) 205–235.

[369] J. L. Feng, I. Galon, F. Kling and S. Trojanowski, *ForwArd Search ExpeRiment at the LHC*, *Phys. Rev.* **D97** (2018) 035001, [1708.09389].

[370] J. P. Chou, D. Curtin and H. J. Lubatti, *New Detectors to Explore the Lifetime Frontier*, *Phys. Lett.* **B767** (2017) 29–36, [1606.06298].

[371] J. A. Evans, *Detecting Hidden Particles with MATHUSLA*, *Phys. Rev.* **D97** (2018) 055046, [1708.08503].

[372] V. V. Gligorov, S. Knapen, M. Papucci and D. J. Robinson, *Searching for Long-lived Particles: A Compact Detector for Exotics at LHCb*, *Phys. Rev.* **D97** (2018) 015023, [1708.09395].

[373] J. R. Cudell, V. Ezhela, P. Gauron, K. Kang, Yu. V. Kuyanov, S. Lugovsky et al., *Hadronic scattering amplitudes: Medium-energy constraints on asymptotic behavior*, *Phys. Rev.* **D65** (2002) 074024, [hep-ph/0107219].

[374] Particle Data Group collaboration, K. Nakamura et al., *Review of particle physics*, *J. Phys.* **G37** (2010) 075021.

[375] French-Soviet collaboration, V. V. Ammosov et al., *pi+- Meson and Proton Production in Inclusive and Semiinclusive Processes in p p Interactions at 69-GeV/c. 2.*, *Nuovo Cim.* **A40** (1977) 237.

[376] M. Aguilar-Benitez et al., *Inclusive particle production in 400-GeV/c p p interactions*, *Z. Phys.* **C50** (1991) 405–426.

[377] A. Anastasi et al., *Limit on the production of a low-mass vector boson in* $e^+e^- \to U\gamma$, $U \to e^+e^-$ *with the KLOE experiment*, *Phys. Lett.* **B750** (2015) 633–637, [1509.00740].

[378] P.-f. Yin, J. Liu and S.-h. Zhu, *Detecting light leptophilic gauge boson at BESIII detector*, *Phys. Lett.* **B679** (2009) 362–368, [0904.4644].

[379] H.-B. Li and T. Luo, *Probing Dark force at BES-III/BEPCII*, *Phys. Lett.* **B686** (2010) 249–253, [0911.2067].

[380] BESIII collaboration, M. Ablikim et al., *Dark Photon Search in the Mass Range Between 1.5 and 3.4 GeV/*c^2, *Phys. Lett.* **B774** (2017) 252–257, [1705.04265].

[381] T. Ferber, *B2tip, to be submitted to ptep*, 2018.

[382] M. A. Arroyo-Ureña, E. Díaz, O. Meza-Aldama and G. Tavares-Velasco, $\tau^- \to \ell_i^- \ell_i^+ \ell_j^- \bar{\nu}_j \nu_\tau$ *decays with a magnetic dipole term*, *Int. J. Mod. Phys.* **A32** (2017) 1750195, [1711.01393].

[383] B. Van de Vyver and P. Zucchelli, *Prompt tau-neutrino background in wide band muon-neutrino beams*, *Nucl. Instrum. Meth.* **A385** (1997) 91–99.

[384] CCFR/NuTeV collaboration, A. Romosan et al., *A High statistics search for muon-neutrino (anti-muon-neutrino) –> electron-neutrino (anti-electron-neutrino) oscillations in the small mixing angle regime*, *Phys. Rev. Lett.* **78** (1997) 2912–2915, [hep-ex/9611013].

[385] S.-F. Ge, M. Lindner and W. Rodejohann, *Atmospheric Trident Production for Probing New Physics*, *Phys. Lett.* **B772** (2017) 164–168, [1702.02617].

[386] H. Nunokawa, S. J. Parke and R. Zukanovich Funchal, *What fraction of boron-8 solar neutrinos arrive at the earth as a nu(2) mass eigenstate?*, *Phys. Rev.* **D74** (2006) 013006, [hep-ph/0601198].

[387] M. Lindner, F. S. Queiroz, W. Rodejohann and X.-J. Xu, *Neutrino-electron scattering: general constraints on* Z' *and dark photon models*, *JHEP* **05** (2018) 098, [1803.00060].

[388] M. Abdullah, J. B. Dent, B. Dutta, G. L. Kane, S. Liao and L. E. Strigari, *Coherent elastic neutrino nucleus scattering as a probe of a Z' through kinetic and mass mixing effects*, *Phys. Rev.* **D98** (2018) 015005, [1803.01224].

[389] Super-Kamiokande collaboration, G. Mitsuka et al., *Study of Non-Standard Neutrino Interactions with Atmospheric Neutrino Data in Super-Kamiokande I and II*, *Phys. Rev.* **D84** (2011) 113008, [1109.1889].

[390] T. Ohlsson, *Status of non-standard neutrino interactions*, *Rept. Prog. Phys.* **76** (2013) 044201, [1209.2710].

[391] M. C. Gonzalez-Garcia and M. Maltoni, *Determination of matter potential from global analysis of neutrino oscillation data*, *JHEP* **09** (2013) 152, [1307.3092].

[392] DUNE collaboration, B. Abi et al., *The DUNE Far Detector Interim Design Report Volume 1: Physics, Technology and Strategies*, 1807.10334.

[393] A. Fradette, M. Pospelov, J. Pradler and A. Ritz, *Cosmological Constraints on Very Dark Photons*, *Phys. Rev.* **D90** (2014) 035022, [1407.0993].

[394] H. C. Harris et al., *The white dwarf luminosity function from sdss imaging data*, *Astron. J.* **131** (2006) 571–581, [astro-ph/0510820].

[395] Krzesinski, J., Kleinman, S. J., Nitta, A., Hügelmeyer, S., Dreizler, S., Liebert, J. et al., *A hot white dwarf luminosity function from the sloan digital sky survey*, *A&A* **508** (2009) 339–344.

[396] S. DeGennaro, T. von Hippel, D. E. Winget, S. O. Kepler, A. Nitta, D. Koester et al., *White Dwarf Luminosity and Mass Functions from Sloan Digital Sky Survey Spectra*, *Astron. J.* **135** (2008) 1–9, [0709.2190].

[397] G. G. Raffelt, *Stars as laboratories for fundamental physics*. Chicago University Press, 1996.

[398] G. Mangano and P. D. Serpico, *A robust upper limit on $N_{\rm eff}$ from BBN, circa 2011*, *Phys. Lett.* **B701** (2011) 296–299, [1103.1261].

[399] G. Steigman, *Neutrinos And Big Bang Nucleosynthesis*, *Adv. High Energy Phys.* **2012** (2012) 268321, [1208.0032].

[400] R. H. Cyburt, B. D. Fields, K. A. Olive and T.-H. Yeh, *Big Bang Nucleosynthesis: 2015*, *Rev. Mod. Phys.* **88** (2016) 015004, [1505.01076].

[401] S. Roy, *Light Weakly Interacting Particles: Constraints and Connection to Dark Matter*. PhD thesis, Durham U., 2012. http://etheses.dur.ac.uk/6386/.

[402] E. Rrapaj and S. Reddy, *Nucleon-nucleon bremsstrahlung of dark gauge bosons and revised supernova constraints*, *Phys. Rev.* **C94** (2016) 045805, [1511.09136].

[403] E. Hardy and R. Lasenby, *Stellar cooling bounds on new light particles: plasma mixing effects*, *JHEP* **02** (2017) 033, [1611.05852].

[404] J. H. Chang, R. Essig and S. D. McDermott, *Revisiting Supernova 1987A Constraints on Dark Photons*, *JHEP* **01** (2017) 107, [1611.03864].

[405] C. Mahoney, A. K. Leibovich and A. R. Zentner, *Updated Constraints on Self-Interacting Dark Matter from Supernova 1987A*, *Phys. Rev.* **D96** (2017) 043018, [1706.08871].

[406] S. Knapen, T. Lin and K. M. Zurek, *Light Dark Matter: Models and Constraints*, *Phys. Rev.* **D96** (2017) 115021, [1709.07882].

[407] V. Popov, *On the experimental search for photon mixing*, *Turkish Journal of Physics* **23** (1999) 943 – 950.

[408] J. Redondo, *Helioscope Bounds on Hidden Sector Photons*, *JCAP* **0807** (2008) 008, [0801.1527].

[409] H. An, M. Pospelov and J. Pradler, *New stellar constraints on dark photons*, *Phys. Lett.* **B725** (2013) 190–195, [1302.3884].

[410] J. Redondo and G. Raffelt, *Solar constraints on hidden photons re-visited*, *JCAP* **1308** (2013) 034, [1305.2920].

[411] CMS collaboration, A. M. Sirunyan et al., *Search for an $L_\mu - L_\tau$ gauge boson using $Z\to 4\mu$ events in proton-proton collisions at $\sqrt{s} = 13$ TeV*, *Submitted to: Phys. Lett.* (2018) , [1808.03684].

[412] P. Foldenauer, *Light dark matter in a gauged $U(1)_{L_\mu - L_\tau}$ model*, *Phys. Rev.* **D99** (2019) 035007, [1808.03647].

[413] F. Zwicky, *Die Rotverschiebung von extragalaktischen Nebeln*, *Helv. Phys. Acta* **6** (1933) 110–127.

[414] V. C. Rubin and W. K. Ford, Jr., *Rotation of the Andromeda Nebula from a Spectroscopic Survey of Emission Regions*, *Astrophys. J.* **159** (1970) 379–403.

[415] M. S. Roberts and R. N. Whitehurst, *The rotation curve and geometry of M31 at large galactocentric distances.*, *Astrophys. J.* **201** (Oct., 1975) 327–346.

[416] V. C. Rubin, N. Thonnard and W. K. Ford, Jr., *Rotational properties of 21 SC galaxies with a large range of luminosities and radii, from NGC 4605 (R = 4k pc) to UGC 2885 (R = 122 kpc)*, *Astrophys. J.* **238** (1980) 471.

[417] A. Bosma, *21-cm line studies of spiral galaxies. 2. The distribution and kinematics of neutral hydrogen in spiral galaxies of various morphological types.*, *Astron. J.* **86** (1981) 1825.

[418] M. Persic, P. Salucci and F. Stel, *The Universal rotation curve of spiral galaxies: 1. The Dark matter connection*, *Mon. Not. Roy. Astron. Soc.* **281** (1996) 27, [astro-ph/9506004].

[419] R. Massey et al., *Dark matter maps reveal cosmic scaffolding*, *Nature* **445** (2007) 286, [astro-ph/0701594].

[420] D. Huterer, *Weak lensing, dark matter and dark energy*, *Gen. Rel. Grav.* **42** (2010) 2177–2195, [1001.1758].

[421] R. Massey, T. Kitching and J. Richard, *The dark matter of gravitational lensing*, *Rept. Prog. Phys.* **73** (2010) 086901, [1001.1739].

[422] C. L. Bennett, A. Banday, K. M. Gorski, G. Hinshaw, P. Jackson, P. Keegstra et al., *Four year COBE DMR cosmic microwave background observations: Maps and basic results*, *Astrophys. J.* **464** (1996) L1–L4, [astro-ph/9601067].

[423] WMAP collaboration, E. Komatsu et al., *Five-Year Wilkinson Microwave Anisotropy Probe (WMAP) Observations: Cosmological Interpretation*, *Astrophys. J. Suppl.* **180** (2009) 330–376, [0803.0547].

[424] W. J. Percival, S. Cole, D. J. Eisenstein, R. C. Nichol, J. A. Peacock, A. C. Pope et al., *Measuring the Baryon Acoustic Oscillation scale using the SDSS and 2dFGRS*, *Mon. Not. Roy. Astron. Soc.* **381** (2007) 1053–1066, [0705.3323].

[425] G. Arcadi, M. Dutra, P. Ghosh, M. Lindner, Y. Mambrini, M. Pierre et al., *The waning of the WIMP? A review of models, searches, and constraints*, *Eur. Phys. J.* **C78** (2018) 203, [1703.07364].

[426] LUX collaboration, D. S. Akerib et al., *Results from a search for dark matter in the complete LUX exposure*, *Phys. Rev. Lett.* **118** (2017) 021303, [1608.07648].

[427] C. Boehm and P. Fayet, *Scalar dark matter candidates*, *Nucl. Phys.* **B683** (2004) 219–263, [hep-ph/0305261].

[428] P. Fayet, *Light spin 1/2 or spin 0 dark matter particles*, *Phys. Rev.* **D70** (2004) 023514, [hep-ph/0403226].

[429] E. Izaguirre, G. Krnjaic, P. Schuster and N. Toro, *Testing GeV-Scale Dark Matter with Fixed-Target Missing Momentum Experiments*, *Phys. Rev.* **D91** (2015) 094026, [1411.1404].

[430] E. Izaguirre, G. Krnjaic, P. Schuster and N. Toro, *Analyzing the Discovery Potential for Light Dark Matter*, *Phys. Rev. Lett.* **115** (2015) 251301, [1505.00011].

[431] R. Essig, T. Volansky and T.-T. Yu, *New Constraints and Prospects for sub-GeV Dark Matter Scattering off Electrons in Xenon*, *Phys. Rev.* **D96** (2017) 043017, [1703.00910].

[432] W. L. Xu, C. Dvorkin and A. Chael, *Probing sub-GeV Dark Matter-Baryon Scattering with Cosmological Observables*, *Phys. Rev.* **D97** (2018) 103530, [1802.06788].

[433] R. Essig, J. Kaplan, P. Schuster and N. Toro, *On the Origin of Light Dark Matter Species*, *Submitted to: Physical Review D* (2010) , [1004.0691].

[434] L. Darmé, S. Rao and L. Roszkowski, *Light dark Higgs boson in minimal sub-GeV dark matter scenarios*, *JHEP* **03** (2018) 084, [1710.08430].

[435] M. Dutra, M. Lindner, S. Profumo, F. S. Queiroz, W. Rodejohann and C. Siqueira, *MeV Dark Matter Complementarity and the Dark Photon Portal*, *JCAP* **1803** (2018) 037, [1801.05447].

[436] L. Darmé, S. Rao and L. Roszkowski, *Signatures of dark Higgs boson in light fermionic dark matter scenarios*, *JHEP* **12** (2018) 014, [1807.10314].

[437] S. Baek and P. Ko, *Phenomenology of $U(1)_{L_\mu - L_\tau}$ charged dark matter at PAMELA and colliders*, *JCAP* **0910** (2009) 011, [0811.1646].

[438] S. Baek, *Dark matter and muon $(g-2)$ in local $U(1)_{L_\mu - L_\tau}$-extended Ma Model*, *Phys. Lett.* **B756** (2016) 1–5, [1510.02168].

[439] G. Arcadi, T. Hugle and F. S. Queiroz, *The Dark $L_\mu - L_\tau$ Rises via Kinetic Mixing*, *Phys. Lett.* **B784** (2018) 151–158, [1803.05723].

[440] M. Bauer, S. Diefenbacher, T. Plehn, M. Russell and D. A. Camargo, *Dark Matter in Anomaly-Free Gauge Extensions*, *SciPost Phys.* **5** (2018) 036, [1805.01904].

[441] S. Patra, S. Rao, N. Sahoo and N. Sahu, *Gauged $U(1)_{L_\mu - L_\tau}$ model in light of muon $g-2$ anomaly, neutrino mass and dark matter phenomenology*, *Nucl. Phys.* **B917** (2017) 317–336, [1607.04046].

[442] A. Biswas, S. Choubey and S. Khan, *Neutrino Mass, Dark Matter and Anomalous Magnetic Moment of Muon in a $U(1)_{L_\mu - L_\tau}$ Model*, *JHEP* **09** (2016) 147, [1608.04194].

[443] P. Fayet, *U-boson production in e+ e- annihilations, psi and Upsilon decays, and Light Dark Matter*, *Phys. Rev.* **D75** (2007) 115017, [hep-ph/0702176].

[444] Y. Kahn, G. Krnjaic, N. Tran and A. Whitbeck, *M^3: a new muon missing momentum experiment to probe $(g-2)_\mu$ and dark matter at Fermilab*, *JHEP* **09** (2018) 153, [1804.03144].

[445] Y. Cui and F. D'Eramo, *Surprises from complete vector portal theories: New insights into the dark sector and its interplay with Higgs physics*, *Phys. Rev.* **D96** (2017) 095006, [1705.03897].

[446] J. D. Wells, *Annihilation cross-sections for relic densities in the low velocity limit*, hep-ph/9404219.

[447] K. Griest and D. Seckel, *Three exceptions in the calculation of relic abundances*, *Phys. Rev.* **D43** (1991) 3191–3203.

[448] P. Gondolo and G. Gelmini, *Cosmic abundances of stable particles: Improved analysis*, *Nucl. Phys.* **B360** (1991) 145–179.

[449] T. Bringmann, *Particle Models and the Small-Scale Structure of Dark Matter*, *New J. Phys.* **11** (2009) 105027, [0903.0189].

[450] T. Bringmann and S. Hofmann, *Thermal decoupling of WIMPs from first principles*, *JCAP* **0704** (2007) 016, [hep-ph/0612238].

[451] M. Hindmarsh and O. Philipsen, *WIMP dark matter and the QCD equation of state*, *Phys. Rev.* **D71** (2005) 087302, [hep-ph/0501232].

[452] K. Huang, *Statistical mechanics*. Wiley, 1987.

[453] G. Steigman, B. Dasgupta and J. F. Beacom, *Precise Relic WIMP Abundance and its Impact on Searches for Dark Matter Annihilation*, *Phys. Rev.* **D86** (2012) 023506, [1204.3622].

[454] F. Ambrogi, C. Arina, M. Backovic, J. Heisig, F. Maltoni, L. Mantani et al., *MadDM v.3.0: a Comprehensive Tool for Dark Matter Studies*, *Phys. Dark Univ.* **24** (2019) 100249, [1804.00044].

[455] V. Mukhanov, *Physical Foundations of Cosmology*. Cambridge University Press, Oxford, 2005.

[456] C. Boehm, M. J. Dolan and C. McCabe, *Increasing Neff with particles in thermal equilibrium with neutrinos*, *JCAP* **1212** (2012) 027, [1207.0497].

[457] C. Boehm, M. J. Dolan and C. McCabe, *A Lower Bound on the Mass of Cold Thermal Dark Matter from Planck*, *JCAP* **1308** (2013) 041, [1303.6270].

[458] Planck collaboration, P. A. R. Ade et al., *Planck 2013 results. XVI. Cosmological parameters*, *Astron. Astrophys.* **571** (2014) A16, [1303.5076].

[459] K. M. Nollett and G. Steigman, *BBN And The CMB Constrain Neutrino Coupled Light WIMPs*, *Phys. Rev.* **D91** (2015) 083505, [1411.6005].

[460] N. Padmanabhan and D. P. Finkbeiner, *Detecting dark matter annihilation with CMB polarization: Signatures and experimental prospects*, *Phys. Rev.* **D72** (2005) 023508, [astro-ph/0503486].

[461] WMAP collaboration, C. L. Bennett et al., *The Microwave Anisotropy Probe (MAP) mission*, *Astrophys. J.* **583** (2003) 1–23, [astro-ph/0301158].

[462] Planck collaboration, P. A. R. Ade et al., *Planck Early Results. I. The Planck mission*, *Astron. Astrophys.* **536** (2011) A1, [1101.2022].

[463] T. R. Slatyer, *Energy Injection And Absorption In The Cosmic Dark Ages*, *Phys. Rev.* **D87** (2013) 123513, [1211.0283].

[464] T. R. Slatyer, N. Padmanabhan and D. P. Finkbeiner, *CMB Constraints on WIMP Annihilation: Energy Absorption During the Recombination Epoch*, *Phys. Rev.* **D80** (2009) 043526, [0906.1197].

[465] T. R. Slatyer, *Indirect dark matter signatures in the cosmic dark ages. I. Generalizing the bound on s-wave dark matter annihilation from Planck results*, *Phys. Rev.* **D93** (2016) 023527, [1506.03811].

[466] Planck collaboration, P. A. R. Ade et al., *Planck 2015 results. XIII. Cosmological parameters*, *Astron. Astrophys.* **594** (2016) A13, [1502.01589].

[467] R. K. Leane, T. R. Slatyer, J. F. Beacom and K. C. Y. Ng, *GeV-scale thermal WIMPs: Not even slightly ruled out*, *Phys. Rev.* **D98** (2018) 023016, [1805.10305].

[468] M. Mateo, *Dwarf galaxies of the Local Group*, *Ann. Rev. Astron. Astrophys.* **36** (1998) 435–506, [astro-ph/9810070].

[469] J. F. Navarro, C. S. Frenk and S. D. M. White, *A Universal density profile from hierarchical clustering*, *Astrophys. J.* **490** (1997) 493–508, [astro-ph/9611107].

[470] Fermi-LAT collaboration, M. Ackermann et al., *Searching for Dark Matter Annihilation from Milky Way Dwarf Spheroidal Galaxies with Six Years of Fermi Large Area Telescope Data*, *Phys. Rev. Lett.* **115** (2015) 231301, [1503.02641].

[471] Fermi-LAT collaboration, M. Ackermann et al., *Dark matter constraints from observations of 25 Milky Way satellite galaxies with the Fermi Large Area Telescope*, *Phys. Rev.* **D89** (2014) 042001, [1310.0828].

[472] Fermi-LAT, DES collaboration, A. Albert et al., *Searching for Dark Matter Annihilation in Recently Discovered Milky Way Satellites with Fermi-LAT*, *Astrophys. J.* **834** (2017) 110, [1611.03184].

[473] HAWC collaboration, A. U. Abeysekara et al., *Extended gamma-ray sources around pulsars constrain the origin of the positron flux at Earth*, *Science* **358** (2017) 911–914, [1711.06223].

[474] S. Profumo, J. Reynoso-Cordova, N. Kaaz and M. Silverman, *Lessons from HAWC pulsar wind nebulae observations: The diffusion constant is not a constant; pulsars remain the likeliest sources of the anomalous positron fraction; cosmic rays are trapped for long periods of time in pockets of inefficient diffusion*, *Phys. Rev.* **D97** (2018) 123008, [1803.09731].

[475] L. Bergstrom, T. Bringmann, I. Cholis, D. Hooper and C. Weniger, *New Limits on Dark Matter Annihilation from AMS Cosmic Ray Positron Data*, *Phys. Rev. Lett.* **111** (2013) 171101, [1306.3983].

[476] S. Palomares-Ruiz and S. Pascoli, *Testing MeV dark matter with neutrino detectors*, *Phys. Rev.* **D77** (2008) 025025, [0710.5420].

[477] R. Primulando and P. Uttayarat, *Dark Matter-Neutrino Interaction in Light of Collider and Neutrino Telescope Data*, *JHEP* **06** (2018) 026, [1710.08567].

[478] A. Olivares-Del Campo, C. Bœhm, S. Palomares-Ruiz and S. Pascoli, *Dark matter-neutrino interactions through the lens of their cosmological implications*, *Phys. Rev.* **D97** (2018) 075039, [1711.05283].

[479] A. Olivares-Del Campo, S. Palomares-Ruiz and S. Pascoli, *Implications of a Dark Matter-Neutrino Coupling at Hyper-Kamiokande*, in *53rd Rencontres de Moriond on Electroweak Interactions and Unified Theories (Moriond EW 2018) La Thuile, Italy, March 10-17, 2018*, 2018. 1805.09830.

[480] M. W. Goodman and E. Witten, *Detectability of Certain Dark Matter Candidates*, *Phys. Rev.* **D31** (1985) 3059.

[481] G. Jungman, M. Kamionkowski and K. Griest, *Supersymmetric dark matter*, *Phys. Rept.* **267** (1996) 195–373, [hep-ph/9506380].

[482] K. Freese, M. Lisanti and C. Savage, *Colloquium: Annual modulation of dark matter*, *Rev. Mod. Phys.* **85** (2013) 1561–1581, [1209.3339].

[483] J. A. Evans, S. Gori and J. Shelton, *Looking for the WIMP Next Door*, *JHEP* **02** (2018) 100, [1712.03974].

[484] R. Essig, J. Mardon and T. Volansky, *Direct Detection of Sub-GeV Dark Matter*, *Phys. Rev.* **D85** (2012) 076007, [1108.5383].

[485] W. Mu and X. Ji, *Ionization Yield from Nuclear Recoils in Liquid-Xenon Dark Matter Detection*, *Astropart. Phys.* **62** (2015) 108–114, [1310.2094].

[486] DARWIN collaboration, J. Aalbers et al., *DARWIN: towards the ultimate dark matter detector*, *JCAP* **1611** (2016) 017, [1606.07001].

[487] J. Kopp, V. Niro, T. Schwetz and J. Zupan, *DAMA/LIBRA and leptonically interacting Dark Matter*, *Phys. Rev.* **D80** (2009) 083502, [0907.3159].

[488] M. J. Dolan, F. Kahlhoefer and C. McCabe, *Directly detecting sub-GeV dark matter with electrons from nuclear scattering*, *Phys. Rev. Lett.* **121** (2018) 101801, [1711.09906].

[489] R. Essig, M. Fernandez-Serra, J. Mardon, A. Soto, T. Volansky and T.-T. Yu, *Direct Detection of sub-GeV Dark Matter with Semiconductor Targets*, *JHEP* **05** (2016) 046, [1509.01598].

[490] S. Derenzo, R. Essig, A. Massari, A. Soto and T.-T. Yu, *Direct Detection of sub-GeV Dark Matter with Scintillating Targets*, *Phys. Rev.* **D96** (2017) 016026, [1607.01009].

[491] C. McCabe, *New constraints and discovery potential of sub-GeV dark matter with xenon detectors*, *Phys. Rev.* **D96** (2017) 043010, [1702.04730].

[492] SuperCDMS collaboration, R. Agnese et al., *Projected Sensitivity of the SuperCDMS SNOLAB experiment*, *Phys. Rev.* **D95** (2017) 082002, [1610.00006].

[493] A. Berlin, N. Blinov, G. Krnjaic, P. Schuster and N. Toro, *Dark Matter, Millicharges, Axion and Scalar Particles, Gauge Bosons, and Other New Physics with LDMX*, *Phys. Rev.* **D99** (2019) 075001, [1807.01730].

[494] XENON collaboration, E. Aprile et al., *Physics reach of the XENON1T dark matter experiment*, *JCAP* **1604** (2016) 027, [1512.07501].

[495] S. Gopalakrishna, S. Jung and J. D. Wells, *Higgs boson decays to four fermions through an abelian hidden sector*, *Phys. Rev.* **D78** (2008) 055002, [0801.3456].

[496] Wolfram Research Inc., *Mathematica, versions 11.1 & 11.2*, 2017.